U.S. Department of the Interior
Bureau of Land Management

BLM Alaska Open File Report 103
BLM/AK/ST-06/001+3090+942
November 2005

An Investigation of the Geology and Gold Mineralization in the Nyac District, Southwest Alaska

Zachary John Wenz

BLM

Alaska

Mission Statement

The Bureau of Land Management (BLM) sustains the health, diversity and productivity of the public lands for the use and enjoyment of present and future generations.

Author

Zachary John Wenz

This report is the outcome of a thesis completed by the author in partial fulfillment of the requirements for a Masters of Science degree at the University of Alaska, Fairbanks. The project was supported in part by the BLM as part of the Aniak Mining District study.

Cover

Geologists Jeff Foley (left) and Zach Wenz examine a gold-bearing sericite-altered quartz-calcite vein zone on Bonanza Ridge, NYAC District, Southwest, Alaska (photo by Nick Enos).

Open File Reports

Open file reports present the results of inventories or other investigations published outside the formal BLM-Alaska technical publication series. These reports can include preliminary or incomplete data and are not published and distributed in quantity.

Reports are available while supplies last from BLM External Affairs, 222 West 7th Avenue, #13, Anchorage, Alaska 99513 (907) 271-5555 and from the Juneau Minerals Information Center, 100 Savikko Road, Mayflower Island, Douglas, AK 99824, (907) 364-1553. Copies are also available for inspection at the Alaska Resource Library and Information Service (Anchorage), the United States Department of the Interior Resources Library in Washington D.C., various libraries of the University of Alaska, the BLM National Business Center Library (Denver), and other selected locations.

A complete bibliography of all BLM-Alaska scientific reports can be found on the Internet at: **http://www.ak.blm.gov/affairs/sci_rpts.html**

Related publications are also listed at: **http://juneau.ak.blm.gov.**

An Investigation of the Geology and Gold Mineralization in the Nyac District, Southwest Alaska

By
Zachary John Wenz

BLM Open File Report 103
November 2005

U.S. Department of the Interior
Bureau of Land Management
Alaska State Office
222 W. 7th Ave., #13
Anchorage AK 99513

Abstract

The Nyac district, southwest Alaska, contains multiple felsic to mafic plutons and dikes intruding the volcano-sedimentary package of the Nyac terrane. Dated plutons and dikes in the Nyac terrane record Early Cretaceous ages; other plutons in southwest Alaska are Late Cretaceous and Tertiary. The Nyac district contains high-temperature and low-temperature gold mineralization. The age of high-temperature and low-temperature mineralization is concordant with plutonism. The high-temperature mineralization occurs in the Bonanza pluton and associated gray granodiorite porphyry dikes. Bonanza pluton mineralization consists of gold-bearing quartz veins with pyrite-chalcopyrite-magnetite-bismuthinite-molybdenite. Fluid inclusions from mineralized quartz veins record trapping temperatures up to 560^{o} C and salinities up to 60 wt% NaCl. Mineralization in the grey granodiorite porphyry dikes consists of gold-bearing quartz veins with tellurobismuthite-tetradymite-chalcopyrite. Fluid inclusions from mineralized quartz veins record trapping temperatures up to 370^{o} C, salinities up to 5 wt% NaCl, and CO_2 concentrations up to 80 vol%. Both types display sericite-chlorite-albite alteration, and the Bonanza Pluton also displays potassic alteration. The low-temperature mineralization occurs at the Bonanza Creek Color Anomaly and along high-angle faults. This type contains anomalous Au and Hg. The alteration assemblage is sericite-kaolinite, indicating low temperature (<240^{o} C) and acidic fluids.

TABLE OF CONTENTS

List of Figures

List of Tables

List of Appendices

1. Introduction

The Nyac district is located approximately 100 kilometers northeast of Bethel in the Kilbuck Mountains, southwest Alaska (Figure 1.1). Calista Corporation, an Alaska native corporation founded under the Alaska Native Claims Settlement Act, owns the surface and subsurface rights to 186 square kilometers in the Nyac area, covering nearly all of the historical placer mining operations in the district. The Nyac district lies in the northeast portion of the Nyac terrane (as defined by Decker et al., 1994). The Nyac terrane is arguably the least understood terrane in southwest Alaska. The only published geologic maps (Box et al., 1993; Hoare and Coonrad, 1959) are highly generalized (1:250,000 scale) and accompanied by a few K-Ar, U-Pb dates, geochemical analyses and major oxide analyses (Box et al., 1993; Robinson and Decker, 1986; and Wilson, 1977). No detailed study of the geology and particularly of the lode gold mineralization is available.

From the early 1900's to 2000, a minimum 500,000 oz. of placer gold has been produced from the Nyac district (Foley, 2000). Despite this enormous placer gold production, no significant lode gold prospects are known. Although known bedrock gold anomalies occur in the district (Gierymski and Werdon, 1997; Frost et al., 1993; RAA, 1975; and Wallace, 1945), no particular lode source or system has been identified as responsible for the accumulation of gold in the streams. Lack of lode gold discovery is related to limited exploration, lack of detailed mapping, and inadequate models for potential mineralization. Therefore the purpose of this study is to produce an accurate geologic map and combine all geochemical data to produce a local model for gold deposition in the study area.

1.1 Regional Geology

Southwestern Alaska is comprised of various tectonostratigraphic terranes, including the Farewell, Goodnews, Nyac, Kilbuck, and Togiak terranes largely overlain by the Cretaceous Kuskokwim Group and unconsolidated Tertiary sediments (Figure 1.1; Decker et al., 1994). The Nyac terrane consists of volcanic and volcaniclastic rocks of Middle and Late Jurassic age intruded by Early Cretaceous felsic to intermediate plutons. The volcanic rocks possess high La/Nb ratios, characteristic of volcanic arc-related magmatism. The volcaniclastic rocks are dominantly epiclastic tuffaceous marine sandstone, shale and conglomerate. Pelecypod fossils found in sedimentary beds are of Bajocian (Early Jurassic) and Tithonian (Late Jurassic) age; the latter are present in the upper sequences outside the study area. Unlike other terranes in southwest Alaska, the Nyac terrane is nowhere overlain by the Kuskokwim Group rocks (Box et al., 1993). The Nyac terrane is also unique among the SW Alaska terranes in that it contains Early Cretaceous plutons whereas plutons in adjacent terranes are latest Cretaceous and early Tertiary in age (Decker et al., 1994).

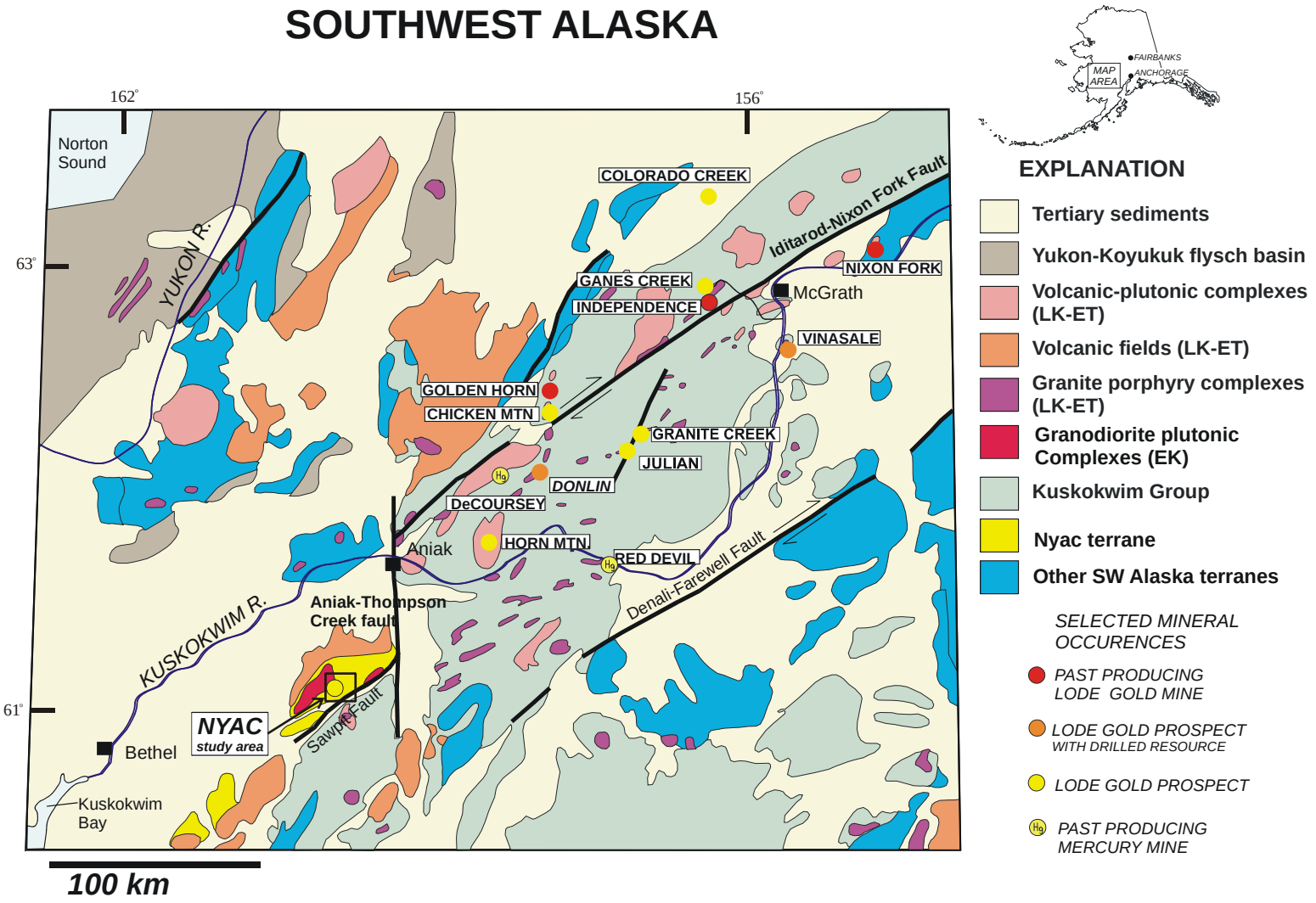

Figure 1.1: Regional geologic map of southwest Alaska. Modified after Bundtzen and Miller (1997)

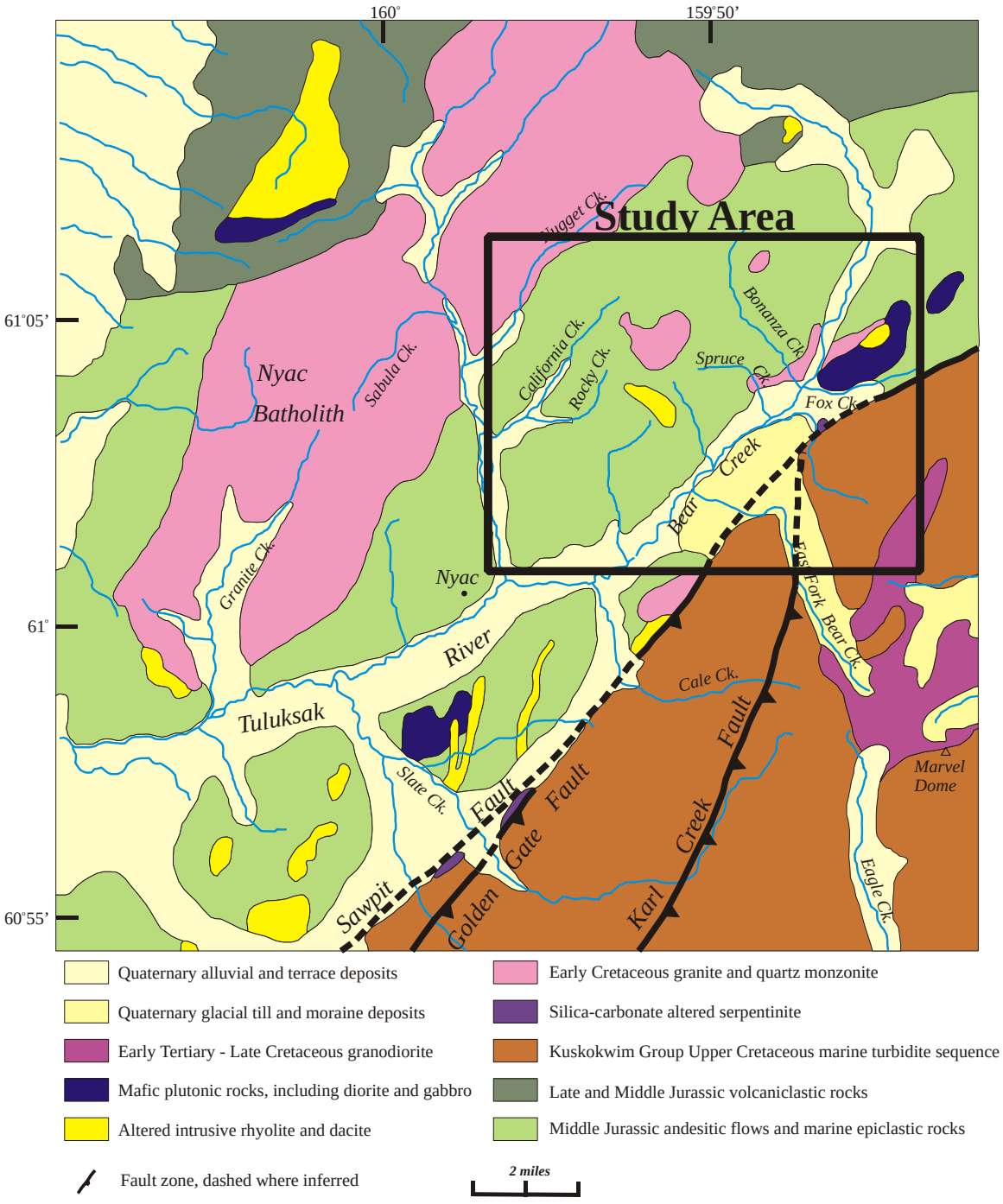

Figure 1.2: USGS 1:250,000-scale geologic map of the Nyac area after Box et al. (1993). Study area enclosed by the outlined box.

Southwest Alaska is dominated by the right-lateral Iditarod-Nixon Fork and Denali-Farewell Fault systems (Figure 1.1). In the Nyac area, the Nyac terrane is bounded on the SE by the right-lateral Golden Gate-Sawpit Fault (Figure 1.2). The Golden Gate-Sawpit Fault is inferred to be a continuation of the Iditarod-Nixon Fork Fault system, offset by the left lateral Aniak-Thompson Creek Fault (Figure 1.1). Miller et al. (2002) found the Iditarod-Nixon Fork Fault system became active in Late Cretaceous time. The Aniak-Thompson Creek Fault appears to offset the Iditarod-Nixon Fork Fault system, but the timing of that movement is uncertain.

1.2 Previous Exploration

Robert E. Wallace made the first documented discovery of lode gold in the Nyac district (Wallace, 1945). He found free gold in quartz-chlorite veins hosted in a granitic porphyry dike at the confluence of California Creek and the Tuluksak River (Figure 1.3). More abundant and occurring with the gold was a soft, silver-gray mineral with laminar cleavage later believed to be a telluride (Gates, 1945a, unpublished letter). Early assays of this occurrence reported gold values up to 1.3 opt/Au (Gates, 1945b, unpublished letter).

Resource Associates of Alaska (RAA; 1975) conducted the first comprehensive exploration study in the Nyac area from 1974 to 1975. RAA conducted 1:63,630 scale mapping and sampling of over 675 square miles in a one and a half month period. RAA documented five areas of anomalous gold values: the Wallace occurrence, a fault zone north of Bonanza Creek, Marvel Creek, Fisher Dome and the Cripple Mountain. Two of these areas, the Wallace occurrence and fault-hosted mineralization north of Bonanza Creek (Figure 1.3), lie in the study area. The mineralization north of Bonanza Creek, as described by RAA, is a 20-foot-wide zone of brecciated, quartz-veined, iron-stained hornfels. RAA believed the anomalous gold was constrained to quartz-dolomite veins with values up to 15.1 ppm Au (J. Foley, written comm., 2004).

Frost (1990) discovered anomalous Hg (up to 2.28 ppm) values associated with gold-bearing, quartz veins, suggesting an epithermal component to some of the mineralization. Frost et al. (1993) later speculated that the spatial association of the mineralized veins with the plutons suggests that the plutons at least supplied a heat source for circulation of hydrothermal fluids.

In 1996 and 1997 Placer Dome Exploration (PDX; Gierymski and Werdon, 1997) conducted the most thorough exploration program in the district. In 1996 an eleven-hole, reverse circular drilling program and nine ground-VLF-resistivity profiles were completed. All efforts were constrained to the Bear Creek and Tuluksak River valleys, in belief that the placers directly overlay their lode sources. Of a total 742 meters of drilling the highest anomalous gold values were eight meters of 30 to 70 ppb Au. The 1997 exploration began with compilation of all the old churn drill and dredging records for the district. PDX geologists determined the data were too limited in extent to be spatially useful, but the old reports did provide

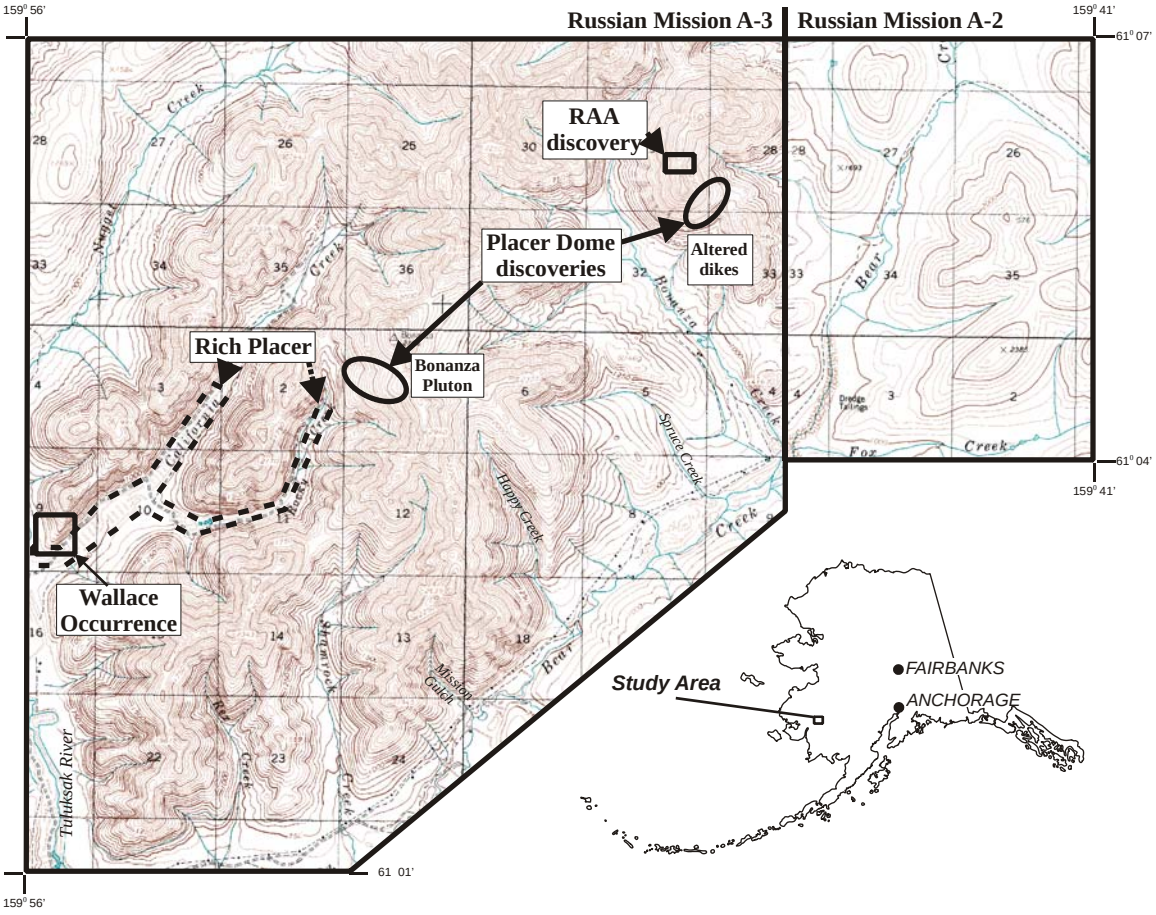

Figure 1.3: Topographic map of the study area. Map depicts previously discovered bedrock gold occurrences and rich placer locations.

references to high-grade placers in Rocky and California Creek drainages (Figure 1.3). PDX geologists mapped and sampled approximately 200 square kilometers at a 1:12000 scale in 200 days. New discoveries found during this exploration included anomalous gold values in the Bonanza pluton and altered dikes north of Bonanza Creek (Figure 1.3; Gierymski and Werdon, 1997).

1.3 Purpose of Study

The main goal of this study is to determine the source of the 500,000 oz of placer gold. To determine the source of the gold, this investigation is focused on two aspects. The first aspect is to better understand and document the geology of the area, especially the intrusions. The second aspect is to better understand and tie together the various prospects and bedrock geochemical anomalies in the area. Thus, the principal goal was to construct an accurate geologic map at 1:25,000 scale employing a combination of field, petrographic, petrologic and dating techniques. Using this map and characteristics of the mineralization/alteration (deduced from field and laboratory observations and statistical analysis in the study area), this study ultimately produced a model for gold mineralization in the region that accounts for the placer deposits.

1.4 Methods

During June and July of 2003 field research was conducted that included geologic mapping and sampling in the Nyac district. The study area is bounded by UTM easting 449000, 463000, UTM northing 6775900 (zone 4 NAD27 datum, Clarke 1866 spheroid) and Bear Creek to the south (Figure 1.2). The terrain is steeply rising foothills covered by talus and vegetation on the lower portions. Outcrop is only exposed on ridge tops. The valleys are entirely covered with vegetation. Access to the base of the ridge tops was made possible by ATV-accessible mining roads. A total of 499 sample locations were collected and recorded using a Garmin 12 GPS unit. Field mapping was aided in part a by regional magnetics map (ADGGS staff et al., 1994). Abbreviated rock sample descriptions and locations are in Appendix A.

1.4.1 Chemical Analysis

A total 204 rock samples were submitted to ALS Chemex Laboratories[1] for trace element and major oxide analysis. The 204 rock samples were sent in two different sets and were analyzed by different techniques. Both sets were prepared for analysis by fine crushing (70% <2 mm), then a split sample (riffle splitter) was pulverized to < 75 microns (85% of sample). Analyses of the first set involved Aqua Regia digestion of the powdered sample followed by ICP-MS analysis for 50 elements. In addition, Ba, W and Sn

[1] Mention of ALS Chemex Labortories does not signify any specific BLM endorsement.

were analyzed by XRF wavelength dispersive methods, Hg by cold-vapor atomic absorption spectroscopy and Au by fire assay with ICP-AES. Analysis of the second set of samples involved a triple acid digestion (HF, HNO_3 and $HClO_4$) and HCl leach followed by ICP-MS analysis. In addition, Au was analyzed by fire assay atomic absorption spectroscopy, Hg by cold-vapor atomic absorption spectroscopy and major oxide analysis of lithium borate fused discs by XRF wavelength dispersive techniques. The triple acid technique was used for all the samples from mineralized areas suspected to have significant tellurium values since this method is more accurate in determining tellurium concentration. Partial digestion, especially for samples treated with aqua regia, make many of the elemental values low. Only results for elements known to completely dissolve are reported here.

Some powders returned from the ALS Chemex were used to prepare pressed pellets for major oxide and trace element analysis at the University of Alaska Fairbanks (UAF). The rock powders were mixed with 0.5 mL polyvinyl (2M) binding agent. The samples were then compressed under 20,000 psi and allowed to dry for 24 hours before analysis. Trace and major element analysis were performed at UAF on a Rigaku 3064 XRF using a program created by Dr. Rainer Newberry (described in Cameron, 2000).

Analytical accuracy for commercial and UAF XRF analyses are $\pm$ 2% amount present for major oxides and $\pm$ 5-10% amount present for trace elements (Cameron, 2000). Duplicate samples were submitted to ALS Chemex. Since heterogeneity and the nugget effect could affect duplicate results, only a general sense of accuracy can be obtained. Duplicate samples varied no more than 12% of the amount present. Appendix B lists chemical data and analytical techniques.

1.4.2 Petrography

Polished and covered thin sections of 34 rock samples were prepared commercially by Spectrum Petrographics. An additional 50 polished and covered thin sections were prepared at UAF. All were examined by standard reflected and transmitted light techniques in conjunction with feldspar staining and major oxide analysis. Thin section petrography was used to determine which samples were good candidates for $^{40}Ar/^{39}Ar$ dating, microprobe analysis and fluid inclusion microthermometry. Anorthite content was calculated using the Michel-Levy technique (Deer et al., 1966).

1.4.3 Magnetic Susceptibilities

Magnetic susceptibilities were taken for all samples collected in the field. Normally three measurements were taken at each station and averaged. For those samples taken from Bonanza Pluton, ten measurements were averaged. All measurements were taken with a Kappameter model KT-6 magnetic susceptibility meter. The meter was held normal to a fresh, smooth surface of the rock. Magnetic susceptibility data are given in Appendix A.

1.4.4 Feldspar Staining

Thirty seven igneous rock samples were etched using HF acid and then stained with sodium cobaltinitrate following the procedure of Ruperto et al. (1964). Using this technique K-feldspar stains yellow, plagioclase etches milky white and quartz is unaffected. Modal abundances of quartz, K-feldspar and plagioclase were estimated using standard abundance charts. In general the modal estimations agree with chemically derived names for the same specimen. Modal data are presented in Appendix C.

1.4.5 Microprobe Analysis

Microprobe analyses were conducted on native gold, Bi and Bi-Te minerals. The analyses were performed at the UAF on a Cameca SX-50 microprobe with a 25 micron beam set at 25kV and 30 mA. On peak was counted for 10 seconds and off peaks for 5 seconds. Working standards were used to ensure data quality. Microprobe data are given in Appendix D.

1.4.6 Fluid Inclusion Microthermometry

Fluid inclusion studies were conducted at UAF on a Fluid Inc. model (Reynold) stage. All samples were doubly polished quartz veins with a thickness of approximately 100 microns. Due to the inability to control low temperatures on this setup, few freezing temperatures were determined and no CO_2 freezing temperatures were attempted. Final homogenization temperatures were the last value measured. A final standardization was run to ensure data quality. The standard used was a pure water inclusion that froze at 0.2 C^{o}. Accurate measurements were acquired by cycling back and forth through phase transitions and averaging the results. In general, repeated measurements varied by <1 degree Celsius. Salinities and vol% CO_2 were calculated using the Macintosh FLINCOR (Brown, 1989) program. Trapping temperatures were estimated after Potter (1997). Fluid inclusion data are presented in Chapter 3.

1.4.7 Radiometric $^{40}Ar/^{39}Ar$ Dating

For $^{40}Ar/^{39}Ar$ analysis, mineral separates and whole rock chips (7 hornblende, 1 muscovite, 9 biotite and 2 whole rock) were submitted to the Geochronology Laboratory at UAF. Mineral separates were obtained from a crushed rock sample by hand-picking. The monitor mineral MMhb-1 (Samson and Alexander, 1987) with an age of 513.9 Ma (Lanphere and Dalrymple, 2000) was used to monitor neutron flux (and calculate the irradiation parameter, J). The samples and standards were wrapped in aluminum foil and loaded into aluminum cans of 2.5 cm diameter and 6 cm height. The samples were irradiated in position 5c of the uranium enriched research reactor of McMaster University in Hamilton, Ontario, Canada for 20 megawatt-hours.

Upon their return from the reactor, the sample and monitors were loaded into 2 mm diameter holes in a copper tray that was then loaded into an ultra-high vacuum extraction line. The monitors were fused, and samples heated, using a 6-watt argon-ion laser following the technique described in York et al. (1981), Layer et al. (1987) and Layer (2000). Argon purification was achieved using a liquid nitrogen cold trap and a SAES Zr-Al getter at 400 degrees Celsius. The samples were analyzed in a VG-3600 mass spectrometer at the Geophysical Institute, UAF. The argon isotopes measured were corrected for system blank and mass discrimination, as well as calcium, potassium and chlorine interference reactions following procedures outlined in McDougall and Harrision (1988).

The detailed analyses are given in Appendix E. Ages are quoted at the $\pm$ 1 sigma level and calculated using the constants of Steiger and Jaeger (1977).

2. Geology and Geophysics

Rock types present in a given district are a good initial indicator of where and how the gold occurs. Since both volcanic and plutonic rocks can produce and host gold deposits (e.g., volcanogenic massive sulfide or copper porphyry type deposits), it is important to characterize these different rock types and determine their relation to gold mineralization. The rocks of the study area are of four major types: (1) variably metamorphosed Jurassic volcano-sedimentary rocks, (2) Jurassic (?) plutonic rocks, (3) Early Cretaceous plutonic rocks and (4) Tertiary (?) dikes. Discrimination between these rock types is based on statistical analysis, cross-cutting relationships, compositional data, Ar dating (discussed in chapter 4) and textural features.

The magnetic susceptibility of a particular rock type can be a useful discriminating characteristic of any rock unit. When surface magnetic susceptibilities are used in conjunction with magnetic surveys an indication of the depth of the rock cover can be estimated. This is useful to understand if the rocks exposed at the surface continue at depth. Table 2.1 lists the magnetic susceptibility range and average for each of the rock units.

The interpretive geologic map of the study area (Figure 2.1), is the most detailed map to date of the Nyac district. The previous most detailed published map is a USGS 1:250,000 scale map (Figure 1.2; Box et al, 1993). The USGS map has no bedding measurements in the Jurassic volcanic rocks, does not have any high-angle faults (besides the Golden Gate-Sawpit Fault) and the plutonic rocks mapped in the study area are the same unit as the Nyac Batholith. The map produced as a result of this study includes bedding measurements in the Jurassic volcanic rocks, identifies six different igneous bodies and four different dike types. This map also includes two fault sets with northeast-southwest and north-south orientations. The northeast-southwest faults include the high-angle, right-lateral Golden Gate-Sawpit fault system and its related faults. The north-south trending high-angle, left-lateral faults, are presumably related to the Aniak-Thompson Creek Fault. This chapter includes a complete description of each rock unit shown on the interpretive bedrock geology map (Figure 2.1).

2.1 Jurassic Volcano-Sedimentary Rocks

The volcano-sedimentary rock group includes two rock units: (1) metavolcanic rocks and (2) metasedimentary rocks. The volcano-sedimentary rocks are most important for determining the stratigraphy in the study area. Although some anomalous mineralization occurs in these rocks, they are relatively unmineralized in comparison to the plutonic rocks. The Jurassic volcano-sedimentary rocks are contact metamorphosed to various hornfels facies depending on proximity to a heat source and initial composition.

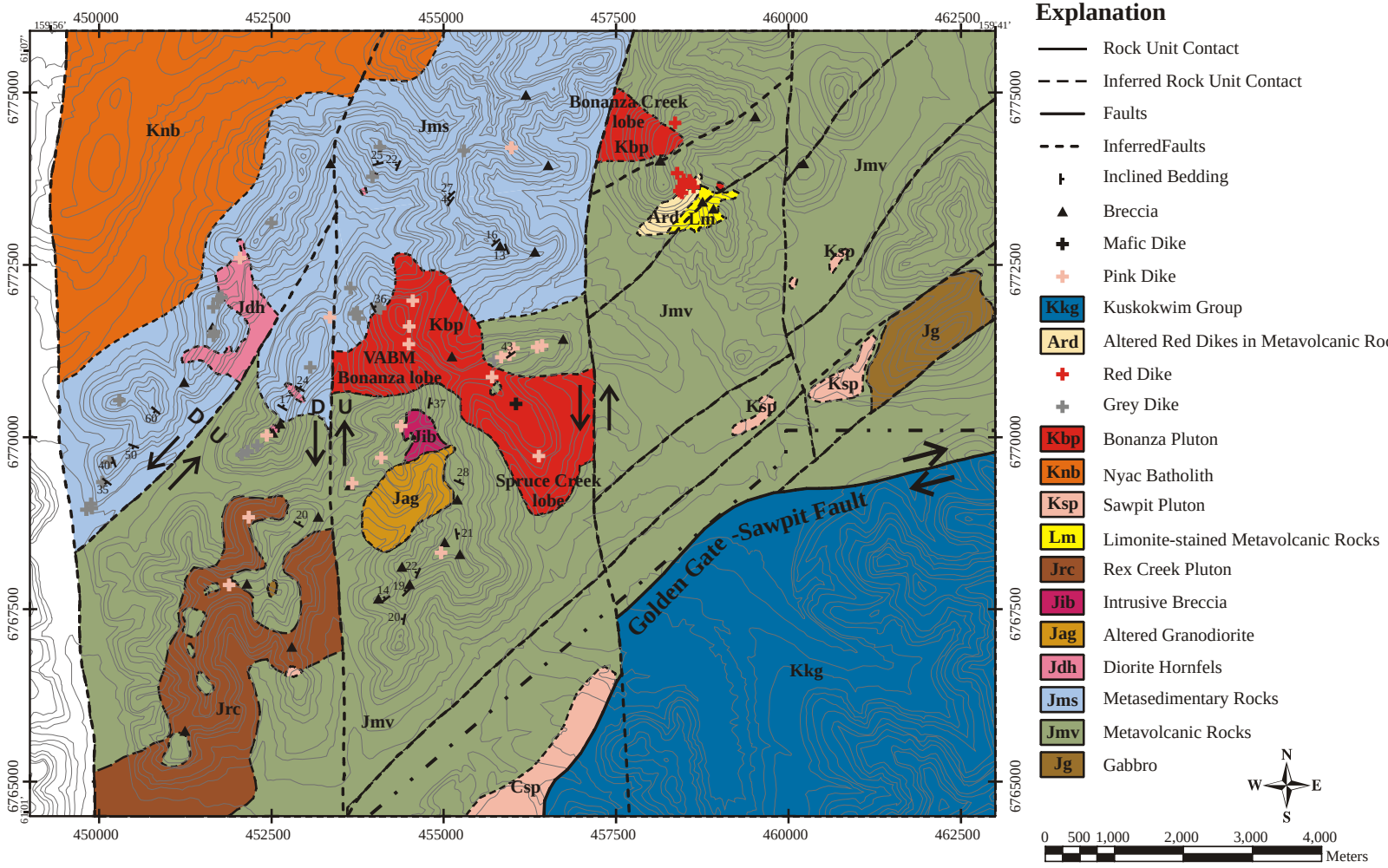

Figure 2.1: Interpretive bedrock map of the Nyac district. Geology southeast of dashed and dotted line is from Gierymski and Werdon (1997).

Table 2.1 Magnetic susceptibility (x10^{-3} SI) ranges and averages for each of the rock units.

Map Unit	Average	Range	Number
Mafic Dike	13.3		1
Pink Dike	4.21	1.39-7.96	16
Bonanza Pluton	8.43	0.14-30.8	54
Gray Dike	3.16	0.19-13.8	16
Red Dike	14.0		1
Nyac Batholith	8	4.0-12.0	13
Sawpit Pluton	3.64	0.11-16.2	8
Rex Creek Pluton	6.75	0.3-25.0	19
Altered Granodiorite	4.88	4.54-5.23	2
Diorite Hornfels	2.29	0.26-16.3	16
Undifferentiated Dikes	2.47	0.01-14.4	17
Metasedimentary Rocks	0.94	0.06-8.76	45
Metavolcanic Rocks	9.61	0.02-108	185
Gabbro	27.5	17.2-37.7	2

Figure 2.2 shows the compositional names for analyzed volcanic rocks using a TAS diagram. Because all of the volcanic rocks have experienced various degrees and types of metamorphism and alteration, the TAS classification may not accurately classify the rocks. The TAS method depends upon Na and K concentrations, which are relatively mobile elements.

TAS volcanic rock classifications were confirmed for samples with trace element data using the Nb/Y vs. Zr/TiO_2 scheme of Winchester and Floyd (1977) (Figure 2.3). These trace element classifications variably agree with the TAS classifications. Most importantly, the trace element classification illustrates that the apparent bimodal volcanic assemblage (basalts and rhyolite) is not accurate and in fact there is a continuum of volcanic compositions (basalt, andesite and rhyodacite). Using the trace element classification scheme none of the volcanic rocks plot as alkali-rich types, suggesting that the volcanic rocks either experienced alkali enrichment by syn-eruptive hydrothermal activity or post-eruptive alteration. Hydrothermal alkali enrichment of volcanic rocks is a common phenomenon for marine volcanic rocks; the resulting alteration is called spilitization (Blatt and Tracy, 1995). Spilitization results in the addition of alkalis from seawater into hot rocks. Since the Nyac terrane is a volcanic-arc and there are fossil beds layered with the flows, it is conceivable that some of the flows were submarine and may have experienced hydrothermal alteration and spilitization. However, since no unaltered varieties of volcanic rocks were identified, and thus analyzed, it is difficult to distinguish between spilitization and post-eruptive alteration as the cause for alkali enrichment.

Trace element data can also provide a means to determine the tectonic setting. Figures 2.4 and 2.5 show trace element based tectonic settings of basaltic composition rocks. In Figure 2.4 all of the basalts plot in the MORB, island-arc tholeiite and calc-alkali basalt field while Figure 2.5 illustrates that all but

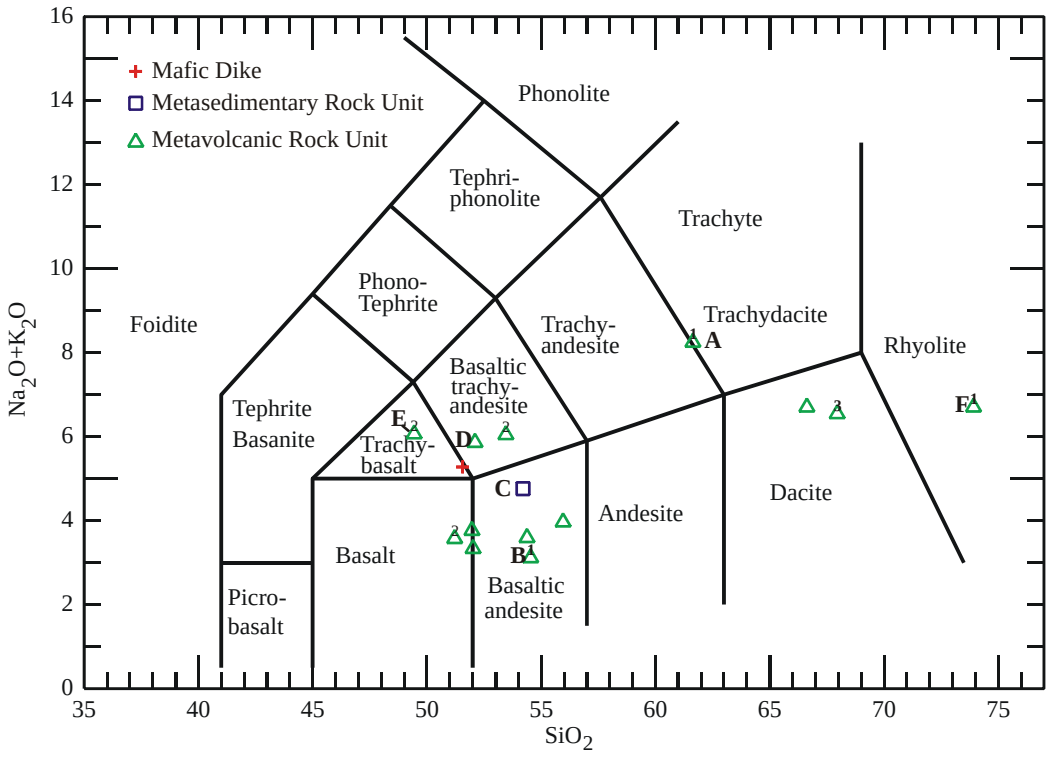

Figure 2.2: TAS diagram for volcanic rocks from the metasedimentary and metavolcanic rock units. and the mafic dike. Lettered samples are those with trace element data that is used on Figure 2.3 for trace element classification. Data are from this study; (1) Gierymski and Werdon (1997), (2) J. Foley written comm. (2004) and (3) T. P. Frost, written comm. (2004). Classification after LeMaitre et al. (1989).

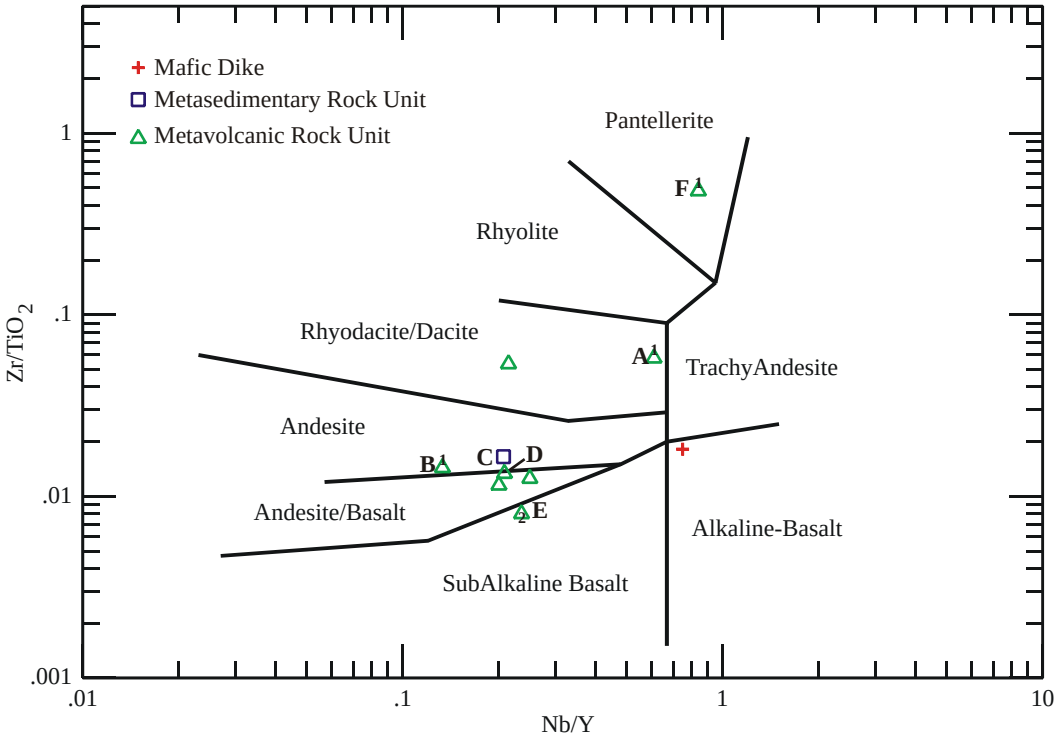

Figure 2.3: Winchester and Floyd (1977) trace element volcanic rock classification diagram for volcanic rocks from the metavolcanic and metasedimentary rock units and the mafic dike. Data are from this study, (1) Gierymski and Werdon (1997), and (2) J. Foley, written comm. (2004).

two of the samples are calc-alkaline basalts. All of the basaltic rocks have trace element characteristics of a volcanic-arc setting; andesite is characteristically of arc origin.

2.1.1 Metavolcanic Rocks

The metavolcanic rock unit is one of the oldest rock units in the study area. Since the bottom contact of this unit is not exposed and due to variable bedding measurements a minimum approximate thickness of 500 meters can be estimated. The unit contains approximately equal parts of volcaniclastic rocks and lava flows. Due to extensive compositional variation and degree of thermal metamorphism, the magnetic susceptibility for this unit is extremely variable (Table 2.1). Only one stratigraphic layer, a wackestone pelecypod-bearing bed, was found to continue across ridges.

The volcaniclastic rocks are extremely variable in composition and texture. The volcaniclastic rocks are dominantly clast supported, but some matrix supported beds exist. Clast supported beds are 1-10 meters thick; matrix supported beds are approximately 2 to <1 meter thick. In clast supported beds the clasts are generally angular and range in size from 2 mm to 10 cm in diameter and account for >50% of the rock volume. Matrix supported beds have more visible quartz grains and rare rounded to sub-angular clasts (2-40 mm in diameter) that account for >10% of the rock volume. In many cases correct classification between volcaniclastic and flow is only possible upon petrographic inspection. Most original volcaniclastic textures are lost due to recrystallization during thermal metamorphism (e.g., porphyritic flows look identical to crystal tuffs).

The flow rocks vary in composition from basalt to andesite with <1% dacite and rhyolite (Figure 2.3). The flows are 2-20 meters thick and presumably represent multiple flows. Flows are gray to gray green, purple and black, variably aphanitic to fine-grained or porphyritic, and/or amygdaloidal fine-grained. Porphyritic flows contain 1-10% plagioclase (1-8 mm) and 0-5% pyroxene (1-5 mm) as phenocrysts, and rarely hornblende. Amygdules are filled with epidote, actinolite or ringed chalcedony. Dacites are typically medium to coarse-grained, follow bedding planes, and may represent sills in the metavolcanic package. A single identified rhyolite is a plagioclase and quartz porphyry with an aphanitic matrix.

In addition to the volcanic and volcaniclastic rocks, other lithologies are present in this unit. They include: a few calcareous beds, a wackestone pelecypod fossil bed, and a clinopyroxenite dike. The calcareous beds are <1 to 20 meters thick and consist of dominantly argillaceous limestone beds, but rare pure limestone is also seen. One calcareous bed located north of Spruce Creek is almost entirely replaced by calc-silicate minerals (described in greater detail in Chapter 3: Gold Mineralization). The wackestone pelecypod-bearing bed consists of rounded to sub-rounded, medium-grained rock fragments in a chlorite altered matrix. Box et al. (1993) reported the pelecypod fossils are Bajocian (Middle Jurassic) in age. A single pyroxenite dike (03ZW328) has a cumulate, coarse-grained texture. Interstitial material is entirely chloritized.

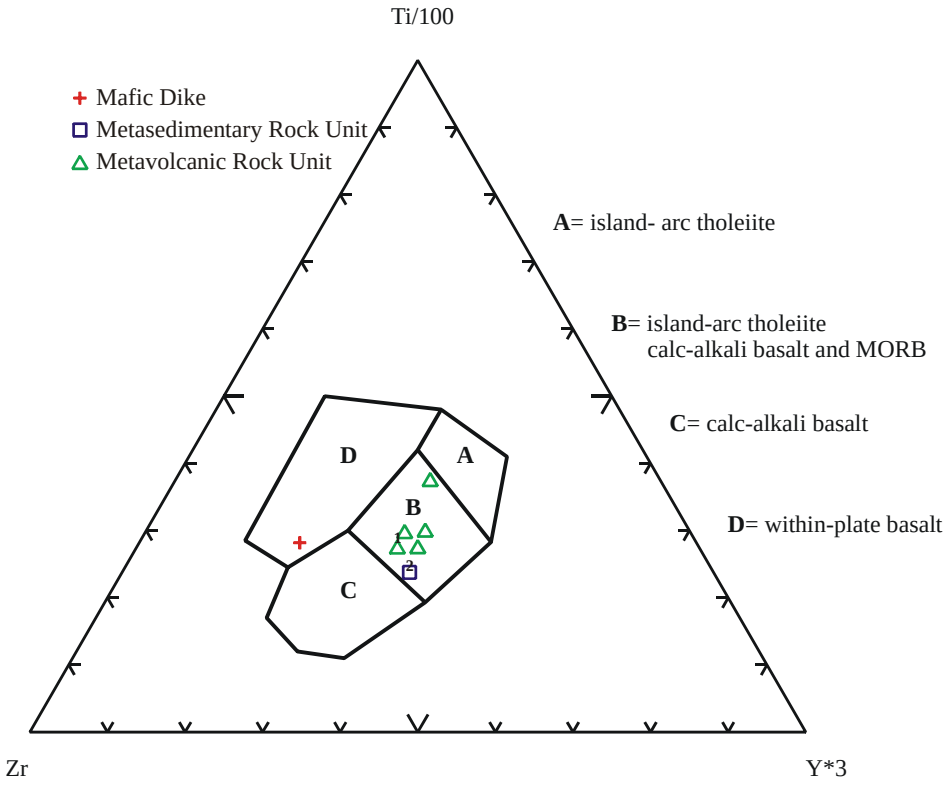

Figure 2.4: Winchester and Floyd (1977) trace element basalt origin diagram for metavolcanic and metasedimentary rock units and the mafic dike. Data are from this study, (1) Gierymski and Werdon (1997), and (2) J. Foley, written comm. (2004).

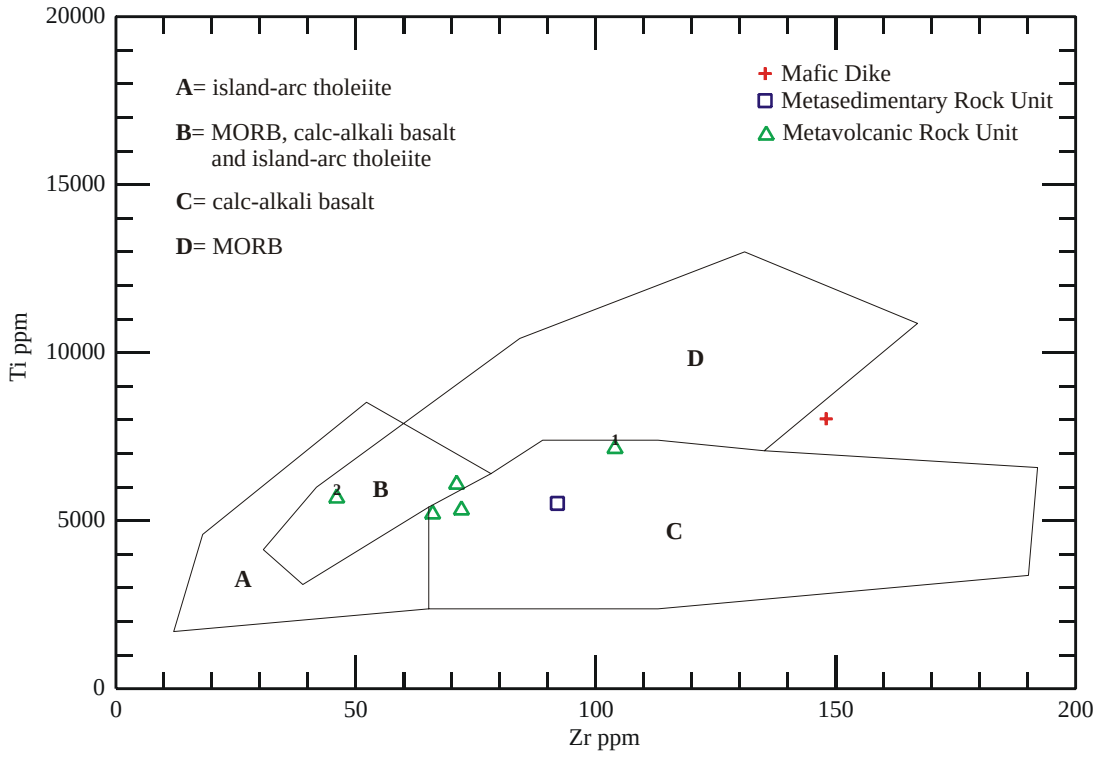

Figure 2.5: Pearce and Cann (1973) Zr vs. Ti discrimination diagram for the origin of basalts and andesites. Data are from this study, (1) Gierymski and Werdon (1997); and (2) J. Foley, written comm. (2004).

In thin section the clast supported volcaniclastic rocks contain approximately 40-85% angular volcanic rock clasts (>2 cm-4 mm diameter), 10-25% feldspar crystals (1-4 mm), <1% quartz (<1mm) and 5-65% fine-grained material. The feldspar crystals are approximately 95% plagioclase and 5% K-feldspar. Feldspar crystals are variably altered to chlorite, epidote and minor sericite (0-10%). The fine-grained material is altered to chlorite and epidote. Matrix supported volcaniclastic rocks are fine grained, occur in 5-mm to 15-cm-sized beds and contain round to sub-angular rock clasts. Some of these clasts form obvious depressions in the bedding and may be bombs. These volcaniclastic rocks contain fine-grained feldspar, minor quartz (80-90%) and larger (2-7 mm) feldspar crystals.

In thin section the volcanic flow rocks are generally porphyrititc and amygdaloidal with a fine-grained to aphanitic groundmass. Plagioclase phenocrysts are most common; pyroxene and hornblende phenocrysts also occur. The pyroxene and hornblende phenocrysts are commonly pseudomorphs replaced by a combination of epidote and actinolite. Amygdules are filled with epidote, actinolite, zeolites and chalcedony. Fine-grained groundmass is altered similar to the phenocrysts. Basalt contains up to 7% magnetite, although it is unclear how much of the magnetite was formed during thermal metamorphism.

In thin section the clinopyroxenite dike contains pyroxene pseudomorphs (2-5 mm, 30-100%) entirely altered to chlorite (50%), actinolite (40%) and epidote (10%). Plagioclase crystals make up 5-10% of the rock, are 10-20 microns in length and, and have been altered to chlorite (85%), epidote (10%) and sericite (5%). Plagioclase has an anorthite content of ~55%.

The volcanic and volcaniclastic rocks generally exhibit albite-epidote hornfels facies mineral assemblages. Higher grade hornblende hornfels and pyroxene hornfels facies are seen locally around the plutons. Metavolcanic rocks in the altered red dikes in metavolcanic rocks unit and near the altered granodiorite contain cordierite (Figure 2.6). Low-grade zeolite facies are present north of Spruce Creek.

2.1.2 Metasedimentary Rocks

This unit occurs in the north and northeastern portion of the study area (Figure 2.1). The metasedimentary unit may be traced from the study area north to the boundary of the Nyac terrane (Box et al, 1993). This unit appears to conformably overlie the metavolcanic unit. The unit is dominantly composed of mudstone/siltstone (55%), conglomerate (35%), volcaniclastic rocks (10%) and flows (<1%) all of which are now hornfels. The mudstone and siltstone beds are tens of meters thick, finely layered (mm's to 2 cm) and characteristically have a purple, biotite-hornfels color. Conglomerates are both clast supported (80%) and matrix supported (20%). The matrix is a fine-grained to aphanitic, quartz poor clay material, now entirely altered to chlorite. The clasts are sand to cobble-sized dominantly porphyritic, medium to fine-grained volcanic rocks with rare (<5%) sedimentary and granitic textured clasts.

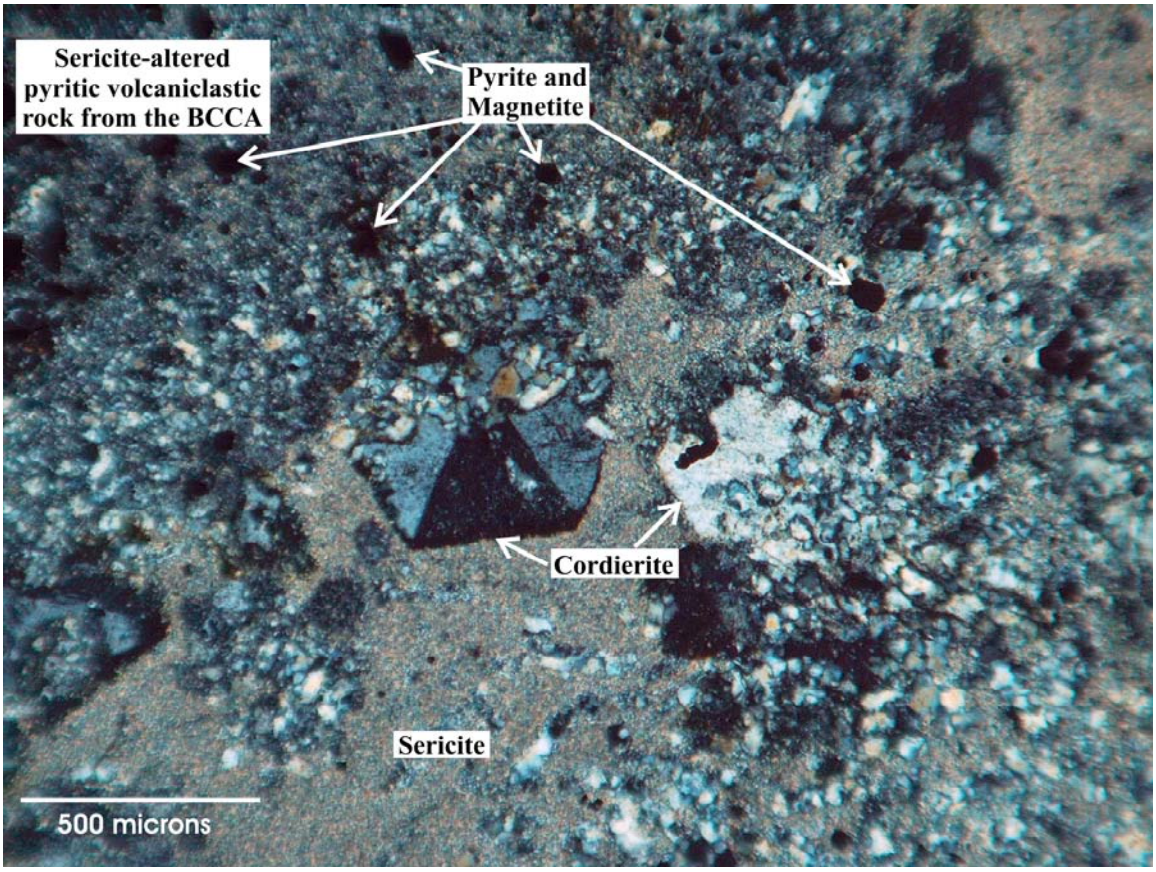

Figure 2.6: Cordierite in pyritic metavolcanic rocks from the BCCA.

In thin section volcaniclastic rocks in the unit have fine layers of feldspar and rock fragment clasts in a fine-grained matrix. In one sample the fine-grained matrix was thermally metamorphosed resulting in a 2/3 scapolite assemblage. The same rock also contains randomly oriented clinopyroxene and hornblende porphyroblasts indicating pyroxene hornfels facies metamorphism. Along the metasedimentary unit and Nyac Batholith contact, many metasedimentary rocks contain calc-silicate veins with sulfides (pyrite, pyrrhotite, chalcopyrite and marcasite) enveloped by garnet, pyroxene, hornblende, epidote, calcite and quartz. This local development of skarn indicates that the sedimentary beds originally contained appreciable calcite.

2.2 Introduction to Plutonic Rocks and Dikes

The correct name for a plutonic igneous rock is determined by IUGS modal abundance (quartz, alkali feldspar and plagioclase; Streckheisen, 1973). A secondary technique uses major oxide composition plotted on a chemical classification diagram (e.g., Streckheisen or R1-R2). The plutonic rocks and dikes were classified using the R1-R2 classification scheme of De la Roche et al. (1980). This method uses most major oxide data (excluding MnO and P_2O_5) from a typical major oxide analysis. The two parameters (R1 and R2) are calculated using the millication proportions of the elements. The formulas for calculating these factors are: R1=[4Si - 11(Na+K) - 2(Fe+Ti)] and R2=(Al + 2Mg + 6Ca). This method does not use normative based methods so a broad comparison of modal abundance versus chemical classification can be made. The R1-R2 diagram then displays mineral compositions relative to major oxide compositions. R1-R2 chemical classifications for plutonic rocks and dikes are given in Figures 2.7a and b. Modal classifications are shown on Figure 2.8.

Statistical methods can be used to group rocks of similar composition. Using discriminant analysis of trace element and major oxide data, the rock units in the study area are statistically distinguishable. Table 2.2 illustrates that 97.8% of the analyzed samples can be statistically distinguished on the basis of composition. Only one specimen from the Bonanza pluton is incorrectly classified.

The oxidation state of a pluton has implication for gold favorability and the type of associated fluids (Thompson and Newberry, 2000). Figure 2.9 shows that all of the Nyac Batholith and Bonanza Pluton rocks are calc-alkaline, relatively high oxidation state felsic rocks. Implications of this will be discussed in greater detail in Chapter 5. Figure 2.10 shows that all the granitic rocks have volcanic-arc trace element signatures.

2.3 Jurassic (?) Plutonic Rocks

This group includes the Rex Creek pluton, altered granodiorite, diorite hornfels and gabbro (Figure 2.1). These plutonic bodies were grouped together due to intense pervasive alteration, composition and unique trace element chemistry. Plutonic rocks grouped in this category have experienced intense thermal metamophism and/or epidote-chlorite-calcite-sericite alteration. The Rex Creek pluton and altered granodiorite display intense epidote-chlorite-calcite-sericite alteration. This alteration has entirely destroyed the original mafic mineralogy. These pervasive alteration types do not occur in the Early Cretaceous plutonic rocks, indicating a different and perhaps longer history of alteration for the Jurassic (?) plutonic rocks.

Table 2.2 Classification results of discriminant analysis for plutonic rocks.

		Predicted Group Membership						
	Rock Unit	Nyac Batholith	Bonanza Pluton	Sawpit Pluton	Rex Creek Pluton	Hornfels Diorite	Altered Granodiorite	Total
Original Count	Nyac Batholith	22	0	0	0	0	0	22
	Bonanza Pluton	1	17	0	0	0	0	18
	Sawpit Pluton	0	0	1	0	0	0	1
	Rex Creek Pluton	0	0	0	2	0	0	2
	Hornfels Diorite	0	0	0	0	1	0	1
	Altered Granodiorite	0	0	0	0	0	2	2
%	Nyac Batholith	100.0	.0	.0	.0	.0	.0	100.0
	Bonanza Pluton	5.6	94.4	.0	.0	.0	.0	100.0
	Sawpit Pluton	.0	.0	100.0	.0	.0	.0	100.0
	Rex Creek Pluton	.0	.0	.0	100.0	.0	.0	100.0
	Hornfels Diorite	.0	.0	.0	.0	100.0	.0	100.0
	Altered Granodiorite	.0	.0	.0	.0	.0	100.0	100.0

*The statistical analysis includes all major oxide and trace element data. The table shows 97.8% of the groups are classified correctly.

The Jurassic (?) plutonic rocks have variable compositions (Figures 2.7a and 2.8). In general these rocks contain significantly more mafic compositions (diorite) in comparison to the Early Cretaceous plutons. It is possible that some of these rocks may have been the feeders for the volcanic rocks in the district. The Jurassic (?) plutonic rocks appear to be more yttrium enriched than the early Cretaceous plutons (Figure 2.11). This difference in yttrium suggests a compositional variation inherent in the source for the two rock groups; thus, the Early Cretaceous plutons likely have originated from a different source.

The final evidence for separating the Jurassic (?) plutonic rocks from the other plutons is illustrated by their fractionation patterns. Since three of the Jurassic (?) plutonic bodies exhibit yttrium enrichment (relative to niobium), their analyses can be grouped together to display a fractionation pattern of trace elements changing with silica content. Figure 2.12 illustrates that the Jurassic (?) plutonic rocks have opposite fractionation patterns from the Early Cretaceous rocks with respect to Ce, Y and Zr. These three elements increase in concentration with increasing silica for the Jurassic (?) plutonic rocks, while for the Early Cretaceous plutonic rocks Ce, Y and Zr concentrations decrease with increasing silica content.

2.3.1 Rex Creek Pluton

The Rex Creek pluton occurs in the southwest portion of the field area (Figure 2.1). The pluton intrudes the metavolcanic unit and is inferred to underlie >4 km^2 of surface area. It is sporadically covered with erosional remnants of metavolcanic rocks a few meters thick. The Rex Creek pluton is a

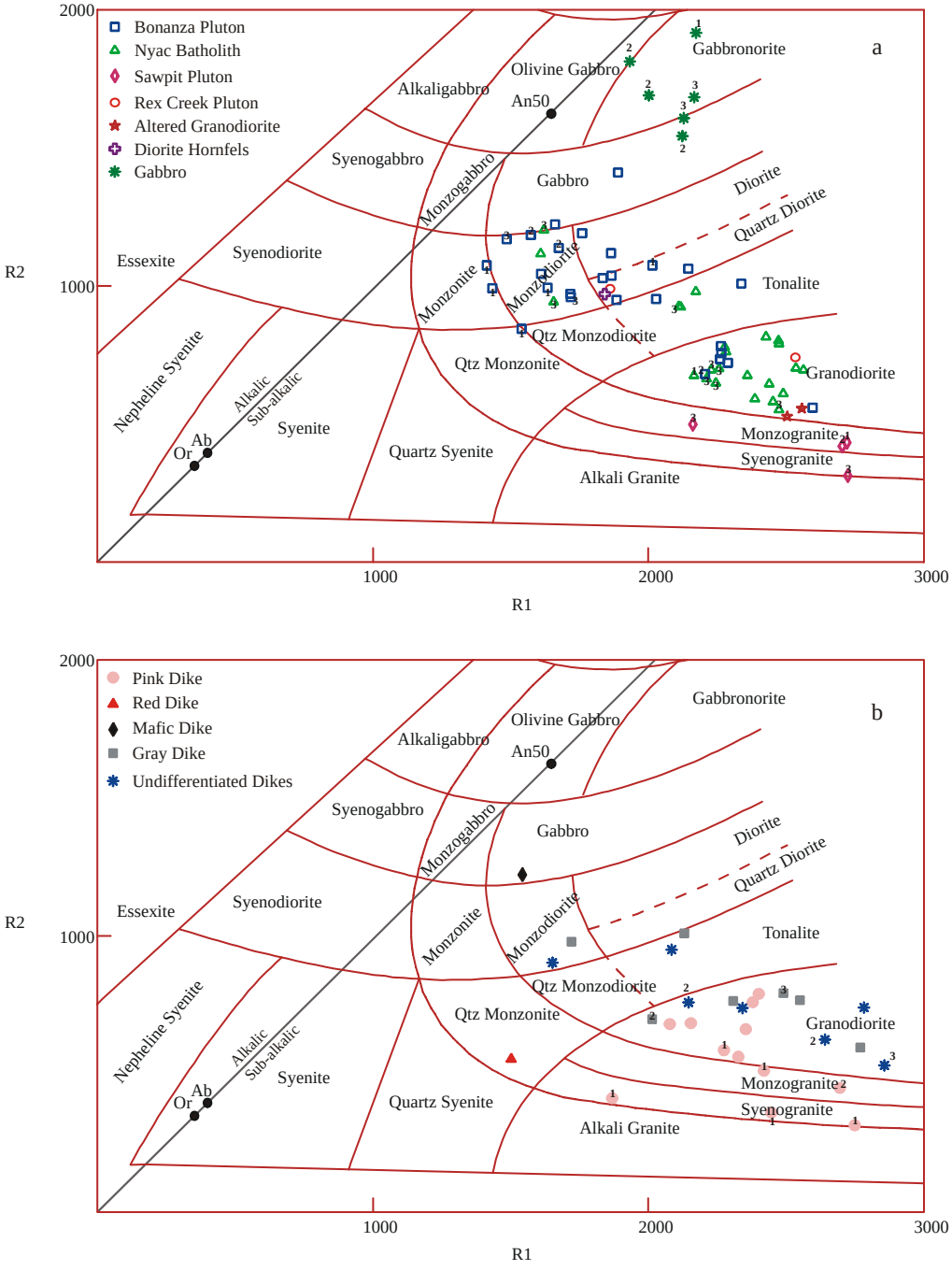

Figure 2.7: R1-R2 chemical classifications for plutons (a) and dikes (b). The two parameters (R1 and R2) are calculated using the millication proportions of the elements, R1=[4Si - 11(Na+K) - 2(Fe+Ti)] and R2=(Al + 2Mg + 6Ca). Data are a compilation from this study; (1) Gierymski and Werdon (1997), (2) J. Foley, written comm. (2004), and (3) T. P. Frost, written comm. (2004). Diagram modified after De la Roche et al. (1980).

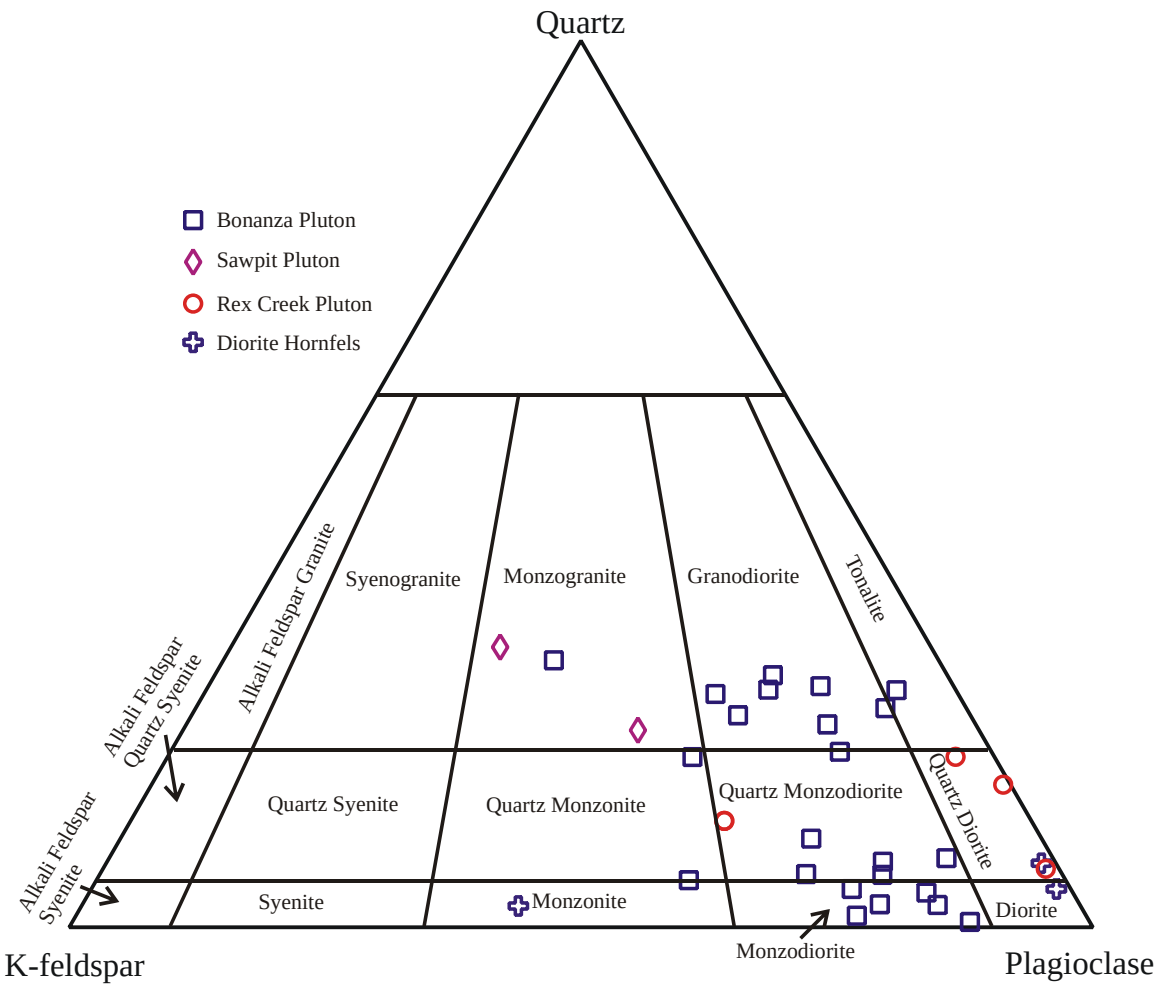

Figure 2.8: IUGS modal igneous classification scheme for igneous rocks. Estimated modal abundances from stained rock slabs containing at least 100 mineral grains. Figure after Strekheisen (1973). Data from this study.

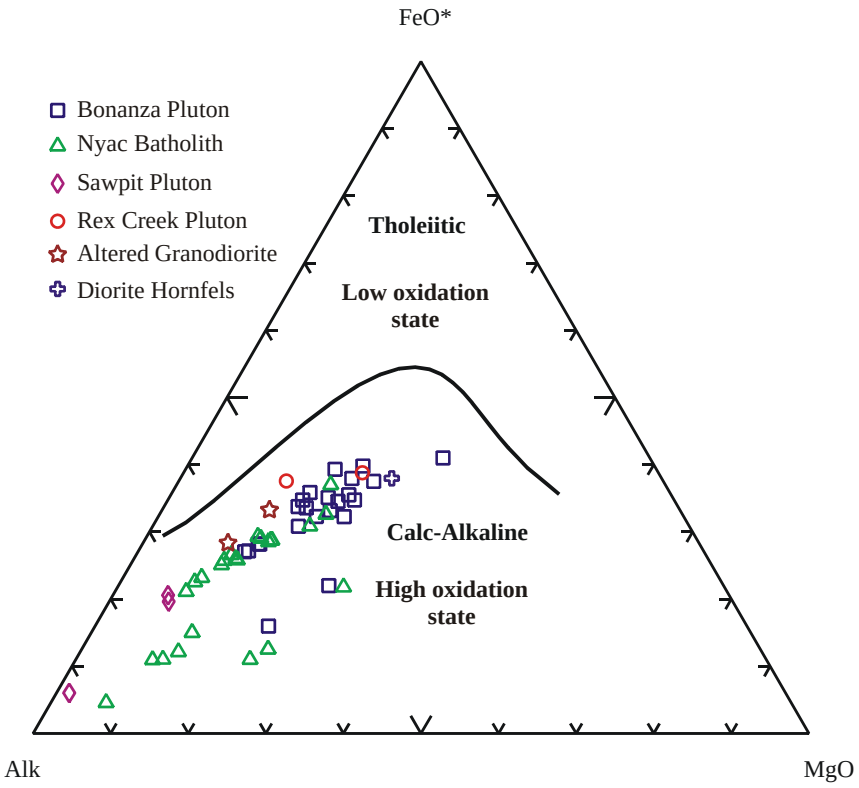

Figure 2.9: AFM classification diagram for the alkalinity of igneous rocks. Tholeiitic rocks have lower oxidation states than calc-alkaline rocks (FeO*= total Fe as Fe^{2+}, Alk= $Na_2O + K_2O$). Figure is modified after Irvine and Baragar (1971). Data are from this study, Gierymski and Werdon (1997), J. Foley, written comm. (2004), and T. P. Frost, written comm. (2004).

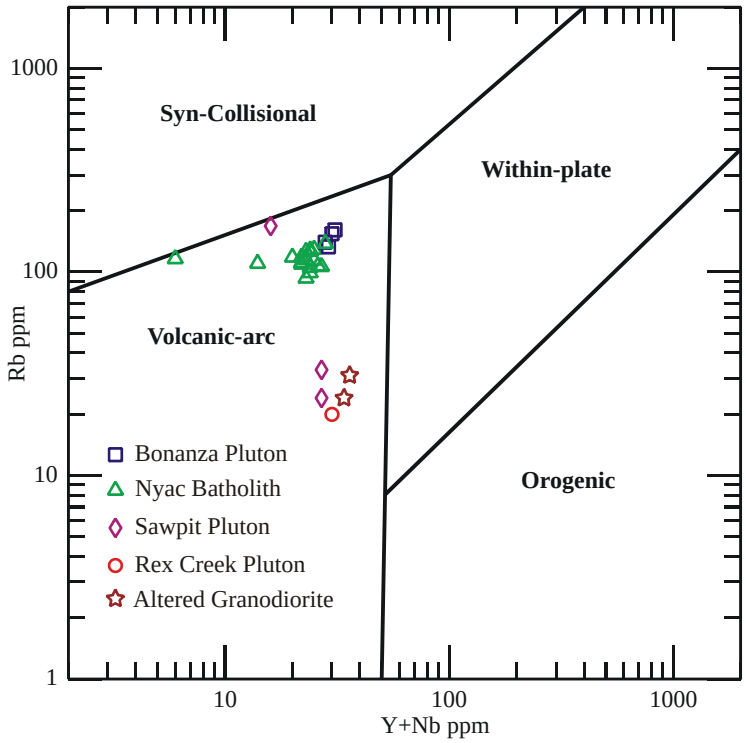

Figure 2.10: Trace element origin classification for felsic to intermediate plutonic rocks. Data are from this study; Gierymski and Werdon (1997), J. Foley, written comm. (2004) and T. P. Frost, written comm. (2004). Figure after Pearce et al. (1984).

medium-grained, generally equigranular, quartz monzodiorite to quartz-diorite and granodiorite body (Figure 2.7a and 2.8). Based on limited exposures, no compositional zoning is seen, but the variation of rock composition suggests that zoning does occur. The pluton displays pervasive epidote-chlorite-calcite-sericite alteration. Epidote veins (1- 20mm wide) comprise <1% of the rock volume, but some areas contain up to 5% veining. Much larger (5-15 cm wide) epidote-magnetite veins are rare. Measured magnetic susceptibilities range from 0.3 to 25.03. The variation is presumably the result of different degrees of magnetite formation during alteration as well as variation in original rock composition (more magnetite present in more mafic rocks).

In thin section, all the original mafic minerals (~ 15-20% of the original volume) are replaced by a combination of epidote, chlorite, calcite, magnetite ± rutile ± pyrite. Evidence of the original mafic mineralogy appears as epidote-chlorite pseudomorphs after hornblende. Plagioclase is 30-80% altered to a combination of epidote + sericite + calcite and minor chlorite. Less altered plagioclase crystals display albite twinning and some are concentrically zoned. K-feldspar crystals are relatively unaffected by the alteration. Trace amounts of apatite and zircon are visible in the feldspars and altered mafics.

2.3.2 Altered Granodiorite

The altered granodiorite, located east of the Rex Creek Pluton, is an inferred 1.5 km^2 body. It is a gray-green, medium to coarse-grained, equigranular granodiorite (Figure 2.7a). All the mafics have been altered to a combination of chlorite and epidote. The top of the body is an intrusive breccia intruded by sericitically altered felsic porphyry dikes.

In thin section all the mafic minerals have been entirely replaced by a combination of epidote, chlorite and calcite. The original mafic minerals constitute approximately 12% of the rock volume. The feldspars are 20-80% replaced by a combination of epidote and sericite. Accessory minerals include apatite and zircon. Chemically, the rock is a granodiorite with a relatively small LOI, indicating that epidote (low water content) is the principal alteration mineral. However, considering the degree of alteration, the original rock composition is uncertain.

The altered dikes in the intrusive breccia have yttrium and niobium concentrations similar to those of the altered granodiorite, but the dikes are slightly more enriched in zirconium. This indicates the altered dikes are likely derived from the altered granodiorite. Similar composition, trace element chemistry, fractionation trends and similar alteration style suggest the altered granodiorite may be part of the Rex Creek pluton.

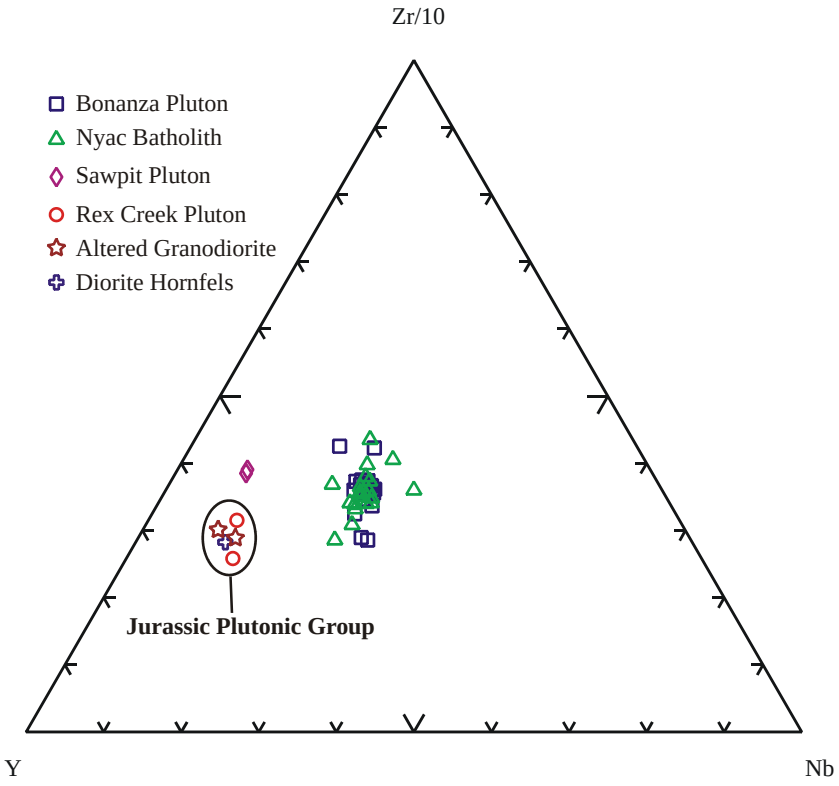

Figure 2.11: Triangular trace element plutonic discrimination diagram for all plutonic rocks. Data are from this study, Gierymski and Werdon (1997), and T. P. Frost, written comm. (2004).

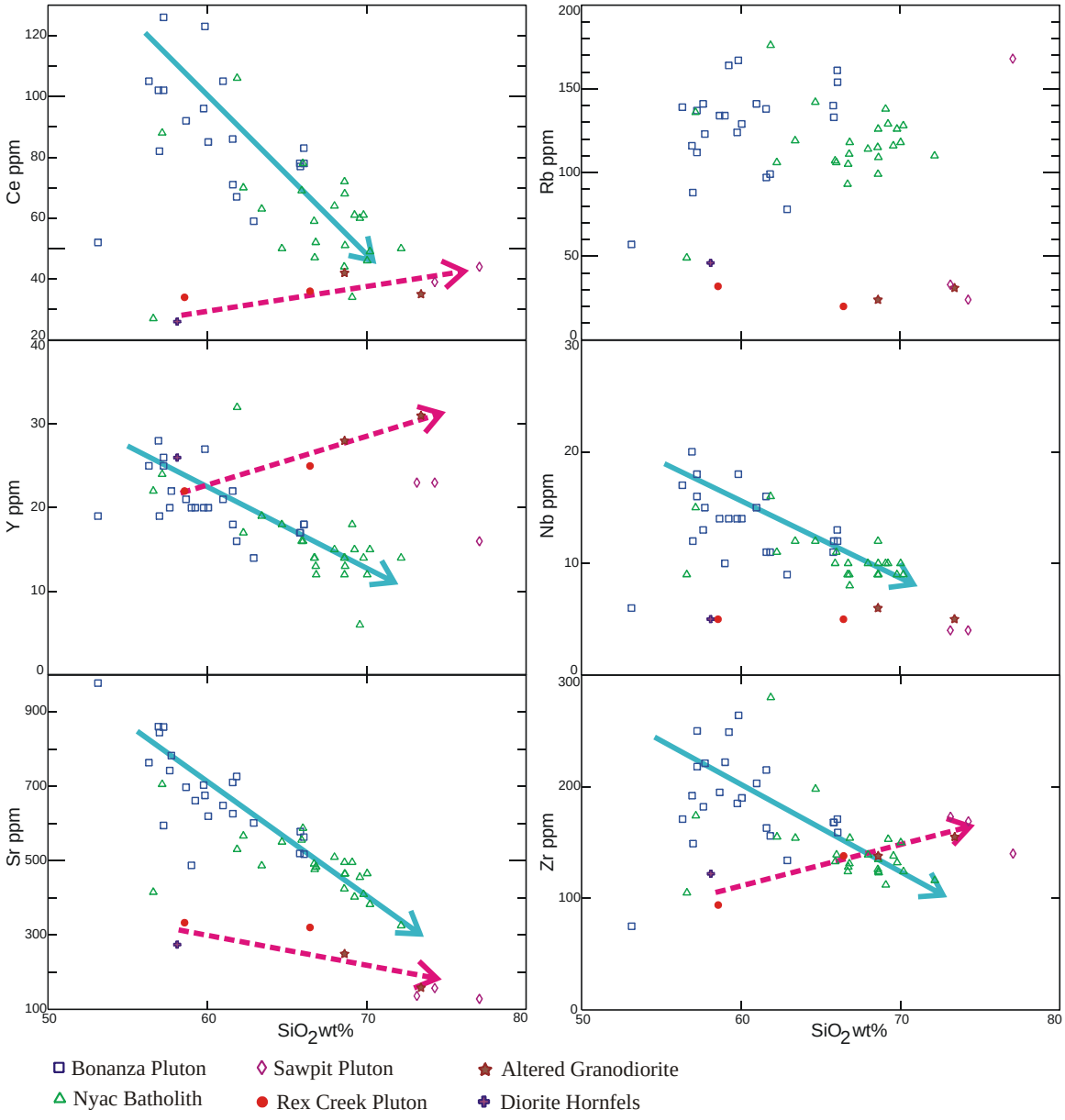

Figure 2.12: Trace element discrimination diagrams for plutonic rocks. Arrows indicate the fractionation trend with increasing silica content. The solid arrow indicates the trend direction for the Nyac Batholith and Bonanza Plutons and the dashed arrow indicates the trend for the Jurassic (?) Plutonic Rocks. Data are from this study, Gierymski and Werdon (1997), J. Foley, written comm. (2004) and T. P. Frost, written comm. (2004).

2.3.3 Diorite Hornfels

The diorite hornfels occurs sporadically in the metasedimentary rock unit (Figure 2.1). It probably is a series of sills and small intrusive bodies, most likely related to Jurassic volcanism. The largest body is located along the metasedimentary contact with the Nyac Batholith. The hornfelsed diorite contains 40-60% plagioclase and 40-60% hornblende and pyroxene (pyroxene is less abundant than hornblende). The plagioclase has a characteristic gray-blue color. The hornblende and pyroxene are partially altered to chlorite and epidote.

In thin section the diorite hornfels does not display epidote-chlorite-calcite-sericite alteration. Instead, the mafics are entirely recrystallized into fine-grained, randomly oriented masses of biotite and hornblende. The plagioclase crystals contain hornblende inclusions. It is unclear whether some plagioclase crystals originally enclosed the hornblende or if this texture is the result of thermal metamorphism. The biotites are light brown, 1-3 mm euhedral grains that form as aggregate masses. The hornblende crystals are green to green-blue, 1-2 x 3-8 mm and elongate with a sub-acicular habit. Within these mafic masses are rare sphene and opaque minerals (presumably magnetite based on crystal shape). This hornfels texture is the best evidence in the study area for pre-Cretaceous plutonism.

2.3.4 Gabbro

Gabbro occurs in two areas on the map. A large body (approximately 2 km^2) is located in the eastern center of the map and a much smaller body is near the Rex Creek Pluton (Figure 2.1). The relationship between these two occurrences is unclear. The largest body is dark green (mafic minerals) and white (plagioclase), coarse-grained and equigranular, approximately 50% plagioclase and 50% pyroxene with zones of up to 60-70% plagioclase. The gabbro also contains few fine-grained mafic enclaves of clinopyroxenite. The gabbro body near Rex Creek pluton appears to intrude the metavolcanic rocks. It is unclear whether this body is associated with the Rex Creek pluton or the large gabbroic body. The small body is dark green and grey in color consisting of 30-40% plagioclase and 70-60% pyroxene.

2.4 Early Cretaceous Plutonic Rocks

The Cretaceous plutonic rocks include: the Nyac batholith, Bonanza pluton, Sawpit pluton, gray dikes and red dikes. Except for the Sawpit pluton, each unit is dated as Early Cretaceous (discussed in Chapter 4). I have grouped the Sawpit Pluton with the Early Cretaceous plutonic rocks because there is no evidence that the Sawpit Pluton cuts any of the Early Cretaceous rocks, it appears to intrude the Rex Creek Pluton (Figure 2.1) and Maddren (1915) reports diabase dikes cut it.

In addition to composition, textures and mineralogy, another factor that can be used to discriminate between igneous bodies is their emplacement depth. The minimum melting

point/crystallization temperature and composition of granite under water saturated conditions is fixed by pressure, so aplite compositions can be used to estimate pressure of crystallization. If the aplite has low calcium concentrations (< 1 wt% CaO), was crystallized under water saturated conditions, and represents the end product of magmatic fractionation, the normative quartz-orthoclase-albite values are a function of pressure (Tuttle and Bowen, 1958). Figure 2.13 shows normative data for the Nyac batholith and Bonanza pluton aplites projected onto the granite ternary diagram. The Nyac batholith aplites plot on the experimental curve at ~1.25 kb (9TF003). A second sample (9TF028B) plots to the right of this value and below the curve. Projecting this value onto the curve yields a pressure of ~1 kb. The third Nyac Batholith value (03ZW357C) plots at the end of the curve near 0.5 kb. This sample displays sericitic alteration and hence the composition does not represent the true pressure. Since one value (9TF003) plots on the expected curve at ~1.25 kb this is the best estimate for the crystallization pressure of the Nyac batholith and represents a depth of ~3 km.

Two samples from Bonanza pluton (8TF036 and 03ZW374B) plot off the experimental curve. Sample 8TF036 is enriched in CaO and therefore does not plot accurately on this projection. Sample 03ZW374B is ~1-3% sericite-chorite-carbonate altered and therefore does not represent the true original composition. Compensation for the alteration effect was calculated by estimating K_2O enrichment and Na_2O depletion in the sample. This calculation yields normative values that plot closer to the experimental curve (Figure 2.13); the crystallization pressure is low, but uncertain. Considering the textures (subporphyritic) in the pluton and the ambiguous aplite compositions, it is reasonable to estimate a pressure of ~0.5 kb or 1.5 km depth for the crystallization of Bonanza pluton.

Despite spatial and compositional variation in Bonanza pluton, trace-element chemistry and age data (discussed in Chapter: 4) indicate that the Bonanza pluton at the three different locations (VABM Bonanza, Spruce and Bonanaza Creek lobes; Figure 2.1) are parts of a single body. Trace element chemistry from Bonanza pluton and the Nyac batholith show a clear pattern of trace element enrichment with decreasing silica content for cerium, yttrium, strontium, niobium and zirconium (Figure 2.12).

2.4.1 Nyac Batholith

The Nyac batholith is located in the northwest corner of the study area (Figure 2.1). The batholith is an approximately 200 km^2 (Box et. al, 1993), elliptical body elongate parallel to the Golden Gate-Sawpit fault. The portion of the batholith that lies in the study area is small, but samples from outside of the map area were collected for comparison to other plutonic rocks.

The Nyac batholith appears to be zoned, with a tonalite and monzodiorite rim grading into a granodiorite center. The batholith is generally equigranular and coarse-grained (locally seriate or porphyritic) with medium and fine-grained textures near the rim. Where porphyritic, the phenocrysts are 1-3 cm K-feldspar. The batholith is cut by numerous aplite dikes and rare medium-grained dikes

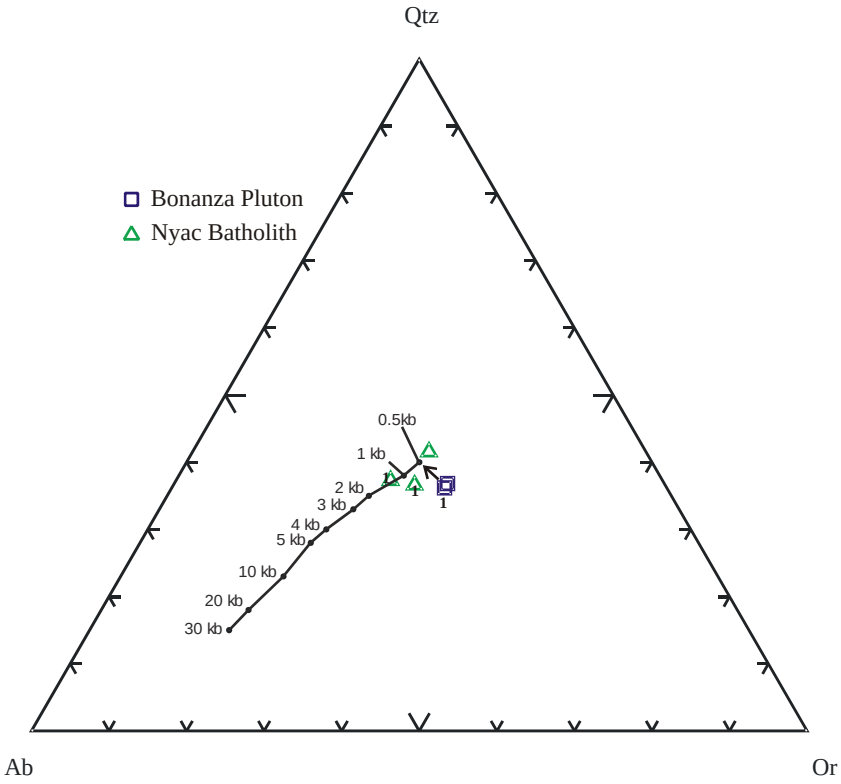

Figure 2.13: Aplite compositional geobarometry for the albite-quartz-orthoclase-H_20 system. Arrow points towards the most likely formation pressure for the Bonanza Pluton at ~0.5 kb equivalent to ~1.5 km depth. Experimental data from Tuttle and Bowen (1958), Steiner et al. (1975), Luth et al. (1964) and Huang and Wyllie (1975). Aplite data is from this study and (1) T. P. Frost, written comm. (2004).

(03ZW357B) similar in composition to the batholith cut the batholith. The medium-grained dikes have slightly more K-feldspar than the granodiorite portions of the batholith they intrude.

In thin section the Nyac batholith displays common plutonic characteristics including randomly oriented, coarse, equigranular crystal grains and concentric zoning of plagioclase. The orthoclase crystals display weak perthitic texture and Carlsbad twinning. Plagioclase crystals display both polysynthetic and Carlsbad twins. Plagioclase anorthite contents range from 23 to 27%. Plagioclase crystals contain 2-5% sericite. In contrast, K-feldspar contains 0-<1% sericite. Samples displaying the most intense sericitization also have intergranular euhedral quartz. Granodiorite portions of the Nyac batholith contain 10-15% mafic minerals with sub-equal biotite and hornblende. Biotite and hornblende are slightly altered along their margins to chlorite; some biotites display up to 5% chloritization. Accessory minerals include allanite, apatite, sphene, and zircon.

2.4.2 Bonanza Pluton

Bonanza pluton is centered on VABM Bonanza peak and extends southeast towards Spruce Creek. A small portion of the pluton is exposed on a ridge north of the main body (Figure 2.1). Bonanza Pluton is dominantly granodiorite with local quartz monzonite and monzonite portions and marginal diorite, quartz diorite, tonalite and monzodiorite (Figures 2.7a and 2.8). The body is typically medium-grained (fine-grained at margins) with central areas exhibiting sub-porphyritic textures. The majority of the Bonanza pluton has lower magnetic susceptibilities than the Nyac Batholith. The higher magnetic susceptibility values for Bonanza pluton are from the mafic (monzodiorite and tonalite) margins of the pluton, which presumably contains more magnetite. Aplite dikes are abundant in portions of the pluton, some are as wide as 10 cm.

In thin section, the Bonanza pluton displays common plutonic characteristics such as, randomly oriented crystal grains and concentrically zoned plagioclase. Orthoclase crystals exhibit Carlsbad twins and microperthitic textures. Plagioclase crystals display both polysynthetic and Carlsbad twins and minor myrmekite. Plagioclase anorthite content ranges from 23 to 40%. The higher anorthite contents are from the more mafic part of the pluton (diorite, quartz-diorite). Sericitic alteration is pervasive. Both feldspars are 5-15% sericitically altered; the plagioclase is more altered than the K-feldspar.

The pluton contains 10-25% mafic minerals. Mafic minerals commonly include biotite and hornblende; minor amounts of pyroxene are also present. A straightforward crystallization order is seen in the granodiorite portion of the pluton where pyroxene grains are entirely enclosed by hornblende rims. The hornblende rim in turn is partially rimmed by biotite, indicating a crystallization order of pyroxene-hornblende-biotite.

The crystallization sequence of the mafic minerals in the monzodiorite portions of the pluton is different. In monzodiorite, pyroxene contains biotite inclusions. The pyroxene is similarly rimmed with

hornblende, but the hornblende rarely entirely encloses pyroxene. Hornblende crystals also occur by themselves, with no pyroxene attached.

The mafic portions of the pluton contain up to 1% apatite. All the rocks contain zircon, but the more mafic varieties have approximately twice as much. Granodiorite portions of pluton contain less apatite and zircon and have trace amounts of sphene. The presence of pyroxene in the pluton indicates that at least initially the pluton had a low water content. All mafics are partially chloritized. Samples displaying the most intense feldspar sericitization also have the most chloritization.

2.4.3 Sawpit Pluton

The Sawpit pluton consists of multiple exposures, all of which lie near or within the Golden Gate-Sawpit fault zone in the study area. The Sawpit pluton lies outside the study area as well and covers approximately 35 km^2 in its entirety (Box et al., 1993). The pluton is a seriate to coarse-grained biotite granite (Figure 2.7a). Portions of the pluton have miarolitic texture. The cavities are filled with chlorite and epidote or quartz. Veinlets of epidote and chlorite 1-3 mm in width cut the pluton, which locally contain pyrite. The pluton has lower average magnetic susceptibility than either the Nyac batholith or the Bonanza pluton (Table 2.1).

In thin section, orthoclase and rare plagioclase are sericitically altered (5-10%). All the mafics are entirely altered to a combination of chlorite (75%), epidote (20%), sphene and magnetite (5%). The feldspars are euheral to subhedral and enclosed by larger optically continuous anhedral quartz crystals. Accessory minerals include apatite, zircon and sphene.

2.4.4 Gray Dikes

The gray dikes are a granodiorite porphyry characterized by their gray color and porphyritic texture. These dikes intrude both the metasedimentary and metavolcanic rocks. The dikes are typically 1-5 meters wide and occur in greatest abundance northwest of the Bonanza pluton (Figure 2.1). The dikes are feldspar-biotite-hornblende-quartz porphyritic and have a gray aphanitic groundmass. The composition is dominantly granodiorite although tonalitic and monzodioritic varieties are also found (Figure 2.7b). Despite compositional variation, the feldspar-biotite-quartz porphyry texture is consistent. Rare (<1% of the rock volume) 5-mm-to 1-cm-sized, amoeba-shaped mafic inclusions occur in some of the dikes. The mafic inclusions consist of fine-grained plagioclase and mafic minerals (pyroxene and hornblende?).

In thin section, phenocrysts include plagioclase (2-15 mm, 10-30%), hornblende (2x1 to 10x3 mm, 1-3%), biotite (1x8 to 4x10 mm, 1-5%), resorbed quartz with groundmass inclusions (2-10 mm, 1-3%) and K-feldspar (5-15 mm, 0-1%) with inclusions of hornblende and biotite. Hornblende and biotite are variably (0-10%) altered to chlorite. The groundmass consists of feldspar and quartz grains both <1 mm in size. Anorthite content of the plagioclase phenocrysts is 27-29%.

2.4.5 Red Dike

Red dikes are quartz monzonite porphyry dikes were seen only as rubble, not in outcrop. Red dike rubble is most abundant on the talus slope north of the limonite-stained metavolcanic rocks (Figure 2.1). The dikes are a biotite-feldspar porphyry with a red fine-grained groundmass. The majority of these dikes are intensely sericite-kaolinite altered. In altered varieties phenocrysts are entirely altered to muscovite, and limonite-sericite lined vugs account for 5-10% of the rock volume.

In thin section, phenocrysts include plagioclase (1-5 mm, 1-3%), K-feldspar (1-3 mm, 1%) and biotite (1-2 mm, 1-2%). Plagioclase is albitically twinned and sometimes concentrically zoned. Plagioclase phenocrysts have anorthite contents of 26-35%. Some K-feldspar crystals display Carlsbad twining. The groundmass is a mixture of <1 mm feldspars, biotite, opaque minerals and minor quartz. Accessory minerals include apatite and zircon. Least altered varieties display weak chlorite alteration of biotite phenocrysts and ~1% sericitic alteration of feldspars. Strongly altered varieties display muscovite rimming vugs and biotite and feldspar phenocrysts entirely altered to muscovite and kaolinite. Complete loss of Ca, Na, Fe and Mg from conversion of the groundmass into sericite, kaolinite and quartz results in the volume loss (vugs).

Trace element analysis indicates altered and unaltered varieties are much more enriched in a variety of elements than the rest of the dikes and plutons (Figure 2.14).

2.5 Tertiary (?) Dikes

The Tertiary (?) dikes are of uncertain age. They include the mafic and pink dikes. Each of these dikes cut the Bonanza pluton, so they are at least younger than that body. Also categorized in this group are some undifferentiated dikes. These dikes include a variety of different textures and compositions and are common in the district. They may represent previously classified dikes, but textural differences and variable compositions make it difficult to categorize these dikes.

2.5.1 Mafic Dikes

Mafic dikes are located in the Bear Creek valley (Maddren, 1915) and on the ridge immediately west of Spruce Creek. Mafic dikes are black, diabasic textured gabbro. A single mafic dike was found at only one location cutting the Bonanza Pluton at Spruce Creek (Figure 2.1).

In thin section the mafic dike is composed of 70% plagioclase (0.1-1 mm), 5% pyroxene (0.1-1.5 mm) and 25% alteration and vesicles. The plagioclase crystals are albitically twinned and weakly (1-5%) altered to sericite. The pyroxenes are concentrically zoned and weakly altered to clinozoisite and chlorite around their rims. The remaining rock is an alteration assemblage of oxy-chlorite, chlorite, biotite, clinozoisite and quartz. This peculiar assemblage is presumably the result of glass recrystallization, because

basaltic glass and this assemblage have roughly equivalent composition. Clinozoisite also rims open cavities.

The mafic dike has trace element signature of continental basalt, suggesting they formed during an extensional event (Figure 2.4).

2.5.2 Pink Dikes

The pink dikes are a granodiorite porphyry found throughout the study area. The dikes are generally 1-5 meters wide and intrude the Bonanza pluton (Figure 2.1). The dikes are feldspar-biotite-hornblende-quartz porphyry with a pink aphanitic groundmass. Pink dikes are dominantly granodiorite in composition, but monzogranite and syenogranite varieties exist (Figure 2.7b).

In thin section, phenocrysts include plagioclase (2x3 to 4x6 mm, 10-20%), biotite (1x2 to 3x3, 2-5%), hornblende (1x2 to 4x8, 1-3%) and resorbed quartz (1-5 mm, 0-7%). The groundmass is a fine-grained mixture of similar composition which presumably contains some K-feldspar. Despite a relatively unaltered appearance in hand specimen, upon petrographic inspection it is evident that these dikes are strongly altered. Feldspar phenocrysts are altered to a combination of equal parts sericite and calcite with minor chlorite. Hornblendes are altered to a combination of chlorite (70%), calcite (25%), and opaque minerals (5%). Calcite commonly replaces the center of the crystal. Biotites are altered to a combination of chlorite (50%), muscovite (40%), calcite (10%) and trace sphene and opaque minerals (<1%). The groundmass is similarly altered. It is unclear how much of the sphene and opaque minerals are primary.

2.5.3 Undifferentiated Dikes

A considerable number of low volume dikes that were not identified enough to be included on the geologic map occur in the field area. Analyzed samples have variable compositions (Figure 2.7a) and textures. Some of these dikes may be Jurassic while others could be related to Early Cretaceous or Tertiary magmatism.

2.6 Regional Geophysics and Structural Geology

In 1994 the Alaska Division of Geological and Geophysical Surveys published a regional magnetic map (ADGGS et al., 1994) of the Nyac area. The flight lines were spaced at quarter-mile intervals with a NW-SE orientation. The magnetic map is useful for identifying the large-scale faults and approximating some lithologic contacts in areas of poor exposure. Mapping in the area is difficult due to limited exposure (outcrops areconstrained mainly to ridges) and limited geophysics (no resistivity maps are available). Without resistivity data it is difficult to determine the number and orientation of faults in the.

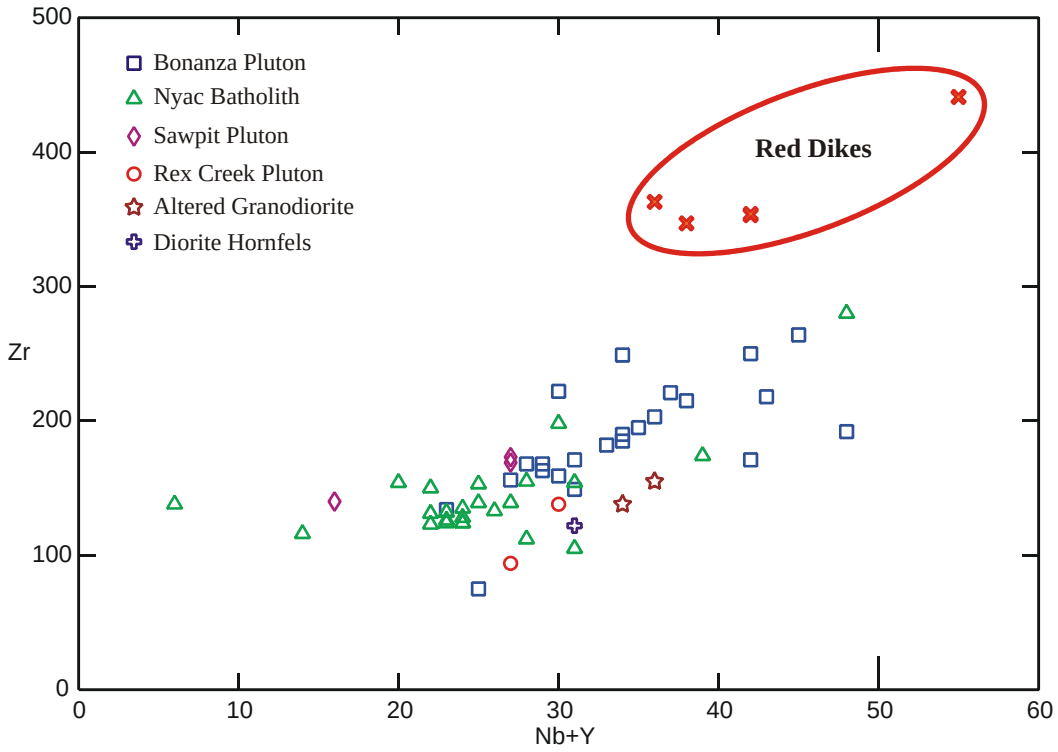

Figure 2.14: Trace element discrimination diagram for plutonic bodies and red dikes. Data are from this study, Gierymski and Werdon (1997), and T. P. Frost, written comm. (2004).

study area. An area so close to the Golden Gate-Sawpit will potentially contain a significant number of subsidiary faults, which could have significant displacement. Many small faults cut the ridges in the study area, but their orientation is difficult to interpret without resistivity data, especially the smaller scale structures that could be locally important in interpreting the stratigraphy

Magnetic susceptibilities vary considerably within and between units (Table 2.1, Figure 2.15). Since no geologic unit has a unique magnetic susceptibility, using the magnetic map to interpret lithologic units in areas of no exposure is problematic. Figure 2.16 shows that magnetic susceptibilities measured on surface samples generally correlate with the magnetic map. This indicates that where the magnetic susceptibilities measured at the surface coincide with magnetic intensity the exposed rock continues at depth or no drastic changes in magnetic character occur. The only obvious rock unit that matches a magnetic signature is the Rex Creek pluton. The body is a magnetic high in surrounding magnetic lows (Figure 2.16). The metasedimentary rocks display an average low magnetic signature except where in contact with the Nyac batholith (Figure 2.16). The high magnetic signature there is probably due to thermal metamorphism (producing secondary magnetite) and an apparent SE dip to the batholith.

Southeast and east of the metasedimentary rocks are the metavolcanic rocks. This unit displays a generally higher magnetic signature than the metasedimentary rocks. Included in the metavolcanic package are areas dominantly composed of metabasalt (>70 of the rock volume). These metabasalt rich areas have average higher magnetic susceptibilities than the other metavolcanic rocks and are easily identifiable on the magnetic map (Figure 2.16). However, their exposure is never seen as a continuous stratigraphic layer in the study area. This is due largely to no exposure in the Bear Creek Valley and possible significant displacment on unidentified faults. If there was exposure in the Bear Creek Valley the magnetic highs seen there may correlate with the metabasaltic unit and would suggest that the metabasalts represent a stratigraphic layer and are likely the lowest and oldest rocks in the study area.

Despite significant surface exposure, the Bonanza pluton displays no unique magnetic anomaly (Figure 2.16). Magnetic susceptibilities taken from the surface span a range of 0.14-30.83 $x10^{-3}$ SI (Table 2.1). Since significant compositional variations exist at different locations in Bonanza pluton and mineralization is focused in two areas, a naming scheme will be used to divide the Bonanza pluton into three different lobes. Thee lobes are, VABM Bonanza lobe (near VABM Bonanza Peak), Spruce Creek lobe and Bonanza Creek lobe (Figure 2.16). The Bonanza pluton appears to be displaced along high angle, north-south faults. Carbonate fault breccia located between the Spruce Creek lobe and VABM Bonanza lobe (Figure 2.1) suggests there is a fault between these two bodies, although the azimuthal orientation is unclear. Recent unroofing is evident at the Spruce lobe where a small metavolcanic raft lies on top of the pluton (Figure 2.1) indicating that this lobe was down-dropped relative to VABM Bonanza lobe. The Bonanza Creek lobe is left laterally displaced north approximately three miles from the Spruce Creek lobe.

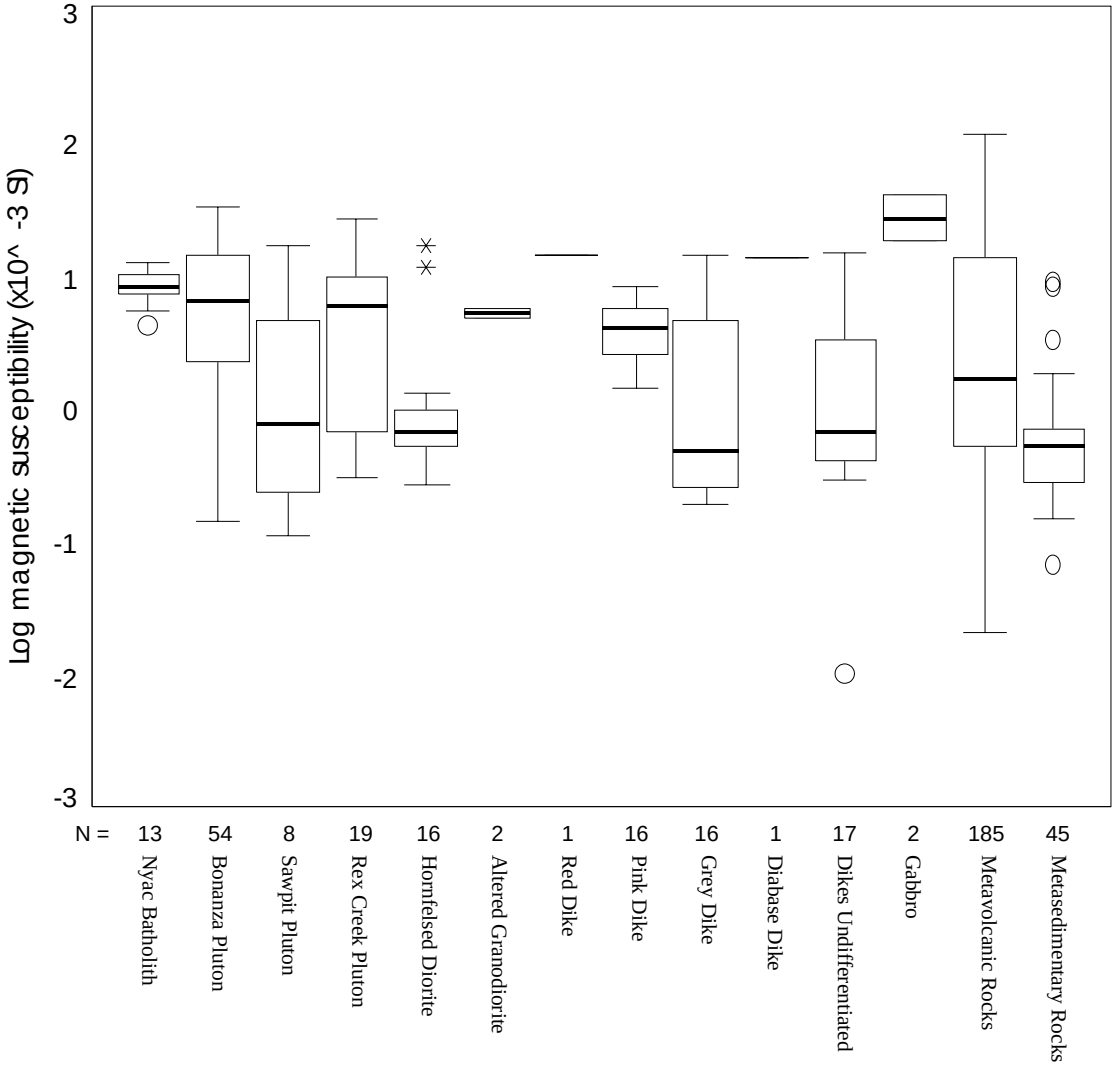

Figure 2.15: Boxplot of the magnetic susceptibilities for the rock units in the study area. Bold lines represent median values and the circles and asterisks represent outside and far outside values, respectively. Data from this study.

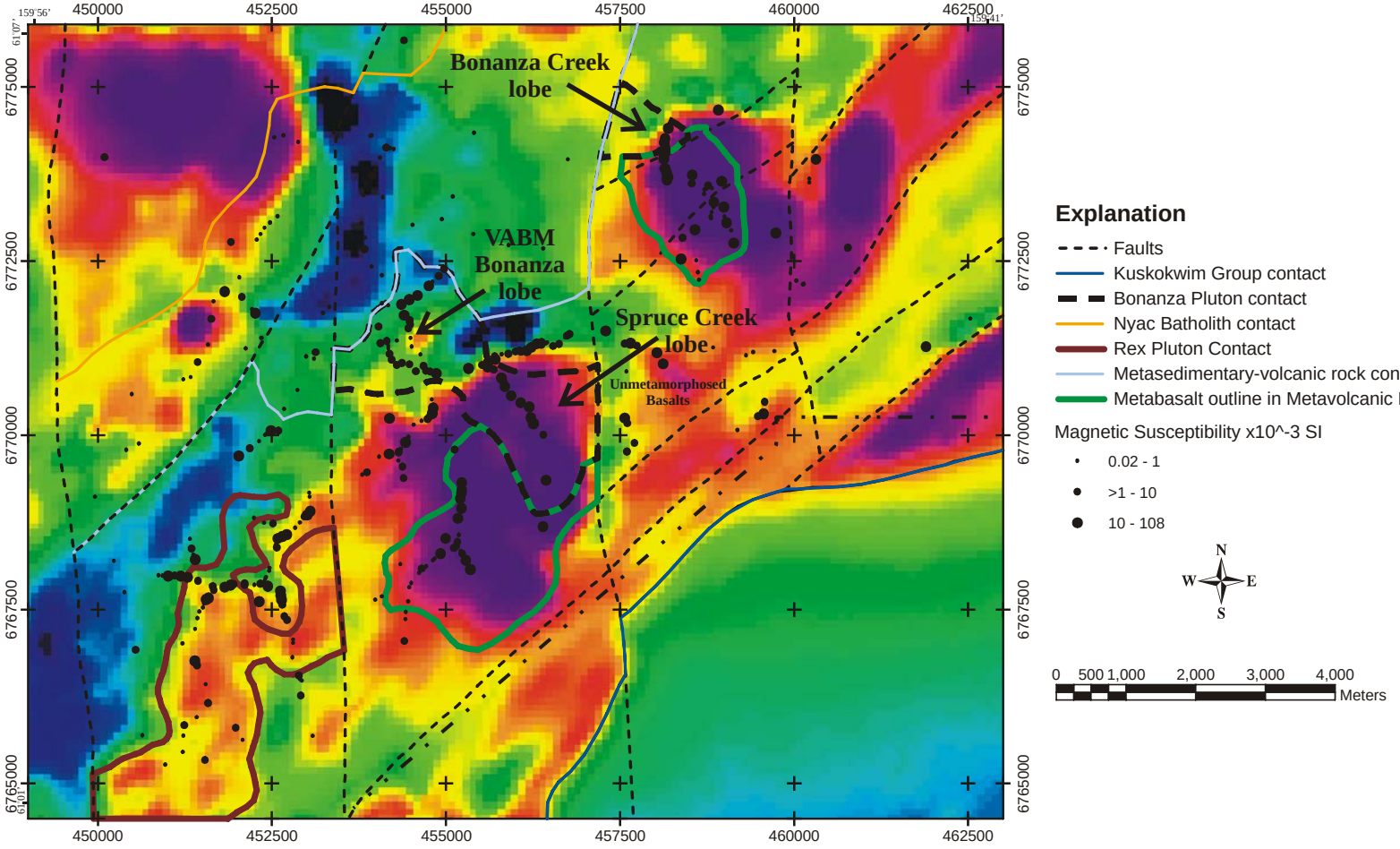

Figure 2.16: Aero-magnetic map of the study area with some ground-based geologic contacts. Map shows the three lobes of the Bonaza Pluton. The red and purple correspond to 54,800-54,500 nT, yellow 54,500-54,480 nT, green 54,480-54,300 nT, and blue 54,300- 54,225 nT. Magnetic data from ADGGS staff et al. (1994).

The Spruce and Bonanza Creek lobes are more mafic in composition and likely represent the near contact surface of the pluton.

The sub-parallel alignment of the Nyac Batholith with the Golden Gate-Sawpit Fault suggests that the batholith occupies an old fault parallel to the Golden Gate-Sawpit Fault. No evidence of crystal deformation was found in the batholith, indicating that its shape is not the result of syn-magmatic deformation. The other possibility for this orientation is brittle deformation of the body by NE-SW trending faults. Detailed mapping of the batholith contact might indicate why the batholith has this orientation.

The faults on the magnetic maps appear as linear magnetic lows or obviously offset anomalous magnetic bodies. Along the contact of the Nyac terrane with the Kuskokwim Group rocks in the southeast part of the study area, a N-S trending fault obviously bisect the northeast trending Golden Gate-Sawpit Fault (Figure 2.16). The Golden Gate-Sawpit Fault must therefore predate the N-S faults.
Metabasalts north of Spruce Creek are the least thermally altered rocks in the study area. During intrusion of the Nyac batholith these rocks were presumably located further to the south and have been displaced left laterally along a north-south trending fault, the same fault that offsets Bonanza pluton (Figure 2.1). The thermal metamorphism effect is weakly imprinted on these rocks because they were presumably located further from the Nyac batholith.

3. Gold Mineralization

The Nyac district is a historically significant placer gold producer. Figure 3.1 shows all the drainages that have been placer mined. Placer mining and exploration are currently taking place on Bear and Shamrock Creeks (Figure 3.1). As of 2000, total placer gold production from the Nyac district is >500,000 oz (Foley, 2000). Placer gold is found in nearly all of the drainages in the study area, and it is important to determine the bedrock source for the gold in order to produce a model for local gold mineralization in the area. Over the years some bedrock gold occurrences have been identified in the district by intensive sample collection and chemical analyses. Over 2,500 rock and soil specimens from the study area have been analyzed for trace elements; however, other than plotting anomalous value locations nothing has been done with this large geochemical database.

Only broad generalizations regarding the styles of mineralization have been made for the Nyac district (RAA 1975, Gierymski and Werdon, 1997). This study uses statistical analysis techniques with the geochemical database to classify the different styles of mineralization. Classification of the styles of mineralization was augmented by field observations, petrographic techniques, fluid inclusion analyses, trace and major oxide data comparisons and microprobe techniques. Three areas were identified within the study area that host the most significant gold mineralizations: the Wallace Occurrence, VABM Bonanza lobe and the Bonanza Creek color anomaly (BCCA) (Figure 3.1). Figure 3.2 is a simplified geologic map showing the location and sample number for each important assay. This chapter focuses on characterizing the different types of alteration and mineralization at each of these locations and uses factor analysis to classify the different types of gold mineralization.

3.1 The Wallace Occurrence

USGS geologist Robert E. Wallace reported finding lode gold along the ridge at the confluence of the Tuluksak River and California Creek (Wallace, 1945; Figure 3.1). The ridge is covered by vegetation making it difficult to find any exposure. The location of the mineralization is only evident from a pile of rubble bull-dozed in the 1970's. Gold mineralization occurs in altered gray dikes. Exposed gold bearing rocks occur over an approximately 10x8 meter area.

The gold occurs in open-spaced quartz-chlorite-calcite veinlets 1 to 8 mm thick that extend for >20 cm (vein dimensions are limited by rubble size). The veining accounts for approximately 1 % of the rock volume. The vein material is approximately 75% quartz, 10% chlorite, 5% calcite and 10% cavities and ore minerals (Figure 3.3). Due to the weathered nature of the mineralized rock the amount of original calcite is uncertain (i.e., the open-spaces in the veins may have once been filled with calcite). The quartz

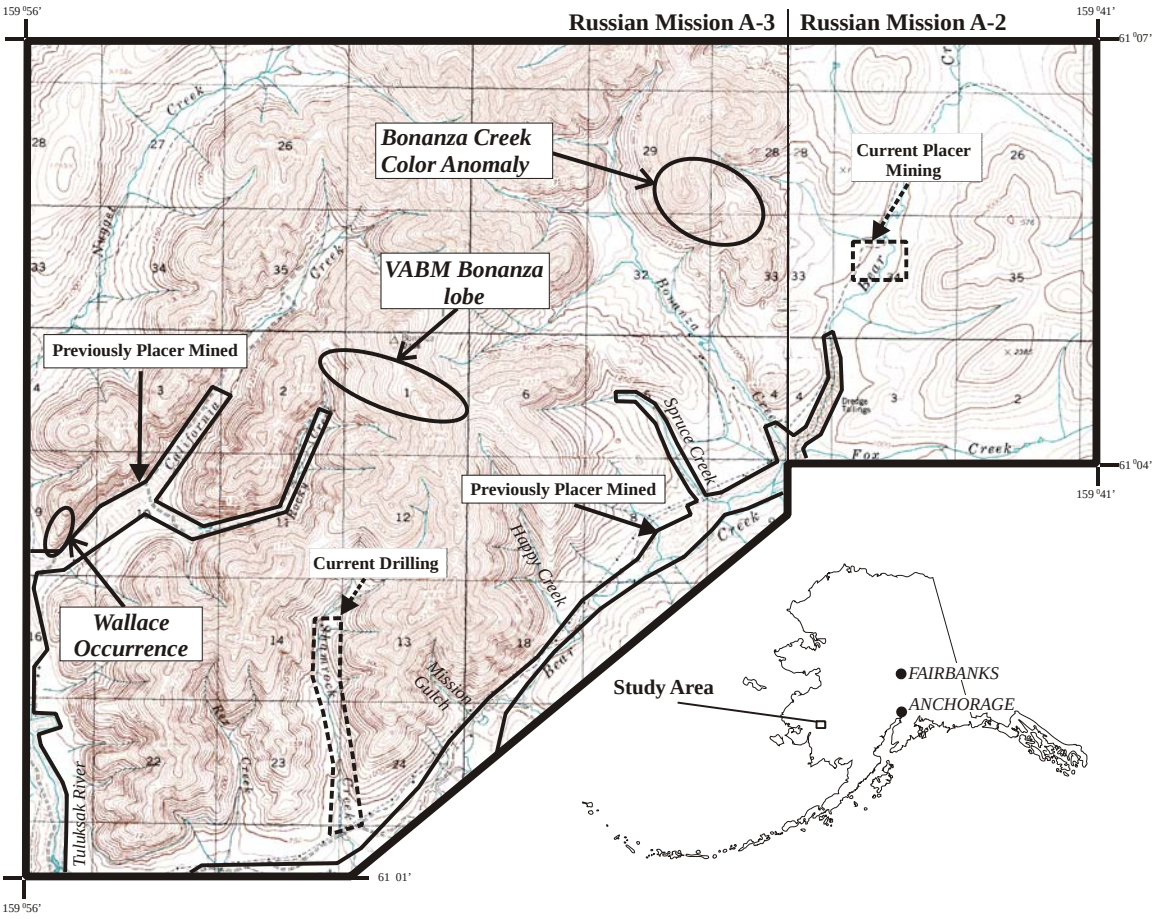

Figure 3.1: Topographic map showing historic and current placer mining locations. The three areas of most significant bedrock gold mineralization are also indicated.

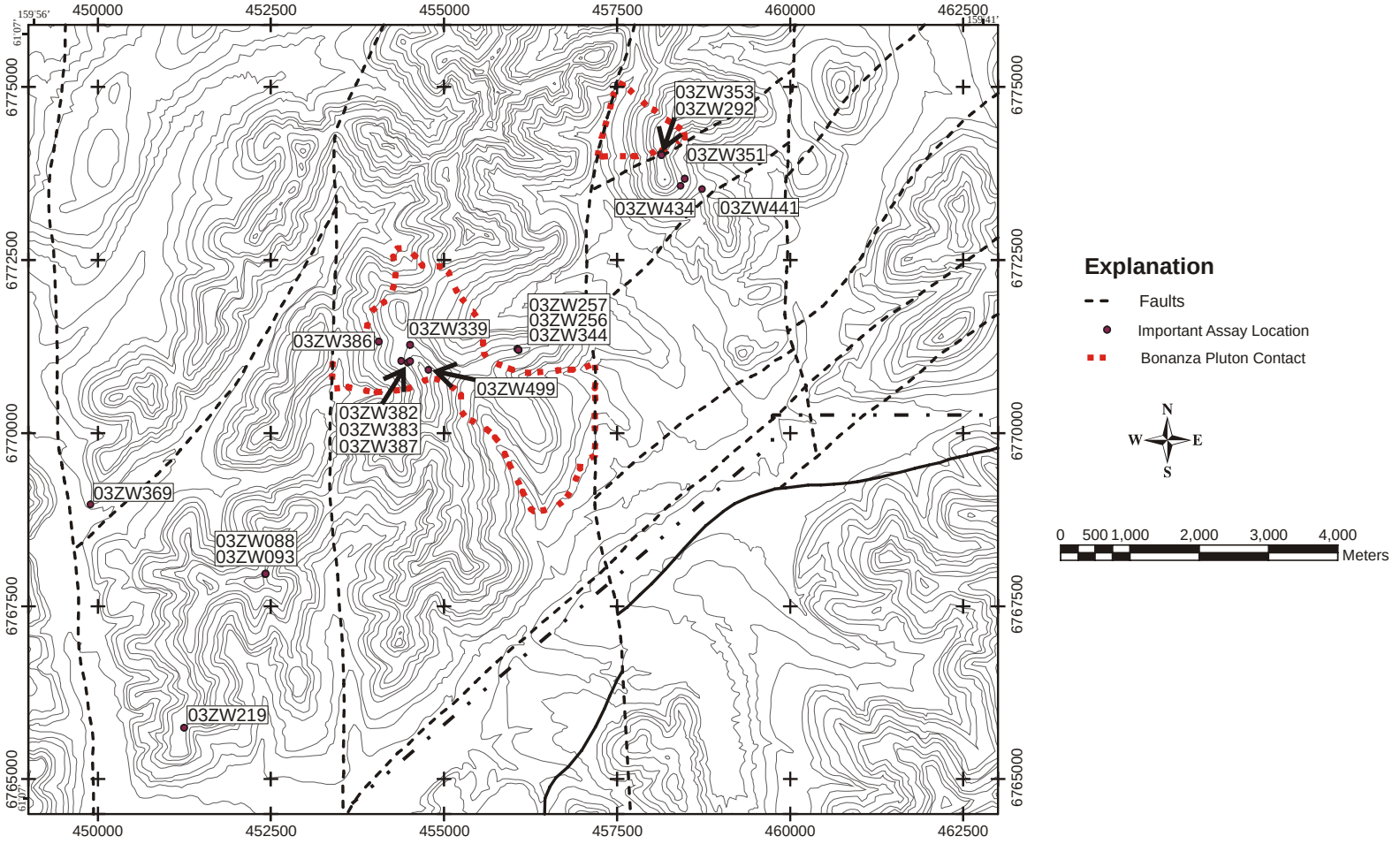

Figure 3.2: Map location and sample number for important assays from this study.

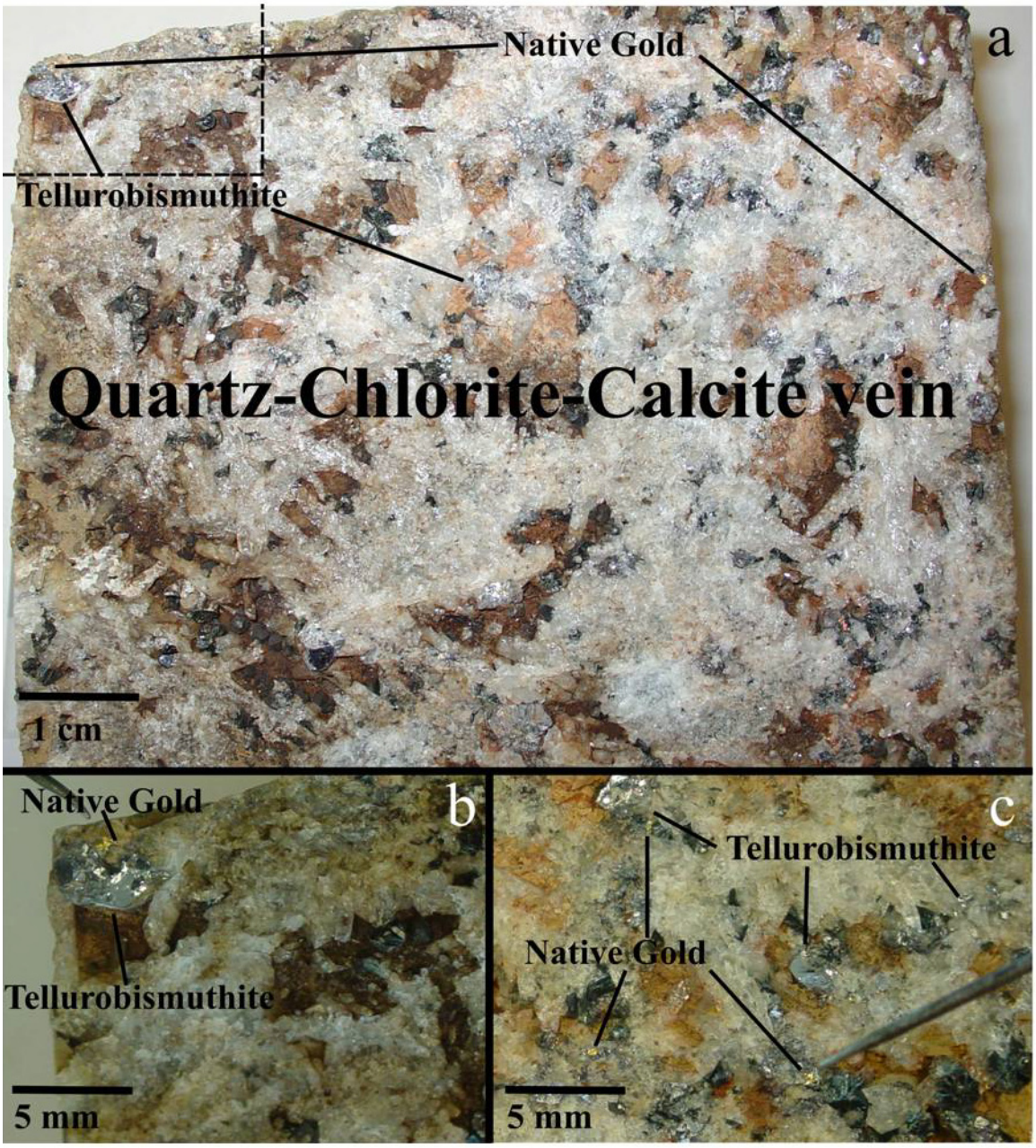

Figure 3.3: Quartz-chlorite-calcite veining and associated tellurobismuthite and native gold from the Wallace occurrence. Figure 3.3b is a higher magnification picture of the top right portion (dotted line) of figure 3.3a. Figure 3.3c is from a different vein.

crystals are euhedral and up to 6 mm wide. The quartz crystals often terminate on adjacent sides of the vein. The chlorite crystals are rosettes 1-6 mm in diameter. In thin section the chlorite is length fast and has anomalous purple blue interference colors indicating a high Fe content. There is no evidence indicating that the cavities in the veins were at one time filled, indicating low pressure during mineralization.

No alteration envelopes were observed adjacent to the quartz veins; instead, the dikes hosting gold-quartz veins are pervasively altered. Feldspar phenocrysts are 10-90% altered to sericite (15-85%), albite (5-15%) and chlorite (<1%). Hornblende phenocrysts are 75-100% altered to a combination of chlorite (85%), calcite (10%), magnetite (2-10%) and rutile (2-3%). Biotite phenocrysts are 90-100% altered to a combination of chlorite (75-80%), magnetite (5-20%) and rutile (2-3%). The groundmass of the dike is almost entirely altered to sericite (40%), albite (30%), quartz (20%) and chlorite (10%).

A standard means of assessing elemental changes during alteration processes is to model them based on Al_2O_3 immobility (Krauskopf and Bird, 1995). Table 3.1 shows composition of altered and unaltered gray dikes. Chemically the altered varieties have experienced CaO, Fe_2O_3, K_2O, MgO, MnO, Na_2O, P_2O_5, SiO_2, Ba and Sr loss and Rb gain. These findings are consistent with the mineralogical alteration. CaO, Fe_2O_3, K_2O, MgO, MnO, Ba and Sr are lost by the replacement of hornblende, biotite, plagioclase and K-feldspar by muscovite, chlorite, epidote and albite. Figure 3.4 shows stained versions of both altered and unaltered varieties of the grey dikes. The unaltered variety has a significant amount of K-feldspar while the altered version has no K-feldspar. The chemistry also reflects this alteration in that the unaltered variety has more K_2O than the less altered variety (Table 3.1) The altered variety has experienced significant CaO loss and relatively little Na_2O loss, so the feldspar in the groundmass must be largely albitic. The higher LOI values for the altered gray dike indicates the presence of CO_2 and water. Therefore the alteration at the Wallace occurrence is sericite-chlorite-carbonate-albite alteration.

Ore minerals identified by reflected light and microprobe analysis include (in order of descending abundance): tellurobismuthite, gold, tetradymite and minor chalcopyrite (Table 3.2). As indicated by microprobe analysis the tetradymite occurs as fine interlayers in the tellurobismuthite. Chalcopyrite was only identified in one slide and was a <1 mm diameter grain.

Table 3.1 Partial chemistry of three variably altered gray dikes from the Wallace occurrence.

Sample	Al_2O_3	CaO	Fe_2O_3	K_2O	MgO	MnO	Na_2O	P_2O_5	SiO_2	BA	RB	SR	LOI	alteration
03ZW474	15.6	3.5	4.67	2.92	1.66	0.09	3.44	0.18	65.2	1548	38	533	0.97	none
7SB020B	16.29	3.74	4.50	1.94	1.46	0.06	4.02	0.19	67.57	815	47	340	4.89	weak
03ZW369	15.94	1.99	4.01	2.11	0.98	0.05	3.89	0.20	70.28	712	53	347		strong
% change	0%	-44%	-16%	-29%	-42%	-43%	-11%	-8%	-5%	-55%	38%	-36%		

* Ba, Rb, Sr values are ppm; all other data are wt%. % change calculated from least altered (03ZW474) and most altered (03ZW369) assuming Al immobility. Data are from this study and T. P. Frost (written comm., 2004).

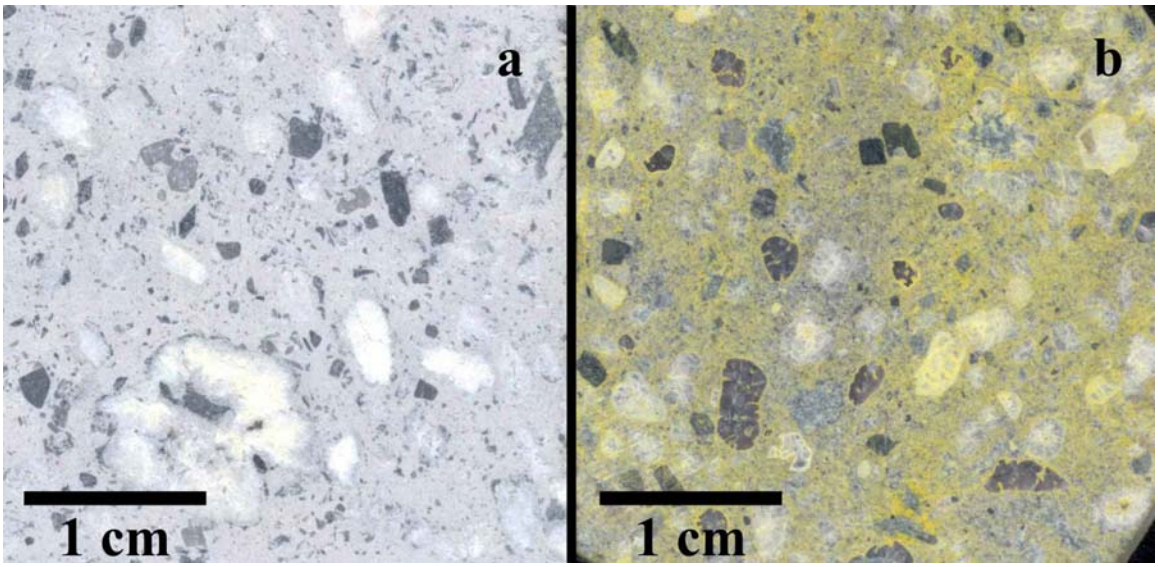

Figure 3.4: Stained gray dike samples from the Wallace occurrence. Figure 3.4a is from an intensely mineralized specimen and Figure 3.4b is from an unmineralized specimen.

Although there are limited data from the Wallace occurrence, mineralized gray dikes throughout the study area can be used to investigate the elemental correlations. Table 3.3 shows the highest correlations are for Sb-As (.736), Bi-Ag (.685), Cu-Zn (.642), and Bi-Au (.630). Au and Ag have either negative or weak correlations with As, Cu, Sb and Zn, demonstrating that while those elements (As, Cu, Sb and Zn) have high correlations with one another they are not associated with Au and Ag. Tellurium data is too limited to determine its correlation with gold; however, visually the gold is attached to and intergrown with tellurobismuthite and tetradymite. Given this physical evidence, it is reasonable to assume that, given more data, Au would correlate well with Te.

Both primary and secondary fluid inclusions are present in quartz veins. Measured primary inclusions (sample 03ZW369) are 9-15 microns in size, have negative crystal shapes, are generally isolated and always have double bubbles (Figure 3.5). The double bubbles indicate the fluids contain high levels of carbon dioxide. The secondary inclusions are 1-4 microns in size, irregularly shaped and define planes in

Table 3.2 Microprobe analysis averages for Bi-Te minerals from the Wallace occurrence.

Sample	Bi %	Te %	S %	Totals	Bi atomic wt%	Te atomic wt%	S atomic wt%	Mineral
03ZW369	51.73	47.9	0.02	99.64	39.7	60.2	0.08	Tellurobismuthite (Bi_2Te_3)
03ZW369	58.35	36.64	4.49	99.48	39.5	40.7	19.8	Tetradymite (Bi_2Te_2S)

Table 3.3 Correlation table for elements from mineralized gray dikes.

		LOG_AG	LOG_AS	LOG_AU	LOG_BI	LOG_CU	LOG_PB	LOG_SB
LOG_AS	Pearson Correlation	.390						
	Sig. (2-tailed)	.066						
	N	23						
LOG_AU	Pearson Correlation	.493*	-.083					
	Sig. (2-tailed)	.017	.707					
	N	23	23					
LOG_BI	Pearson Correlation	**.685****	.114	**.630****				
	Sig. (2-tailed)	.000	.604	.001				
	N	23	23	23				
LOG_CU	Pearson Correlation	.380	.168	-.087	-.030			
	Sig. (2-tailed)	.074	.445	.694	.892			
	N	23	23	23	23			
LOG_PB	Pearson Correlation	.540**	.209	.104	.320	.379		
	Sig. (2-tailed)	.008	.338	.636	.137	.074		
	N	23	23	23	23	23		
LOG_SB	Pearson Correlation	.574**	**.736****	.047	.500*	.190	.545**	
	Sig. (2-tailed)	.004	.000	.830	.015	.386	.007	
	N	23	23	23	23	23	23	
LOG_ZN	Pearson Correlation	.134	.211	-.281	-.271	**.642****	.300	.109
	Sig. (2-tailed)	.541	.334	.195	.212	.001	.164	.620
	N	23	23	23	23	23	23	23

*. Correlation is significant at the 0.05 level (2-tailed).

**. Correlation is significant at the 0.01 level (2-tailed).

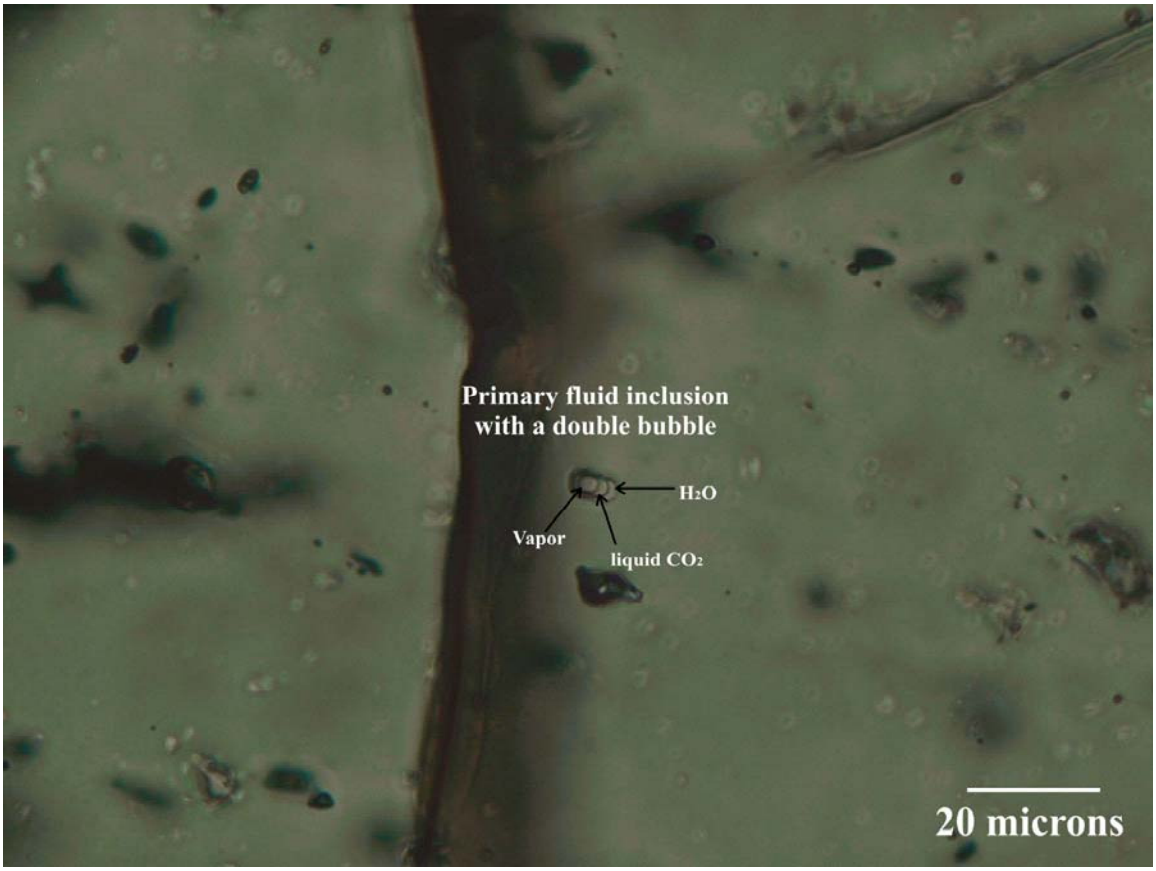

Figure 3.5: Fluid inclusion in mineralization associated quartz veining from the Wallace occurrence. Double bubble is due to the presence of water and liquid CO_2. Sample 03ZW369.

the quartz vein and quartz phenocrysts. The secondary fluid inclusions variably have double bubbles. No measurements were taken on the secondary fluid inclusions.

Upon heating, the vapor bubble and the carbon dioxide bubble expanded to a vapor. This indicates the fluids were under low pressures. Since there is no direct evidence for the exact pressure under which these fluid inclusions formed under exists, an estimate of 0.5 kilobars was used to calculate the trapping temperature. Fluid inclusions from the Wallace occurrence record homogenization temperatures of 301-325 ^{o} C, trapping temperatures of 346-370 ^{o} C, salinities of 2-5 wt % NaCl, and 45-80 vol% carbon dioxide (Table 3.4).

Table 3.4 Primary fluid inclusion measurements from the Wallace 0ccurrence.

Sample	T_h	T_t	wt% NaCl	T_{clath}	T_{CO_2}	xCO_2
03ZW369	325	370	2	9	30	45
	311	356	5	8	30	75
	324	369	4	8	30	80
	315	360	5	7	24	45
	301	346	3	9	31	55

* Th = final homogenization temperature, Tt = trapping temperature, Tclath= clathrate melting temperature, TCO_2 = CO_2 bubble homogenization and xCO_2 = volume percent CO_2.

The oxidation and sulfidation of the mineralizing system at the Wallace occurrence can only be roughly estimated. However, because the dominant ore mineral is tellurobismuthite the system must be at relatively low sulfidation state in comparison to the activity of Te. If the sulfidation were higher one would expect more tetradymite or bismuthinite.

3.2 VABM Bonanza Lobe

Placer Dome geologists discovered gold mineralization at VABM Bonanza lobe (Gierymski and Werdon, 1997). The mineralization is hosted in the Bonanza Pluton and north-south trending high angle fault zones adjacent to the pluton. For this study the area was resampled and more thorough chemical analyses were performed on the samples. Of particular interest was tellurium, for which no samples had been previously analyzed.

Mineralized rock in the VABM Bonanza lobe occurs throughout the entire body and partly into the Spruce Creek lobe. The bulk of the intense gold mineralization is constrained to the west side of the

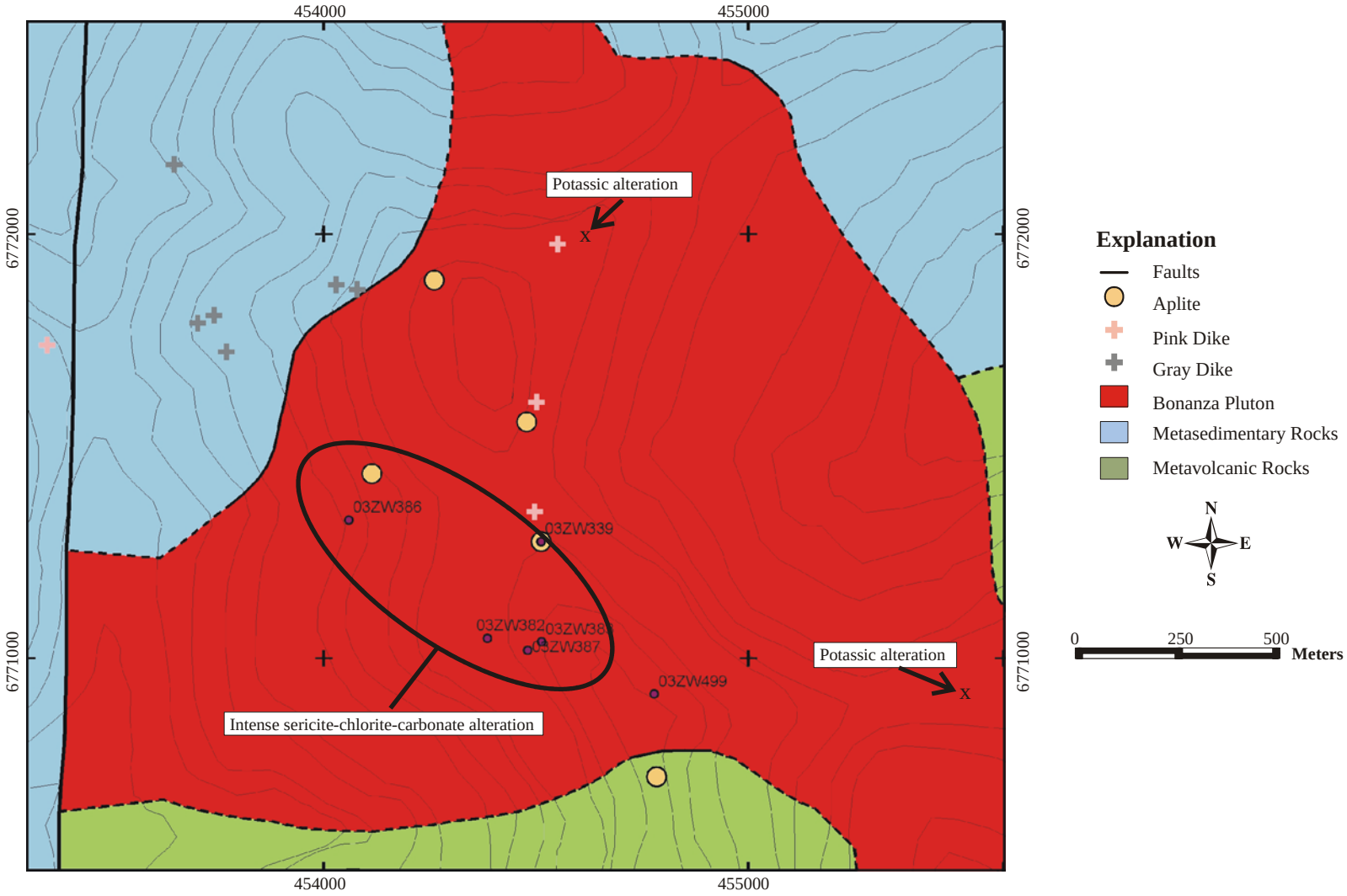

Figure 3.6: Geologic map of the VABM Bonanza lobe showing the location of different styles of alteration and aplite dikes.

pluton (mineralized sample specimens; Figure 3.6). Rock exposure at the VABM Bonanza lobe is limited to boulder fields. Due to the tendency for the veins to weather and the boulders to break along quartz veins, it is difficult to estimate the actual amount of veining and to find unoxidized sulfide specimens. Areas of the most intense veining constitute approximately 1-2% volume of the rock. Ore minerals are more concentrated in or near quartz veins, but significant alteration and mineralized rock do occur were no veining is visible.

Types of alteration in the VABM Bonanza lobe include potassic and sericite-chlorite-carbonate (Figure 3.6). Significant gold mineralization is only found associated with the sericite-chlorite-carbonate alteration.

The potassic alteration consists of <1-3 mm wide quartz veinlets (length is limited by specimen size up to ~15 cm) that have narrow K-feldspar envelopes (<1-1mm) and rare (found at one location) 1-cm-wide K-feldspar veins (length is limited by specimen size up to ~5 cm). Pyrite, magnetite and chalcopyrite are the only opaque minerals found in or near these veins. Potassic alteration is also present in one sample from the Bonanza Creek lobe (03ZW293).

The entire Bonanza pluton exhibits variable sericitic alteration of feldspars (Chapter 2). At the VABM Bonanza lobe an area of intense sericitic-chlorite-carbonate alteration consisting of 2-20 mm wide and >1m long sized quartz -calcite- chlorite-sericite veins with sericite envelopes occurs over a 400x900 meter area (Figure 3.6). The vein material is approximately 80% quartz, 5% calcite, 2-3% chlorite, 2-3% sericite and 1-2% ore minerals. Feldspars within 4 cm of the veins are 5-90% replaced by sericite. All the mafic minerals are 75-100% replaced by a combination of chlorite (85-90%), calcite (5-10%) and rutile (<1%). Under the petrographic microscope the chlorite has green-brown anomalous interference colors and is length slow indicating low to moderate Fe contents.

Chemically the effects of the alteration are obvious. Table 3.5 shows geochemical data for mineralized and unmineralized granodiorite from VABM Bonanza. Altered granodiorite exhibits CaO, Fe_2O_3, MgO, MnO, Na_2O, P_2O_5 and Sr loss and K_2O and Rb gain. The K_2O enrichment is expected with sericitic alteration since K is a significant component in sericite. The loss of CaO, Fe_2O_3, MgO, MnO and Na_2O can be explained by the replacement of plagioclase and biotite by sericite and albite. Since CaO is depleted in altered samples and Na_2O is relatively unchanged, the dominant non-potassic feldspar must be albite. Therefore the alteration at VABM Bonanza is sericite-chlorite-carbonate-albite assemblage.

Rb is a relatively incompatible element and is concentrated in the residual melt as a pluton cools. If the Rb is concentrated in the residual melt and thus in the fluids inherent to the pluton, one would expect increased Rb concentrations in the altered and mineralized parts of the pluton if in fact magmatic fluids are responsible for the mineralization. The fact that this phenomenon is seen is direct evidence that the fluids responsible for the mineralization are magmatic. For this style of alteration, a direct inverse correlation between Sr and Rb can be used to evaluate the extent of alteration. Figure 3.7 shows increased Rb/Sr ratios

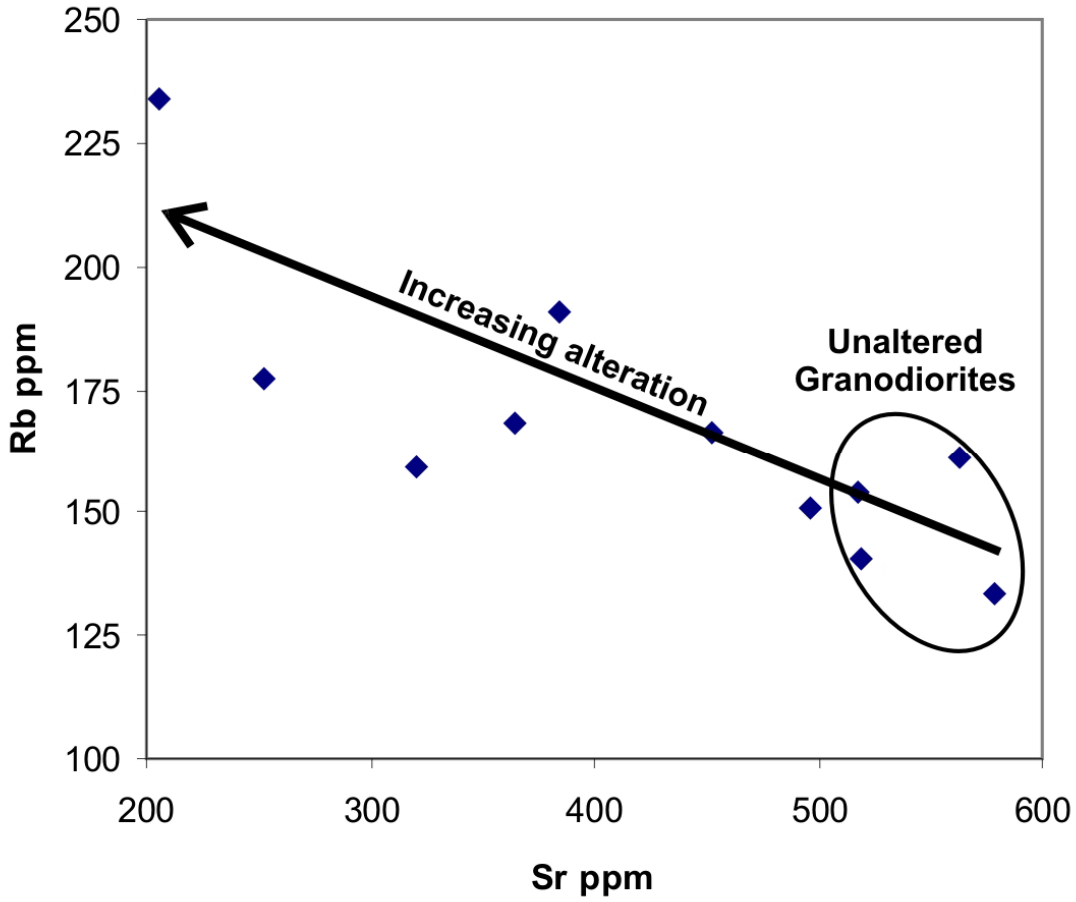

Figure 3.7: Sr vs. Rb plot for altered and unaltered granodiorite samples from VABM Bonanza lobe. Increasing Rb/Sr ratios indicate stronger alteration.

increasing with alteration. Table 3.5 ranks the rocks by this method, and it illustrates that rocks with higher Rb/Sr ratios similarily have lower CaO, Fe_2O_3, MgO, MnO, Na_2O concentrations.

Identified ore minerals in sericite-enveloped veins include (in order of decreasing abundance): pyrite, chalcopyrite, magnetite, bismuthinite, molybdenite, native gold, arsenopyrite, pyrrhotite and bismuth. Chalcopyrite and pyrite are by far the most common minerals in the quartz veins. Pyrite is roughly twice as abundant as chalcopyrite. Although no Te-bearing minerals were identified, Te concentrations in excess of 3 ppm indicate some Te-bearing minerals must be present. The mineral assemblage in the zone of intense sericite-chlorite-carbonate alteration is pyrite, chalcopyrite, bismuthinite, molybdenite and native gold (Figure 3.8). Arsenopyrite was only observed in one specimen (03ZW349) from Spruce Creek.

Neither of the samples containing pyrrhotite (03ZW142) or bismuth (03ZW496) contain significant Au; both are located outside of the zone of intense sericite-chlorite-carbonate alteration (Figure 3.6). At these two occurrences chlorite is more abundant than sericite and there is essentially no sericitic envelope.

Table 3.5 Partial chemistry for granodiorite samples from the VABM Bonanza lobe.

Sample	Al_2O_3	CaO	Fe_2O_3	K_2O	MgO	MnO	Na_2O	P2O5	Rb	Sr	Alteration
03ZW378	16.2	3.5	3.8	3.6	1.8	0.06	3.3	0.19	133	578	0
03ZW391	15.6	3.4	3.6	3.7	1.7	0.06	3.2	0.18	140	519	0
03ZW395	16.0	3.0	3.8	3.7	1.8	0.05	3.2	0.19	161	563	0
03ZW482	15.7	3.2	3.6	3.8	1.6	0.05	3.2	0.17	154	517	0
03ZW382	16.0	2.7	3.4	3.2	1.7	0.04	3.4	0.19	151	497	1
03ZW386	15.8	2.2	3.2	3.7	1.5	0.04	3.3	0.16	167	453	2
03ZW379	16.5	1.3	3.4	3.9	1.6	0.05	3.3	0.19	191	385	3
03ZW387	15.8	2.6	3.1	3.5	1.3	0.04	3.3	0.18	169	364	4
03ZW340	15.3	1.4	2.9	4.0	1.2	0.05	3.1	0.16	159	320	5
03ZW339	15.1	1.1	2.9	3.5	1.3	0.03	2.9	0.16	178	252	6
03ZW377	17.4	0.3	2.6	4.1	1.0	0.03	3.0	0.19	234	206	7
%change	0%	-92%	-36%	7%	-49%	-52%	-14%	-5%	64%	-67%	

* Rb and Sr data are ppm; all other data are wt%. % change calculated from least altered (03ZW378) and most altered (03ZW377) assuming Al immobility. Alteration increases from 0 (unaltered) to 7 (most altered). Unaltered samples (0) are unmineralized.

Due to limited exposure and the inability to properly sample the anomaly, bulk grades from the VABM Bonanza lobe are uncertain. However, hand specimens collected from the most altered zone are generally anomalous in gold. Mineralized hand specimens assay up to 20.8 ppm Au.

Regression of all mineralized samples from the VABM Bonanza lobe show gold correlates best with tellurium (.822) and bismuth (.581) (Table 3.6). Samples containing >100 ppb Au report correlation coefficients of .812, .737 and .712 for Bi, Ag and Cu, respectively (Table 3.7). For strongly mineralized samples (>200 ppb Au) Au correlates best with Te (.919). It appears that, the higher the Au concentration, the greater the Au correlation with Bi and Te, and the lower the Au concentration, the better the correlation with Cu.

Primary fluid inclusions (Figure 3.9) were identified only in one vein sample (03ZW339) from VABM Bonanza. They are 3.75-15 microns in size, have roughly negative crystal shapes, are generally isolated and variably contain daughter minerals. The infrequency of primary inclusions is presumably the result of their destruction by later secondary inclusions. The secondary inclusions are much more abundant and are found both in the quartz veins and in quartz crystals in the pluton. Measured inclusions are 4-6.5 microns in size, irregular in shape, define planes and lack daughter minerals.

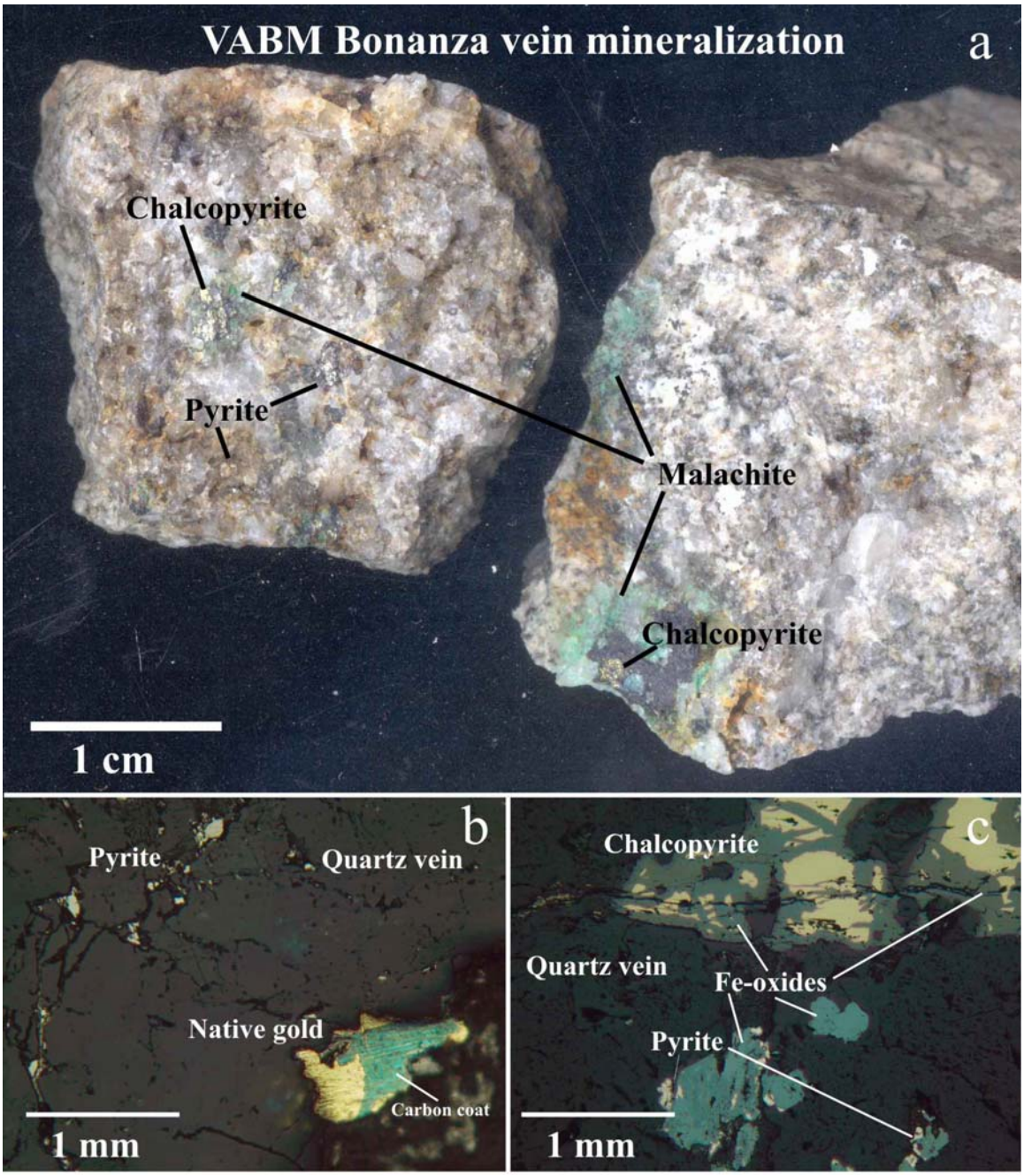

Figure 3.8: Mineralization in quartz veining from VABM Bonanza lobe. Bottom pictures (b and c) are photomicrographs from polished thin sections of vein material.

Table 3.6 Correlation table for all mineralized samples from the VABM Bonanza lobe.

		AG	AS	AU	BI	CU	HG	PB	SB	TE
AS	Pearson Correlation	.348**								
	Sig. (2-tailed)	.010								
	N	54								
AU	Pearson Correlation	.526**	.233							
	Sig. (2-tailed)	.000	.089							
	N	54	54							
BI	Pearson Correlation	.518**	.129	**.581****						
	Sig. (2-tailed)	.000	.354	.000						
	N	54	54	54						
CU	Pearson Correlation	.717**	.141	.481**	.429**					
	Sig. (2-tailed)	.000	.309	.000	.001					
	N	54	54	54	54					
HG	Pearson Correlation	.234	-.171	.022	.029	.150				
	Sig. (2-tailed)	.105	.240	.881	.844	.302				
	N	49	49	49	49	49				
PB	Pearson Correlation	.425**	.412**	.015	.215	.037	-.057			
	Sig. (2-tailed)	.001	.002	.911	.119	.793	.698			
	N	54	54	54	54	54	49			
SB	Pearson Correlation	.496**	.311*	.104	.350**	.260	.506**	.464**		
	Sig. (2-tailed)	.000	.022	.456	.009	.057	.000	.000		
	N	54	54	54	54	54	49	54		
TE	Pearson Correlation	.211	-.083	**.822****	.764**	.195	-.103	-.127	.130	
	Sig. (2-tailed)	.416	.751	.000	.000	.454	.693	.626	.619	
	N	17	17	17	17	17	17	17	17	
ZN	Pearson Correlation	.303*	.373**	-.022	.085	.252	.337*	.569**	.628**	-.340
	Sig. (2-tailed)	.026	.005	.874	.539	.066	.018	.000	.000	.182
	N	54	54	54	54	54	49	54	54	17

**. Correlation is significant at the 0.01 level (2-tailed).

*. Correlation is significant at the 0.05 level (2-tailed).

Table 3.7. Correlation table for samples with >100 ppb Au from the VABM Bonanza lobe.

		AG	AS	AU	BI	CU	HG	PB	SB	TE
AS	Pearson Correlation	.423								
	Sig. (2-tailed)	.080								
	N	18								
AU	Pearson Correlation	**.737****	.152							
	Sig. (2-tailed)	.000	.548							
	N	18	18							
BI	Pearson Correlation	.734**	.117	**.812****						
	Sig. (2-tailed)	.001	.644	.000						
	N	18	18	18						
CU	Pearson Correlation	.901**	.310	**.712****	.753**					
	Sig. (2-tailed)	.000	.210	.001	.000					
	N	18	18	18	18					
HG	Pearson Correlation	.332	.206	.238	.149	.184				
	Sig. (2-tailed)	.178	.412	.341	.555	.466				
	N	18	18	18	18	18				
PB	Pearson Correlation	.737**	.471*	.541*	.525*	.631**	.218			
	Sig. (2-tailed)	.000	.049	.021	.025	.005	.386			
	N	18	18	18	18	18	18			
SB	Pearson Correlation	.706**	.729**	.421	.391	.461	.444	.645**		
	Sig. (2-tailed)	.001	.001	.082	.108	.054	.065	.004		
	N	18	18	18	18	18	18	18		
TE	Pearson Correlation	-.304	.198	.600	.491	-.464	-.749	-.446	.402	
	Sig. (2-tailed)	.507	.671	.154	.263	.295	.053	.316	.372	
	N	7	7	7	7	7	7	7	7	
ZN	Pearson Correlation	.644**	.610**	.348	.374	.563*	.560*	.725**	.741**	-.584
	Sig. (2-tailed)	.004	.007	.157	.126	.015	.016	.001	.000	.168
	N	18	18	18	18	18	18	18	18	7

**. Correlation is significant at the 0.01 level (2-tailed).

*. Correlation is significant at the 0.05 level (2-tailed).

Primary fluid inclusions from quartz veins (sample 03ZW339) record final homogenization temperatures of 221-486 ^{o} C, trapping temperatures 266-536 ^{o} C and salinities of 21-55 wt% NaCl (Table 3.8). Secondary fluid inclusions from quartz veins (sample 03ZW382) report final homogenization temperatures of 87-146 ^{o} C, trapping temperatures of 132-191 ^{o} C, and salinities of 5-9 wt% NaCl. The secondary fluid inclusions most likely represent younger cooler fluids unrelated to mineralization. The mineral assemblage of pyrite-chalcopyrite-magnetite allows an estimate of the oxidation and sulfidation state of the system. In reflected light these three minerals and native gold were observed in a single quartz vein. Figure 3.10 shows the possible range of oxidation and sulfidation state conditions for the mineralizing system.

Table 3.8 Primary and secondary fluid inclusion measurement data from the VABM Bonanza lobe.

Sample	Th	Tt	Ts	Tfd	wt% NaCl
03ZW339	220	536	486		55
	207	529	479		54
	204	522	472		53
	211	477	427		49
	425	470	332		40
	362	407	227		33
	346	391	337		41
	320	365			
	212	350	305		38
	226	334	289		37
	261	306			
	256	301			
	255	300			
	252	297		-19	21
	247	292			
	247	292		-20	23
	246	291			
	244	289			
	240	286		-20	22
	221	266			
03ZW382	146	191		-6	9
	133	178		-3	5
	87	132		-3	5

* Th = liquid homogenization temperature, Tt = trapping temperature, Ts = solid homogenization temperature and Tfd = freezing point depression.

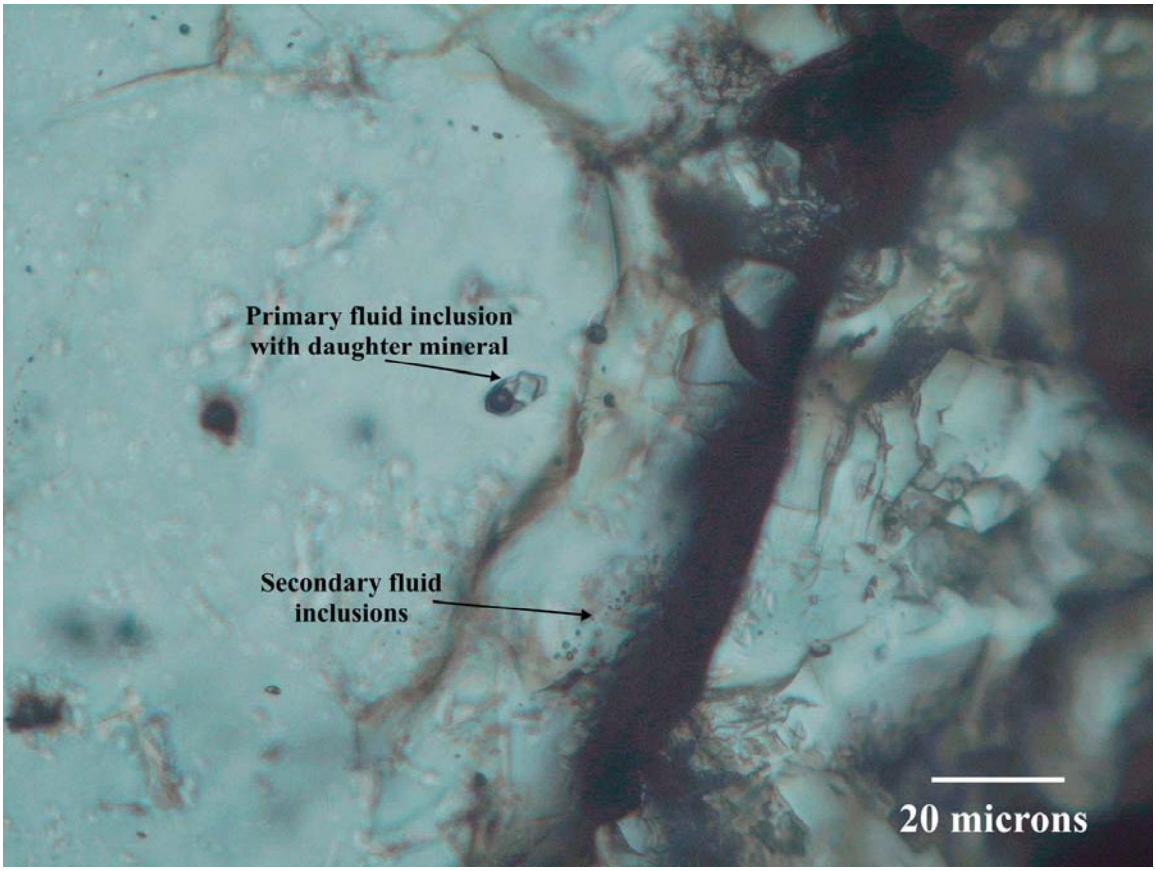

Figure 3.9: Fluid inclusion from a quartz vein hosting mineralization in the VABM Bonanza lobe. The primary fluid inclusion is large, has negative crystal shape and a daughter mineral (halite). In contrast, secondary fluid inclusions are smaller and occur in lines. Sample 03ZW339.

3.3 Bonanza Creek Color Anomaly

A prominent altered zone, informally named the Bonanza Creek Color Anomaly (BCCA; Figure 3.1) is an area of extensive limonite stained pyritic metavolcanic hornfels, easily seen from miles away (Figure 3.11). The pyritic hornfels contains up to 10% pyrite, but does not contain appreciable gold concentrations (generally < 20 ppb Au). The pyritic rocks do contain variably high tellurium contents (up to 5 ppm). However, no tellurium minerals were observed in reflected light, presumably because the Te replaces sulfur in pyrite (Fe $(S,Te)_2$). Much of the pyritic hornfels at the BCCA is brecciated, indicating faulting, which facilitated supergene fluid flow to produce limonite by oxidation of pyrite. Within the pyritic hornfels are isolated areas containing calc-silicate veinlets. The calc-silicate veinlets have garnet cores with pyroxene and epidote envelopes. Opaque minerals associated with the veinlets include pyrite, chalcopyrite and pyrrhotite. The veinlets do not occur in great enough frequency to be economically important, but they do demonstrate that some of the mineralization at the BCCA is plutonic-related. Anomalous gold values at the BCCA include high-T and low-T mineralization.

3.3.1 High-T Mineralization

The high-T mineralization at the BCCA is of two types: Au-Bi and Cu-Au. The Au-Bi mineralization is restricted to two samples collected by PDX geologists. The specimens include a limonite gossan and a granitic rock cut by quartz-chlorite-limonite veins. This mineralization is presumably related to the Bonanza Creek lobe at the BCCA.

The high temperature Cu-Au mineralization occurs near the contact of the Bonanza Creek lobe with the metavolcanic rock unit (Figure 3.12). The Cu-Au mineralization extends for approximately 100 meters from the contact; the most intense veining is within ten meters of the contact. This mineralization consists of quartz-chlorite-calcite veins with associated magnetite, chalcopyrite and native gold (Figure 3.13). The quartz veins are up to 3 cm wide, >30 cm long and composed of approximately 70% quartz, 10% chlorite, 5% calcite, 10% magnetite, 5% chalcopyrite and <1% pyrite. Total veining near the contact constitutes approximately 2-5% of the rock volume. Metabasalt that hosts the veining is pervasively altered. Plagioclase phenocrysts in the metabasalt are 5-15% sericitized. The groundmass is ~75% altered to 75% biotite, 15% chlorite, 10% sericite and 10% magnetite. Chlorite in the veins has anomalous green-brown interference colors and is length fast. Biotite (<1%) is also present in and surrounding mineralized

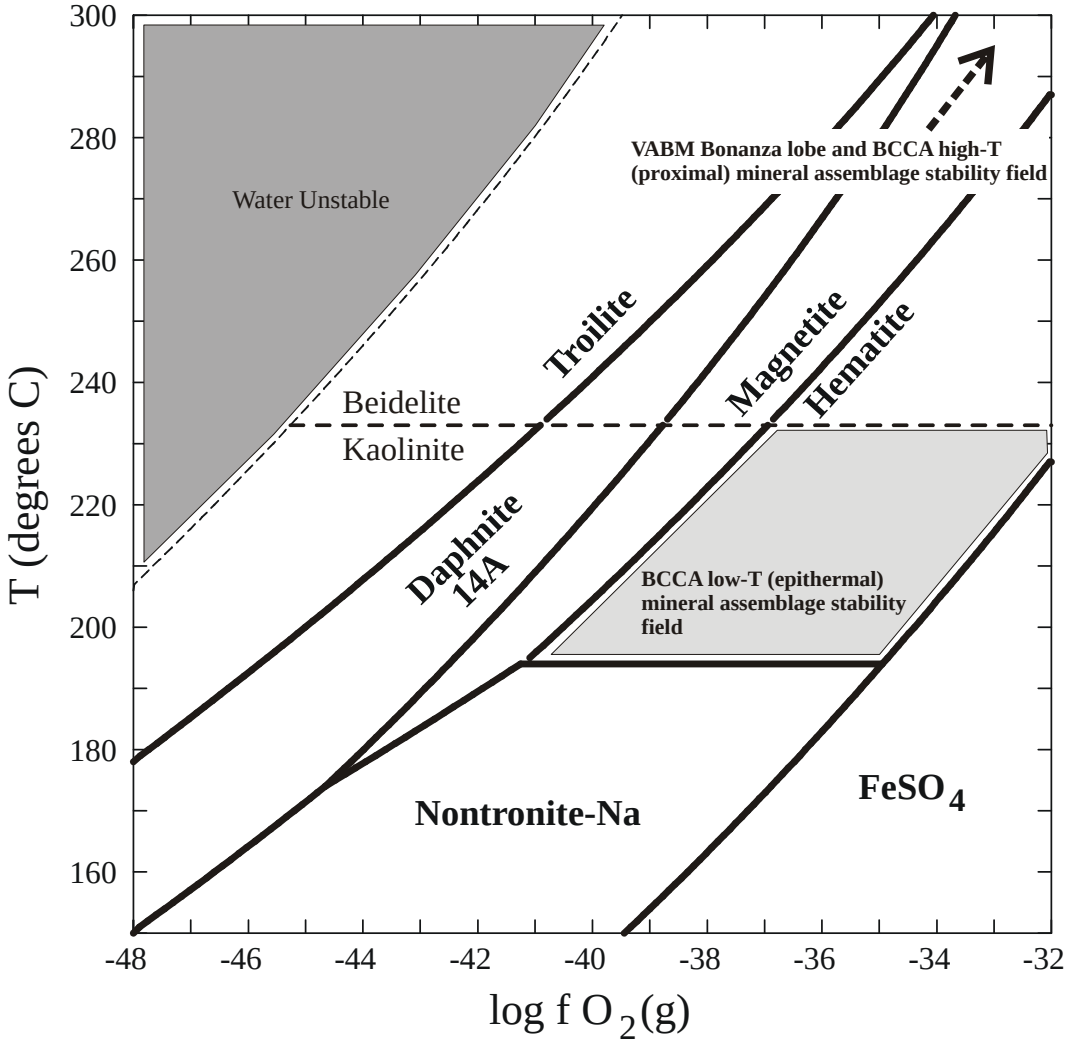

Figure 3.10: Oxidation vs. Temperature mineral stability diagram at 500 bars. The diagram includes the presence of quartz, pyrite, chalcopyrite, muscovite, K-feldspar and albite. The diagram illustrates the possible range of temperature and oxidation state for the mineral assemblage of pyrite, chalcopyrite and hematite for the low-T mineralization at the BCCA. In contrast, the pyrite-chalcopyrite-magnetite mineral assemblage at the VABM Bonanza lobe and high-T (proximal) mineralization at the BCCA is higher temperature and presumably lower oxidation than the BCCA low-T (epithermal) mineralization. Diagram calculated using Geochemist's Workbench (Bethke, 1998) and thermodynamic data of Delany and Lundeen (1990).

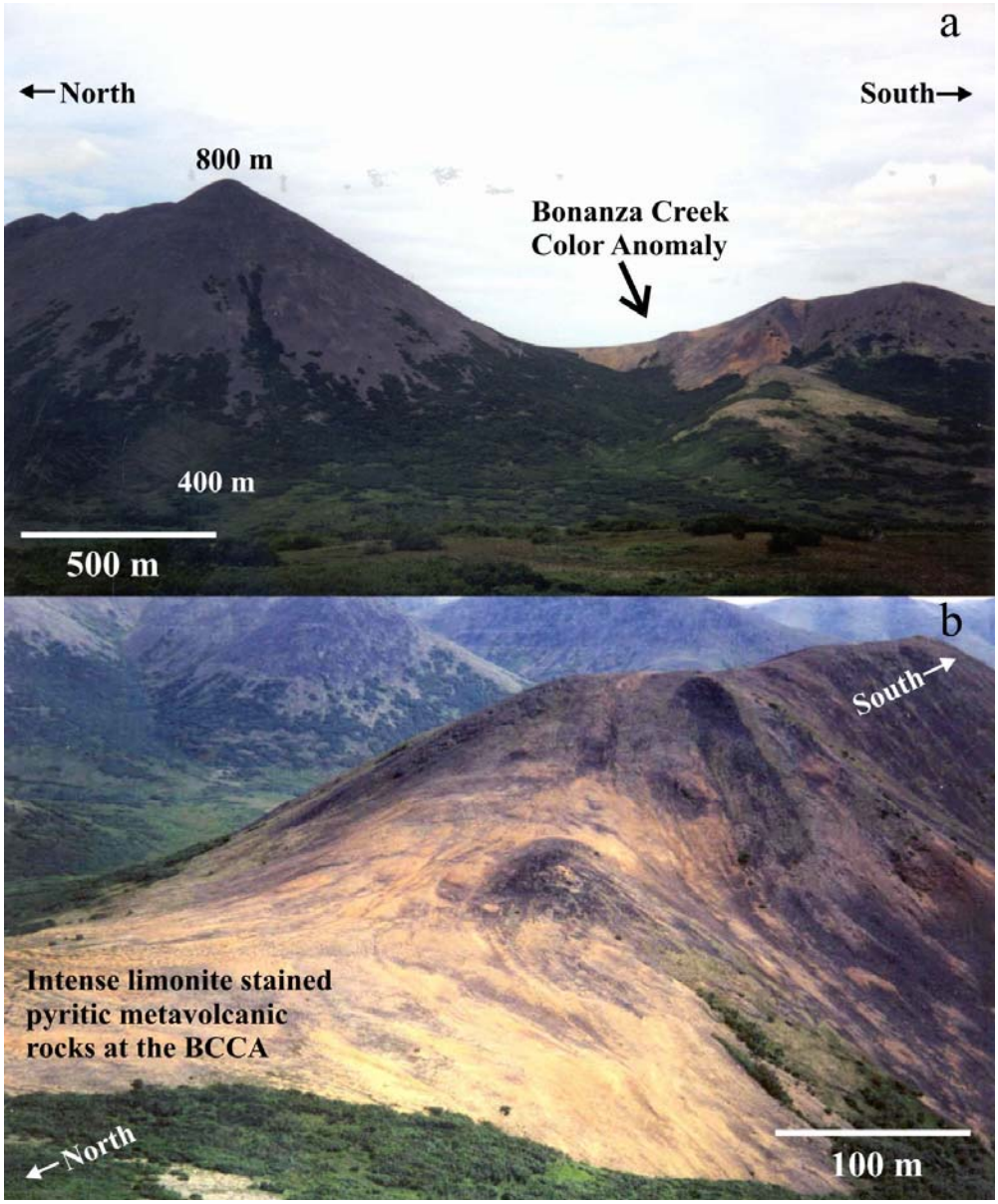

Figure 3.11: Two pictures of the limonite stained pyritic metavolcanic rocks at the BCCA. Figure 3.11a is looking east from Spruce Creek and Figure 3.11b is looking southeast down the ridge north of the color anomaly.

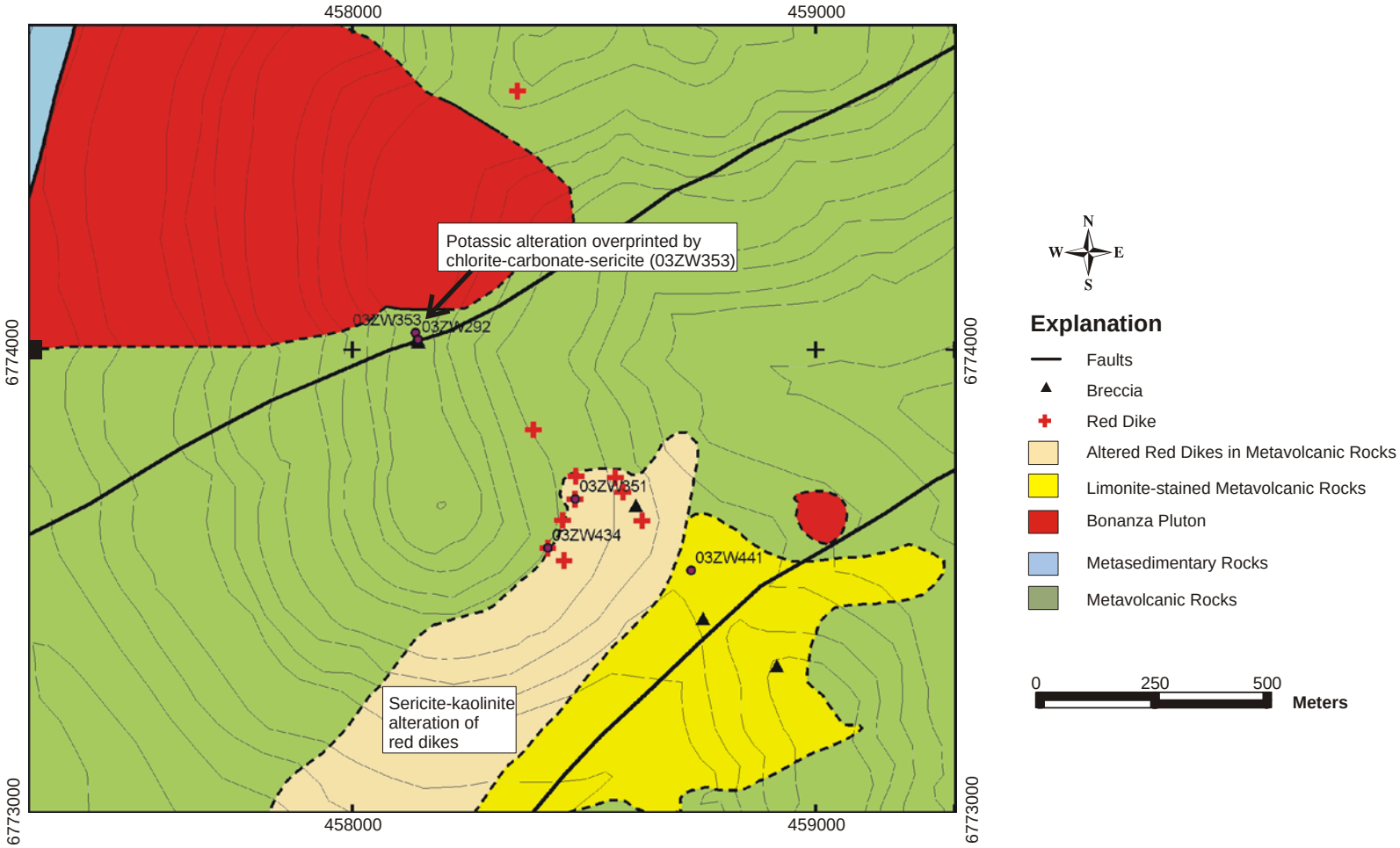

Figure 3.12: Geologic map of the BCCA showing the location of different styles of alteration. Faults mapped in part by regional geophysics.

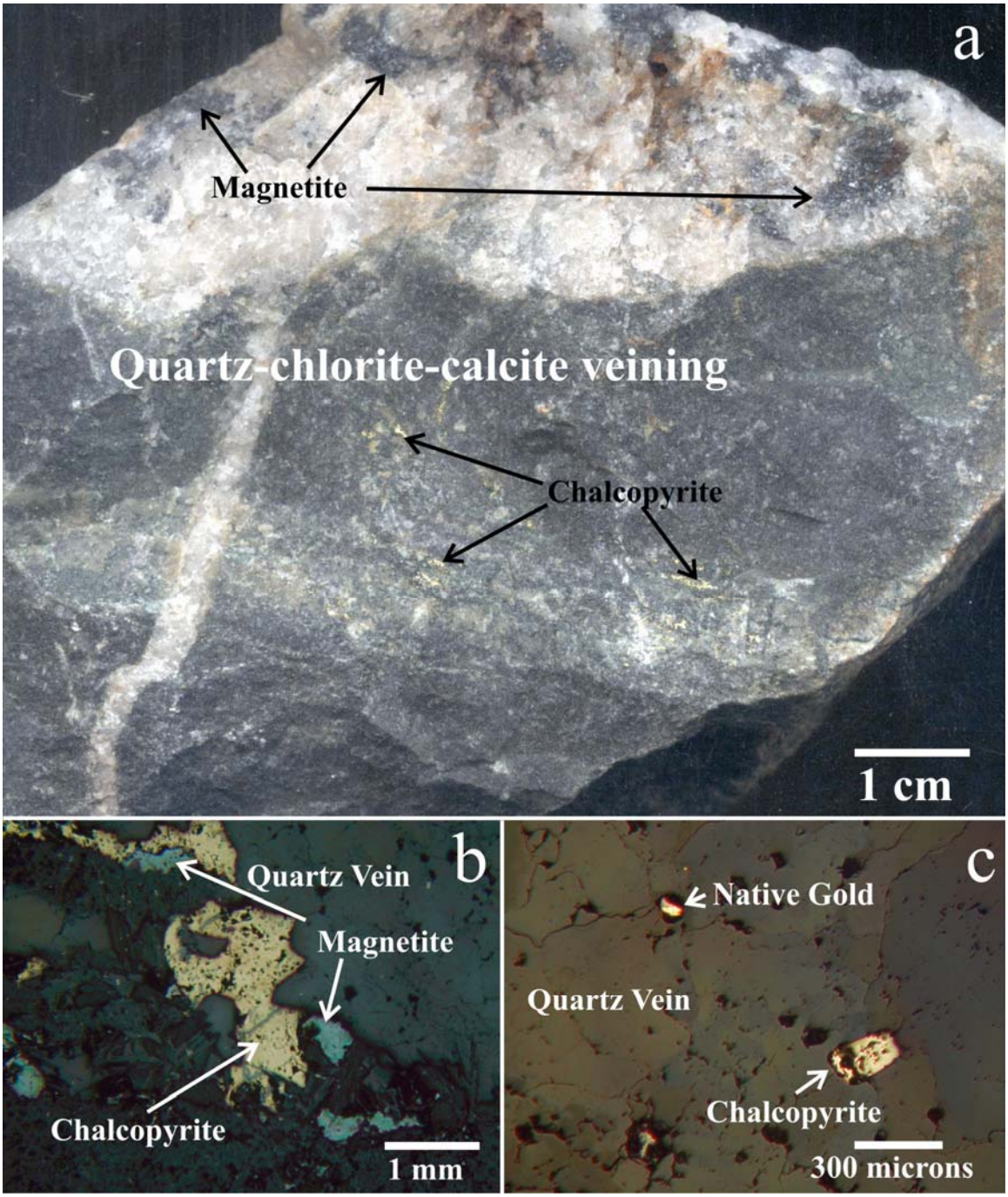

Figure 3.13: Quartz vein mineralization from the high-T mineralization at the BCCA. Figure 3.13a is a mineralized metavolcanic rock near the contact with the Bonanza Creek lobe. Figures 3.13a and b are photomicrographs of quartz veins from polished thin sections in reflected light.

quartz veins. The appearance of secondary biotite is the only evidence for mineralization associated with potassic alteration in the study area. Figure 3.13: Quartz vein mineralization from the high-T mineralization at the BCCA. Figure 3.13a is a mineralized metavolcanic rock near the contact with the Bonanza Creek lobe. Figures 3.13a and b are photomicrographs of quartz veins from polished thin sections in reflected light.

On the aeromagnetic map (Figure 2.16) the BCCA is a large magnetic high. The highest magnetic anomaly measurement is at this mineralization locality. The high magnetic signature is likely related to the significant amount of magnetite at the occurrence. This suggests that the mineralization may continue to significant depths. A single mineralized specimen (03ZW353) from this area assayed 10.9 ppm Au and 1,860 ppm Cu.

Analyzed primary fluid inclusions from mineralized quartz veins (03ZW353) are 3-17.5 microns in size, have negative crystal shapes, and approximately 90% have NaCl daughter minerals (Figure 3.14). The fluid inclusions record final homogenization temperatures of 237-507 degrees C, trapping temperatures of 282-557 degrees Celsius, and salinities of 17-57 wt% NaCl (Table 3.9). The lower homogenization temperatures typically have low salinities as well and presumably indicate conditions when the system was cooling. The wide range of trapping temperature is reflected in the alteration-associated minerals, chlorite

Table 3.9 Primary fluid inclusion measurement data from high-T mineralization at the BCCA.

Sample	Th	Tt	Ts	Tfd	wt% NaCl
03ZW353	232	557	507		57.
	225	543	493		56
	398	443	331		40
	291	415	370		43
	302	358	313		39
	258	357	312		39
	257	355	310		39
	270	351	306		38
	268	349	304		38
	271	339	294		38
	208	320	275		36
	275	320	245		34
	244	311	266		36
	195	310	265		36
	207	293	248		35
	246	291	214		33
	244	289		-20	23
	237	282		-13	17

T_h = liquid homogenization temperature, T_t = trapping temperature, T_s = solid homogenization temperature and T_{fd} = freezing point depression.

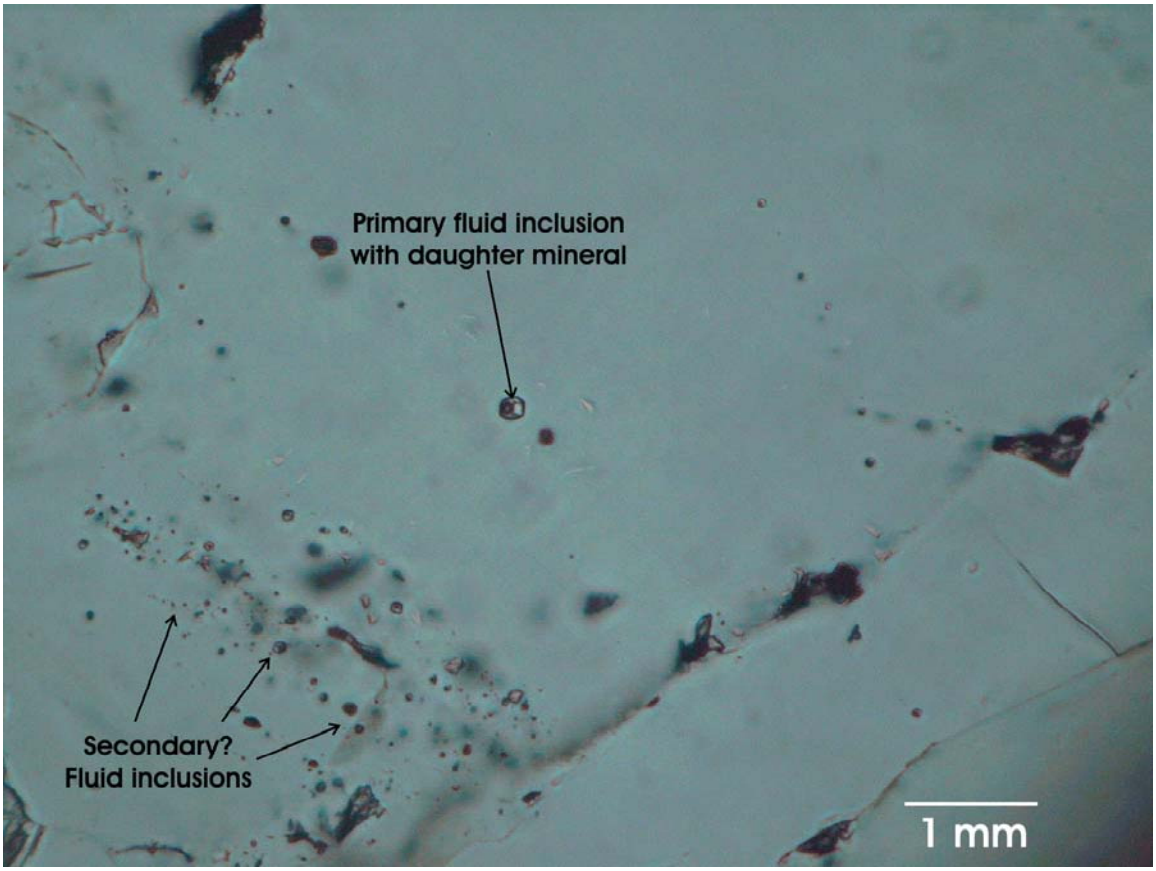

Figure 3.14: Fluid inclusions in quartz veins from the high-T mineralization at the BCCA. Primary fluid inclusions exhibit negative crystal shapes, are generally isolated and have daughter minerals (halite). Secondary fluid inclusions are generally irregular in shape, occur along fractures and variably contain daughter minerals. Sample 03ZW353.

and biotite. The biotite presumably formed during high temperatures and chlorite replaced biotite (evident from significant sphene in the chlorite) during cooling. A continuum of trapping temperatures also suggests this is the case.

The combination of pyrite-chalcopyrite-magnetite is a similar assemblage to the mineralization at the VABM Bonanza lobe. Again this assemblage defines a range of oxidation-sulfidation state conditions for the mineralizing system (Figure 3.10).

3.3.2 Low-Temperature Mineralization

The low-temperature mineralization at the BCCA occurs in a variety of different forms including vuggy chalcedonic veining, sericitically altered red dikes, and mineralized fault (hydrothermal?) breccia (Figure 3.15).

Vuggy chalcedonic veining is found in the limonite stained pyritic hornfels and in close proximity to the sericitically altered dikes. The chalcedonic veins are up to 15 cm wide and their length is limited to 20 cm by rubble occurrence. Open cavities account for approximately 5% of the rock by volume. Of two specimens analyzed in this study the highest ore element values were 0.723 ppm Au, 9.88 ppm Ag and 0.28 ppm Hg.

Sericitically altered red dikes are concentrated on the ridge north of the BCCA (Figure 3.12). The sericitically altered dikes are characteristically pink to orange in color with open vugs accounting for 5-15% of the rock volume. The vugs are lined with sericite, kaolinite and oxidized sulfides. The original feldspar and biotite phenocrysts of the dikes are entirely altered to muscovite. The groundmass is a combination of 40% quartz, 35% sericite, 15% feldspar (albite?) and 10% kaolinite. No visible ore minerals were observed in the dikes. However, some of the altered dikes exhibit square shaped cavities were pyrite presumably occurred. Table 3.10 shows chemistry for the altered and unaltered varieties of the red dikes. The red dikes have experienced loss for all of the major oxides and some trace elements. The loss of most major elements is apparent in the vuggy nature of the dikes. The increased Al_2O_3 and SiO_2 in the altered

Table 3.10: Partial chemistry for altered and unaltered red dikes.

Sample	Al_2O_3	CaO	Fe_2O_3	K_2O	MgO	MnO	Na_2O	P_2O_5	SiO_2	TiO_2	Ba	Rb	Sr	
03ZW297	16.84	1.70	4.27	5.15	0.94	0.11	4.13	0.19	64.49	0.61	1449	217	354	
03ZW427	17.95	0.06	1.57	4.31	0.15	0.01	4.25	0.03	71.49	0.18	1514	78	117	alt
03ZW434	17.80	0.12	3.19	4.21	0.37	0.01	4.27	0.07	69.67	0.29	1328	69	157	alt
03ZW435	17.52	0.08	3.25	4.08	0.38	0.01	4.43	0.07	69.90	0.27	1204	69	141	alt
03ZW351	21.90	0.01	2.99	3.76	0.51	0.01	1.16	0.02	69.45	0.21	1186	76	55	alt
%change	0%	-100%	-46%	-44%	-58%	-96%	-78%	-91%	-17%	-74%	-37%	-73%	-88%	

* Ba, Rb and Sr are ppm; all other data are wt%. % change calculated from least altered (03ZW297) and most altered (03ZW351) assuming Al immobility. Data are from this study.

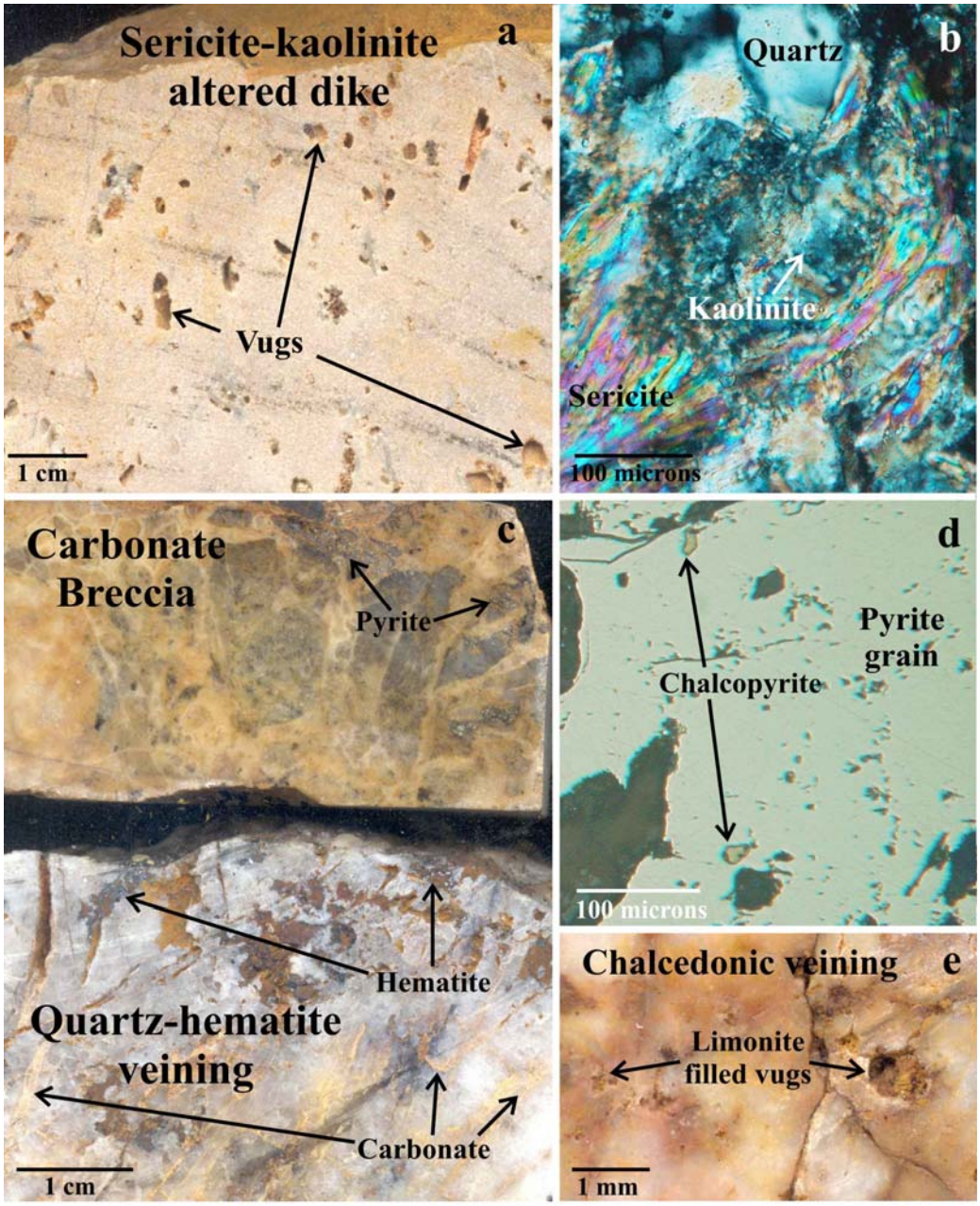

Figure 3.15: Pictures of sericitic-kaolinite altered dikes, chalcedonic veining and quartz veined carbonate breccia of the low-T mineralization at the BCCA. Figure 3.15a and b are examples of the altered red dikes in hand specimen (a) and thin section (b). Figure 3.15c shows carbonate breccia and quartz-hematite veining from low-T (epithermal) mineralization. Figure 3.15d is a photomicrograph of pyrite with chalcopyrite inclusions from the hydrothermal breccia. Figure 3.15e shows limonite filled vugs in a chalcedonic vein.

varieties is the result of intense sericite-kaolinite-silica alteration. The lack of Rb enrichment suggests the major alteration mineral is kaolinite rather than sericite (as seen at VABM Bonanza).

The mineralized fault breccia (sample 03ZW292) is located on top of the ridge north of the limonite stained metavolcanic rocks. The breccia consists of carbonate-replaced metabasalts cut by quartz veins. The carbonate-replaced breccia contains minor pyrite and chalcopyrite (Figure 3.15). The quartz veins contain clasts of carbonate-replaced breccia and 1-5% specular hematite. Despite the apparent lack of abundant ore minerals the breccia assays up to 15.1 ppm Au (J. Foley, written comm., 2004) and 1.6 ppm Hg.

Regression of Au values >200 ppb from the low-T mineralization do not show any significant correlation with other ore elements. However, if some data points are removed Au correlates well with Hg .987 (Figure 3.16). The reason for not seeing any significant correlations with the unedited data is due to limited sample analyses from this style of mineralization or poor chemical analysis for data not from this study.

The mineral assemblage of pyrite-chalcopyrite and hematite can be used to approximate the oxidation-sulfidation state conditions for the mineralizing system (Figure 3.10). The presence of kaolinite allows a maximum temperature estimate to be made, since at higher temperatures kaolinite dehydrates into pyrophyllite. Figure 3.10 illustrates that under quartz saturated conditions the maximum temperature for kaolinite formation is 240 degrees Celsius.

3.4 Other Styles of Mineralization

In addition to the three main gold mineralized areas described above, two additional areas of weak gold mineralized areas occur in the study area. These are the Spruce Creek skarn and Cu-mineralization near the Rex Creek pluton. Although neither of these types contain significant gold, they are important to the mineralization history.

The skarn consists of approximately 50% epidote, 30% calcite, 5-7% hornblende, 5% garnet, 5% scapolite and 2-3% pyroxene. The garnet, pyroxene and scapolite minerals represent the prograde assemblage while the calcite, epidote and hornblende represent the retrograde assemblage. Sulfides observed in the skarn include pyrite (85%), chalcopyrite (10%), pyrrhotite (5%) and covellite (<1%). The pyrrhotite always occurs as inclusions in the pyrite, indicating low oxidation-sulfidation conditions progressing to more oxidized conditions during mineralization. Covellite rims chalcopyrite and represents supergene alteration. Of the three samples analyzed, none contained Au in excess of 100 ppb, but all contained anomalous Cu and one sample reported 96 ppm W (Table 3.11).

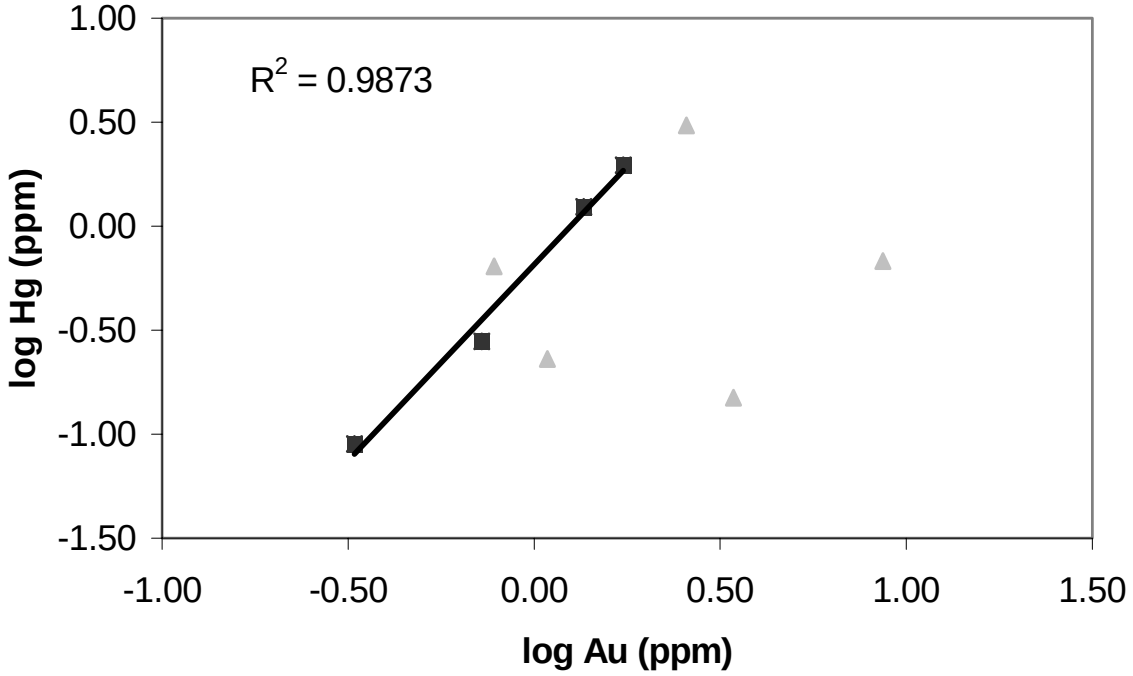

Figure 3.16: Linear regression plot for Au and Hg from low-T (epithermal) mineralization at the BCCA (samples plotted have >200 ppb Au). The squares are data from this study while the triangles are from Gierymski and Werdon (1997). The data as a whole indicate a poor correlation between Au and Hg. Regression of the four samples from this study, however, result in a strong correlation between Au and Hg.

Table 3.11: Partial assays for Spruce Creek skarn specimens; values are ppm.

Sample	Ag	Au	Bi	Cu	Hg	Mo	Pb	Sb	Te	W	Zn
03ZW256	0.27	0.02	0.02	193	0.01	0.52	5.4	0.76	0.01	10	39
03ZW257	0.32	0.04	2.97	580	0.05	6	2.9	6.41	0.14	96	33
03ZW344	0.88	0.09	0.83	658	0.01	1.03	0.9	1.42	0.14	<10	29

Originally, the Spruce Creek skarn (Figure 3.2) was a carbonate rich bed approximately 10-15 meters wide. Volcaniclastic textures (volcanic rock and plagioclase crystal fragments in a fine-grained matrix) are evident in thin section from portions of the skarn, presumably at the boundary of the carbonate bed.

The Rex Creek pluton does not appear to be related to the mineralization in the VABM Bonanza lobe. The alteration mineral assemblage at the Rex Creek pluton is epidote-chlorite-carbonate-sericite. Ore minerals associated with the alteration include malachite, chalcopyrite, magnetite and pyrite. Where metavolcanic rocks shallowly overlie the pluton there are rare, open-spaced, malachite-stained quartz veins with chalcopyrite (samples 03ZW219, 03ZW093). These veins have associated anomalous Cu and Ag values (Table 3.12). The open-spaced nature of the quartz veins indicates that the mineralization formed under low-pressure conditions. An intensely malachite stained portion of the metavolcanic rocks (03ZW088) exists at the NE end of the Rex Creek pluton (Figure 3.1). This zone is approximately 10 meters in width and assays over 1% Cu (Table 3.12). The pluton itself exhibits 1-150 mm sized epidote veins that variably contain up to 1-5% pyrite and magnetite. Mafic minerals are 0-100% replaced by pyrite. Pyrite that replaces mafic minerals is accompanied by epidote, chlorite, calcite and magnetite. Pyrite is largely restricted to the pluton, while chalcopyrite is dominantly found outside the pluton.

Table 3.12. Partial assays for Rex Creek pluton associated mineralization; values are ppm.

SAMPLE	Ag	As	Au	Bi	Cu	Hg	Mo	Pb	Sb	Te	Zn
03ZW219	0.03	1	<0.001	<0.01	244	<0.01	0.51	1.2	0.08	<0.01	15
03ZW088	1.16	0.6	0.002	1.16	13200	<0.01	0.61	11	0.13	0.51	393
03ZW093	0.6	1.8	0.008	0.19	676	0.01	1.66	50.1	0.14	0.1	40

Fluid inclusions in quartz veins from the Rex Creek pluton are irregular in shape and generally <2 microns in size and always define planes. The morphology and geometry of these fluid inclusions indicate they are all secondary. If primary inclusions did exist the likelihood of finding any unaffected by the secondary inclusions is doubtful.

3.5 Placers

The location of historic and current placer mining operations include Bear Creek, the Tuluksak River and most of their tributaries (Figure 3.1). In the early 1900's high grade placers were found at the mouths of California and Rocky Creeks (Figure 3.1; Gierymski and Werdon, 1997). In the mid 1990's the most productive placer mining was on Spruce Creek; a minimum 25,000 oz. of gold was produced from that drainage (J. Foley, written comm., 2004). Bear Creek was being mined in 2003 and Shamrock Creek is expected to be mined soon.

Despite a long history of placer mining, limited data exist on the placer gold from the Nyac district. A preliminary SEM placer gold study by Dan McCoy (in Gierymski and Werdon, 1997) focused on the morphology and leached rims of placer grains from the Nyac district. These data (Table 3.13) show that placer gold from Spruce and Happy Creeks is irregular in shape and has thin (5-10 micron) partially concentric (15-20%) rims. Placer gold from Bear Creek is craggy and fully rimmed (10-40 microns).

In reflected light the placer grains appear homogenous (Figure 3.17a-d). No pores or dark yellow rims are visible which would indicate that the gold was leached of Ag and thus had traveled a significant distance. Placer gold is occasionally attached to quartz and tetradymite (Figure 3.17c and 3.17d).

Gold occurs in nature as a solid solution of Ag and Au, known as electrum. Traditional measurements of Au composition are reported as fineness (= (Au/Au+Ag)*1000). As gold travels in a stream environment, the Ag in solid solution becomes oxidized and is leached from the gold grain (Knight et al., 1999; Figure 3.17e). Removing Ag from the electrum results in gold enrichment, hence increasing fineness.

Microprobe analyses of placer grains prepared for SEM study (Table 3.14) show both leached and unleached rims. Placer grains from Spruce and Happy Creeks show no compositional rimming, indicating minimal transport. In contrast, nearly pure gold rims (indicative of Ag-leaching) are present on gold grains from Bear Creek. These grains experienced significant stream transport.

Table 3.14 also lists average gold finenesses for Bear and Bonanza Creeks and the Tuluksak River. The production average finenesses must be carefully interpreted since they could represent the

Table 3.13. SEM morphology of placer gold from the study area.

Sample	Location	Size (microns)	Shape	Leached Rim (% of Circumference)	Rim Width (microns)	Average Width
975727	Spruce Creek	500x200	craggy, attached quartz	20	1-5	2
975842	Happy Creek	50x50	craggy	15	1-10	3
975721	Bear Creek	100x100	craggy	100	10-40	25

* Data in Gierymski and Werdon (1997).

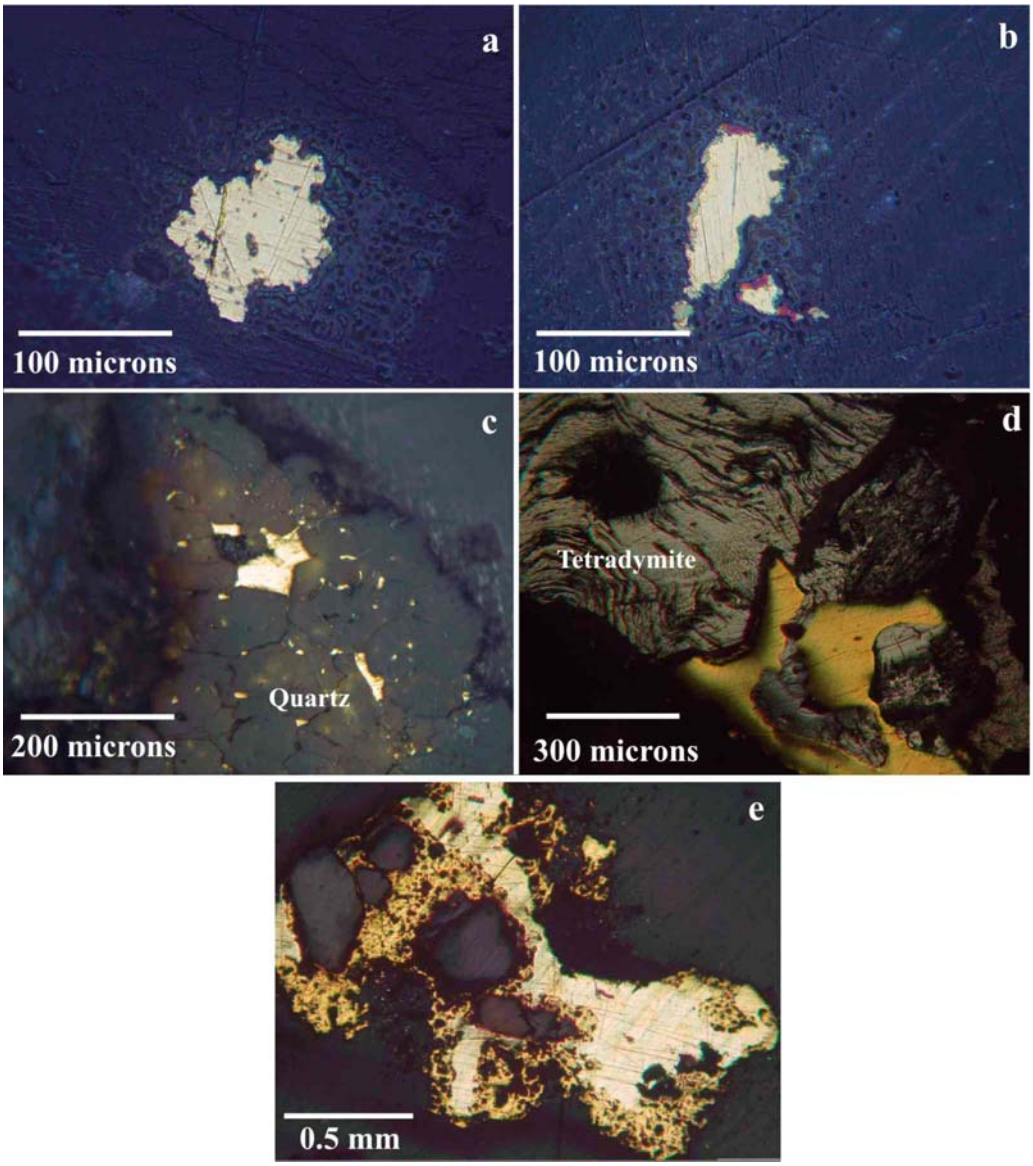

Figure 3.17: Photomicrographs of placer gold from the study area. Samples are from: (a) Bear Creek (975721), (b) Happy Creek (975842), (c) and (d) Spruce Creek (975727 and placer sample), and (e) weathered gold grain (courtesy of R. Newberry). Figure 3.17e is a weathered gold grain exhibiting a porous appearance where Ag has been leached out. None of the grains from the study area exhibit visible Ag-leached rims and are irregular in shape or are attached to quartz (c) or tetradymite (d) indicative of minimal stream transport.

average of several gold populations. Figure 3.18 shows the location for each of the placer grains and production average finenesses. The average fineness location for Bonanza Creek is constrained to the mouth of the creek since placer operations stopped approximately 1000 meters upstream. The location of the Bear Creek production average fineness could have come from anywhere from the mouth of Bear Creek to approximately 1000 m upstream from the Bonanza Creek confluence. The production average fineness for the Tuluksak River is the most problematic. Historic placer mining began on the Tuluksak River outside of the study area and continued along it until the confluence of California Creek. So this bulk average fineness could be located anywhere along the river to the confluence of California Creek.

Table 3.14 Placer gold microprobe and production average placer fineness data.

Sample	Location	%Ag	%Au	total	Fineness	Grain	Measurement location
975727	Spruce Creek	10.2	88.8	98.9	897	1	center
		10.3	88.8	99.1	896	1	center
		9.8	87.9	97.7	899	1	rim
975842	Happy Creek	3.8	93.4	97.2	961	1	center
		3.9	93.6	97.5	960	1	rim
		3.6	93.0	96.6	962	1	rim
975629	Tiny Gulch	4.6	94.4	99.0	954	1	center
		0.3	97.9	98.2	997	1	rim
		4.2	94.5	98.7	957	2	center
975121	Bear Creek	8.4	88.9	97.3	914	1	center
		0.5	94.9	95.4	994	1	rim
		0.3	94.4	94.6	997	1	rim
Spruce Placer	Spruce Creek	6.0	93.2	99.3	939	1	rim
		5.9	95.2	101.1	942	1	center
		6.3	94.9	101.3	938	1	rim
	Bonanza Creek				893		placer average
	Tuluksak River				922		placer average
	Bear Creek				931		placer average

*Microprobe fineness data from this study; placer average data from Metz and Hawkins (1981).

3.6 Relationship of the Placer and Bedrock Gold

Maddren (1915) first postulated that the gold in Bear Creek was locally derived. This study used microprobe analysis to measure gold fineness from placer and bedrock in the study area to determine if the gold is truly locally derived and the extent of fineness variations.

A summary of gold fineness data is listed on Table 3.15. For placer grains the reported values are single measurements or averages from the center of the grain and bedrock values are the average of multiple measurements. More than one style of mineralization is present in the study area, so it is

conceivable that the gold fineness could be quite variable. Of the styles of mineralization classified bedrock gold fineness data exists for the Wallace occurrence, VABM Bonanza lobe and the high-T Cu-Au mineralization at the BCCA. These fineness values are 937, 875 and 913, respectively (Table 3.15). These three occurrences likely represent the same mineralization event; and the fineness variation depicts a typical natural range.

Table 3.15. Summarized table of all gold fineness data from the study area.

Sample	Location	fineness	type
975721	Bear Creek	914	placer grain
975727	Spruce Creek	897	placer grain
975842	Happy Creek	961	placer grain
Spruce Placer	Spruce Creek	940	placer grain
03ZW353	Bonanza Creek lobe (high-T, BCCA)	913	outcrop
03ZW369	Wallace occurence	937	outcrop
03ZW382	VABM Bonanza lobe	875	outcrop
	Bonanza Creek	893	placer average
	Tuluksak	922	placer average
	Bear Creek	931	placer average

* Microprobe analyses fineness values have analytical uncertainties of ~ +/- 5 parts/thousand. Microprobe fineness data from this study; placer average data from Metz and Hawkins (1981).

Interestingly, the high fineness gold from the Wallace occurrence (937) is essentially the same as a placer grain with attached tetradymite (940) taken from Spruce Creek. There may be a mineralogical link between Bi-Te minerals and associated high fineness gold in the district.

Placer grain sample 975727 and the Spruce placer sample are essentially outcrop values. The Spruce placer 940 fineness gold grain is attached to tetradymite, a very soft mineral (hardness of 1.5-2) with a perfect cleavage, which would be destroyed quickly in a stream environment. Sample 975727 finenesses were obtained from a placer specimen with gold enclosed in quartz.

Since the gold finenesses reported in Table 3.15 represent either unweathered gold from bedrock or the center of placer grains (unaffected by Ag-leaching), a direct comparison between Au-source and placer location can be made. Fineness of placer grains is both higher and lower than those from outcrop (Figure 3.18). Excluding sample 975842 the placer gold from the study area is all within error of the predicted bedrock fineness range. The highest placer fineness value (961) comes from a homogeneous, apparently unleached placer grain (Figure 3.17b). This sample comes from a small drainage (Happy Creek) and could not have traveled far. The most likely source for this gold is from the headwaters of Happy Creek (Figure 3.1), which is in Bonanza Pluton. The bulk average fineness of gold from Bonanza Creek is especially significant. Only approximately 1000 meters of Bonanza Creek were mined from its confluence

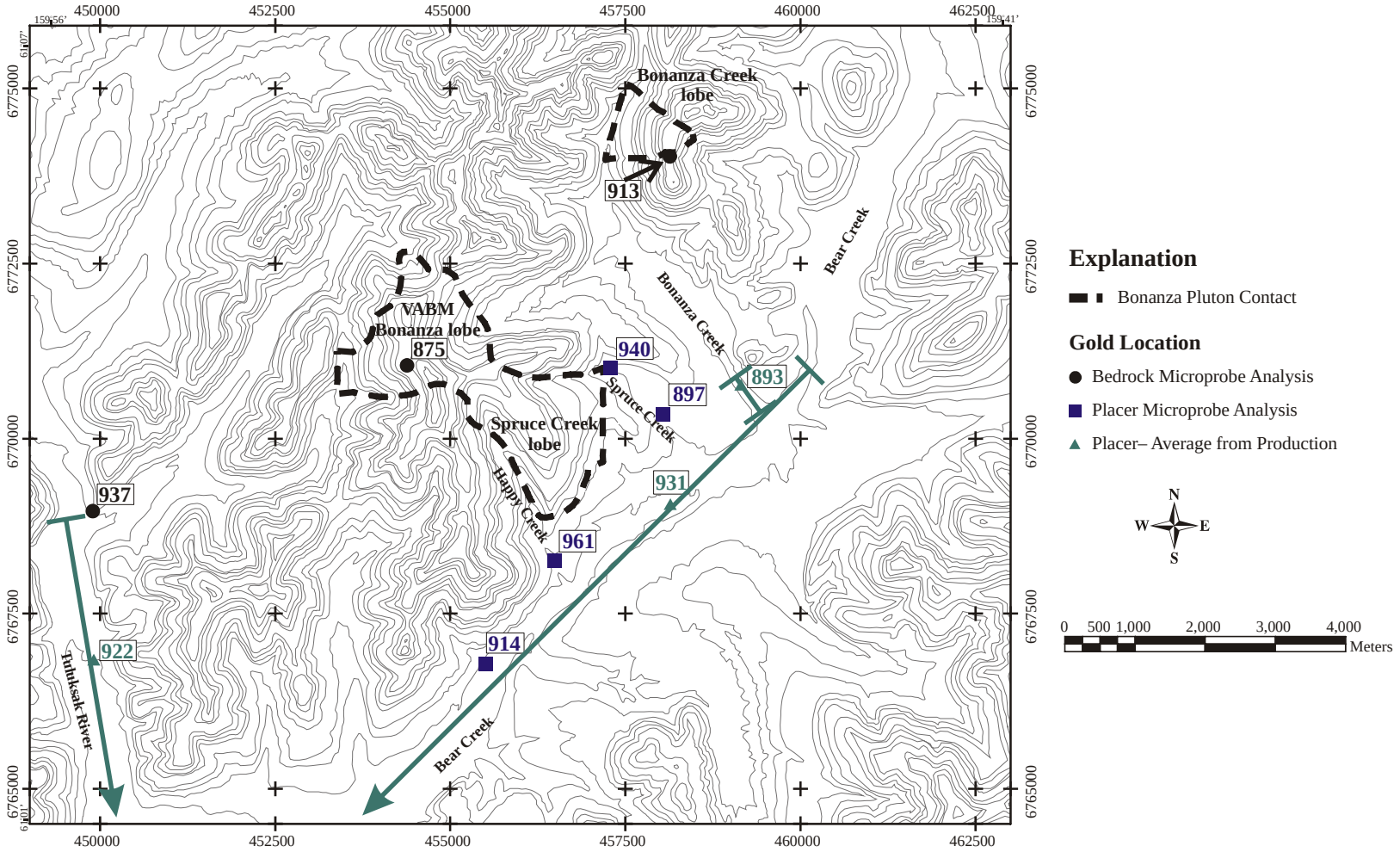

Figure 3.18: Map of sample location and gold fineness for bedrock, placer and production average. Line markers indicate the possible location for production average values.

with Bear Creek (Figure 3.1). The gold fineness average there reflects the fineness of a relatively small area. Upstream sources for this gold have high finesses (913) suggesting that this production average is possibly a mixture of low-T (lower fineness) and high-T (high fineness, 913) gold from the BCCA. The remaining bulk Au fineness values do not provide any direct evidence to provenance except that they are likely of local derivation. The highest and lowest placer grains with finesses of 915 (Bear Creek) and 961 (Happy Creek) indicate that a significant compositional range exists in the district. Beside the 961 fineness sample all of the other Au finenesses fall in the natural range of the mineralizing system and thus are clearly of local derivation.

3.7 Classification of Mineralization Style

Classification of the types of mineralization was characterized by principal component factor analysis (Davis, 2002). Factor analysis is a data reduction process that takes many variables (in this case element concentrations) and determines their correlations to one another. Factor analysis combines variables that correlate well with one another into a factor, hence this process thus reduces the number of variables. All rock samples that contained >200 ppb Au from the compiled data set (Gierymski and Werdon, 1997; J. Foley, written comm., 2004; and this study) were used to perform the analysis. Elements included in the analysis are Ag, As, Au, Bi, Cu, Hg, Pb, Sb and Zn. Figure 3.19 shows the statistical results of the factor analysis. The factor analysis identified three factors with eigen values greater than one, that explain 77% of the variance of the data. Elements that have high loading values for each factor indicate they correlate with one another. The three factors can be geologically classified as distal, proximal and epithermal style mineralization (Figure 3.19).

Factor 1 has high loading values for Pb-Ag-Zn-As-Sb. These elements have relatively high solubilities, particularly Pb, Zn and Sb, and thus do not precipitate as readily as Au or Bi. Therefore factor 1 is called a distal mineralization factor because these elements and the minerals they form are typically found distal to the mineralizing source. This type of mineralization in the Nyac area is often found in fault breccia.

Factor 2 has high loading values for Bi, Au, Cu and Ag. Wood et al. (1987) found Bi has a lower solubility than Ag, Pb, Zn and Sb and thus precipitates near the hydrothermal source. Therefore, factor 2 is called the proximal mineralization factor.

Factor 3 has high loadings for Au and Hg. Hg mineralization is commonly associated with low temperature hydrothermal systems. Since Hg is a significant attribute to this type of mineralization, factor 3 is classified as an epithermal mineralization factor.

Figure 3.20 shows the location and dominant geologic factor for the 41 samples at each of the three anomalous gold occurrences: the Wallace occurrence, VABM Bonanza lobe and the BCCA. The Wallace occurrence and VABM Bonanza lobe are characterized by proximal mineralization. The BCCA contains both proximal and epithermal style mineralization.

The end result of the factor analysis shows that mineralization at VABM Bonanza lobe, the Wallace Occurrence and Bi-Au mineralization at the BCCA are similar geochemically and thus likely represent similar origins. The low-T type mineralization at the BCCA anomaly and a few scattered locations throughout the study area are classified as epithermal type mineralization.

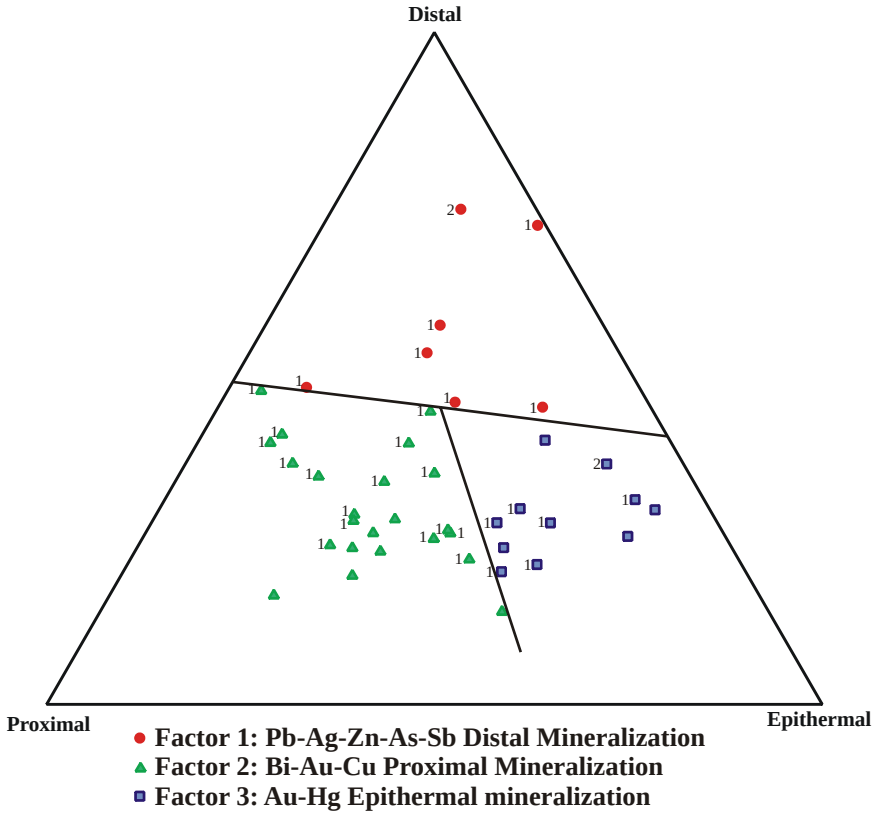

Figure 3.19: Triangular plot of mineralization factors. Diagram illustrates three types of mineralization in the study area: distal mineralization, proximal mineralization, and epithermal mineralization. Data are from this study, (1) Gierymski and Werdon (1997), and (2) J. Foley, written comm. (2004).

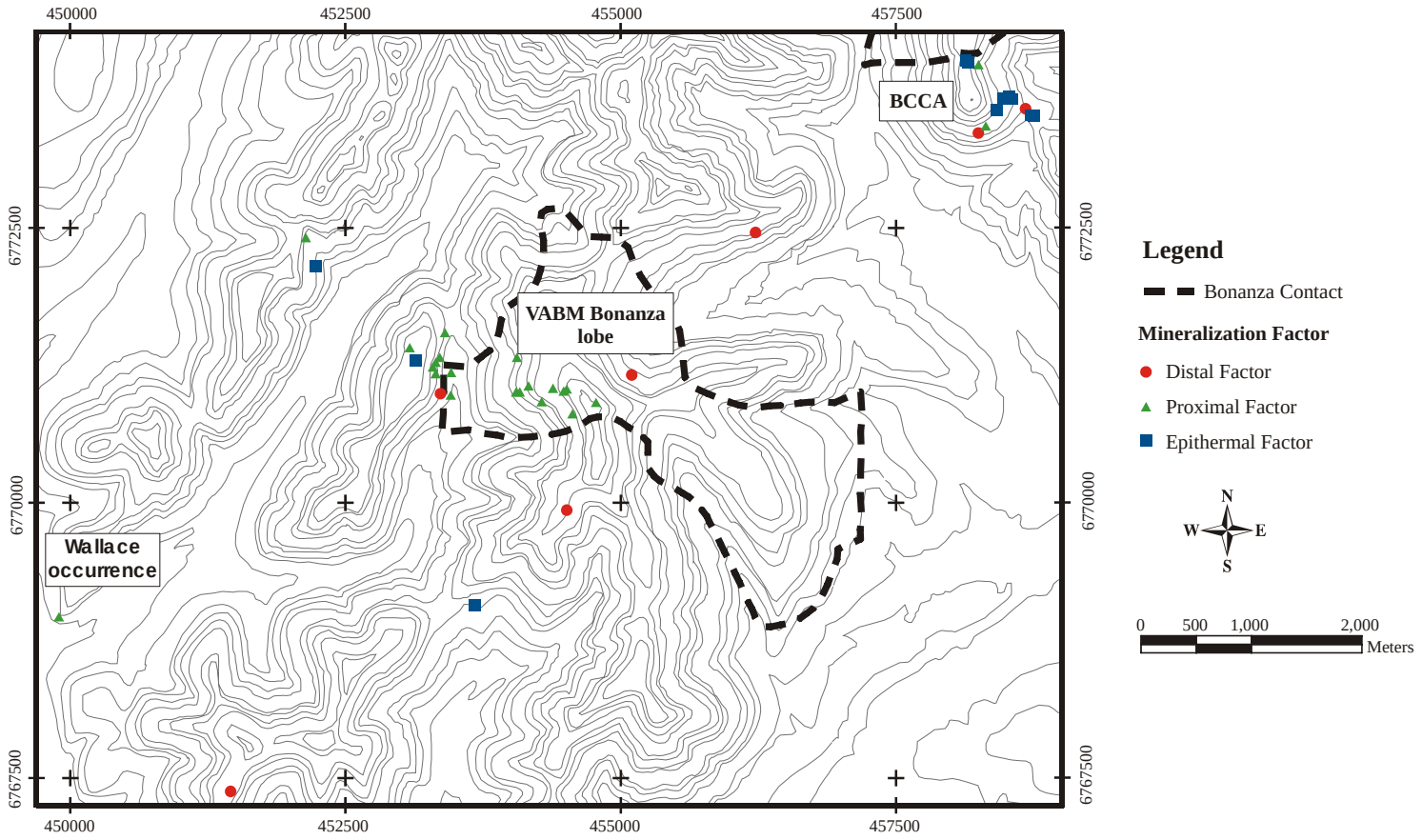

Figure 3.20: Map of samples with Au concentrations >200 ppb and their factor classification.

4. Geochronology

The Nyac terrane contains a tremendous number of plutonic bodies and dikes that intrude the Jurassic volcano-sedimentary rock package. Because textural variations and chemistry can vary significantly in a single pluton or series of dikes, other criteria must be to group the different igneous bodies. The most definitive way to accomplish this is by isotope geochronology.

Previously dated igneous bodies from the Nyac terrane are Early Cretaceous ages (Box et al., 1993; Robinson and Decker, 1986; and Wilson, 1977). Most of the plutonic complexes in SW Alaska have ages of Late Cretaceous and early Tertiary (Bundtzen and Miller, 1997). Previous determinations from the Nyac terrane have large analytical uncertainties ($\pm$ 5 Ma), and were obtained by K-Ar and U-Pb methods. Ages for this study were determined by $^{40}Ar/^{39}Ar$ laser step-heating of a mineral separate or whole rock chip (York et al., 1981; Layer et al.; 1987; and Layer 2000).

This technique is based on the ratio of ^{40}Ar to ^{39}Ar. Samples are irridated in a reactor to produce ^{39}Ar from ^{39}K. The ratio of ^{40}Ar to ^{39}Ar increases with the age of the rock. Because Ar is a gas, it diffuses from and into minerals, especially at high temperatures. Different minerals have different temperatures at which the mineral retains Ar called the closure temperature. The three minerals measured in this study are hornblende, muscovite and biotite. These minerals have closure temperatures of approximately 450, 350 and 300 ^{o} C, respectively (McDougall and Harrison, 1988). After the mineral cools to its closure temperature it has locked a finite amount of ^{40}K into its crystal lattice. The radiogenic ^{40}K decays into ^{40}Ar. The $^{40}Ar/^{39}Ar$ method requires using a standard irridated under the same conditions as the samples to determine the age. The step heating technique results in an age spectrum. The age spectrum is a series of steps (increasing temperature with each step). The Ar released at a given step yields an apparent age. Consecutive steps produce an age spectra. A weighted average of all steps is equivalent to a K-Ar date. Three consecutive steps that account for >60% of argon released within $\pm 2\sigma$ of one another define a plateau. A plateau gives the most reliable age.

The $^{40}Ar/^{39}Ar$ laser step-heating technique provides insight into the thermal history of the material dated. Two different geologic processes can affect a mineral's Ar concentration: reset heating and argon addition. After a mineral cools below its closure temperature and is reheated, raising the temperature above the mineral's closure temperature, Ar is lost by diffusion out of the mineral. Ar can be added to a mineral by remobilization of Ar in a hydrothermal system and depositing Ar into the mineral. In both cases a K-Ar age will be erroneous. The $^{40}Ar/^{39}Ar$ laser step-heating technique step releases Ar from increasingly tightly held sites; at higher temperatures the Ar released comes from the most tightly held sites. This is advantageous because alteration typically occurs on the outside portion of a crystal grain. In such a case, the first few heating steps can be ignored due to Ar loss, while Ar released at higher temperature gives the closure age of the mineral.

In addition to the $^{40}Ar/^{39}Ar$ age spectrum this method also provides atomic Ca/K and Cl/K spectra through reactor-produced ^{37}Ar from ^{40}Ca and ^{38}Ar from ^{35}Cl. These spectra are useful in determining the composition of the mineral that released Ar at each of the heating steps. Table 4.1 shows typical atomic Ca/K and Cl/K ratios for the minerals of interest.

Table 4.1: Typical atomic Ca/K and Cl/ K ratio ranges for dated minerals. Pyroxene and hornblende data is from Deer et al. (1997a and 1997b) and biotite and muscovite data is from Middelaar and Keith (1990).

Mineral	Ca/K	Cl/K
Muscovite	.001-.002	[.001]-.006
Biotite	.001-.005	.005-.016
Hornblende	4.8-76	.01-.21
Pyroxene	45->300	[.02-.1]

* Bracketed values used .0025 for Cl %.

Previous K-Ar and U-Pb data will not be discussed because those techniques do not offer means of assessing Ar or Pb loss or gain, whereas the $^{40}Ar/^{39}Ar$ spectra approach will. In one case the biotite K-Ar age is older than the hornblende age from a sample taken from the Nyac batholith. Hornblende has a higher closure temperature and it should yield an older age than biotite from the same sample. Opposite results (as in this case) indicates open system behavior in the K-Ar data or serious analytical uncertainties.

The following presents interpretations for the different $^{40}Ar/^{39}Ar$, Ca/K and Cl/K age spectra.

4.1 Sample Selection

A large number of rock types exist in the study area, samples selected for this study include: metabasalts in the metavolcanic rock unit, Nyac batholith, Spruce Creek lobe, Bonanza Creek lobe, grey dike and red dike. Besides the fossil age in the metavolcanic rocks no other dates exist for the volcanic rocks. Although radiometric ages already existed for the Nyac batholith the previous data had associated large errors, were measured by less precise methods and the biotite ages are older than the hornblende indicating that the methods used were not producing correct ages. Both the Spruce creek and Bonanza creek lobes of the Bonanza Pluton were dated to determine whether they are the same age as the VABM Bonanza lobe. Since significant mineralization is hosted in the gray dikes, it is important to determine their age to indicate their relationship to any of the plutons. Muscovite from a mineralized red dike was dated to determine the age of epithermal mineralization from the BCCA.

Placer Dome previously submitted three samples to the UAF Geochronology lab for $^{40}Ar/^{39}Ar$ dating, and these data were made available for this thesis. These samples include a biotite age from VABM

Bonanza lobe, a muscovite age from VABM Bonanza alteration and a biotite age from the red dike. Interpretation of those ages will be included in this chapter. Locations for all of the dated samples are illustrated in Figure 4.1. The age data are tabulated on Table 4.2.

4.2 Volcanic Rock Ages

While mapping in the field, an area of apparently unaltered basalts were identified. It appeared that these basalts might represent post-Cretaceous magmatism. In thin section the basalt is weakly altered, but otherwise unmetamorphosed. The groundmass is composed of fine-grained plagioclase and pyroxene. Phenocrysts include pyroxene and plagioclase. The pyroxene crystals have a small rim of chlorite-epidote alteration along their rims. Two samples of basalt rock chips (03ZW232) were analyzed. The age spectra (Figures 4.2, 4.3) are complex and show that basalt is reset at ~119 Ma, but a high Ca phase, presumably pyroxene, preserves an older age as a pseudo-plateau. The best eruption age is the variance-averaged results of the two pseudo-plateaus, of 180 ± 7 Ma. These two pseudoplateaus only account for 23.1% and 24.2% of the total Ar released and thus only serve as a minimum estimate of the original age. The reset pseudo-plateaus account for 45.9% and 56.5% of the total Ar released. The best age for reset is the variance-averaged results of these pseudo-plateaus, 119 ± 3 Ma.

4.3 Plutonic Rock Ages

The plutonic rocks can be divided into two different age suites: the Nyac batholith and Bonanza pluton group. Most of the mineral separates contain inclusions of other minerals and such inclusions can have a dramatic effect on the age spectrum. There are two characteristics found in nearly all of the plutonic rock age spectra. First, most of the age spectra display Ar gain followed by Ar loss. The Ar loss is likely attributed to alteration during a younger event, which will be described in greater detail later in this chapter. The Ar gain is extraneous Ar normally concordant with the biotite phase. Biotite has a lower closure temperature than other phases (in particular hornblende), and as a pluton cools Ar from other phases is released. If biotite has not yet reached its closure temperature it can take the released Ar into its crystal lattice. The extraneous Ar contributed by this process will result in a hump in the age spectrum and result in an erroneously old age. The second characteristic has to do with initial high Ca/K and/or Cl/K ratios for most of the spectra. The initial high Ca/K ratios are the result of alteration of biotite and hornblende to epidote and/or calcite. The initial high Cl/K ratios are likely the result of Cl released from inclusions.

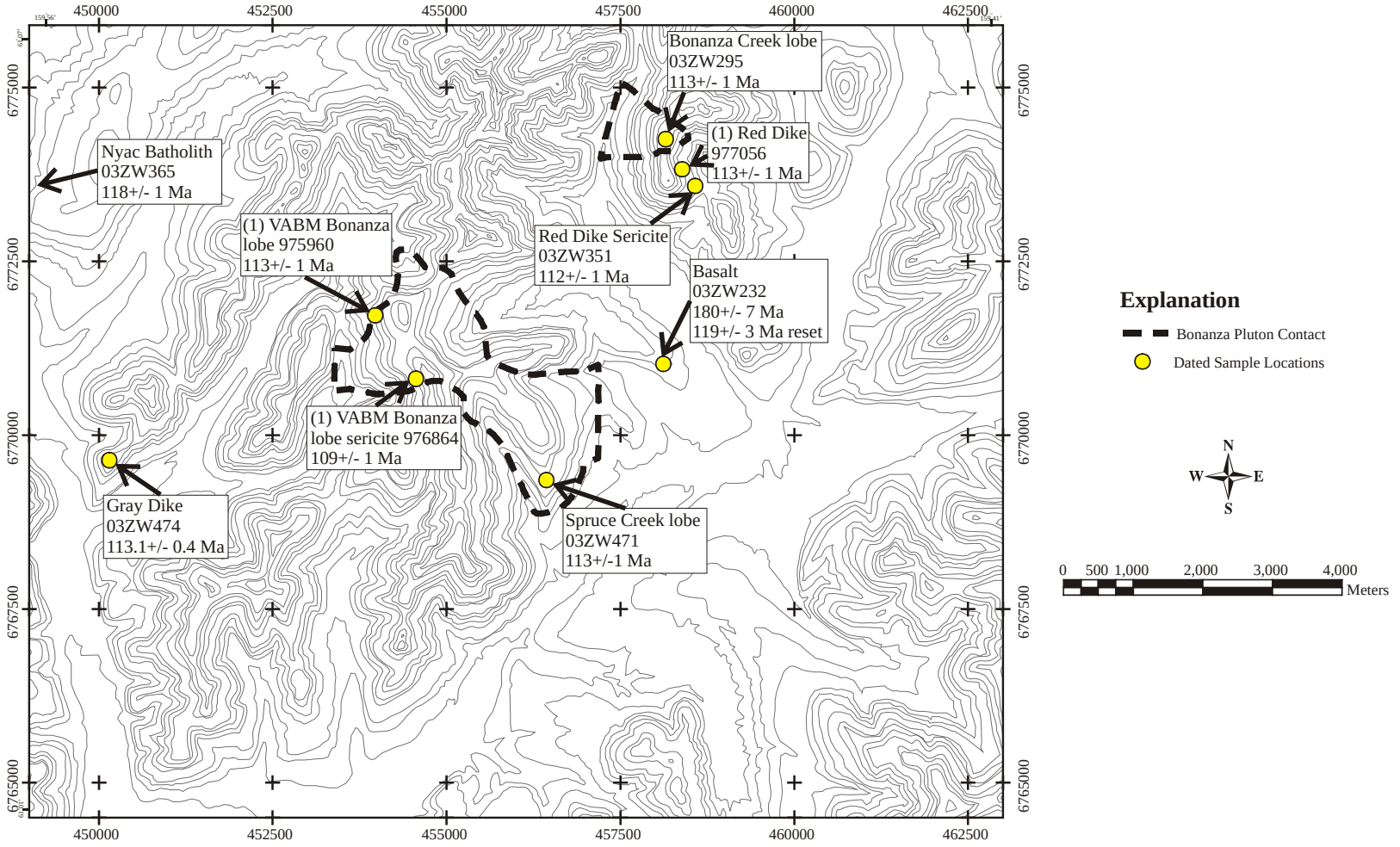

Figure 4.1: Map of sample location for all rock ages. Listed ages are best estimate. Data are from this study and (1) Gierymski and Werdon (1997). See Table 4.2.

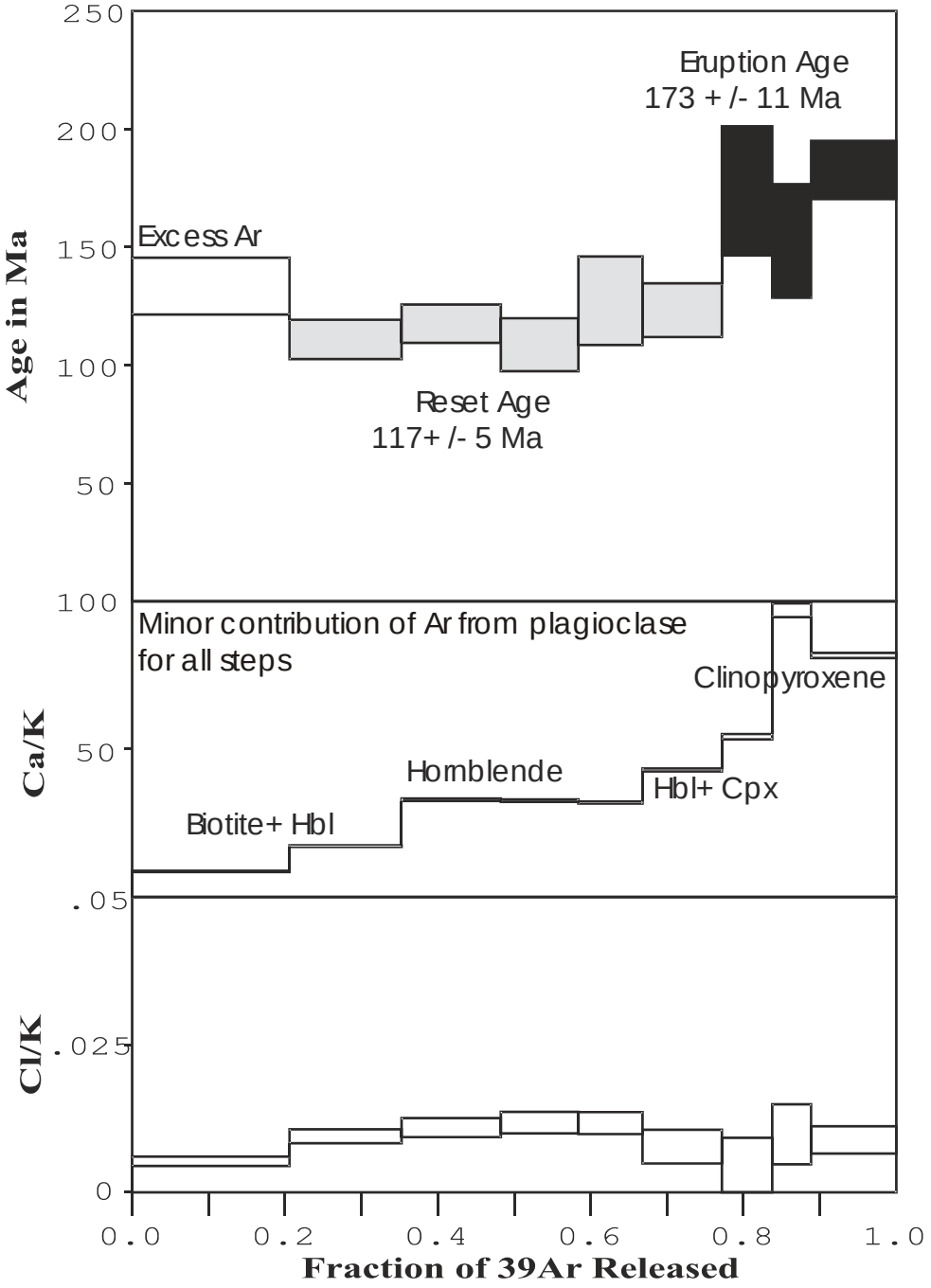

Figure 4.2: Age, Ca/K and Cl/K spectrum diagram for whole rock basalt sample 03ZW232. Age spectrum depicts two pseudo-plateaus, an original age (black steps) and a reset age (grey steps). A high calcium phase (pyroxene and/or plagioclase?) has retained the initial Ar concentration in the basalt.

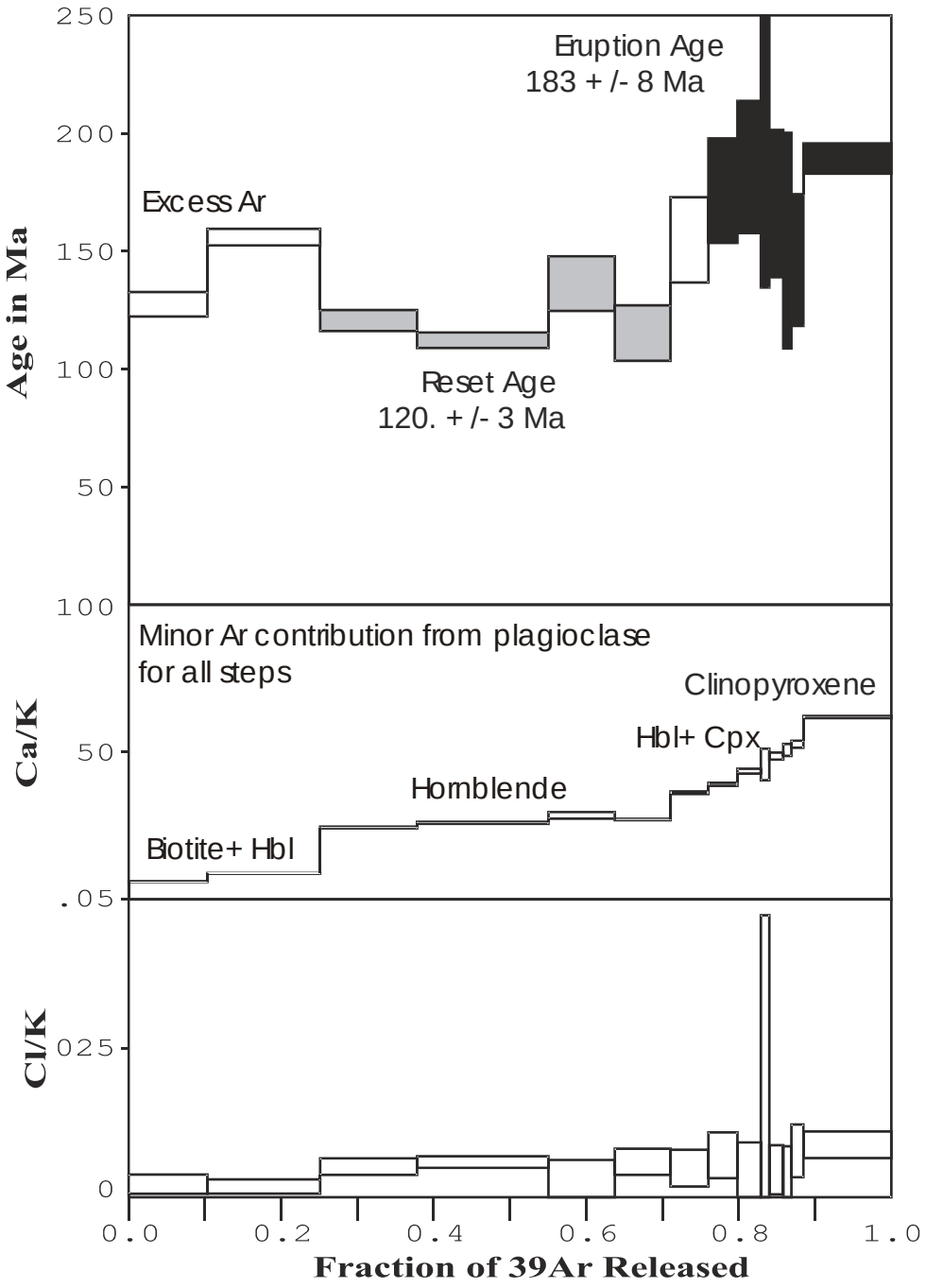

Figure 4.3: Age, Ca/K and Cl/K spectrum diagram for the second whole rock basalt sample 03ZW232. Age spectrum depicts two pseudo-plateaus, an original age (black steps) and a reset age (grey steps). A high calcium phase (pyroxene and/or plagioclase) has retained the initial Ar concentration in the basalt.

Table 4.2: Abbreviated $^{40}Ar/^{39}Ar$ age data for all dated samples.

Sample	Location	Rock Type	Mineral	Integrated Age (Ma)	Plateau Age (Ma)	# Fractions	% 39Ar	MSWD	Best Age (Ma)
03ZW232	Spruce Ck A	Basalt	WR	133.3+/ 4.6	173.4+/- 11.3	3	23.1	0.66	180+/- 7
03ZW232	Spruce Ck B	Basalt	WR	142.9+/- 2.8	182.8+/- 8.2	7	24.2	0.61	
03ZW232	Spruce Ck A	Basalt	WR	133.3+/ 4.6	116.8+/- 4.9	5	56.5	0.42	119+/- 3
03ZW232	Spruce Ck B	Basalt	WR	142.9+/- 2.8	119.6+/- 3.4	4	45.9	2.42	
03ZW295	Bonanza Ck	QtzMzDi	B	110.6+/- 0.5	111.0+/- 0.5	10	97.6	0.75	
03ZW295	Bonanza Ck	QtzMzDi	H	112.8+/- 0.8	113.4+/- 0.8	8	95.1	0.79	~113
03ZW365	Nyac Batholith	Grd	B	110.7+/- 0.4	113.2+/- 0.4	9	96.7	9.49	
03ZW365	Nyac Batholith	Grd	B	111.3+/- 0.4	113.3+/- 0.4	8	94.2	5.83	
03ZW365	Nyac Batholith	Grd	B	112.1+/- 0.4	116.3+/- 0.4	5	79	0.59	
03ZW365	Nyac Batholith	Grd	H	109.8+/- 0.8	112.7+/- 1.0	3	69.2	0.9	
03ZW365	Nyac Batholith	Grd	H	105.8+/- 4.5	117.8+/- 0.7	3	76.1	0.28	118+/- 1
03ZW471	Spruce Ck	QtzMzDi	B	110.9+/- 0.4	111.0+/- 0.4	6	80.3	0.36	
03ZW471	Spruce Ck	QtzMzDi	H	114.2+/- 0.6	115.1+/- 0.8	6	65.9	0.93	113+/- 1
03ZW474	Wallace	Grd Dike	B	98.6+/- 1.1	109.1+/- 1.2	7	81.7	10.1	
03ZW474	Wallace	Grd Dike	B	112.8+/- 0.5					
03ZW474	Wallace	Grd Dike	H	112.2+/- 0.8	113.5+/- 0.7	8	95.6	3.83	113.1+/- 0.4
03ZW474	Wallace	Grd Dike	H	110.2+/- 0.8	112.5+/- 0.8	3	90.1	0.78	
975960	VABM	Grd	B	108.5+/- 0.5	108.8+/- 0.5	8	61.3	2.43	~113
976864	VABM	Grd	M	109.4+/- 0.9	109.2+/-1.2	6	68.9	0.21	~111
977056	BCCA	QtzMz Dike	B	110.4+/- 0.5	111.2+/- 0.5	9	81.8	1.11	~113
03ZW351	BCCA	QtzMz Dike	M	112.1+/-0.6	111.9+/-0.6	6	80	0.5	112+/-1

4.3.1 Nyac Batholith

Two hornblende and three biotite separates were dated from a granodiorite sample (03ZW365) from the Nyac batholith. Of the two hornblende age spectra, the second yields the most precise age (Figure 4.4). The Ca/K ratio for the first split (Figure 4.5) is low throughout the spectrum and gradually increases. I interpreted this to indicate that the hornblende from the first analysis have a significant amount of biotite inclusions. In thin section some of the hornblendes have obvious biotite inclusions. Since biotite has an order of magnitude more K than hornblende, the biotite age will dominate the age spectrum and will not yield an accurate hornblende age. The second split yielded a higher Ca/K ratio and represents the best hornblende age for the pluton. Of the three biotites analyzed, the first two analyses exhibit age spectra that gradually step to a peak and then decline from the peak (Figures 4.6 and 4.7). The peak is likely the closure age of the biotite and the decreased values represent diffusion of Ar out of the crystal from alteration. The third biotite split produced an age spectrum without a hump (Figure 4.8). The third split yields the best

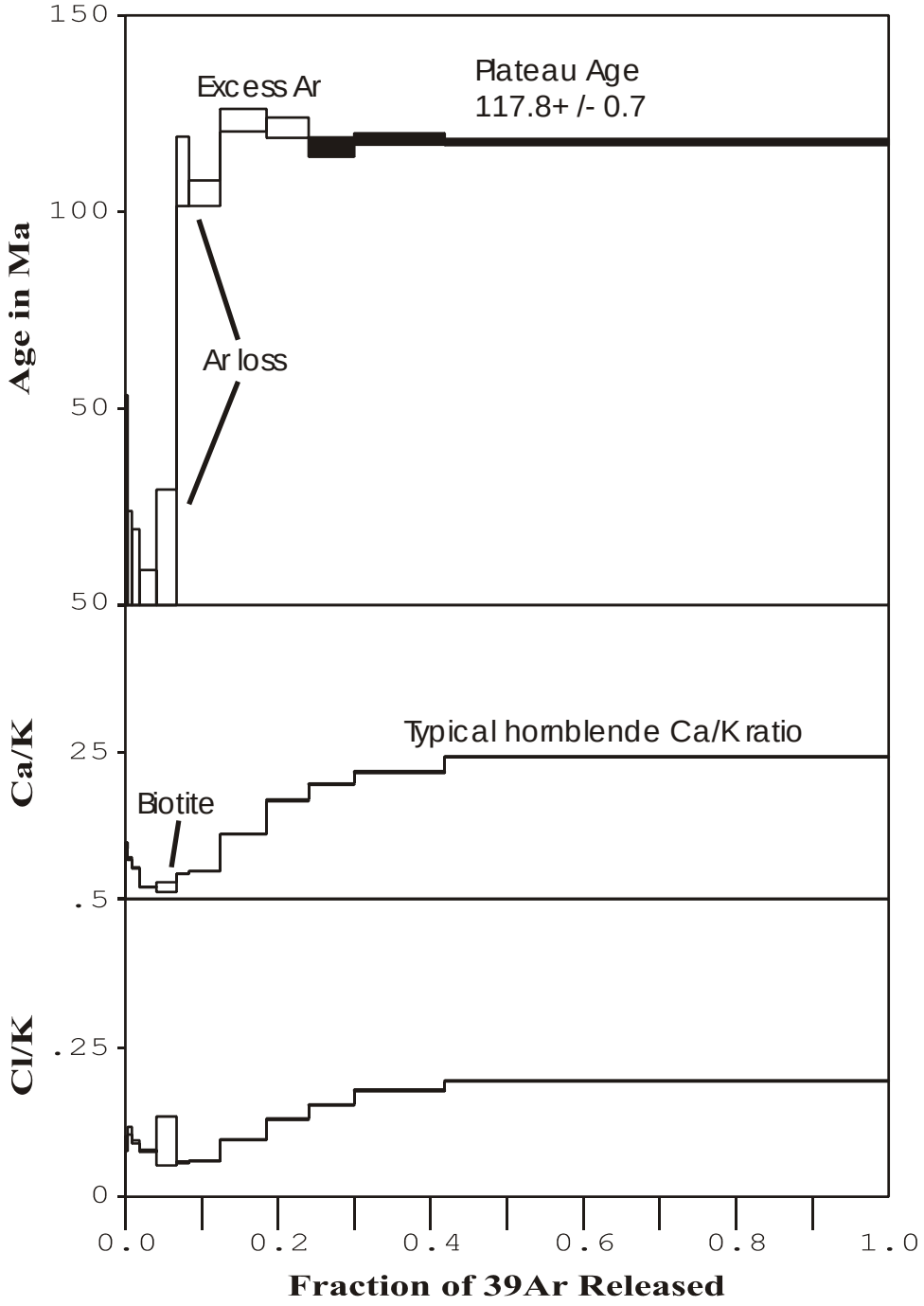

Figure 4.4: Age, Ca/K and Cl/K spectra for hornblende from the Nyac batholith (03ZW365). Despite the majority of the Ar being released in one step, the Ca/K spectrum is typical of a hornblende composition.

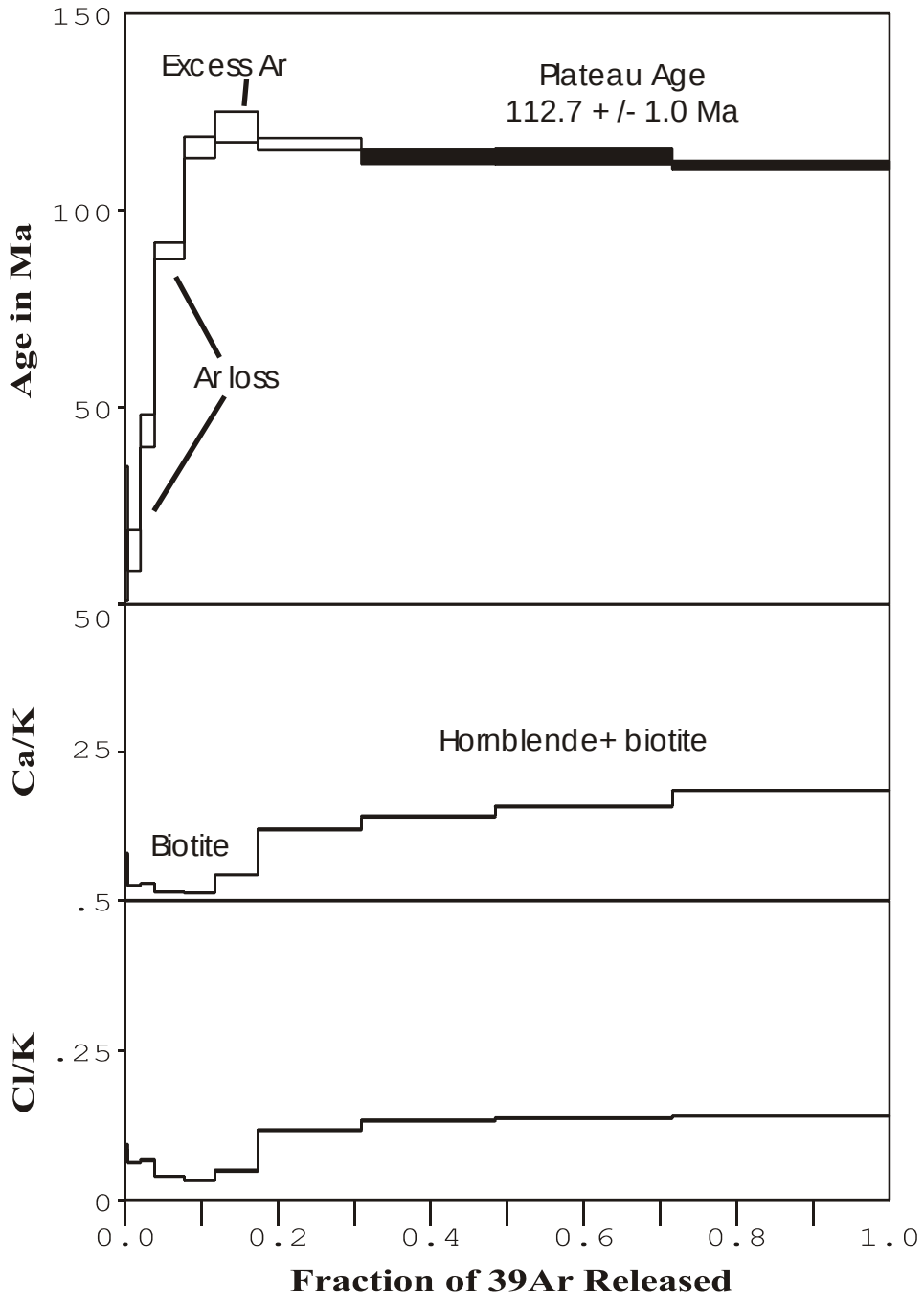

Figure 4.5: Age, Ca/K and Cl/K spectrum diagram for hornblende from the Nyac batholith (03ZW365). The Ca/K spectrum gradually steps up and never reaches a Ca/K ratio higher than the first (03ZW365) hornblende sample.

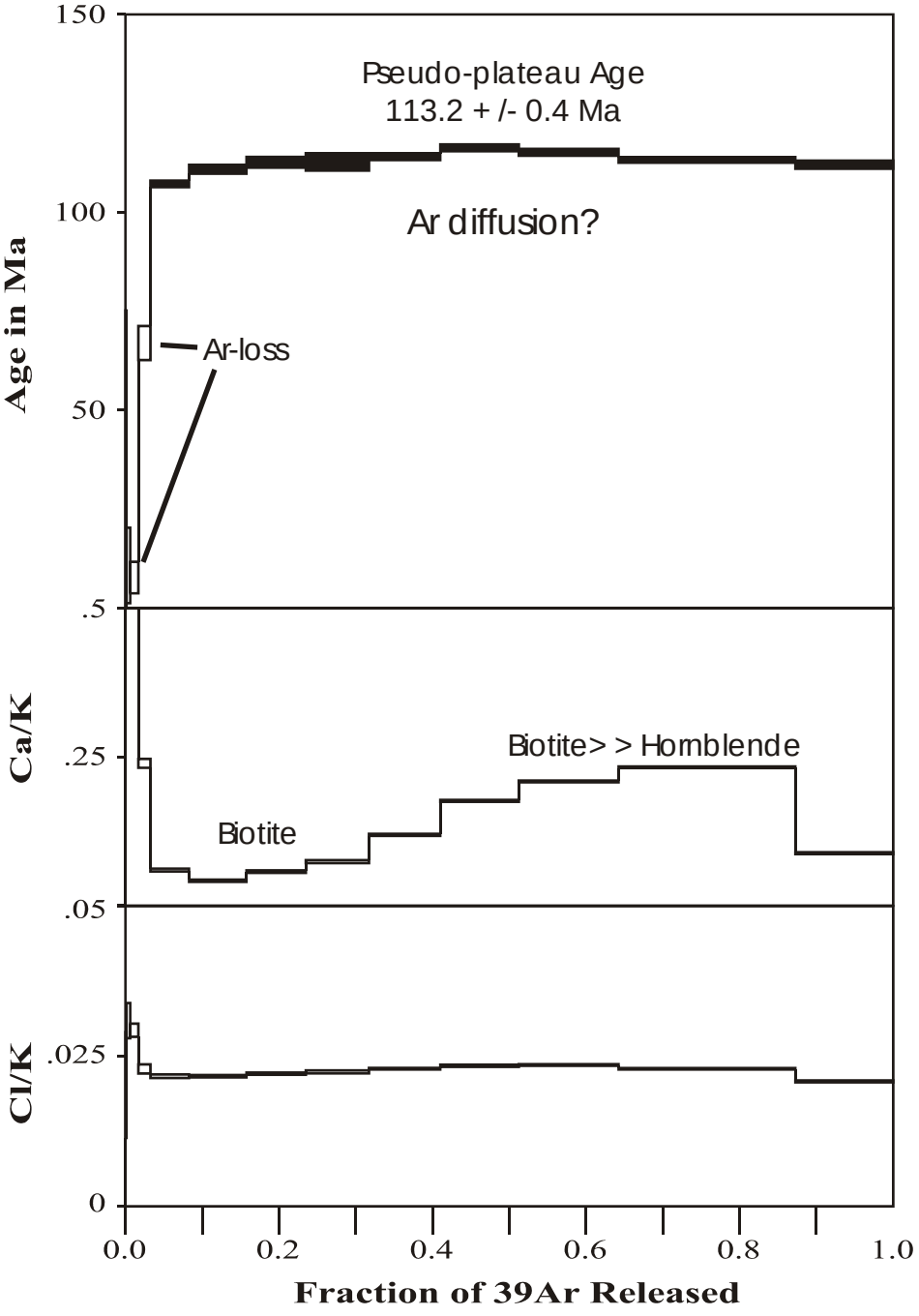

Figure 4.6: Age, Ca/K and Cl/K spectrum diagram for biotite from the Nyac batholith (03ZW365). The age spectrum exhibits a convex shape indicating Ar loss by diffusion.

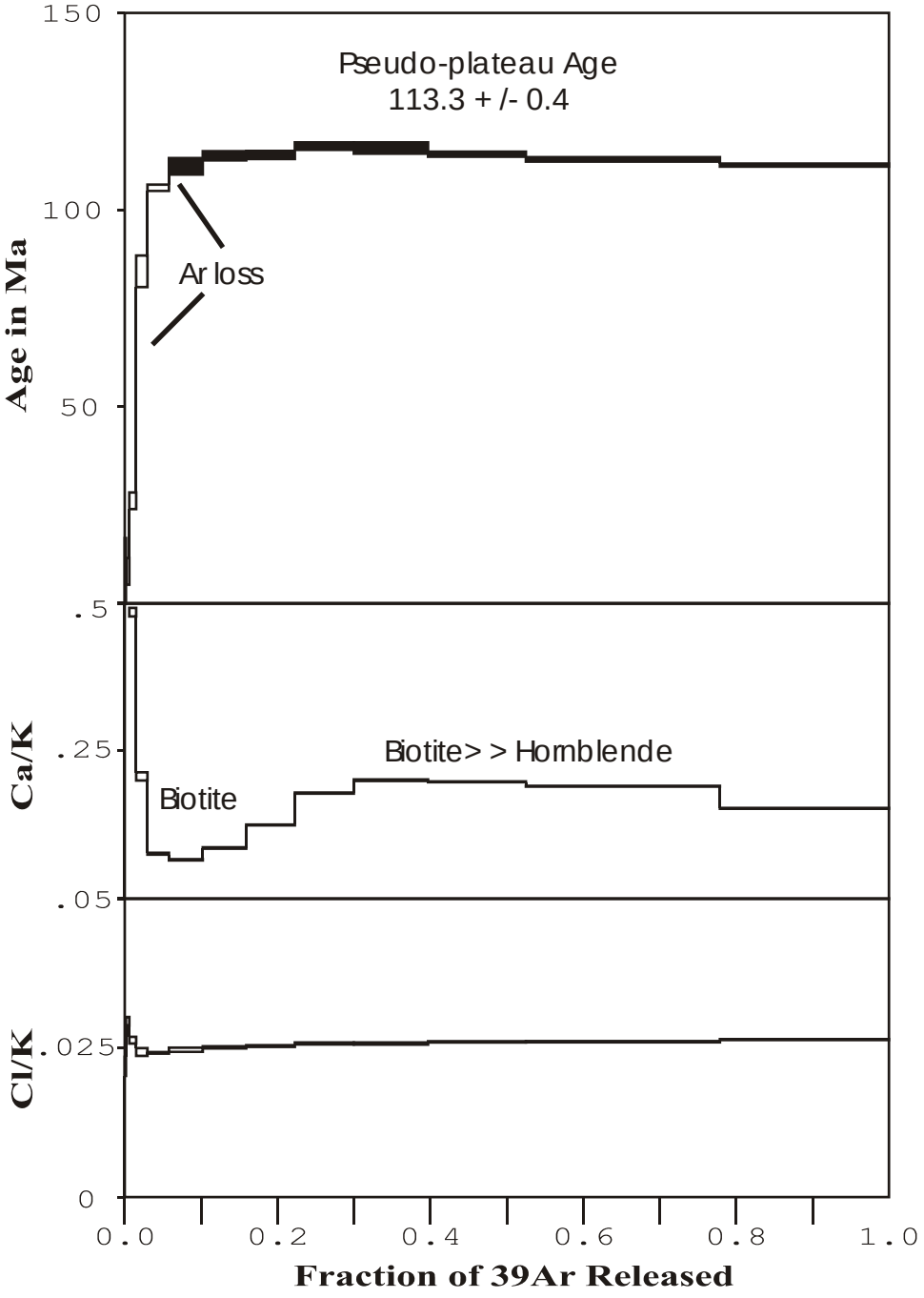

Figure 4.7: Age, Ca/K and Cl/K spectrum diagram for biotite from the Nyac batholith (03ZW365). The age spectrum exhibits a convex shape indicating Ar loss or Ar recoil.

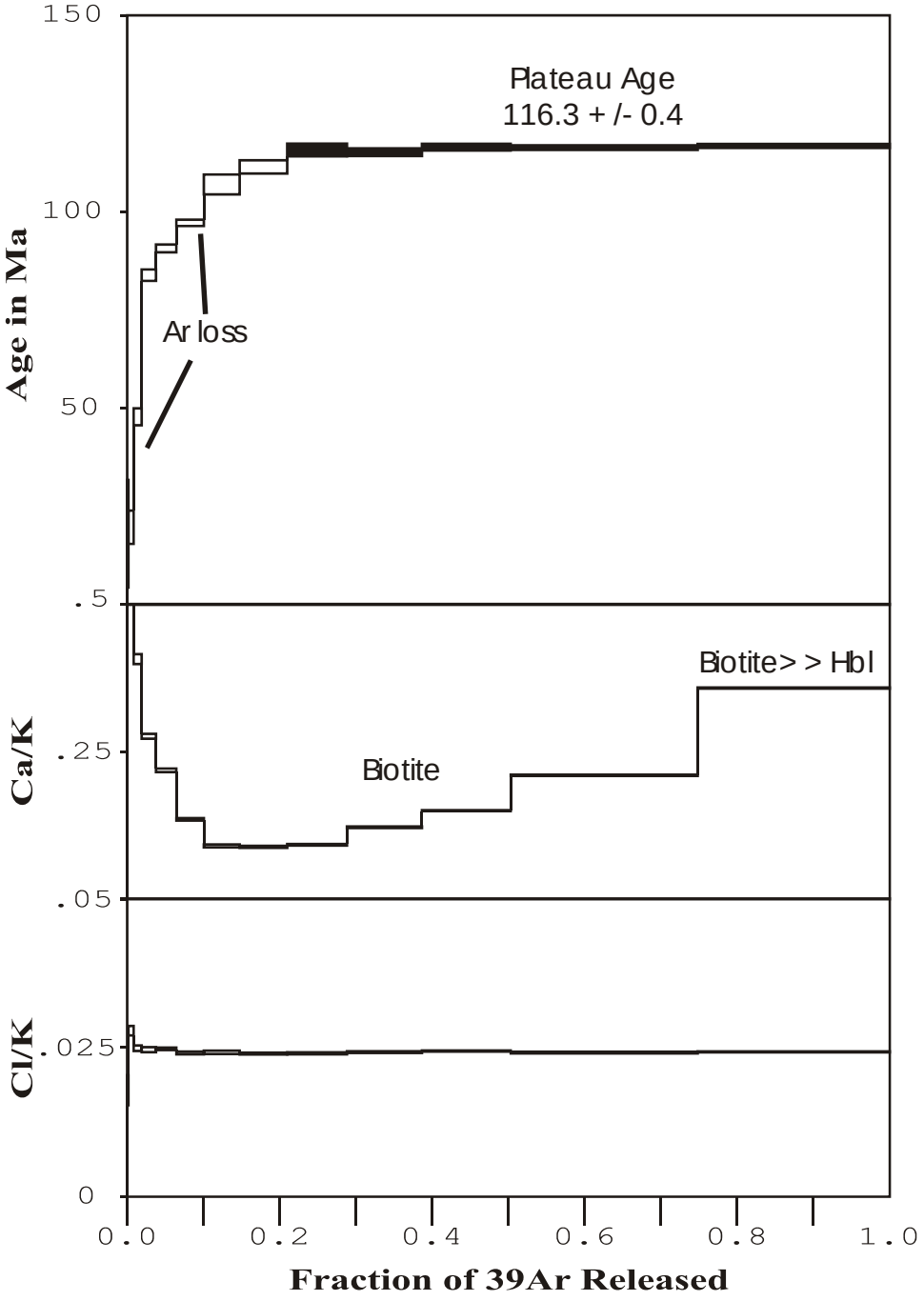

Figure 4.8: Age, Ca/K and Cl/K spectrum diagram for biotite from the Nyac batholith (03ZW365). The age spectrum levels out into a true plateau and gives the best biotite age for the Nyac batholith.

biotite age for the Nyac batholith since it levels into a true plateau. All of the biotite Ca/K and Cl/K spectra display ratios expected for biotite.

The most precise hornblende and biotite analyses from the Nyac batholith record ages of 117.8 ± 0.7 and 116.3 ± 0.4 Ma, respectively. Both of the age spectra level off into flat plateaus accounting for more than 75% of the total argon released and have plateau MSWDs of less than 0.6. Although, approximately 60% of the ^{39}Ar for the first hornblende analysis was released in a single step, the Ca/K ratio remained high, indicating that the hornblende crystal is homogenous. Since hornblende traps Ar at much higher temperatures than biotite, the best estimate for emplacement of the Nyac batholith is 118 ± 1 Ma.

4.3.2 Bonanza Creek Lobe

One hornblende and one biotite separate were dated from a quartz diorite sample (03ZW295) from the Bonanza Creek lobe. In thin section hornblende, pyroxene and biotite are generally separate from one another. The Ca/K spectra for the hornblende and biotite (Figures 4.9 and 4.10) indicate the samples analyzed were nearly pure. Some, often high temperature, Ar released from the biotite sample reveals high Ca/K ratios (Figure 4.10), which likely represent small inclusions of hornblende.

The hornblende and biotite dates from the Bonanza Creek lobe yield ages of 113.4 ± 0.8 and 111.0 ± 0.5 Ma, respectively (Figures 4.9 and 4.10). Both age plateaus account for over 95% of the total Ar released and have MSWD less than 0.8. The best estimate emplacement age for the Bonanza Creek lobe is 113 ± 1 Ma.

4.3.3 VABM Bonanza Lobe

One biotite and one muscovite separate were dated from theVABM Bonanza lobe. The biotite came from a least altered portion of the pluton. In thin section the biotites are unaltered. The muscovite sample was taken from a gold mineralized quartz vein (Gierymski and Werdon, 1997).

The biotite (Figure 4.11) and muscovite (Figure 4.12) samples from VABM Bonanza lobe yield ages of 109.0 ± 0.5 and 110.9 ± 0.7 Ma, respectively. The muscovite Ca/K spectrum has unusually high values, most likely due to remnant plagioclase inclusions in the sericite. Both of the age spectra level off into flat plateaus accounting for more than 70% of the total argon released and have plateau MSWDs of less than 0.6. Since no hornblende age exists for VABM Bonanza Pluton the best estimate for emplacement is ~111 Ma (the estimated age is 2 Ma older than the biotite age, consistent with the Bonanza Creek lobe). The best age for the muscovite and thus the age of mineralization is also ~111 Ma. The older age for the muscovite is not necessarily due to being older, but from having a higher closure temperature than biotite.

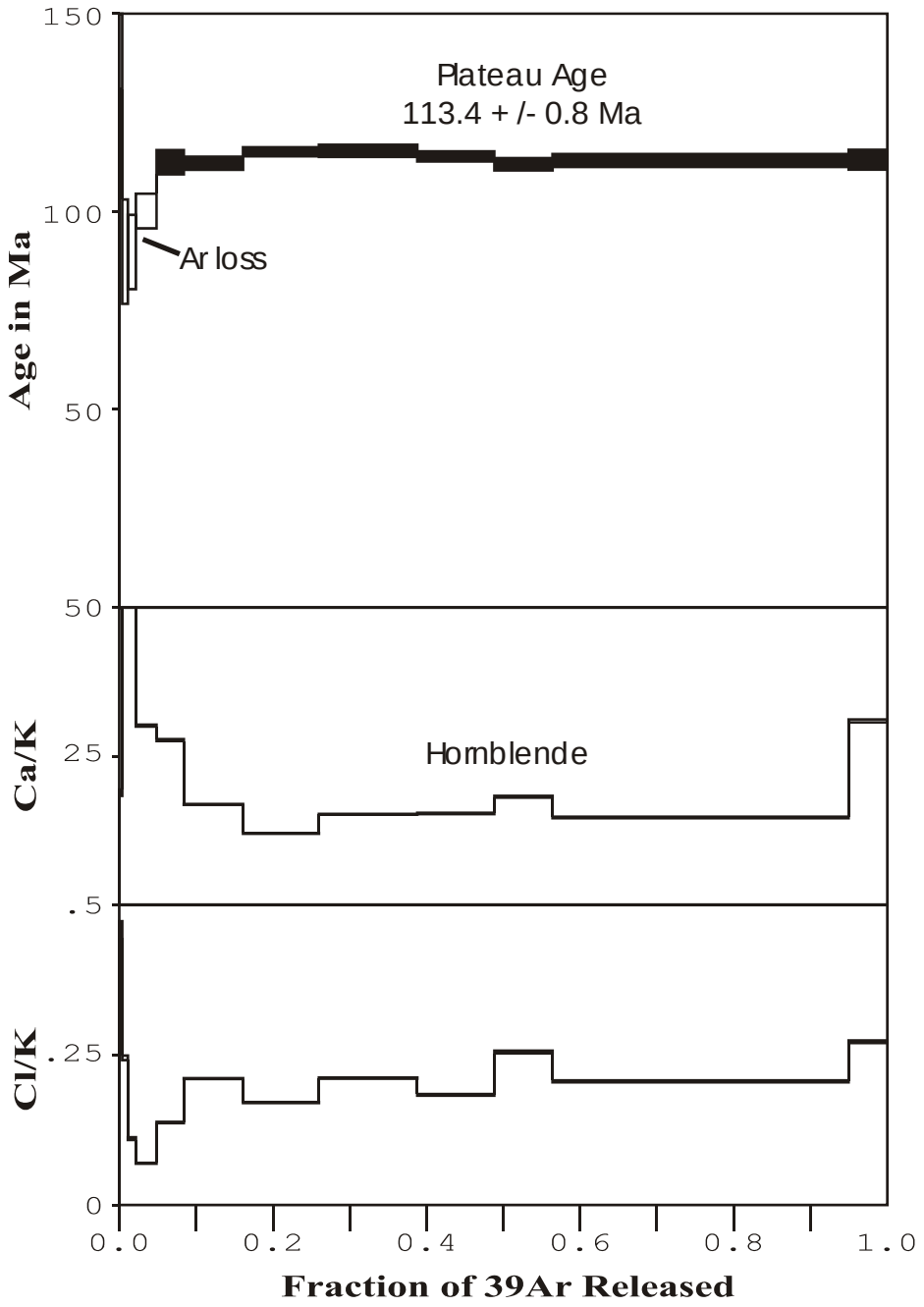

Figure 4.9: Age, Ca/K and Cl/K spectrum diagram for hornblende from the Bonanza Creek lobe (03ZW295).

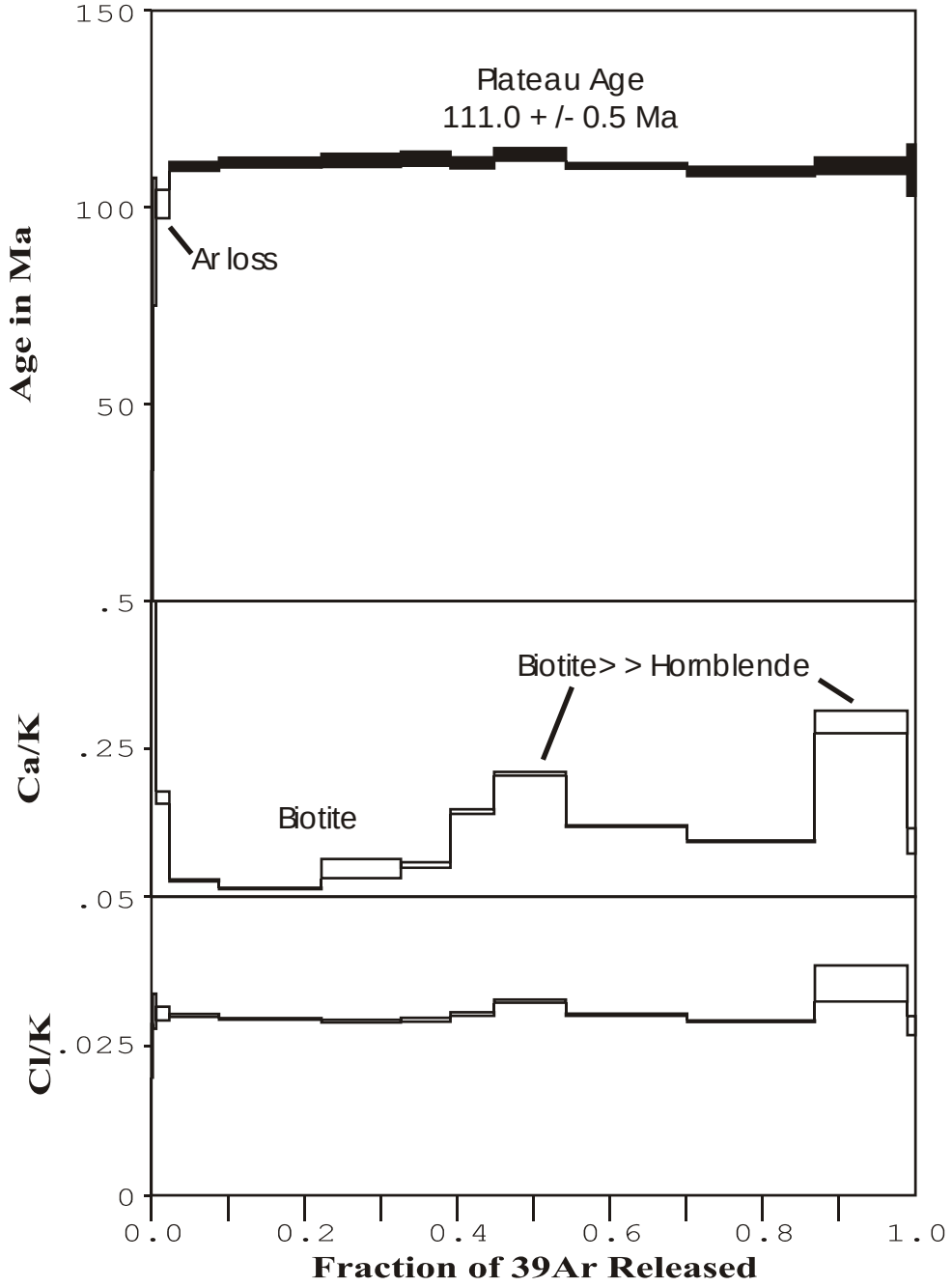

Figure 4.10: Age, Ca/K and Cl/K spectrum diagram for biotite from the Bonanza Creek lobe (03ZW295).

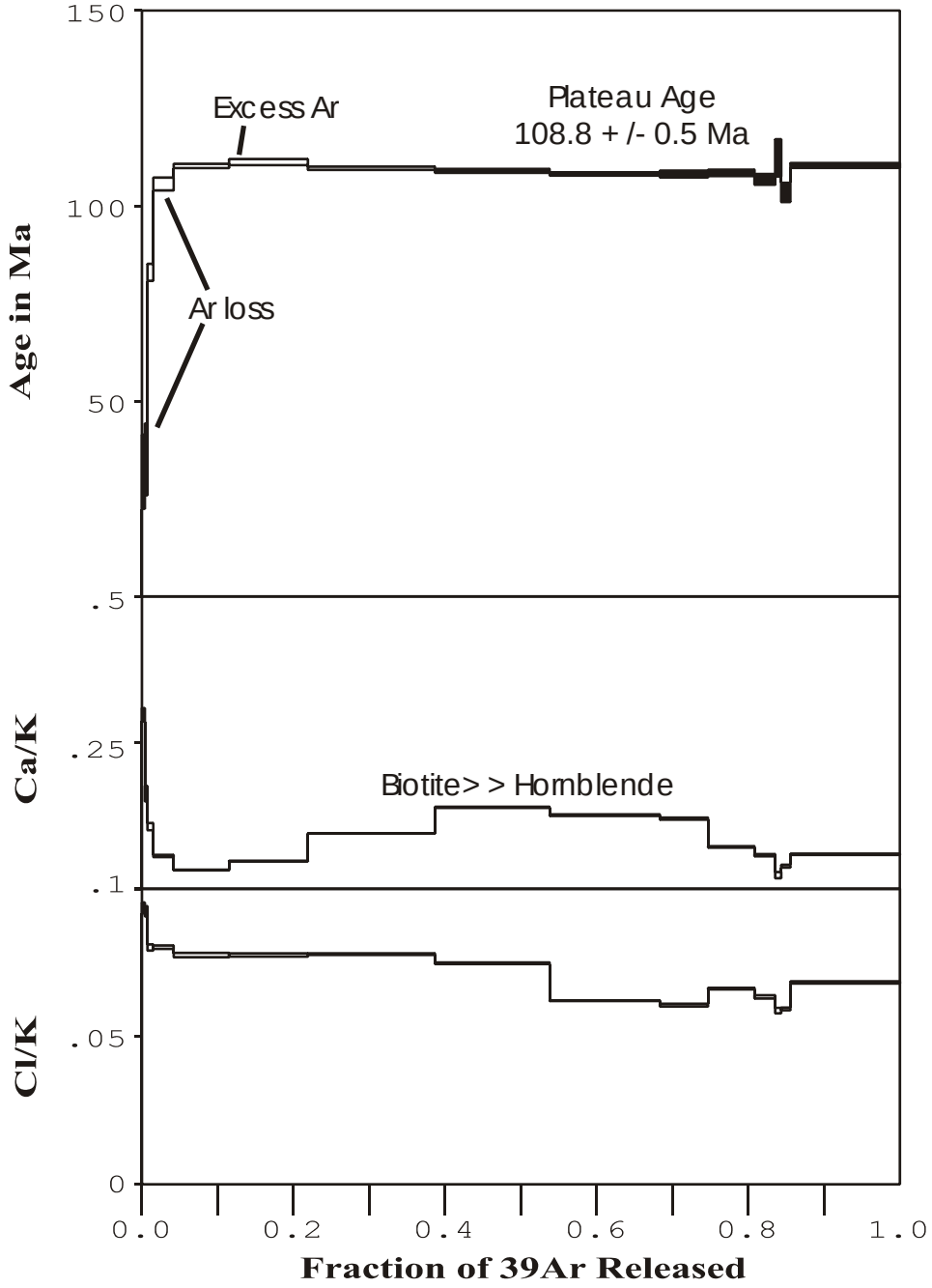

Figure 4.11: Age, Ca/K and Cl/K spectrum diagram for biotite from VABM Bonanza lobe (975960).

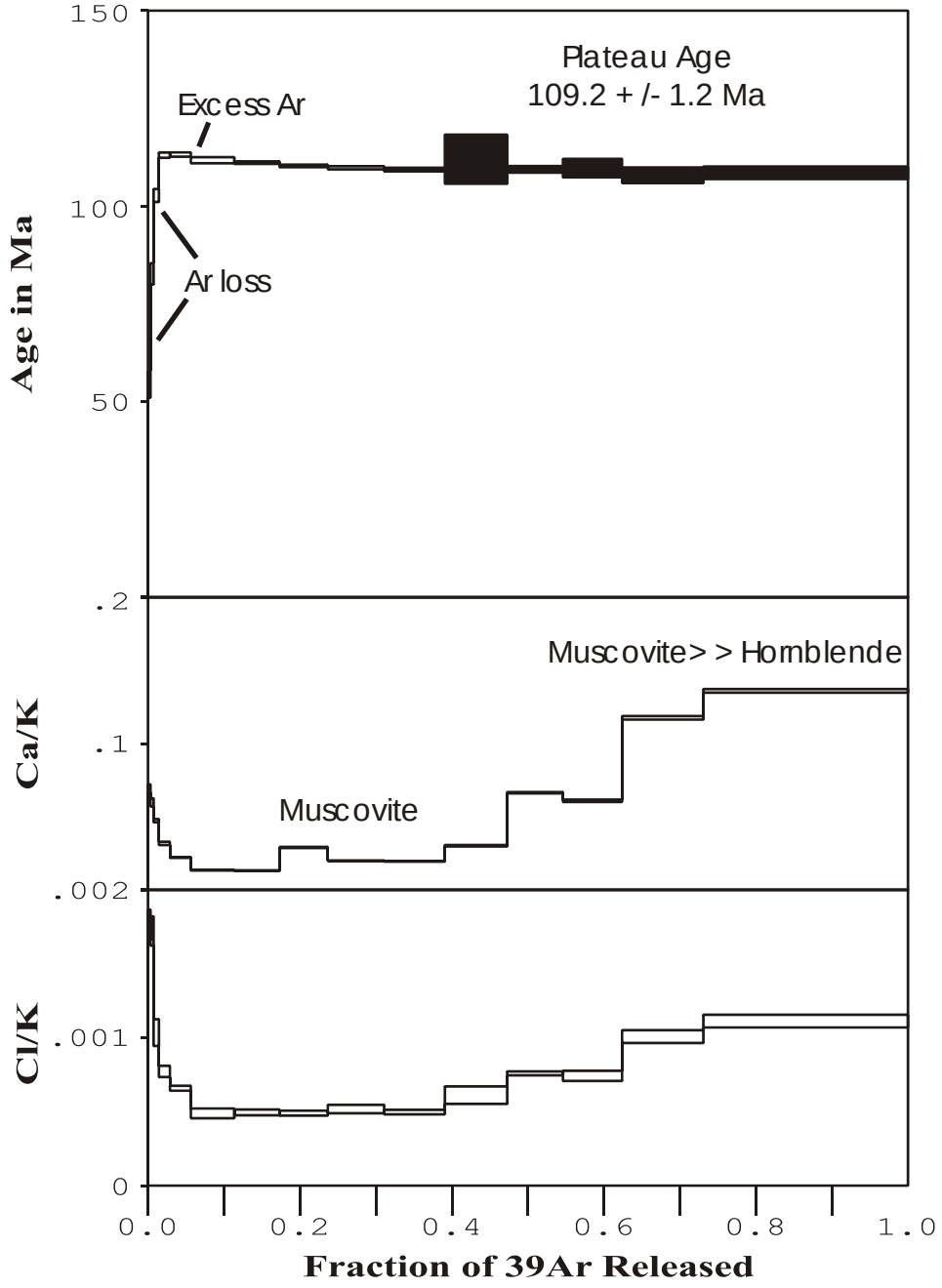

Figure 4.12: Age, Ca/K and Cl/K spectrum diagram for muscovite from VABM Bonanza lobe (976864). The age plateau for muscovite is a good estimate for the time of mineralization.

4.3.4 Spruce Creek Lobe

One hornblende and one biotite separate were dated from a quartz diorite sample (03ZW471) from the Spruce Creek lobe. Petrographic examination of the mineral separates revealed that the dated crystals were a combination of biotite, hornblende, and pyroxene (Figure 4.13). Hornblende rims pyroxene, and the biotite both occurs as small inclusions in pyroxene and rims around hornblende. The hornblende Ca/K (Figure 4.14) spectrum shows extreme variations in Ca/K ratios. Since the age spectrum reflects a combination of minerals, the Ca/K spectrum can be used to determine which heating steps represent Ar released from the three different minerals. Biotite has the lowest Ca/K ratio (nearly zero), and since it has the lowest Ar-retention temperature it should release its Ar first. The Ca/K spectrum shows that the early heating steps released Ar from a low Ca mineral. With increasing laser energy the Ca/K ratio rises, indicating Ar released from both hornblende and biotite. At higher energy high Ca/K ratios indicate hornblende released Ar with a small contribution from clinopyroxene. Finally, at the highest heating temperature very high Ca/K ratios indicate clinopyroxene released its Ar (Figure 4.14). In contrast, the biotite analysis (Figure 4.15) resulted in a near perfect age plateau and a flat and low Ca/K spectrum indicating the biotite separate was nearly pure biotite.

The hornblende and biotite from the Spruce Creek lobe yield ages of 115.2 ± 0.8 and 111.2 ± 0.4 Ma, respectively. For the hornblende age spectrum, Ar was primarily released from hornblende for steps seven through twelve (Figure 4.14). The plateau accounts for 65.9% of the total Ar released and has a MSWD of 0.93. The biotite plateau (Figure 4.15) accounts for 98.1% of the total Ar released and has a MSWD of 1.22. The hornblende age is older than expected (relative to the biotite) and is probably the result of extraneous Ar in biotite inclusions in the dated mineral grain. Since the biotite occurs as inclusions and attached to hornblende and pyroxene, Ar released from those minerals can still enter the biotite since it has a lower closure temperature. Considering this problem and consistent with a typical 2 Ma difference between biotite and hornblende ages the best estimate emplacement age for the Spruce Creek lobe is ~113 Ma, similar to that of the Bonanza Creek lobe.

4.3.5 Gray Dikes

Two hornblende and two biotite samples were dated from a gray dike (03ZW474) at the Wallace Occurrence. All of the age, Ca/K and Cl/K spectra (Figure 4.16 and 4.17) are similar for each hornblende analysis. The hornblende crystals are large (dated specimens >1x1 mm), weakly chloritized along their margins, and have rare biotite inclusions (Figure 4.18). The defined plateaus account for over

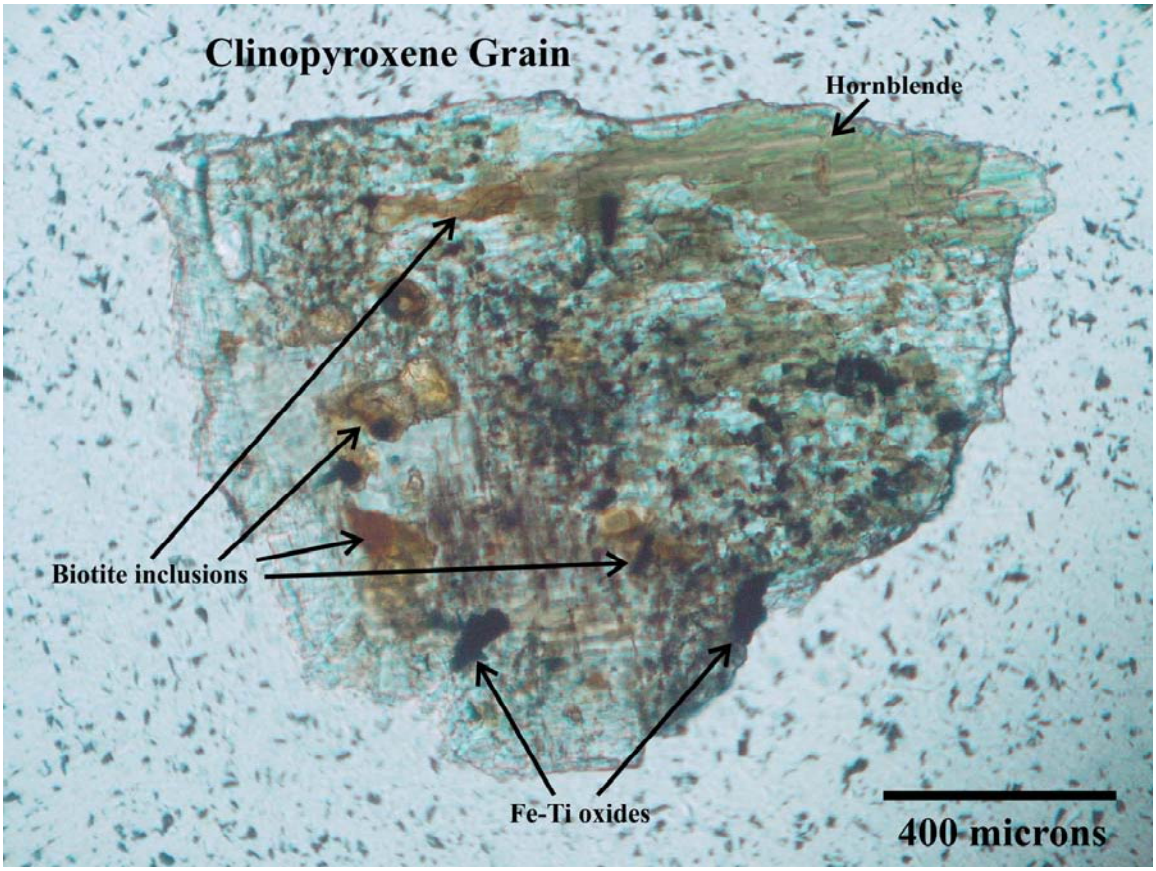

Figure 4.13: Spruce Creek lobe mineral aggregate separate (sample 03ZW471). The majority of the grain is clinopyroxene with biotite, hornblende and Fe-Ti oxide inclusions with a partial hornblende rim.

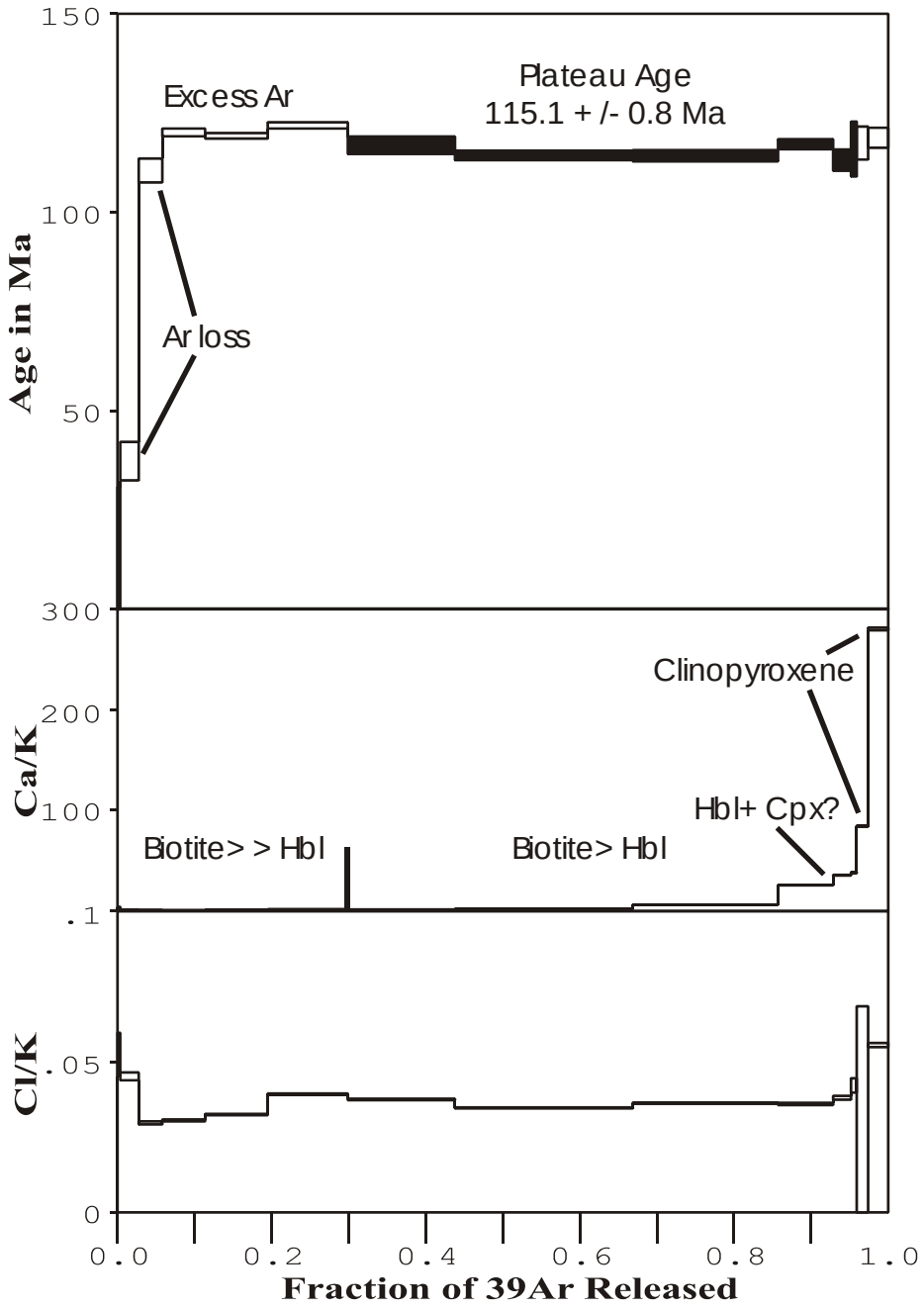

Figure 4.14: Age, Ca/K and Cl/K spectrum diagram for hornblende from the Spruce Creek lobe (03ZW471). The analyzed samples were mineral aggregates. Only heating steps 7-12 have Ca/K ratios diagnostic of hornblende.

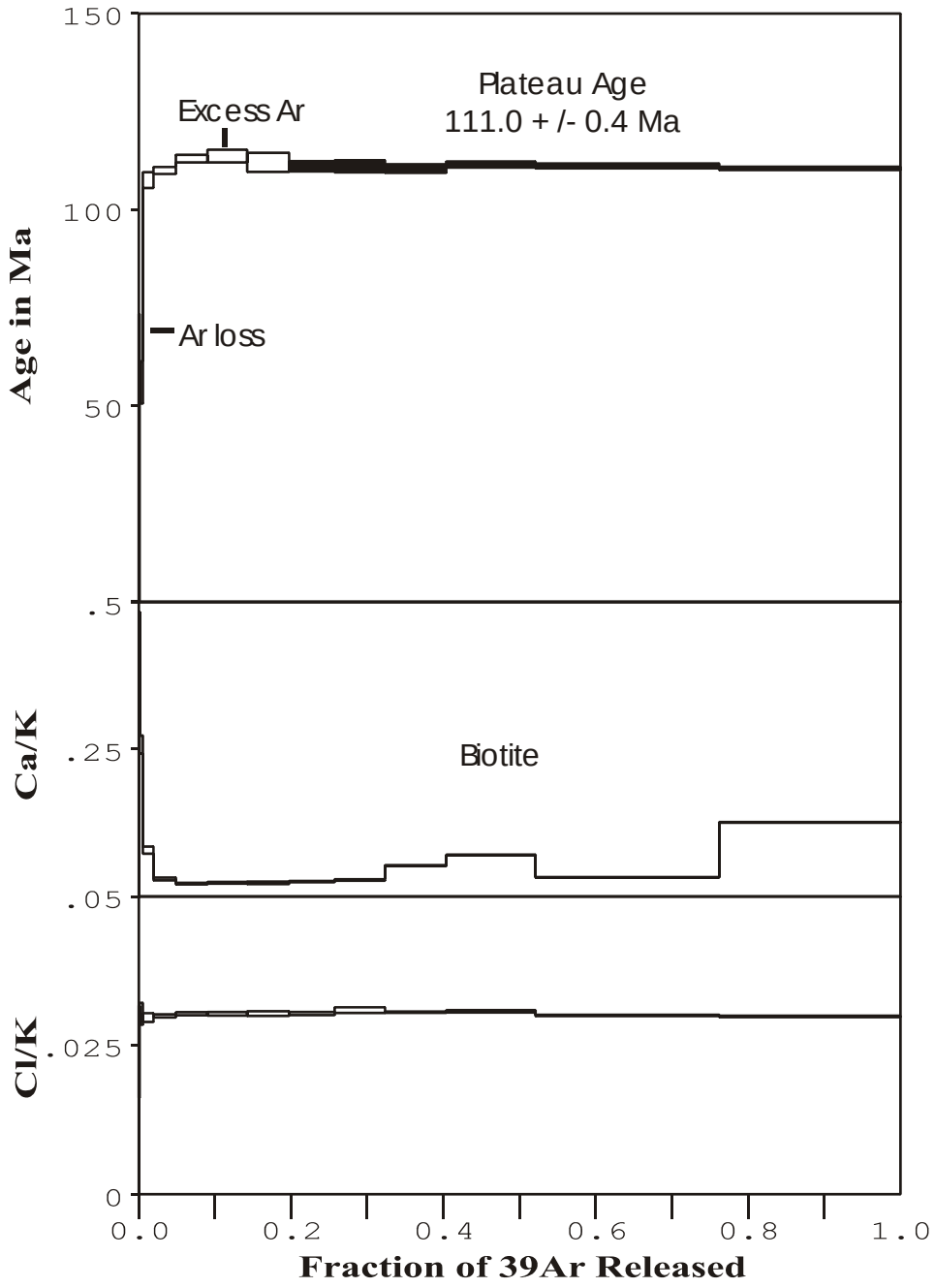

Figure 4.15: Age, Ca/K and Cl/K spectrum diagram for biotite from the Spruce Creek lobe (03ZW471).

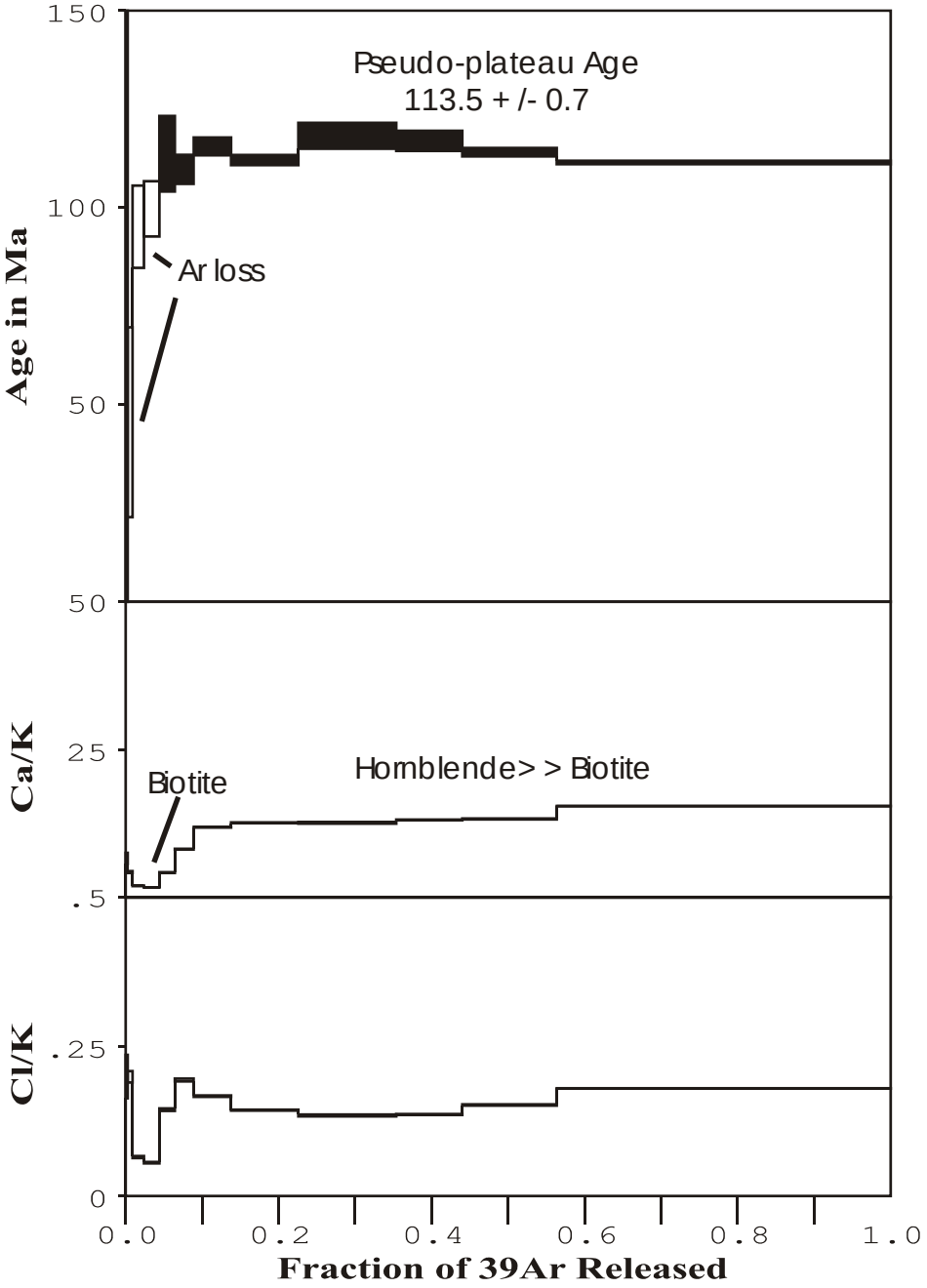

Figure 4.16: Age, Ca/K and Cl/K spectrum diagram for hornblende from the gray dike (03ZW474).

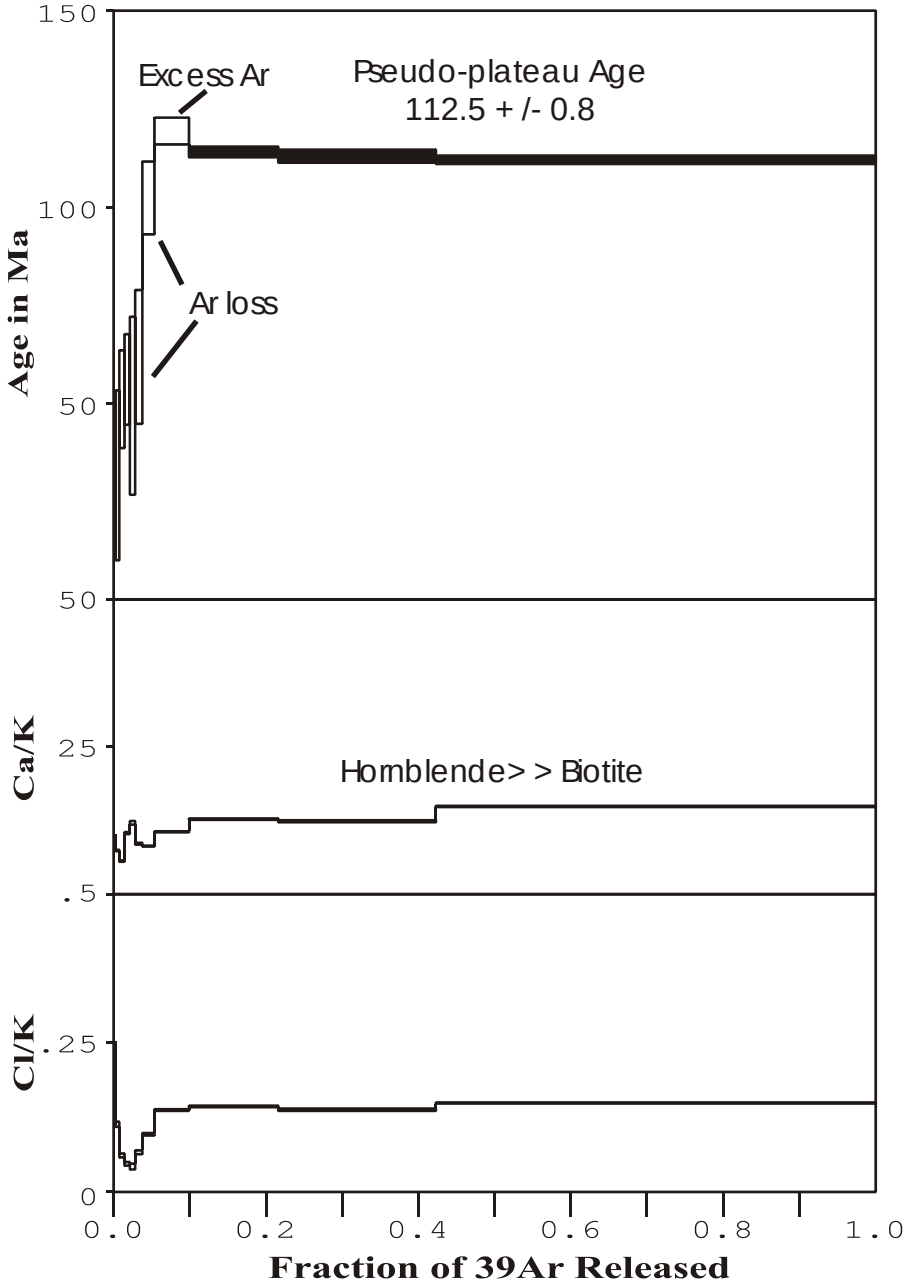

Figure 4.17: Age, Ca/K and Cl/K spectrum diagram for hornblende from the gray dike (03ZW474).

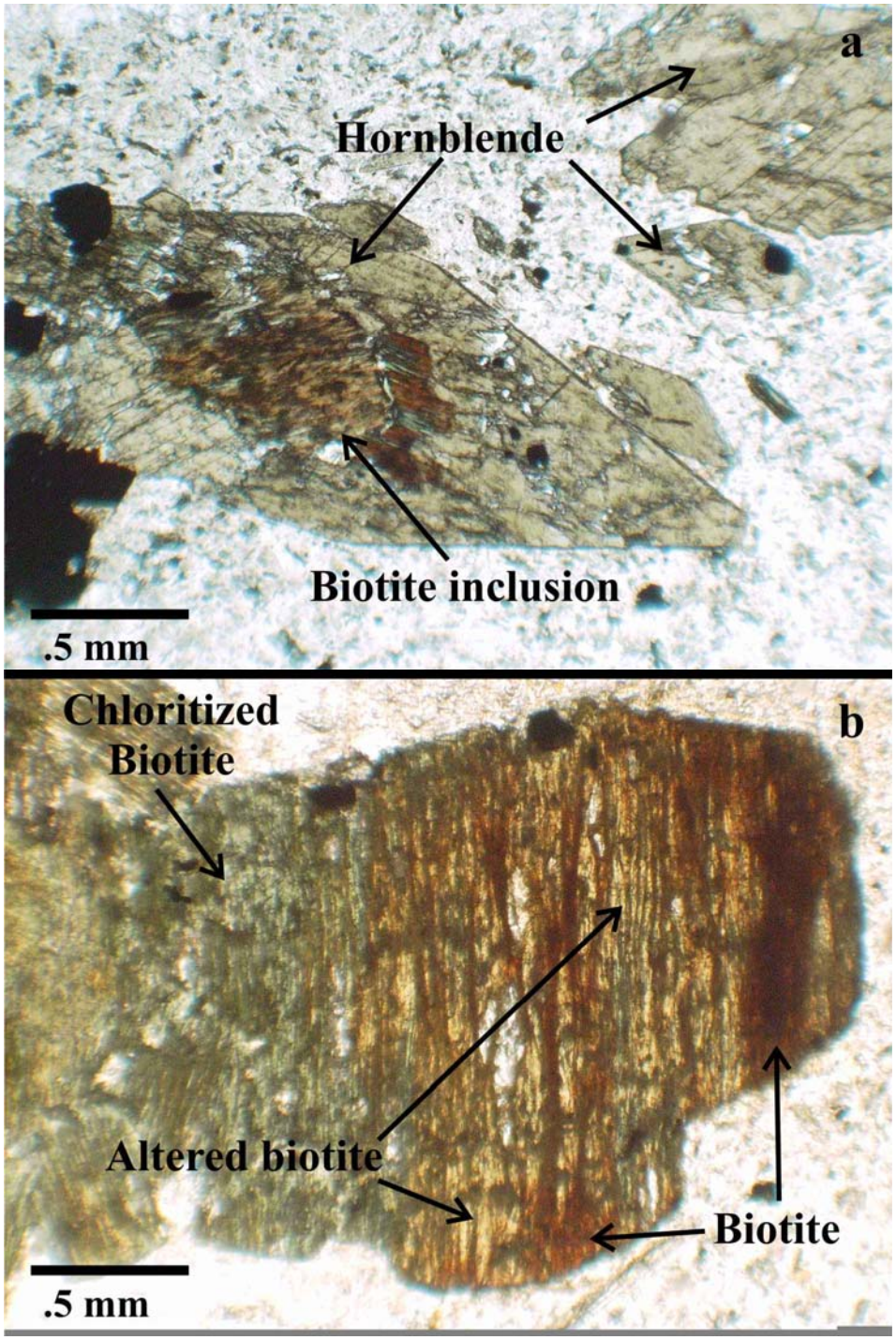

Figure 4.18: Photomicrographs of hornblende (a) and biotite (b) from the gray dike at the Wallace occurrence. Figure 4.18 (a) shows an extreme example of biotite inclusions in hornblende grains and Figure 4.18 (b) shows extensive chloritization of biotite. Biotite photomicrograph is rotated 90 degrees.

95.6% and 90.1% of the total Ar released. The plateaus have MSWDs of 3.81 and 0.78. The two plateau ages weighted by variance and averaged report a hornblende age of 113.1 ± 0.4.

Biotites from the grey dike are variable chloritized. The grains separated were visibly altered to chlorite apparent in their green discoloration; only the grains with minimal chlorite alteration were selected for dating. In thin section it is obvious that the biotites are altered (Figure 4.18), but in some grains the alteration is not as intense. Both biotite samples analyzed yielded complex results. The first biotite age spectrum is very noisy (Figure 4.19). The age spectrum never levels off into a true plateau. A pseudo-plateau gives a biotite age of 109.1 ± 1.2 Ma. A second analysis, with the hope of obtaining a better plateau, was no better: no plateau was ever reached (Figure 4.20). The last two steps, which each account for approximately 25% of the total argon released, differ in age by more than 15 Ma. All of the previous steps gradually increase in age with successive heating steps. The biotite age spectra from the second analysis records ^{39}Ar recoil. The biotite analyzed in the second analysis was presumably more altered and thus ^{39}Ar was easily redistributed in the crystal during irridation. Due to the unreliability of the biotite analyses from this dike it is unclear whether the 109.1 ± 1.2 Ma age reflects the magmatic cooling biotite age or rather a later mineralizing event at the Wallace occurrence. The best crystallization age for the gray dike is 113.1 ± 0.4 Ma.

4.3.6 Red Dikes

One biotite and one muscovite sample were dated from the red dike at the BCCA. The biotite came from an unaltered variety of the dike and the muscovite from the most altered variety which hosts gold mineralization. Biotites from the unaltered variety display weak chlorite alteration along their rims (Gierymski and Werdon, 1997). The biotite records an age of 111.2 ± 0.5 Ma (Figure 4.21). The variation of the Ca/K ratio is likely the result of hornblende or sphene present as inclusions in the biotite. Nonetheless, the Ca/K ratio is low indicating nearly pure biotite. The muscovite grains are large (up to 4mm diameter) and coherent crystals. The muscovite appears to have completely replaced former biotite grains. The age spectrum for the muscovite sample records a mineralization age of 111.9 ± 0.6 Ma (Figure 4.22).

4.4 ^{40}Ar/^{39}Ar Rock Age Summary

All the plutonic and volcanic age data are illustrated on Figure 4.23. I propose that there were four different geologic events in the study area: Jurassic volcanic-arc formation, Nyac Batholith plutonism, Bonanza Pluton plutonism and Tertiary hydrothermal activity.

The first event is the formation of the volcanic arc. The basalt dated in this study records an age of 180 ± 7 Ma. This age is similar to the Bajocian age of the pelycypod fossils (Box et al., 1993). Several

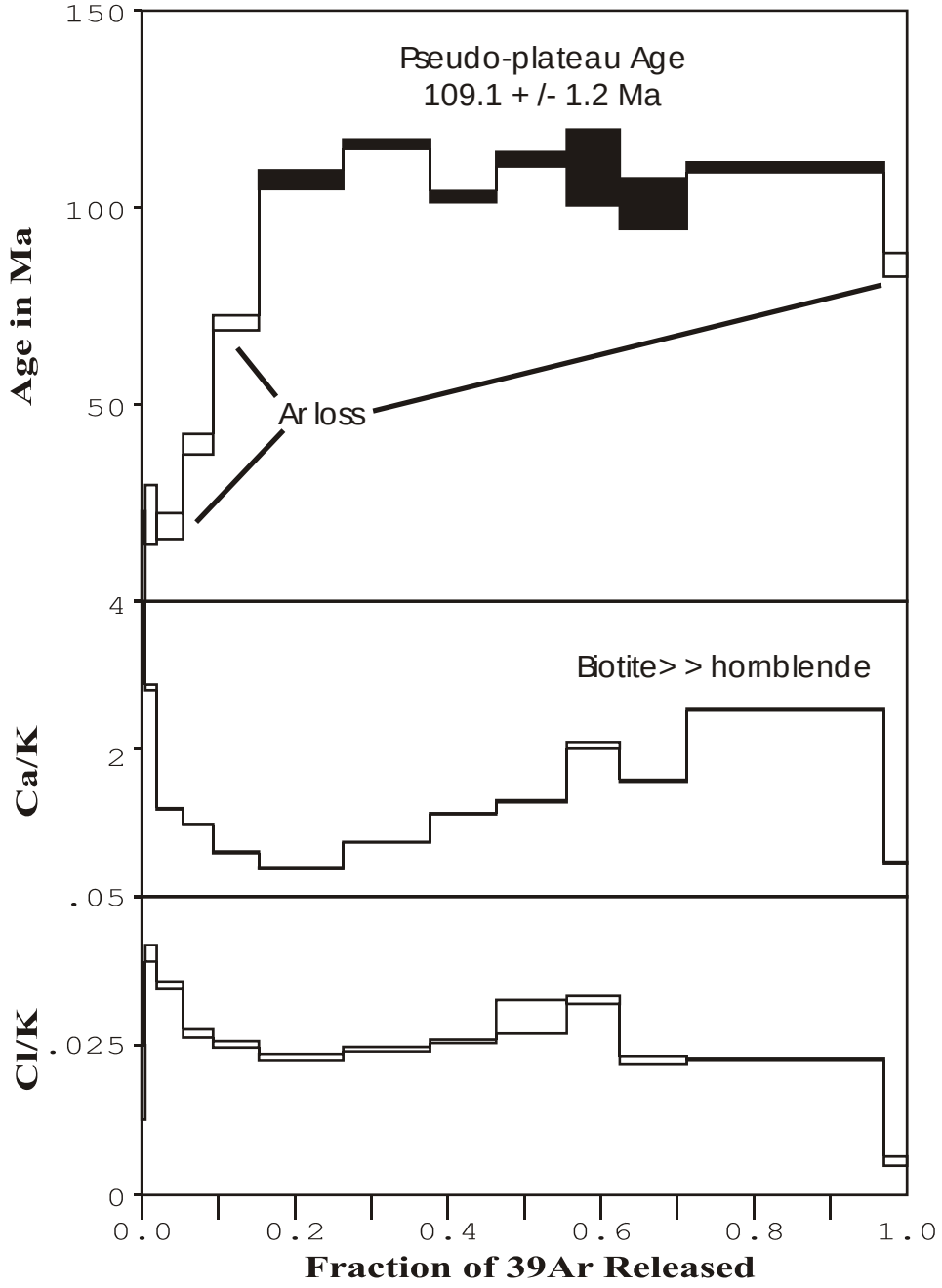

Figure 4.19: Age, Ca/K and Cl/K spectrum diagram for biotite from the gray dike (03ZW474). The age spectrum indicates substantial Ar loss, but a pseudo-plateau does give an indication of either the biotite age or time of alteration.

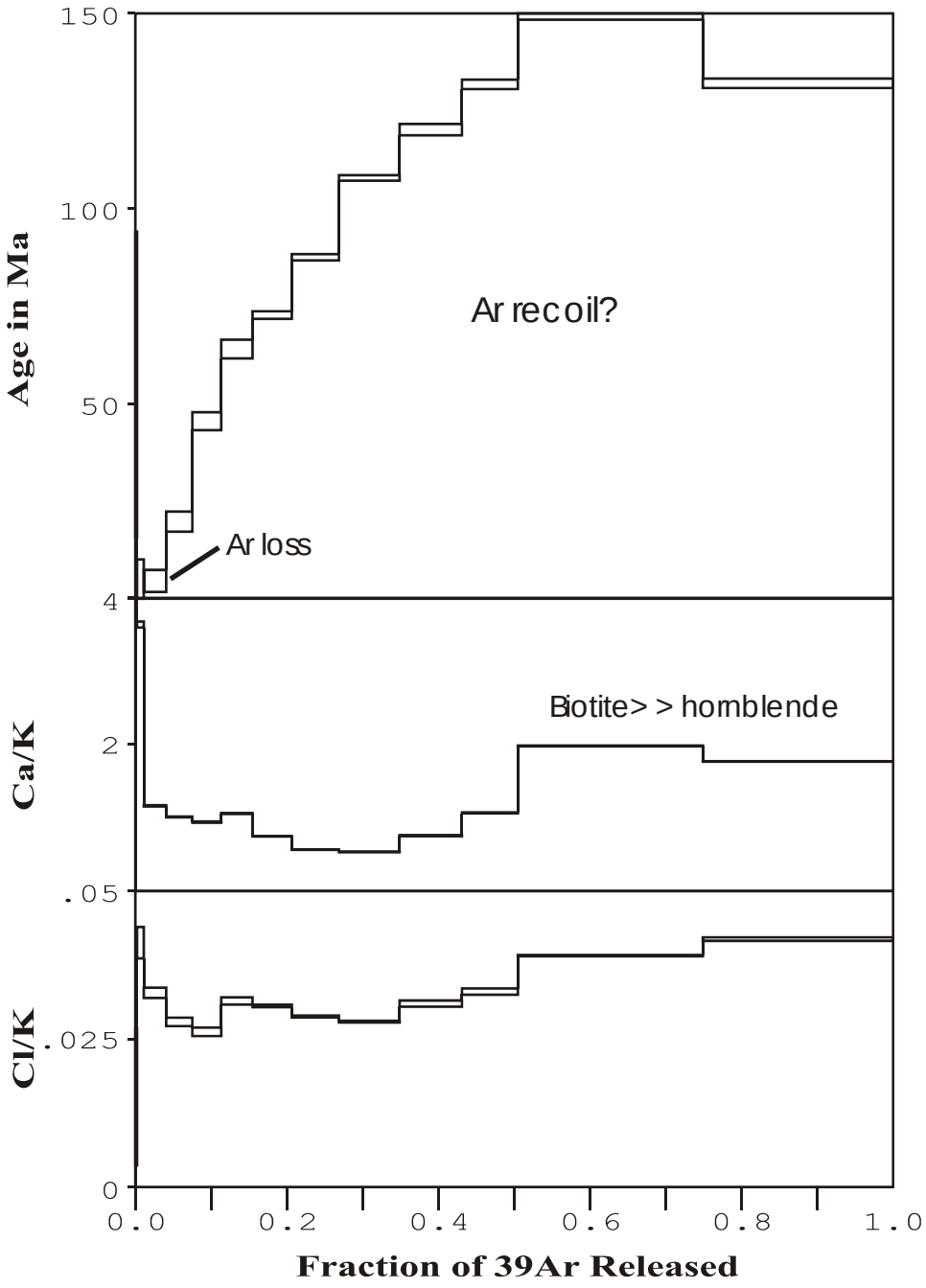

Figure 4.20: Age, Ca/K and Cl/K spectrum diagram for biotite from the gray dike (03ZW474). The age spectrum never levels off into a plateau. The appearance of the age spectrum is the result of either Ar gain followed by Ar loss or more likely Ar recoil since the integrated age is similar to the other biotite age (Table 4.1).

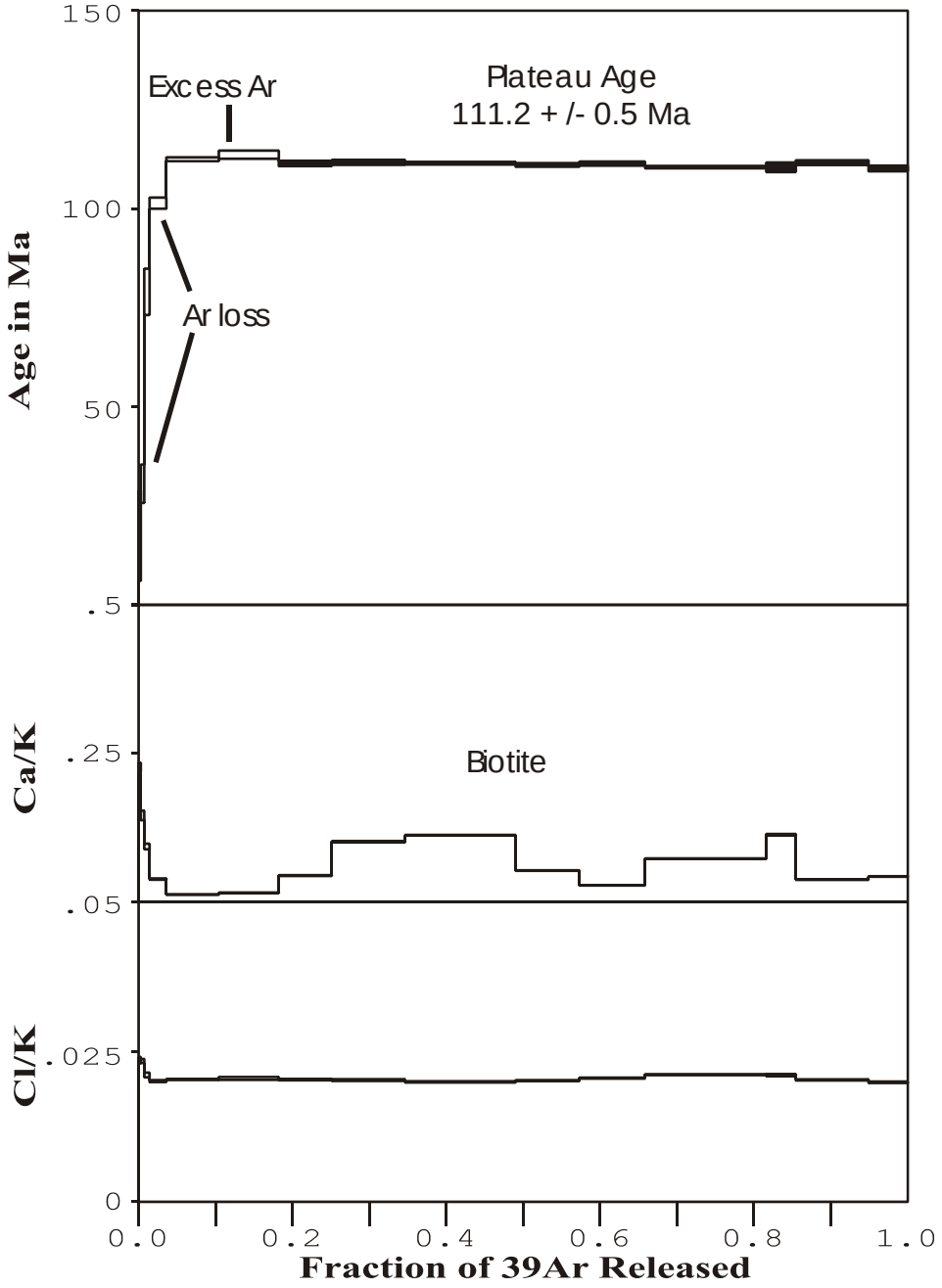

Figure 4.21: Age, Ca/K and Cl/K spectrum diagram for biotite from the red dike (977056).

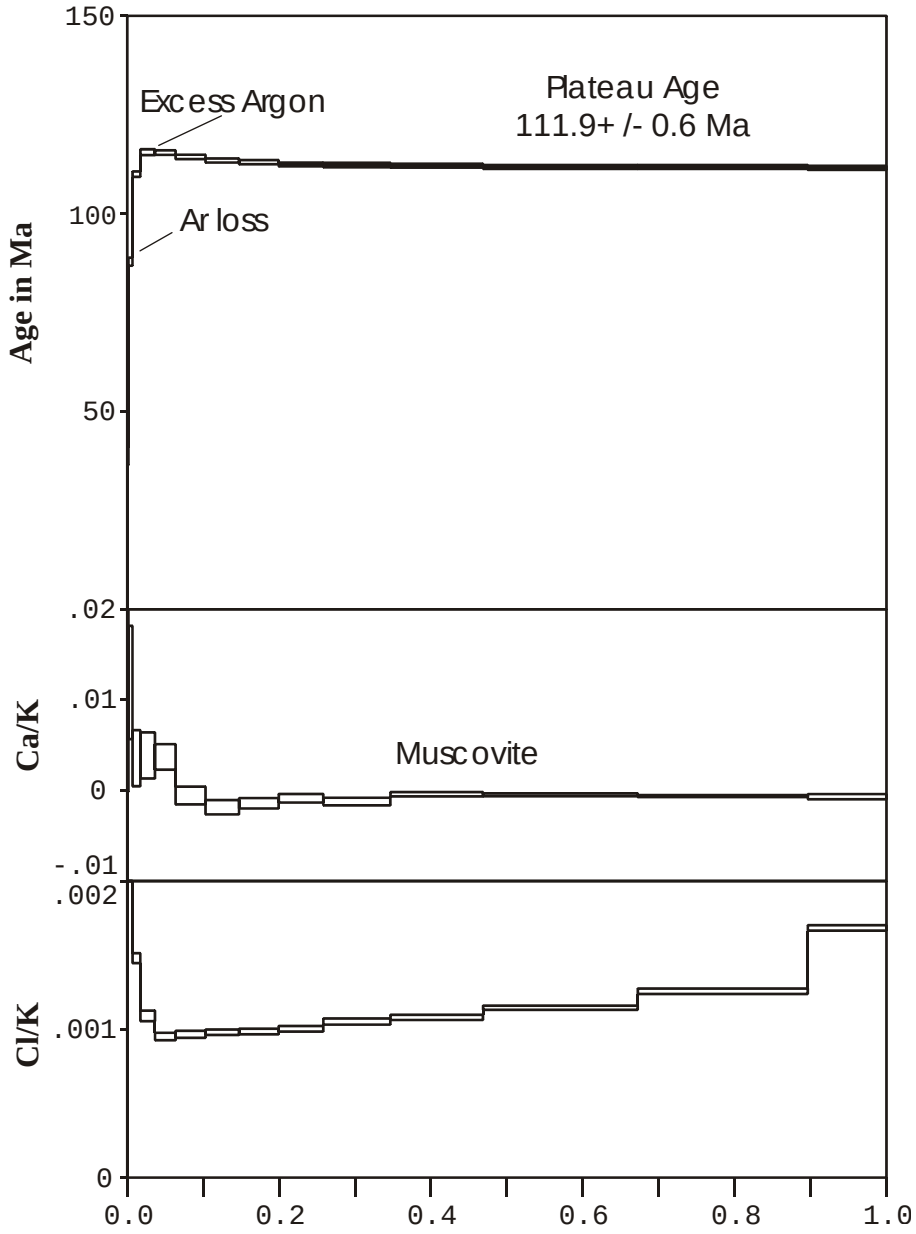

Figure 4.22: Age, Ca/K and Cl/K spectrum diagram for muscovite from a mineralized red dike (03ZW351).

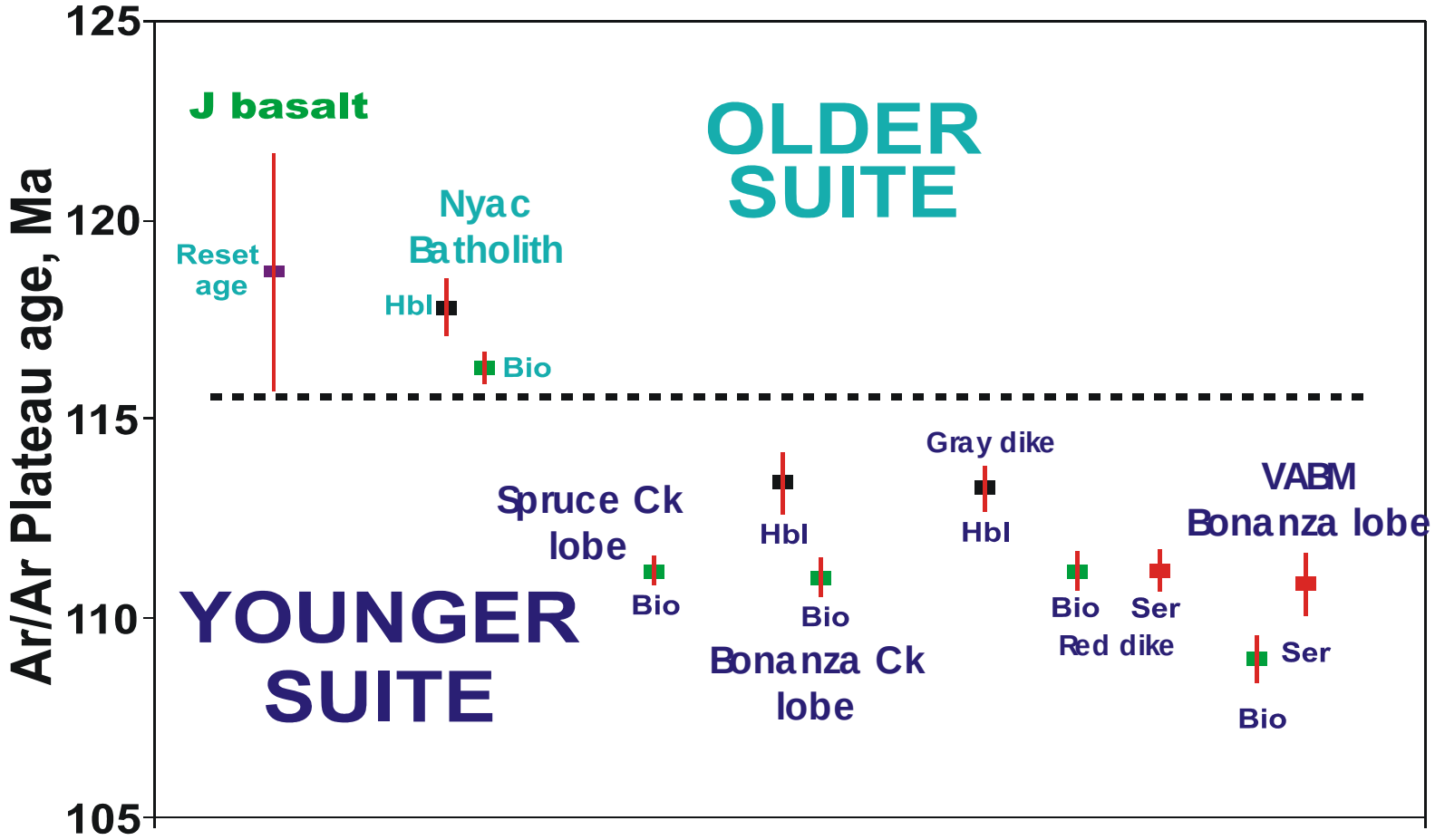

Figure 4.23: Figure of dated samples illustrating two distinct age suites. The old suite is the Nyac batholith. The young suite includes all portions of the Bonanza pluton, the gray dikes and the red dikes (bars represent 1 sigma error).

plutons (diorite hornfels, Rex Creek pluton, and altered granodiorite; discussed in Chapter: 2) also appear to be related to this event.

The second event is the intrusion of the Nyac batholith into the volcanic-arc complex. The Nyac batholith is 118 ± 1 Ma. The reset age of the metavolcanic rock unit (119 ± 3 Ma) is statistically the same (at $\pm 1\sigma$) as the hornblende age from the Nyac Batholith (Figure 4.22). The Nyac Batholith is thus responsible for the regional thermal metamorphism in the study area and perhaps the entire northern portion of the Nyac terrane.

The third event is Bonanza pluton plutonism. This event includes the Bonanza pluton, grey dikes, red dikes, mineralization at the VABM Bonanza lobe at ~111 Ma, and mineralization at the BCCA at ~112 Ma . The biotite age from Bonanza Pluton was likely affected by the mineralization event and Ar loss resulting in a younger age. Biotite from the Bonanza Creek and Spruce Creek lobes, red dike and the grey dike are statistically indistinguishable (Figure 4.22). Similarly, the hornblende ages from Bonanza Pluton and the grey dike are statistically indistinguishable at the $\pm 2\sigma$ confidence level. The muscovite age from the VABM Bonanza lobe is statistically indistinguishable from the biotite age of the Bonanza pluton. Therefore, the Bonanza pluton is most likely responsible for the mineralization at VABM Bonanza lobe. The later mineralization age at the BCCA likely reflects the later stages of mineralization. This topic will be futher discussed in Chapter 5.

The fourth event is a widespread heating event. All of the mineral samples analyzed yield an initial Ar loss. This Ar loss is most likely due to hydrothermal activity related to a regional Tertiary heating event. The undated mafic dikes may be responsible for this event.

5. Mineralization Model

This study presented mineralogical and petrological data of the rocks, evidence for alteration styles, ore mineralogy, and fluid chemistry and age data from the study area. All of these aspects provide the information needed to produce a geological model that explains the mineralization in the study area. Mineralization in the study area accompanied three separate events: Jurassic (?) plutonism, Early Cretaceous plutonism and Tertiary hydrothermal activity.

5.1 Jurassic (?) Plutonism

The timing of the earliest mineralizing event can only be inferred because the causative pluton (Rex Creek pluton ?) age cannot be determined with certainty. Biotite and hornblende in the pluton are altered to a combination of epidote-chlorite-calcite-magnetite-rutile rendering $^{40}Ar/^{39}Ar$ dating useless. As evidenced by intense alteration and similar trace element chemistry to the diorite hornfels the Rex Creek pluton is at least older than 118 Ma, because the large scale thermal metamorphism in the study area is likely the result of Nyac batholith plutonism. Mineralization associated with this pluton includes quartz-chalcopyrite veining, disseminated chalcopyrite in volcanic rocks now replaced by malachite, and pyritization of mafics in and around the Rex Creek pluton.

This style of alteration and mineralization is different from that at VABM Bonanza lobe in that it has no associated anomalous Au, Bi or Te and a different alteration assemblage of epidote-chlorite-carbonate-sericite. This pluton also hosts epidote veins not seen at VABM Bonanza.

5.2 Early Cretaceous Plutonism

The Early Cretaceous event includes mineralization resulting from the intrusion of the Nyac batholith and Bonanza pluton. Before discussing the source and relationship between the two igneous bodies it is important to review the chemical processes responsible for plutonic-related mineralization. First, both the Nyac batholith and Bonanza pluton are volcanic-arc plutons with high oxidation states (Figures 2.9 and 2.10). Plutons with original high oxidation states are not gold favorable because at these conditions gold is in the Au^{3+} valence state and thus goes into magmatic magnetite. If the oxidation state is too low gold will be in the Au^{1+} valence state and will be lost to magmatic sulfide (Mirsa, 2000). The Bonanza pluton contains both native gold and magmatic magnetite, indicating it was relatively oxidized, but the oxidation state was not high enough for all the gold to be lost to magmatic magnetite. Another implication of volcanic-arc high oxidation plutons is their fluid chemistry. HS^- and Cl^- are the two most common complexing agents for Au (Mirsa, 2000). High oxidation fluids cannot contain significant

amounts of HS^- (sulfur is instead present as SO_4^{2-}). Hence, in such fluids, if metal complexing occurs, it is through Cl^- complexation. The Bonanza pluton's high oxidation state, high salinities and high temperature fluid inclusions indicate that the Au complexing agent at Bonanza pluton was Cl^- ion. The low salinities calculated from fluid inclusions at the Wallace occurrence suggest instead a HS^- complex.

The Nyac batholith is most likely responsible for the large-scale thermal metamorphism throughout the study area. During cooling it is likely that fluids were released from the crystallizing batholith. It is these far-reaching fluids that are likely responsible for most of the uneconomic mineralization in the volcano-sedimentary package. The majority of the calc-silicate veinlets that have associated sulfides are located on the metasedimentary-Nyac batholith contact (discussed in Chapter 4). These sulfide occurrences are likely the result of fluids from the Nyac batholith traveling through the wallrocks, locally mobilizing Fe and Cu, to be later precipitated as pyrite, pyrrhotite and chalcopyrite. The magmatic fluids could have also contained inherent appreciable amounts of Cu and Fe. The mineralization is dominantly small calc-silicate veinlets with associated pyrite, pyrrhotite, chalcopyrite and marcasite. Rocks of the volcano-sedimentary package ubiquitously contain pyrite, pyrrhotite and chalcopyrite with no associated calc-silicates. It is unclear whether the sulfides with no associated calc-silicates are related to the Nyac batholith or earlier Jurassic volcanism.

It is unclear whether the skarn at Spruce Creek is the result of the regional thermal event (Nyac batholith plutonism)or the later intrusion of the Bonanza pluton. The abundance of scapolite, a Cl-rich mineral, in the Spruce Creek skarn is a strong indication that the responsible fluids had high salinities. Fluid inclusions from Bonanza pluton have high salinities, indicating that the Bonanza pluton is possibly responsible for the Spruce Creek skarn. However, scapolite also occurs in unmineralized hornfels along the contact of the metasedimentary rocks and the Nyac batholith. The scapolite here has small pyroxene inclusions (hence, high temperature) indicating that the close proximity of the Nyac batholith must be responsible for the scapolite at this locality. This evidence indicates the Nyac Batholith may be responsible for the Spruce Creek skarn.

Mineralized rock in and around the Bonanza pluton have the highest gold concentrations of lode prospects in the study area. There are four different subtypes of mineralization: the proximal Bi-Cu-Au mineralization in and around the VABM Bonanza lobe, proximal Cu-Au mineralization at the BCCA, epithermal Au-Hg mineralization at the BCCA and proximal Te-Bi-Au mineralization at the Wallace occurrence. All four subtypes of mineralization are likely to be related to the Bonanza Pluton. Each subtype has its own unique alteration and mineralization characteristics.

The VABM Bonanza lobe displays sericite-chlorite-carbonate alteration with associated pyrite, chalcopyrite, bismuthinite, molybdenite and native gold. The chlorites associated with this style of mineralization are length fast and have anomalous green-brown interference colors, characteristic of

moderate to low Fe composition. The fluid inclusions from VABM Bonanza lobe yield trapping temperatures from 536 to 266 degrees Celsius and have salinities of 55-21 wt% NaCl.

BCCA high-T, Cu-Au mineralization displays potassic alteration (secondary biotite) overprinted by chlorite-sericite-carbonate alteration with associated magnetite, chalcopyrite, pyrite and native gold. The chlorite associated with the mineralization is optically indistinguishable from chlorite at VABM Bonanza Pluton. Fluid inclusions from the high-T Cu-Au mineralization yield trapping temperatures from 557 to 282 degrees Celsius and salinities of 57-13 wt% NaCl. The high-T BCCA mineralization is different from the VABM Bonanza Pluton mineralization in that Bi contents are low, chlorite is more abundant than sericite, and the mineralization occurs outside of the pluton.

BCCA epithermal mineralization is older than VABM Bonanza lobe mineralization (112 Ma) and likely represents a later stage of Bonanza pluton mineralization as the system was cooling. Epithermal-type mineralization is seen throughout the entire study area but is concentrated at the BCCA. The sporadic occurrences of epithermal mineralization in the study area are localized along faults, which serve as major fluid conduits. At the BCCA, epithermal mineralization is hosted in the red dikes and fault breccia and also occurs in vuggy chalcedonic quartz veins. This style of mineralization is different from VABM Bonanza mineralization in its elemental association, oxidation-sulfidation conditions and alteration assemblage. The epithermal mineralization has associated high levels of Hg, higher than any other style of mineralization in the study area. The oxidation and sulfidation conditions are higher than that of the Bonanza pluton mineralization. The most defining different characteristic of this style of mineralization is the sericite-kaolinite alteration assemblage. This assemblage indicates both lower temperature and more acidic conditions than sericite-chlorite alteration (Figure 5.1).

The Wallace occurrence displays sericite-chlorite-carbonate-albite alteration with associated tellurobismuthite, tetradymite, native gold and minor chalcopyrite. The chlorites associated with this style of mineralization have purple-blue anomalous interference colors and are length slow, indicating high Fe content. Fluid inclusions from the Wallace occurrence yield trapping temperatures from 370 to 346 ^{o} C, salinities of 2 wt% NaCl and high CO_2 concentrations. The Wallace occurrence is different from Bonanza Pluton mineralization in its alteration assemblage, ore mineralogy, chlorite composition and fluid chemistry. The Wallace occurrence exhibits the most intense albite alteration, has higher Fe chlorites, a greater abundance of Bi-Te bearing minerals and a much lower abundance of chalcopyrite. The fluid inclusions have much lower salinities and much higher CO_2 concentrations than VABM Bonanza Pluton mineralization.

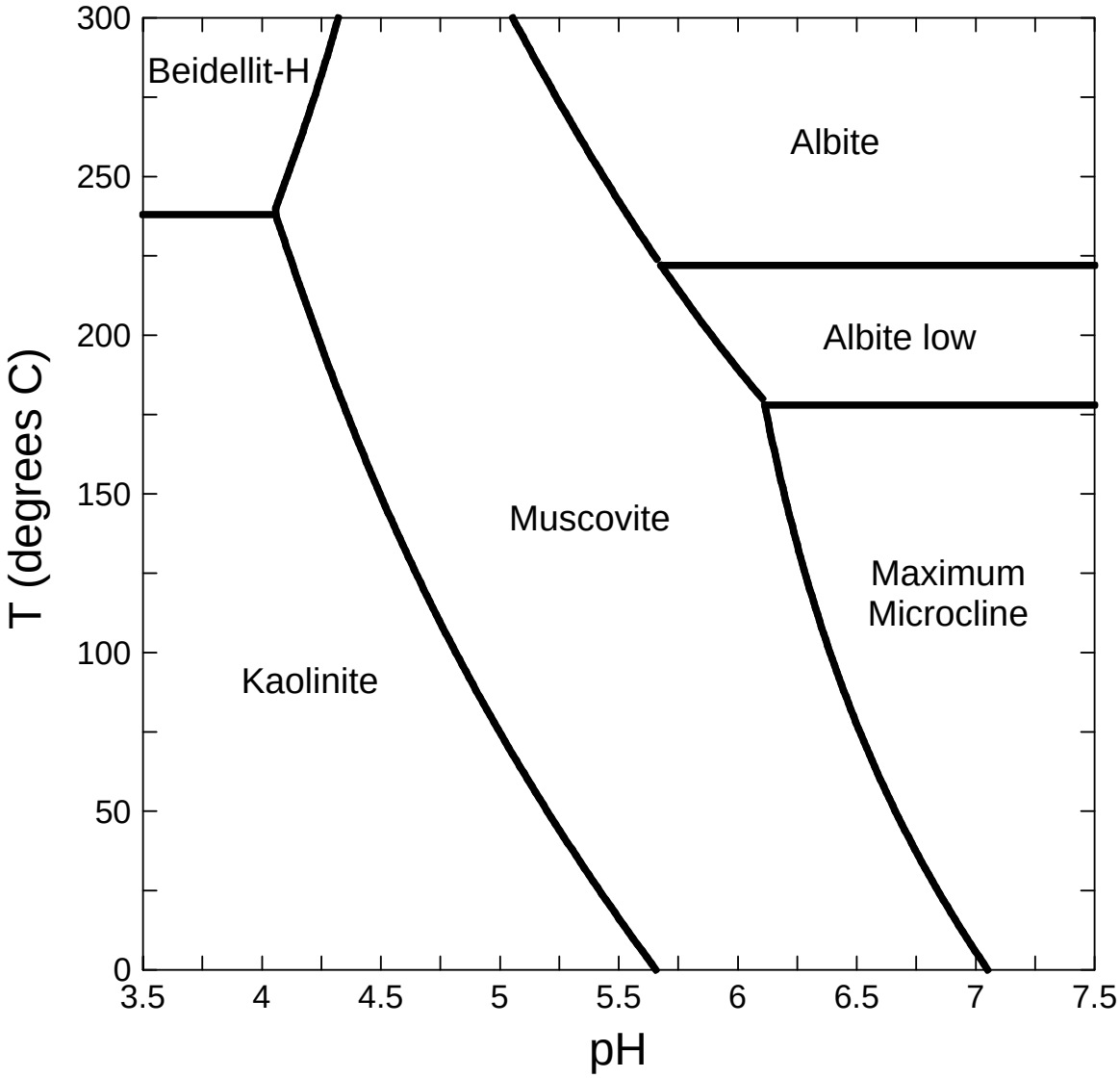

Figure 5.1: pH vs. Temperature diagram for Al alteration minerals. The diagram illustrates that kaolinite is the stable species at low pH. Conditions are under quartz saturation, K^+ activity of 0.01 and Na^+ activity of 0.3. Increasing K^+ activity by a factor of ten shifts all boundaries 1 pH unit lower. Diagram calculated using Geochemist's Workbench (Bethke, 1998) and thermodynamic data of Delany and Lundeen (1990).

5.3 Tertiary (?) Hydrothermal Activity

Tertiary (?) hydrothermal activity likely occured in the district. Although, no igneous body was identified that is responsible for this mineralization; the mafic dikes that cut the Bonanza and Sawpit plutons (Maddren, 1915) could be responsible for this event. The Ar loss seen in all age spectra in the study area supports this hypothesis. The single analyzed mafic dike has continental trace element signatures suggesting that it originated from an extensional event (Figure 2.4).

5.4 Mineralization Model

Figure 5.2 is a schematic cross section through Bonanza pluton that illustrates the structural history and location of the most significant mineralization in the study area.

Originally the volcano-sedimentary package overlay all of the Bonanza pluton. Movement on the N-S faults uplifted the pluton at VABM Bonanza and the Spruce and Bonanza lobes. At the Wallace occurrence the metasedimentary rocks presumably still overlie the pluton. Here the gray dikes may be related to the underlying Bonanza pluton (the grey dikes have similar age and composition as the Bonanza pluton). The Spruce lobe is likely down dropped from the VABM Bonanza lobe as is evident from the small raft of metavolcanic rocks that lie on top of the pluton and more mafic compositions here (Figure 2.1). The Bonanza Creek lobe is roughly at the same exposure level as the Spruce Creek lobe, but is left-laterally displaced north along N-S faults.

The differences in the type of mineralization can be explained by a phase separation of fluids expelled from Bonanza pluton resulting in an aqueous phase and a gas-rich phase. Several authors (Candela and Piccoli, 1995; Hedenquist, 1995; and Gammons and Williams-Jones, 1997) have proposed a similar phase separation resulting in a gas-rich phase and a hypersaline liquid. In this case, the aqueous phase is a high temperature, high salinity, and low CO_2 phase with an associated Cu-Bi-Au mineralization (eg. VABM Bonanza lobe). The gas-rich phase is a lower temperature, low salinity, and high CO_2 phase with an associated Te-Bi-Au mineralization (eg. Wallace occurrence).

The aqueous phase is responsible for the proximal mineralization at VABM Bonanza lobe and the high temperature Cu-Au mineralization at the BCCA. The high salinity of this style of mineralization suggests that the ore minerals were dominantly complexed with Cl^-. At high temperature and oxidation state Au can complex with Cl^- (Wood et al., 1987; and Hayashi and Ohmoto, 1991).

In contrast, the gas-rich phase is responsible for the mineralization at the Wallace occurrence. Au transport as a chloride complex dominates bisulfide complex, but at lower temperatures bisulfide dominates Au complexing (Hiyashi and Ohmoto, 1991). Since chloride complexes dominate at high temperature and

their solubility is strongly affected by temperature, at lower temperature all available Cu could have already precipitated and thus is not seen with the gas-rich phase.

Magmatic fluids were concentrated as the magma body (Bonanza Pluton) crystallized and then were subsequently expelled. At some point lower pressure resulted in a phase separation (aqueous and gas-rich) of the magmatic fluid. The gaseous phase being less dense would ascend with the dikes or use them as conduits. It is more likely that the dikes acted as conduits since early crystallization of Bonanza pluton (the mafic outer zone) yielded mostly plagioclase and pyroxene, indicating that water contents were initially low and it was not until later that H_2O was sufficiently concentrated to be expelled from the pluton. If the fluids were expelled from the pluton after a significant amount of crystallization, the dikes would likely have been in place and thus serve as conduits for the fluids.

The reason both fluid phases resulting styles of mineralization are seen on the surface is due to significant vertical displacement along the high-angle N-S faults. At the Wallace occurrence gray dikes intrude the metasedimentary rocks and host the gas-rich mineralization style. In contrast, the uplifted, VABM Bonanza lobe hosts the aqueous mineralization. It is possible that beneath the surface at the Wallace occurrence the Bonanza pluton would contain the aqueous style of mineralization.

The epithermal mineralization at the BCCA likely represents a largely meteoric fluid dominating late, low temperature circulation through the uppermost part of the Nyac system. A later epithermal mineralization could be related to a regional Late Cretaceous and early Tertiary magmatic arc and extensional event in SW Alaska (Gray et al., 1997). The mafic dikes with continental signatures that cut the Bonanza pluton are direct evidence for such a magmatic event.

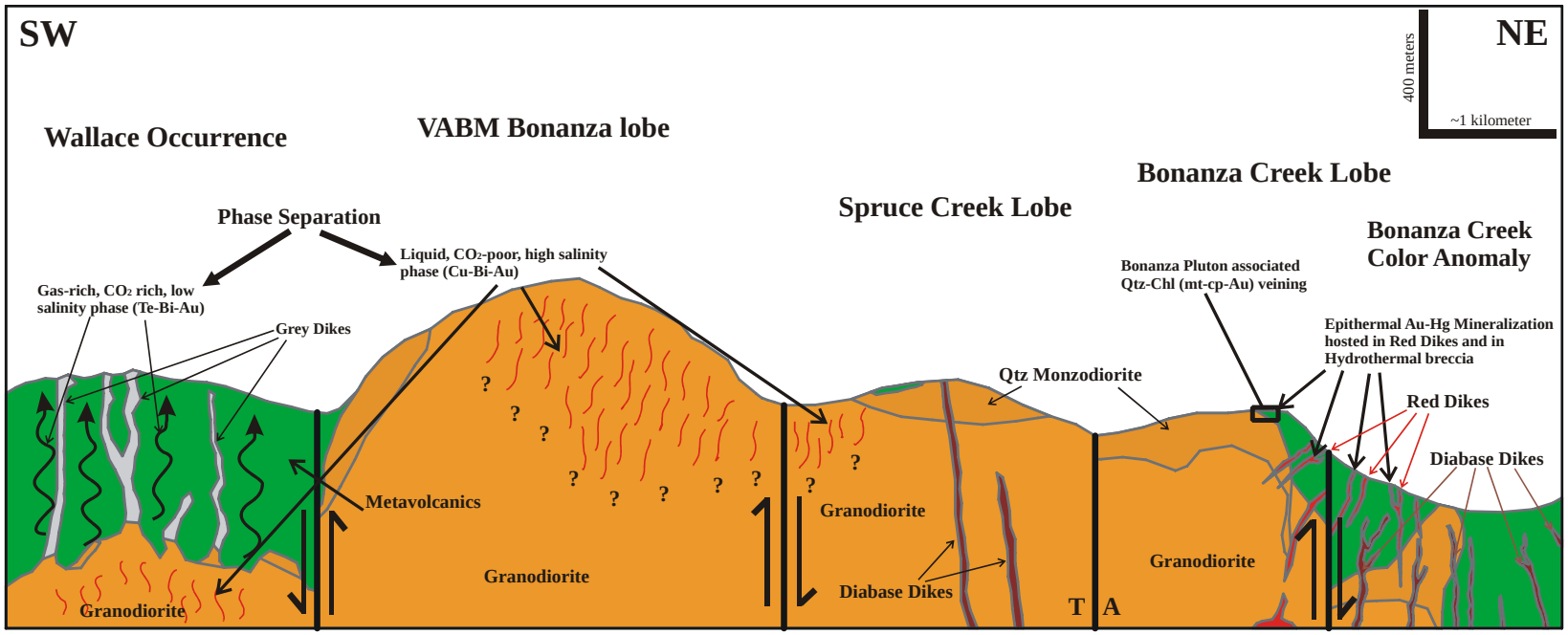

Figure 5.2: Schematic cross section through Bonanza pluton.

6. Conclusions

During the field and analytical portions of this study six important conclusions were determined.

1. Placer gold mined from the study area is definitely locally derived. All of the placer grain (excluding sample 975842) finenesses and placer averages fall within the range of finenesses taken from outcrop. All analyzed placer grains were either attached to tetradymite (a soft mineral which would be destroyed quickly in a stream environment), had experience little Ag-leaching or had irregular shapes indicating local derivation.
2. The Nyac batholith is significantly older than Bonanza pluton and dated mineralization. The Nyac batholith is thus unrelated to any of the mineralization in the study area. The hornblende age for the gray dikes at the Wallace occurrence are younger than the hornblende age of the Nyac Batholith, illustrating that the batholith cannot be responsible for this mineralization.
3. All portions of the Bonanza pluton have statistically indistinguishable biotite ages, distinct trace element fractionation patterns and similar mineralogy. All these lines of evidence indicate that the VABM Bonanza lobe, Spruce Creek lobe and Bonanza Creek lobe are part of the same pluton. The differences in composition are likely the result of different levels of exposure of the zoned pluton. Mineralization from mineralized quartz muscovite veins at VABM Bonanza lobe yield an age slightly older than the biotite, but definitely younger than hornblende. The closure temperature of muscovite is higher than biotite and lower than hornblende, thus the mineralization occurred during cooling of the Bonanza pluton.
4. The gray dikes yield statistically indistinguishable ages from dated hornblende (and biotite?) from Bonanza pluton, and the red dikes have a statistically indistinguishable biotite age from that of the Bonanza pluton. The similar ages suggest that the grey dikes, the Bonanza pluton and possibly the red dikes were derived from a common magmatic body. The extreme trace element enrichment of the red dikes suggests they are not compositionally related to the Bonanza pluton. It is possible that multiple magma bodies existed at ~113 Ma ago.
5. Bedding measurements indicate that the metasedimentary rocks overlie the metavolcanic rocks. This finding is consistent with dated fossils (Box et al., 1993). Variable bedding measurements are likely due to the significant movement along faults and original non-horizontal bedding due to an active volcanic-arc formation.
6. The high temperature Cu-Bi-Au mineralization in the study area is unique to the Nyac terrane in SW Alaska. The dated mineralization is older than all other dated Au occurrences of the region. The style of mineralization is also different with respect to high salinities, essentially no arsenopyrite and the association of chalcopyrite. Since this is the first documentation of this style

of mineralization in southwest, Alaska the economic potential for this type of mineralization is unknown.

6.1 Recommended Work

It is the author's hope that the results presented in this study will provide a solid basis for continued exploration in the Nyac district. The following is a summary of recommendations for further study and exploitation.

1. Due to poor exposure, geologic mapping in the Nyac terrane is difficult. There appears to be a tremendous number of faults that cut the study area. Producing a more accurate map requires more geophysical data. Tighter flight lines for a magnetic survey and a resistivity survey would make mapping the geology simpler and more accurate.
2. Three areas of the most intense gold mineralization have been outlined: the Wallace occurrence, the VABM Bonanza lobe and the BCCA. Continued work should be focused on these areas. Gridded soil sampling, trenching, and drilling these targets should be conducted to estimate the economic potential of the Nyac district.
3. What role do the pink dikes play in Au mineralization in the Nyac district? Although no mineralization was ever found in the pink porphyry dikes significant mineralization occurs in close proximity to these dikes. The closest spatially associated mineralized areas are at the Bonanza pluton contact with the metavolcanic rocks at Spruce Creek and in the center of VABM Bonanza lobe. A sample should be dated to see if the age is similar to that of the muscovite from VABM Bonanza lobe mineralization.
4. Obtain a U-Pb date of the Rex Creek pluton to determine its true age.
5. Dating the scapolite from the contact at the Spruce Creek skarn and from the metasedimentary rock unit will indicate which igneous body is responsible for the skarn mineralization.
6. Dating of secondary biotite from the High-T, Cu-Au mineralization at the BCCA, and dating sericite from the Wallace occurrence would show if all these styles of mineralization are related to a single event (Bonanza Pluton) and give a time constraint on how long the system lasted.
7. Are the mafic dikes in the study area responsible for the Ar loss seen in all the age spectra and later epithermal mineralization? Dating the mafic dike from the Spuce Creek lobe will answer part of this question.

References

ADGGS, WGM, Dighem, 1994, Digital gridded data of total field magnetics for entire survey of Nyac mining district: Alaska Division of Geological & Geophysical Surveys, Public Data File 94-34, 1 disk.

Bethke, C.M., 1998, The Geochemist's Workbench (computer program). University of Illinois, Urbana.

Box, S.E., Moll-Stalcup, E.J., Frost, T.P., and Murphy, J.R., 1993, Preliminary geologic map of the Bethel and southern Russian Mission quadrangles, southwestern Alaska: U.S. Geological Survey Miscellaneous Field Studies Map MF-2226-A, scale 1:250,000, 20 p.

Blatt, H., and Tracy, R.J., 1995, Petrology Igneous, Sedimentary, and Metamorphic, Houndsmills, Basingstoke, England, 2nd edition: W. H. Freeman and Company, 529 p.

Brown, P.E., 1989, FLINCOR: A microcomputer program for the reduction and investigation of fluid inclusion data: American Mineralogist, v. 74, p. 1390-1393.

Bundtzen, T.K., and Miller, M.L., 1997, Precious metals associated with Late Cretaceous-Early Tertiary igneous rocks of southwestern Alaska: Economic Geology Monograph 9, p. 242-295.

Cameron, C.E., 2000, Fault-hosted Au Mineralization, Ester Dome, Alaska: M.S. Thesis, University of Alaska, Fairbanks, 115 p.

Candela, P.A., and Piccoli, P.M., 1995, Model ore-metal partitioning from melts into vapor and vapor/brine mixtures, *in* Thompson, J. F. H., ed., Magmas, Fluids, and Ore Deposits: Mineralogical Association of Canada Short Course, v. 23, p. 101-127.

Davis, J.C., 2002, Statistics and Data Analysis in Geology: New York, John Wiley & Sons, 638 p.

Decker, J., Bergman, S.C., Blodgett, R.B., Box, S.E., Bundtzen, T.K., Clough, J.G., Coonrad, W.L., Gilbert, W.G., Miller, M.L., Murphy, J.M., Robinson, M.S., and Wallace, W.K., 1994, Geology of Southwestern Alaska, in Plafker, G., and Berg, H.C., eds., v. G1, The Geology of Alaska: Boulder, Colorado, Geological Society of America, Geology of North America, p. 285-310.

Deer, W.A., Howie, R.A., and Zussman, J., 1997a, Rock-Forming Minerals: Single Chain Silicates, 2nd ed, Oxford UK, Alden Press, Osney Mead, v. 2A, 668 p.

Deer, W.A., Howie, R.A., and Zussman, J., 1997b, Rock-Forming Minerals: Double Chain Silicates, 2nd ed, Oxford UK, Alden Press, Osney Mead, v. 2B, 758 p.

Deer, W.A., Howie, R.A., and Zussman, J., 1966, An Introduction to the Rock-Forming Minerals: Longman Group Limited, London, 528 p.

Delany, J.M., and Lundeen, S.R., S.R., 1990, The LLNL thermodynamic database: Lawrence Livermore National Laboratory Report UCRL-21658, 150 p.

De la Roche, H., Leterrier, J., Grande Claude, P., and Marchal, M., 1980, A classification of volcanic and plutonic rocks using R1-R2 diagrams and major element analyses—its relationships and current nomenclatures: Chemical Geology, v. 29, 183-210.

Foley, J., 2000, The Nyac mining district, southwestern Alaska: Calista Corporation, unpublished company report, 13 p.

Frost, T.P., Box, S.E., and Moll-Stalcup, E.J., 1993, Summary of results of the mineral resource assessment of the Bethel and southeastern part of the Russian Mission 1^{o} and 3^{o} quadrangles, Alaska: U.S. Geological Survey Bulletin 2041, p. 30-48.

Frost, T.P., 1990, Geology and geochemistry of mineralization in the Bethel quadrangle, southwestern Alaska, in Goldfard, R.J., Nash, J.T., and Stoeeser, J.W., eds., Geochemical studies in Alaska by the U.S. Geological Survey: U.S. Geological Survey Bulletin 1950, p. C1-C10.

Gammons, C.H., and Williams-Jones, A.E., 1997, Chemical mobility of gold in the porphyry-epithermal environment: Economic geology, v. 92, p. 45-59.

Gates, G., 1945a, Letter from USGS geologist George Gates to USGS geologist Robert Wallace, July 9, 1945. (Calista Corporation holdings)

Gates, G., 1945b, Letter from USGS geologist George Gates to USGS geologist Robert Wallace, July 17, 1945. (Calista Corporation holdings)

Gierymski, C., and Werdon, M. B., 1997, 1997 Summary report: Placer Dome Exploration, unpublished company report, Nyac- project 8A-25, 2 volumes.

Gray, J.E., Gent, C.A., Snee, L.W., and Wilson, F.H., 1997, Epithermal mercury-antimony and gold bearing vein lodes of southwestern Alaska: Economic Geology Monograph 9, p. 287-305.

Hayashi, K-I., and Ohmoto, H., 1991, Solubility of gold in NaCl- and H_2S-bearing aqueous solutions at 250-350 ^{o} C: Geochemica et Cosmochemica Acta, v. 55, p. 2111-2126.

Hedenquist, J.W., 1995, The ascent of magmatic fluid: discharge versus mineralization, in Thompson, J. F. H., ed., Magmas, Fluids, and Ore Deposits: Mineralogical Association of Canada Short Course, v. 23, p. 101-127.

Hoare, J.M., and Coonrad, W.L., 1959, Geology of the Russian Mission quadrangle, Alaska: U.S. Geological Survey Miscellaneous Investigations Map I-292, scale 1:250,000.

Huang, W-L., and Wyllie, P.J., 1975, Melting relations in the system $NaAlSi_3O_8$-$KAlSi_3O_8$-SiO_2 to 35 kilobars, dry and excess water: Journal of Geology, v. 83, p. 737-748.

Irvine, T.N., and Baragar, W.R.A., 1971, A guide to the chemical classification of the common volcanic rocks: Canadian Journal of Earth Science, v. 8, p. 523-548.

Knight, J.B., Morison, S.R., and Mortensen, J.K., 1999, The relationship between placer gold particle shape, rimming, and distance of fluvial transport as exemplified by gold from the Klondike district, Yukon Territory, Canada: Economic Geology, v.94, p. 635-648.

Krauskopf, K.B., and Bird, D.K., 1995, Introduction to Geochemistry: New York, Mc-Graw Hill, 647 p.

Lanphere, M.A., and Dalrymple, G.B., 2000, First-principles calibration of ^{38}Ar tracers: Implications for the ages of $^{40}Ar/^{39}Ar$ fluence monitors: U.S. Geological Survey Professional Paper 1621, 10 p.

Layer, P.W., 2000, $^{40}Ar/^{39}Ar$ age of the El'gygytgyn impact event, Chukotka, Russia: Meteoritics and Planetary Science, v. 35, p. 591-600.

Layer P. W., Hall C. M. and York D., 1987, The derivation of $^{40}Ar/^{39}Ar$ age spectra of single grains of hornblende and biotite by laser step heating: Geophysical Research Letters, v. 14, p. 757-760.

LeMaitre, R.W.[ed.], Bateman, P., Dudek, A., Keller, J., Lemeyre, J., Le Bas, M.J., Sabine, P.A., Schmid, R., Sorenson, H., Sreckheisen, A., Wooley, A.R., and Zanettin, B., 1989, A classification of igneous rocks and glossary of terms: Blackwell Science Publishing, Oxford, 193 p.

Luth, W.C., Jahns, R.H., and Tuttle, O.F., 1964, The granite system at pressures of 4-10 kbar: Journal of Geophysical Research, v. 69, p. 759-773.

Maddren, A.G., 1915, Gold placers of the lower Kuskokwim, with a note on copper in the Russian mountains, in Brooks, A.H. ed., Mineral Resources of Alaska: U.S. Geological Survey Bulletin 622, p. 292-355.

McDougal, I., and Harrison, T.M., 1988, Geochronology and Thermochronolgy by the $^{40}Ar/^{39}Ar$ Method: New York, Oxford University Press, 212 p.

Metz, P.A. and Hawkins, D.B., 1981, A summary of gold fineness values from Alaska placer deposits, University of Alaska, Mineral Industry Research Lab, Report No. 45, 63 p.

Middelaar, W.T. van, and Keith, J.D., 1990, Mica chemistry as an indicator of oxygen and halogen fugacities in the CanTung and other W-related granitoids in the North American Cordillera, in Stein, H.J., and Hannah, J.L., eds.: Geological Society of America Special Paper 246, p. 205-220.

Miller, M.L., Bradley, D.C., Bundtzen, T.K., and McClelland, W., 2002, Late Cretaceous through Cenozoic strike-slip tectonics of southwestern Alaska: Journal of Geology, v. 110, p. 247-270.

Mirsa, K.C., 2000, Understanding Mineral Deposits: Dordrecht Netherlands, Kluwer Academic Publishers, 845p.

Pearce, J.A., and Cann, J.R., 1973, Tectonic setting of basic volcanic rocks determined using trace element analyses: Earth and Planetary Science Letters, v. 19, p. 290-300.

Pearce, J.A., Harris, N.B.W., and Tindle, A.G., 1984, Trace element discrmination diagrams for the tectonic interpretation of granitic rocks: Journal of Petrology, v. 25, p. 956-983.

Potter, R.W, II, 1977, Pressure corrections for fluid inclusion homogenization temperatures based on the volumetric properties of the system H_2O-NaCl: U.S. Geological Survey Journal of Research, v. 5, p. 603-607.

Resource Associates of Alaska (RAA), 1975, Mineral resource evaluation for Calista Corporation: Final report of exploration activities during 1975, unpublished report, 29p.

Robinson, M.S., and Decker, J., 1986, Preliminary age dates and analytical data for selected igneous rocks from the Sleetmute, Russian Mission, Taylor Mountains, and Bethel quadrangles, southwestern: Alaska Division of Mining and Geological and Geophysical Surveys, Public Data File 86-99, 3 p.

Ruperto, V.L., Stevens, R.E., and Norman, M.B., 1964, Staining of plagioclase feldspar and other minerals with F.D. and C. Red No. 2: U.S. Geological Survey Professional Paper 501B, p. 152-153.

Samson S. D., and Alexander E. C., 1987, Calibration of the interlaboratory $^{40}Ar/^{39}Ar$ dating standard, MMhb-1: Chemical Geology, v. 66, p. 27-34.

Streckheisen, A.L., 1973, Classification and nomenclature recommended by the IUGS Subcommission on the systematics of igneous rocks: Geotimes, v. 18, p. 26-30.

Steiger, R.H. and Jaeger, E., 1977, Subcommission on geochronology: Convention on the use of decay constants in geo and cosmochronology: Earth and Planetary Science Letters, v. 36, p. 359-362.

Steiner, J.C., Jahns, R.H., and Luth, W.C., 1975, Crystallization of alkali feldspars and quartz in the haplogranite system $NaAlSi_3O_8$-$KAlSi_3O_8$-SiO_2-H_2O at 4 kb: Bulletin of the Geological Society of America, v. 86, p. 83-98.

Thompson, J.F.H. and Newberry, R.J.J., 2000, Low fO_2 intrusion-related gold deposits: An important class of Phanerozoic ores: Reviews in Economic Geology, v. 14, p. 12-38.

Tuttle, O.F., and Bowen, N.L., 1958, The origin of granite in the light of experimental studies in the system $NaAlSi_3O_8$-$KAlSi_3O_8$-SiO_2 - H_2O: Geological Society of America Memoir, no. 74.

Wallace, R.E., 1945, Free-gold lode deposit on Tuluksak River, Kuskokwim Region, Alaska: US Department of the Interior Press Release, August 4, 1945.

Wilson, F.H., 1977, Some plutonic rocks of southwestern Alaska, a data compilation: U.S. Geological Survey Open-File Report 77-501.

Winchester, J.A., and Floyd, P.A., 1977, Geochemical discrimination of different magma series and their differentiation products using immobile elements: Chemical Geology, v. 20, p. 325-343.

Wood, S.A., Crear, D.A., and Borcsik, M.P., 1987, Solubility of the assemblage, pyrite-pyrrhotite magnetite-sphalerite-galena-gold-stibnite-bismuthinite-argentite-molybdenite in H_2O-NaCl-CO_2 solutions from 200^o to 350^o C: Economic Geology, v. 82, p. 1864-1887.

York, D., Hall, C.M., Yanase, Y., Hanes, J.A., and Kenyon, W.J., 1981, $^{40}Ar/^{39}Ar$ dating of terrestrial minerals with a continuous laser: Geophysical Research Letters, v. 8, p. 1136-1138.

Appendices

Appendix A: List of samples, location, rock type, veining style, ore mineralogy and magnetic susceptibility.

Abbreviations are as follows: asp= arsenopyrite, cc= calcite, chl= chlorite, co= chalcopyrite, bis= bismuthinite, ep=epidote, hm= hematite, il= ilmenite, lim= limonite, mal= malachite, mg=magnetite, musc= muscovite, po= pyrrhotite, py=pyrite, qtz= quartz, rt= rutile, ser= sericite, tebis= tellurobismuthite and tet= tetradymite.

Sample	UTM E	UTM N	Lithology	Ore Minerals	Veins	Magnetic Susceptibility
03ZW001	460927	6771453	Conglomerate Hornfels	py		0.90
03ZW002	460929	6771463	Andesite Hornfels	py		0.46
03ZW003	461899	6771273	Gabbro	mg,il		17.23
03ZW004	462537	6771678	Andesite Hornfels	py,co	ep	0.31
03ZW005	462278	6772703	Granodiorite Dike			0.45
03ZW006	449959	6769116	Andesite Hornfels	co,py	chl(2%)	0.57
03ZW007	455115	6768387	Basalt Hornfels	py	chl	6.17
03ZW008	455169	6768473	Andesite Hornfels		chl	5.57
03ZW009	455189	6768578	Volcaniclastic Hornfels	py	qtz-chl	0.35
03ZW010	455151	6768405	Basalt Hornfels	co,py	ep-chl-qtz	2.04
03ZW011	455369	6768066	Basalt Hornfels			8.50
03ZW012	455353	6768078	Basalt Hornfels	co		11.55
03ZW013	455293	6768198	Basalt Hornfels			4.94
03ZW014	455291	6768209	Volcaniclastic Hornfels	mg		20.43
03ZW015	455234	6768305	Volcaniclastic Hornfels	co,py	chl-ep-qtz(80%)	1.22
03ZW016	455216	6768337	Andesite Hornfels			0.43
03ZW017	454998	6768516	Basalt Hornfels	py	ep	14.03
03ZW018	455015	6768481	Breccia	lim	qtz,lim	0.44
03ZW019	454962	6768320	Pink Dike			5.04
03ZW020	454953	6768322	Volcaniclastic Hornfels		chl	0.31
03ZW021	454925	6768303	Basalt Hornfels			16.73
03ZW022	454839	6768229	Volcaniclastic Hornfels		ep-chl-qtz(2%)	0.41
03ZW023	454816	6768210	Volcaniclastic Hornfels		ep	0.64
03ZW024	454719	6768122	Dacite Sill Hornfels			0.79
03ZW025	454651	6768087	Basalt Hornfels			5.73
03ZW026	454617	6768030	Volcaniclastic Hornfels	po		0.52
03ZW027	454348	6768150	Volcaniclastic Hornfels	py		0.44
03ZW028	454393	6768124	Breccia	lim		0.33
03ZW029	454507	6767881	Dacite Sill Hornfels			0.72
03ZW030	454505	6767869	Breccia	lim		0.25
03ZW031	454474	6767820	Volcaniclastic Hornfels	py		0.62
03ZW032	454456	6767618	Andesite Hornfels	lim		0.51
03ZW033	454449	6767549	Felsic Dike	py(15%)		0.87
03ZW034	453985	6767638	Volcaniclastic Hornfels	py	qtz-ep-chl-cc(5%)	0.61
03ZW035	454052	6767662	Breccia	lim	lim-cc	0.48

Sample	UTM E	UTM N	Lithology	Ore Minerals	Veins	Magnetic Susceptibility
					(pervasive)	
03ZW036	454080	6767687	Volcaniclastic Hornfels			0.88
03ZW037	454428	6767467	Dacite Sill Hornfels			0.41
03ZW038	454420	6767364	Volcaniclastic Hornfels			0.25
03ZW039	454404	6767048	Volcaniclastic Hornfels	py,co	ep (pods)	5.31
03ZW040	450992	6763935	Siltstone Hornfels	py,lim	ep-qtz-cc	0.58
03ZW041	459579	6770483	Sawpit Pluton		qtz-ep-Na-spar	1.45
03ZW042	459579	6770483	Volcaniclastic Hornfels			0.58
03ZW043	452626	6767767	Basalt Hornfels	co,hm	ep-cc	30.40
03ZW044	452632	6767704	Basalt Hornfels		ep-cc	17.47
03ZW045	452641	6767636	Basalt Hornfels	hm?	ep-cc (5%)	12.77
03ZW046	452649	6767587	Altered Porphyry (Dike?)	lim		0.69
03ZW047	452652	6767567	Basalt Hornfels	hm?	ep-cc	1.54
03ZW048	452682	6767402	Basalt Hornfels		ep-qtz-cc (10%)	1.55
03ZW049	452718	6767350	Volcaniclastic Hornfels	hm?	ep-cc (2%)	6.55
03ZW050	452749	6767283	Altered Porphyry (Dike?)	lim		0.29
03ZW051	452790	6767199	Altered Porphyry (Dike?)	lim		0.40
03ZW052	452808	6767067	Volcaniclastic Hornfels		ep-cc	0.43
03ZW053	452806	6767020	Alt Metavolcanic Hornfels	lim,py		0.26
03ZW054	452795	6766961	Breccia	lim		0.39
03ZW055	452799	6766816	Tonalite Hornfels	lim		0.61
03ZW056	452885	6766555	Monzogranite			2.26
03ZW057	452901	6766505	Altered Diorite Hornfels	lim		0.35
03ZW058	452931	6766480	Volcaniclastic Hornfels		ep-cc	0.85
03ZW059	452921	6766261	Basalt Hornfels			2.39
03ZW060	453089	6765687	Andesite Hornfels	py		0.48
03ZW061	450236	6768195	Volcaniclastic Hornfels			0.29
03ZW062	450385	6767749	Andesite Hornfels			0.61
03ZW063	450872	6767990	Andesite Hornfels	py		0.76
03ZW064	450933	6767985	Volcaniclastic Hornfels	py (2-3%)		0.83
03ZW065	451010	6767984	Basalt Hornfels			17.43
03ZW066	451108	6767987	Basalt Hornfels	py	ep-cc	7.74
03ZW067	451197	6767981	Basalt Hornfels	py (2%)		18.30
03ZW068	451296	6767961	Quartz Diorite Hornfels			25.03
03ZW069	451364	6767905	Altered Porphyry (Dike?)	lim		0.37
03ZW070	451441	6767916	Diorite Hornfels		ep	3.36
03ZW071	451626	6767843	Volcaniclastic Hornfels		ep-cc (5%)	0.88
03ZW072	451541	6767900	Diorite Dike Hornfels			1.40
03ZW073	451402	6768220	Basalt Hornfels	py	ep-chl-cc	37.47
03ZW074	451373	6768288	Andesite Hornfels	py, lim (3%)	lim	0.45
03ZW075	451349	6768376	Andesite Hornfels	py(3%)		1.91
03ZW076	451324	6768514	Volcaniclastic Hornfels			0.42
03ZW077	453156	6768868	Quartz Veined Breccia	py,lim	silica	0.20
03ZW078	453054	6768913	Basalt Hornfels		ep	35.10
03ZW079	453010	6768852	Basalt Hornfels	py	ep	21.67
03ZW080	452970	6768832	Basalt Hornfels	py		9.08

Sample	UTM E	UTM N	Lithology	Ore Minerals	Veins	Magnetic Susceptibility
03ZW081	452905	6768750	Volcaniclastic Hornfels			0.34
03ZW082	452836	6768674	Andesite Hornfels	py	ep	0.55
03ZW083	452714	6768574	Basalt Hornfels		ep	12.36
03ZW084	452648	6768549	Basalt Hornfels			25.80
03ZW085	452589	6768516	Basalt Hornfels		qtz-ep	21.00
03ZW086	453180	6768847	Breccia	lim,cc(30%)		
03ZW087	451262	6765472	Epidote-Quartz Vein			0.46
03ZW088	452421	6767968	Alt Metavolcanic Hornfels	mal(5%)		0.51
03ZW089	452557	6768430	Dacite Hornfels			0.41
03ZW090	452554	6768438	Diorite Dike Hornfels			2.41
03ZW091	452467	6768095	Andesite Hornfels		cc	0.50
03ZW092	452459	6768054	Andesite Hornfels	py	cc-qtz	0.58
03ZW093	452425	6767969	Quartz Vein	lim,co	qtz-cc-mal	0.21
03ZW094	452409	6767945	Andesite Hornfels	py	cc	0.34
03ZW095	452365	6767886	Alt Metavolcanic Hornfels	hm,py,mal	ep-qtz-cc(5%)	0.51
03ZW096	453040	6769173	Andesite Hornfels		ep-qtz-cc	0.59
03ZW097	453045	6769117	Andesite Hornfels	py	ep-qtz-cc-chl	0.76
03ZW098	452574	6768393	Andesite Hornfels		ep	1.67
03ZW099	452391	6767901	Alt Metavolcanic Hornfels	lim,py?		0.51
03ZW100	452333	6767870	Andesite Hornfels	py,lim	qtz	1.01
03ZW101	452249	6767856	Andesite Hornfels	py		0.38
03ZW102	452143	6767873	Breccia	py,lim	qtz	0.20
03ZW103	452111	6767879	Dacite Hornfels			5.06
03ZW104	451950	6767867	Quartz Diorite Hornfels		ep (2%)	6.65
03ZW105	451909	6767850	Diorite Hornfels		ep (2%)	17.07
03ZW106	451886	6767855	Pink Dike			4.74
03ZW107	451824	6767817	Diorite Hornfels	lim		11.40
03ZW108	451669	6767780	Quartz Monzodiorite H		ep-qtz	7.81
03ZW109	451650	6767835	Intrusive Breccia	lim	qtz-cc	3.06
03ZW110	452110	6767853	Dacite Hornfels			4.85
03ZW111	452292	6767716	Quartz Veined Breccia	lim		0.12
03ZW112	452319	6767614	Basalt Hornfels			13.57
03ZW113	452445	6767837	Gabbro			37.73
03ZW114	452570	6767805	Quartz Veined Breccia	lim	qtz	0.08
03ZW115	460143	6772174	Andesite Hornfels			0.19
03ZW116	460126	6772171	Monzogranite			0.11
03ZW117	460036	6772223	Monzogranite			0.37
03ZW118	459741	6772908	Dacite Hornfels			11.10
03ZW119	460222	6773629	Alt Metavolcanic Hornfels	lim	qtz-ser	0.27
03ZW120	460224	6773681	Alt Metavolcanic Hornfels	lim	qtz-ser	0.29
03ZW121	460317	6773963	Dacite Hornfels			10.42
03ZW122	460219	6773976	Shear	lim	qtz-ser	0.18
03ZW123	453638	6769305	Breccia	lim	silica	0.06
03ZW124	453672	6769328	Pink Dike			3.21
03ZW125	453803	6769439	Alt Metavolcanic Hornfels		chl-qtz-cc	0.42
03ZW126	453868	6769470	Volcaniclastic Hornfels			4.35

Sample	UTM E	UTM N	Lithology	Ore Minerals	Veins	Magnetic Susceptibility
03ZW127	453997	6769592	Quartz Vein	lim, py	qtz-chl	0.07
03ZW128	454045	6769695	Mudstone Hornfels	lim	silica	0.14
03ZW129	454097	6769696	Pink Dike			7.60
03ZW130	454145	6769719	Mudstone Hornfels	py(2%),co	chl	0.77
03ZW131	454184	6769731	Basalt Hornfels		qtz-ep-chl-cc	40.97
03ZW132	454379	6769551	Alt Metavolcanic Hornfels	py(2%),lim	ep-qtz-cc-chl	8.11
03ZW133	454317	6769638	Alt Metavolcanic Hornfels	lim,py,co	silica	0.29
03ZW134	455188	6768566	Volcaniclastic Hornfels			0.52
03ZW135	455171	6768805	Alt Metavolcanic Hornfels	lim	silica	16.80
03ZW136	455225	6768954	Diorite Hornfels	py(2%)		13.73
03ZW137	455199	6769078	Alt Metavolcanic Hornfels	py(3%)		7.05
03ZW138	455211	6769095	Andesite Hornfels		qtz-cc-ep	22.33
03ZW139	455224	6769168	Alt Metavolcanic Hornfels	py,po		23.37
03ZW140	455232	6769210	Basalt Hornfels			16.67
03ZW141	455232	6769321	Volcaniclastic Hornfels	py(2%)		50.23
03ZW142	455124	6769795	Granodiorite	py, bis	qz-chl-py-po-bth	4.54
03ZW143	453819	6773447	Diorite Hornfels	py		0.63
03ZW144	453853	6773622	Mudstone Hornfels	py,po		0.43
03ZW145	453946	6773723	Mudstone Hornfels	py,po, lim		1.01
03ZW146	453908	6773724	Mudstone Hornfels			0.24
03ZW147	453970	6773777	Gray Dike			4.44
03ZW148	453992	6773809	Diorite Hornfels	py		0.52
03ZW149	454053	6773990	Mudstone Hornfels	py	silica	0.99
03ZW150	454072	6774212	Gray Dike			0.37
03ZW151	453915	6774303	Mudstone Hornfels		qtz-chl	0.44
03ZW152	453933	6774309	Conglomerate Hornfels			0.48
03ZW153	454142	6774130	Andesite Hornfels			8.76
03ZW154	454203	6774126	Dacite Hornfels			0.23
03ZW155	454251	6774116	Monzonite Hornfels			0.81
03ZW156	454093	6773420	Mudstone Hornfels	py		0.38
03ZW157	452268	6771755	Diorite Hornfels			11.10
03ZW158	452214	6771810	Mudstone Hornfels	py		0.82
03ZW159	452074	6771988	Volcaniclastic Hornfels	py		1.74
03ZW160	452038	6772272	Diorite Hornfels		chl	0.55
03ZW161	452044	6772597	Pink Dike			2.83
03ZW162	451914	6772775	Diorite Hornfels			1.27
03ZW163	452284	6772813	Mudstone Hornfels		chl-qtz-cc(2%)	0.50
03ZW164	452343	6772891	Diorite Hornfels			0.34
03ZW165	452398	6772980	Mudstone Hornfels	py	chl-qtz-cc,silica	0.69
03ZW166	452475	6773058	Mudstone Hornfels		chl-qtz(3%)	0.27
03ZW167	452475	6773058	Diorite Hornfels		chl-qtz(3%)	0.26
03ZW168	452503	6773109	Gray Dike			0.25
03ZW169	452582	6773149	Conglomerate Hornfels			0.46
03ZW170	452880	6774216	Mudstone Hornfels		chl-qtz(15%)	0.19
03ZW171	452667	6774311	Mudstone Hornfels	py	silica	0.30
03ZW172	452536	6774276	Dacite Hornfels			0.98

Sample	UTM E	UTM N	Lithology	Ore Minerals	Veins	Magnetic Susceptibility
03ZW173	452377	6774063	Peraluminous Aplite Dike			1.46
03ZW174	453393	6774348	Mudstone Hornfels	py	chl-qtz	0.54
03ZW175	453358	6773978	Breccia		cc(20%)	13.55
03ZW176	456487	6772736	Granodiorite Dike			3.06
03ZW177	456399	6772687	Volcaniclastic Hornfels	py?		0.47
03ZW178	456325	6772692	Breccia	lim	cc(5%)	0.34
03ZW179	456220	6772668	Granodiorite Dike			4.46
03ZW180	456120	6772672	Quartz Vein		qtz	0.14
03ZW181	455955	6772712	Aplite Dike		qtz	0.16
03ZW182	455902	6772732	Mudstone Hornfels			0.26
03ZW183	455819	6772778	Breccia	lim		0.22
03ZW184	455746	6772828	Aplite Dike			0.69
03ZW185	455391	6772889	Volcaniclastic Hornfels			0.54
03ZW186	453790	6773047	Mudstone Hornfels	py,lim	chl(2%)	0.50
03ZW187	454519	6773022	Conglomerate Hornfels		cc-chl	0.63
03ZW188	454944	6773103	Mudstone Hornfels	py		0.58
03ZW189	455143	6773134	Tonalite?			0.66
03ZW190	455098	6773431	Mudstone Hornfels			0.58
03ZW191	455403	6774344	Conglomerate Hornfels			0.62
03ZW192	455586	6774424	Gray Dike			4.11
03ZW193	455985	6774203	Pink Dike			1.98
03ZW194	456757	6773963	Volcaniclastic Hornfels	py		0.61
03ZW195	456044	6774108	Tonalite Dike			0.37
03ZW196	455980	6774194	Pink Dike			2.16
03ZW197	455292	6774155	Gray Dike			0.45
03ZW198	452085	6765630	Volcaniclastic Hornfels			0.39
03ZW199	451985	6765800	Intrusive Breccia	py?		2.67
03ZW200	451595	6767669	Quartz Diorite Hornfels	py	ep-qtz(2%)	12.87
03ZW201	451560	6767647	Diorite Hornfels			6.85
03ZW202	451560	6767647	Basalt Hornfels	py	ep-qtz(3%)	19.23
03ZW203	451526	6767580	Andesite Hornfels	py	ep-qtz(2%)	0.82
03ZW204	451512	6767531	Altered Diorite Hornfels	lim		0.31
03ZW205	451459	6767474	Volcaniclastic Hornfels	py(2%)	qtz-ep	0.47
03ZW206	451431	6767375	Alt Metavolcanic Hornfels	lim		0.02
03ZW207	451400	6767219	Diorite Hornfels			0.61
03ZW208	451360	6767127	Altered Porphyry (Dike?)	lim		0.52
03ZW209	451355	6767115	Altered Porphyry (Dike?)	lim(25%)		0.21
03ZW210	450542	6766921	Andesite Hornfels	py		1.35
03ZW211	451218	6767013	Diorite Hornfels	py	ep(2%)	0.30
03ZW212	451396	6766765	Quartz Diorite Hornfels			10.94
03ZW213	451425	6766700	Granodiorite		ep-qtz	5.47
03ZW214	451550	6766427	Granodiorite Hornfels			0.48
03ZW215	451583	6766159	Diorite Hornfels			3.74
03ZW216	451540	6765339	Volcaniclastic Hornfels	mg	cc(2%)	8.14
03ZW217	451222	6765452	Volcaniclastic Hornfels	py	ep-qtz-cc(2%)	0.48
03ZW218	451234	6765691	Basalt Hornfels	py	cc	0.59

Sample	UTM E	UTM N	Lithology	Ore Minerals	Veins	Magnetic Susceptibility
03ZW219	451245	6765742	Quartz Vein	co, mal	qtz-chl(95-5%)	0.08
03ZW220	451241	6765840	Quartz Diorite Hornfels	lim		8.28
03ZW221	451421	6765952	Alt Metavolcanic Hornfels	mg		0.28
03ZW222	450645	6765696	Andesite Hornfels	py		0.93
03ZW223	459892	6771320	Epidote Rock	py(2%)		0.71
03ZW224	459718	6771209	Alt Metavolcanic Hornfels	py(2%)	ep-qtz(3%)	0.13
03ZW225	459411	6771198	Chlorite Rock	co,py		0.92
03ZW226	459312	6771149	Volcaniclastic Hornfels	py	chl(5%)	0.49
03ZW227	459605	6770283	Quartz Vein	co, py		
03ZW228	459601	6770283	Quartz Monzonite		qtz-Kspar-ep	
03ZW229	459601	6770283	Altered Quartz Monzonite	py	qtz-Kspar-ep	
03ZW230	459483	6770272	Sawpit Pluton			8.20
03ZW231	459188	6770080	Sawpit Pluton	py		0.25
03ZW232	458123	6771026	Basalt Hornfels		qtz-chal	14.93
03ZW233	458034	6771189	Basalt Hornfels		qtz-chal	23.63
03ZW234	457744	6771285	Basalt Hornfels			8.58
03ZW235	457654	6771322	Basalt Hornfels			16.83
03ZW236	457567	6771319	Altered Metabasalt			5.01
03ZW237	457294	6771495	Basalt Hornfels			11.01
03ZW238	456775	6771456	Volcaniclastic Hornfels	mg	qtz-chl	1.64
03ZW239	456738	6771430	Andesite Hornfels			1.73
03ZW240	456735	6771429	Breccia	lim(10%)		0.57
03ZW241	456722	6771415	Alt Metavolcanic Hornfels	lim		0.15
03ZW242	456710	6771401	Volcaniclastic Hornfels	py	chl-qtz(2%)	0.56
03ZW243	456630	6771314	Volcaniclastic Hornfels	py	chl-qtz-musc(3%)	5.13
03ZW244	456538	6771280	Volcaniclastic Hornfels		ep-qtz-chl-musc	1.76
03ZW245	456457	6771336	Volcaniclastic Hornfels		ep-qtz-chl-musc	0.53
03ZW246	456439	6771326	Volcaniclastic Hornfels		ep-qtz-chl(5%)	0.82
03ZW247	456429	6771327	Pink Dike			4.82
03ZW248	456372	6771302	Basalt Hornfels		chl(2%)	4.33
03ZW249	456385	6771341	Volcaniclastic Hornfels		qtz-chl(2%)	0.34
03ZW250	456376	6771341	Basalt Hornfels	mg		3.12
03ZW251	456355	6771305	Pink Dike			1.97
03ZW252	456306	6771313	Andesite Hornfels	mg(2%)	qtz-chl-musc-mg	42.40
03ZW253	456277	6771292	Alt Metavolcanic Hornfels	py, lim(2%)		0.16
03ZW254	456231	6771263	Dacite Hornfels	mg(2%)		19.57
03ZW255	456168	6771213	Basalt Hornfels	mg(2%)		107.97
03ZW256	456081	6771199	Skarn	mg, co, cv, py	qtz	8.75
03ZW257	456075	6771204	Skarn	py-po(3%),co,mg		3.07
03ZW258	456113	6771212	Alt Metavolcanic Hornfels	lim(5%)		0.14
03ZW259	459564	6770310	Sawpit Pluton		ep	16.23
03ZW260	452349	6771400	Quartz Diorite Hornfels			1.00
03ZW261	452349	6771399	Andesite Hornfels	py	chl-qtz	0.15
03ZW262	456708	6771401	Epidote-Chlorite vein	py(2%)	ep-chl(90%)	4.18
03ZW263	456005	6771205	Andesite Hornfels	py	chl-ep	2.95
03ZW264	455993	6771201	Alt Metavolcanic Hornfels	py(2%),lim		0.41

Sample	UTM E	UTM N	Lithology	Ore Minerals	Veins	Magnetic Susceptibility
03ZW265	455955	6771194	Pink Dike			5.70
03ZW266	455896	6771173	Basalt Hornfels	py(2%)		4.45
03ZW267	455836	6771161	Pink Dike			1.39
03ZW268	455804	6771164	Volcaniclastic Hornfels	py	qtz-chl	0.42
03ZW269	455733	6771125	Quartz Vein		qtz(99%)	0.21
03ZW270	455733	6771125	Gray Dike			13.77
03ZW271	455704	6771134	Alt Metavolcanic Hornfels	mg(5%),py(2%)	qtz-ep-chl-ser(2%)	9.89
03ZW272	455607	6771045	Monzodiorite			10.25
03ZW273	455603	6770976	Diorite			16.90
03ZW274	455774	6770835	Granodiorite	lim(10%)		0.22
03ZW275	455799	6770823	Quartz Diorite	co	qtz-chl	13.53
03ZW276	455812	6770796	Tonalite Dike			14.40
03ZW277	455824	6770773	Granodiorite			5.18
03ZW278	455850	6770697	Tonalite			18.17
03ZW279	455938	6770568	Monzodiorite			16.77
03ZW280	456191	6770296	Granodiorite	lim(5%), hem		0.14
03ZW281	456261	6770172	Monzodiorite	mg	chl-py	17.23
03ZW282	456225	6770254	Gabbro	mg		20.07
03ZW283	456075	6770466	Quartz Diorite			11.40
03ZW284	456047	6770481	Diabase Dike			13.27
03ZW285	458179	6773669	Basalt Hornfels		chl	22.90
03ZW286	458176	6773690	Basalt Hornfels	mg	chl-mg	49.10
03ZW287	458190	6773709	Alt Metavolcanic Hornfels	mg	chl-mg	32.13
03ZW288	458171	6773765	Alt Metavolcanic Hornfels	mg	chl-mg(80%)	34.40
03ZW289	458148	6773831	Basalt Hornfels	mg	chl-mg(3%)	66.87
03ZW290	458131	6773965	Basalt Hornfels	mg		71.20
03ZW291	458125	6773999	Breccia	py		0.69
03ZW292	458140	6774021	Breccia	lim(15%), hem		0.30
03ZW293	458150	6774125	Monzodiorite			30.83
03ZW294	458135	6774201	Tonalite			14.70
03ZW295	458152	6774259	Monzodiorite			29.50
03ZW296	458196	6774408	Quartz Monzodiorite			19.60
03ZW297	458355	6774558	Quartz Monzonite Dike			13.97
03ZW298	458914	6774673	Volcaniclastic Hornfels	py	qtz-ep	12.63
03ZW299	459519	6774652	Breccia	lim(10%)		0.68
03ZW300	458377	6772530	Volcaniclastic Hornfels	lim(5%)		13.34
03ZW301	458636	6772231	Basalt Hornfels			0.60
03ZW302	458619	6772342	Alt Metavolcanic Hornfels	lim(10%)		0.62
03ZW303	458601	6772509	Basalt Hornfels	lim(5%)		0.98
03ZW304	458576	6772951	Basalt Hornfels	py		24.33
03ZW305	459034	6773055	Basalt Hornfels		chl-qtz(2%)	21.97
03ZW306	458992	6773280	Alt Metavolcanic Hornfels	py(3%)		11.21
03ZW307	458976	6773640	Monzodiorite			5.40
03ZW308	458961	6773649	Andesite Hornfels			34.00
03ZW309	458739	6773535	Alt Metavolcanic Hornfels	py(5%)		0.71
03ZW310	453236	6771760	Conglomerate Hornfels			0.27

Sample	UTM E	UTM N	Lithology	Ore Minerals	Veins	Magnetic Susceptibility
03ZW311	452024	6769705	Basalt Hornfels			18.47
03ZW312	452069	6769746	Gray Dike			4.17
03ZW313	452183	6769814	Mudstone hornfels	py	qtz-chl-py	1.01
03ZW314	452317	6769917	Siltstone Hornfels			0.52
03ZW315	452406	6770007	Diorite Hornfels	py?	qtz-cc-chl	0.48
03ZW316	452419	6770016	Alt Metavolcanic Hornfels	py		0.09
03ZW317	452433	6770025	Pink Dike			3.02
03ZW318	452488	6770066	Andesite Hornfels	py	qtz-chl-cc	17.03
03ZW319	452522	6770068	Breccia	lim(10%)		0.63
03ZW320	452555	6770067	Diorite Hornfels	py	chl	0.67
03ZW321	452596	6770066	Basalt Hornfels	py	chl(10%)	1.61
03ZW322	454177	6771867	Dacite Hornfels	lim	qt-cc-mus	0.22
03ZW323	454258	6771891	Aplite Dike			0.33
03ZW324	454322	6769755	Andesite Hornfels	py		3.31
03ZW325	454328	6769768	Intrusive Breccia	py		2.09
03ZW326	454358	6769806	Intrusive Breccia	py(2%)		0.16
03ZW327	454404	6769884	Intrusive Breccia	py		0.66
03ZW328	454421	6769898	Clinopyroxenite Hornfels			36.73
03ZW329	454462	6769978	Intrusive Breccia	py(3%)		0.33
03ZW330	454188	6770244	Volcaniclastic Hornfels			18.57
03ZW331	454384	6770159	Pink Dike			7.96
03ZW332	454536	6770154	Intrusive Breccia	py(2%)		0.68
03ZW333	454586	6770173	Altered Felsic Dike	py(2%)		0.42
03ZW334	454650	6770211	Intrusive Breccia	red lim(2%)		0.02
03ZW335	454736	6770235	Volcaniclastic Hornfels	py	chl(4%)	2.40
03ZW336	454803	6770316	Intrusive Breccia	mg, py	chl(3%)	11.17
03ZW337	454819	6770392	Basalt Hornfels	py		35.33
03ZW338	454802	6770517	Mudstone hornfels		chl	0.63
03ZW339	454510	6771275	Quartz Monzodiorite	co,py,mo,rt	qtz-ser-sul	0.34
03ZW339B	454510	6771275	Aplite Dike			
03ZW340	454569	6770918	Quartz Monzodiorite	co,py, bis	qtz-ser-sul	4.73
03ZW341	454395	6769384	Granodiorite	py		5.23
03ZW342	454138	6769321	Aplite Dike			0.19
03ZW343	456012	6771285	Pink Dike			7.41
03ZW344	456060	6771220	Skarn	co,py,po		4.31
03ZW345	455805	6771159	Basalt Hornfels	py(3%)		0.76
03ZW346	455709	6771094	Basalt Hornfels	mg,py(2%)		22.90
03ZW347	455521	6771006	Diorite	lim, co, bis	qtz	7.46
03ZW348	455327	6770960	Quartz Diorite?	co,py, bis	qtz	10.14
03ZW349	455824	6770769	Granodiorite	co,py,asp	qtz-musc	2.98
03ZW350	455689	6770947	Diorite?	co,py	qtz-chl	2.83
03ZW351	458480	6773677	Quartz Monzonite Dike	lim(3%)		0.09
03ZW352	458532	6773613	Skarn	py(2%)		4.46
03ZW353	458135	6774036	Basalt Hornfels	py,co,mg, Au	qtz-chl-sulfide(3%)	92.27
03ZW354	458141	6774016	Breccia			0.64
03ZW355	454402	6775667	Tonalite		qtz	4.00

Sample	UTM E	UTM N	Lithology	Ore Minerals	Veins	Magnetic Susceptibility
03ZW356	456142	6776399	Tonalite		qtz and qtz-Kspar	10.00
03ZW357	454785	6777734	Granodiorite			5.00
03ZW358	453706	6779070	Granodiorite		qtz-Kspar	7.00
03ZW359	453175	6777346	Granodiorite			5.00
03ZW360	449666	6778440	Monzodiorite		qtz-Kspar	12.00
03ZW361	446934	6775776	Granodiorite			7.00
03ZW362	450099	6773992	Granodiorite			9.00
03ZW363	445813	6772869	Granodiorite			8.00
03ZW364	444359	6771884	Granodiorite			7.00
03ZW365	443643	6769271	Granodiorite			8.00
03ZW366	446620	6769360	Granodiorite			11.00
03ZW367	447902	6771398	Granodiorite			11.00
03ZW368	449815	6768948	Gray Dike			0.25
03ZW369	449896	6768969	Gray Dike	tebis,tet,Au,co	qtz-chl	0.19
03ZW370	450411	6769796	Diorite Hornfels		chl	0.48
03ZW371	450591	6769883	Limestone			0.29
03ZW372	450492	6770593	Volcaniclastic Hornfels			0.54
03ZW373	454033	6771560	Quartz Diorite			6.08
03ZW374	454112	6771435	Quartz Monzonite			
03ZW374B	454112	6771435	Aplite Dike			7.20
03ZW375	454155	6771357	Granodiorite	co		2.44
03ZW376	454176	6771288	Granodiorite	py,co	qtz	0.82
03ZW377	454175	6771252	Granodiorite	py,co	qtz	0.49
03ZW378	454191	6771174	Granodiorite			4.82
03ZW379	454222	6771086	Quartz Monzodiorite	lim	qtz-ser	3.97
03ZW380	454294	6771008	Granodiorite		qtz	1.90
03ZW381	454367	6771039	Quartz Monzodiorite	py,lim		2.10
03ZW382	454384	6771047	Quartz Monzodiorite	co,Au,py, bis	qtz-ser-chl-cc	0.38
03ZW383	454511	6771039	Quartz Vein		qtz-cc-ser	
03ZW384	454508	6770122	Altered Felsic Dike	py(3%)		0.42
03ZW385	454768	6770268	Intrusive Breccia	py		1.31
03ZW386	454058	6771326	Granodiorite	co,py, bis, Au	qtz	1.43
03ZW387	454479	6771019	Quartz Monzodiorite	co,py, bis, Au	qtz	2.15
03ZW388	454782	6770720	Aplite Dike	lim		
03ZW389	454865	6770887	Gabbro		qtz-Kspar	13.63
03ZW390	454828	6770899	Altered Igneous	lim(15%)		0.34
03ZW391	454716	6770930	Granodiorite			7.84
03ZW392	454682	6770998	Tonalite	co,py	qtz-co-py	1.25
03ZW393	454467	6771538	Granodiorite			2.39
03ZW394	454479	6771636	Quartz Diorite			2.69
03ZW395	454483	6771655	Granodiorite			4.74
03ZW396	454976	6772391	Tonalite			1.42
03ZW397	454897	6772289	Quartz Monzodiorite			4.25
03ZW398	454811	6772207	Altered Igneous	lim(10%)	qtz	0.19
03ZW399	454760	6772141	Quartz Monzodiorite			10.73
03ZW400	454594	6772005	Quartz Monzodiorite	lim	qtz	11.92

Sample	UTM E	UTM N	Lithology	Ore Minerals	Veins	Magnetic Susceptibility
03ZW401	454473	6771951	Quartz Monzodiorite			10.10
03ZW402	454366	6771882	Quartz Monzodiorite			11.12
03ZW403	454398	6771723	Quartz Diorite			11.41
03ZW404	454028	6771881	Gray Dike	py	qtz-chl-sulfide	0.22
03ZW405	453934	6772424	Altered Metaconglomerate	py(2%)		0.16
03ZW406	454078	6772299	Altered Metaconglomerate	py		0.06
03ZW407	454081	6771895	Mudstone hornfels		qtz-chl-sul?	0.27
03ZW408	452586	6770172	Breccia	lim		0.46
03ZW409	452628	6770198	Breccia	lim		0.71
03ZW410	452694	6770238	Breccia	lim		0.31
03ZW411	452677	6770377	Conglomerate Hornfels		chl	0.42
03ZW412	452873	6770652	Quartz Diorite Hornfels	py	chl-qtz	0.70
03ZW413	453066	6771011	Grey Dike			0.20
03ZW414	453108	6771104	Conglomerate Hornfels	py		0.92
03ZW415	458400	6772836	Basalt Hornfels	py		3.72
03ZW416	458620	6772980	Alt Metavolcanic Hornfels	lim		0.18
03ZW417	458809	6773117	Altered Metabasalt	lim		0.34
03ZW418	458805	6773131	Altered Metabasalt	lim		0.24
03ZW419	458802	6773149	Altered Metabasalt	lim, py(2-3%)		0.13
03ZW420	458818	6773207	Altered Metabasalt	lim, py(2-3%)		0.21
03ZW421	458844	6773272	Altered Metabasalt	lim		0.44
03ZW422	459136	6772758	Basalt Hornfels			25.57
03ZW423	459100	6772941	Altered Metabasalt	lim		0.22
03ZW424	459006	6773144	Altered Metabasalt	lim		0.60
03ZW425	458915	6773317	Breccia	lim		0.08
03ZW426	458852	6773348	Basalt Hornfels			30.60
03ZW427	458624	6773630	Quartz Monzonite Dike	py, lim		0.22
03ZW428	458611	6773664	Breccia	lim		0.36
03ZW429	458583	6773692	Quartz Monzonite Dike			4.80
03ZW430	458566	6773724	Quartz Monzonite Dike			0.55
03ZW431	458541	6773734	Basalt Hornfels	co,py		29.60
03ZW432	458482	6773727	Quartz Monzonite Dike			0.28
03ZW433	458453	6773631	Quartz Monzonite Dike			0.68
03ZW434	458421	6773571	Quartz Monzonite Dike			0.34
03ZW435	458456	6773545	Quartz Monzonite Dike			0.24
03ZW436	458712	6773532	Altered Metabasalt	lim		0.25
03ZW437	458708	6773468	Altered Metabasalt	lim		0.07
03ZW438	458756	6773419	Breccia	lim		0.16
03ZW439	458826	6773545	Altered Metabasalt	lim		0.28
03ZW440	458767	6773590	Altered Metabasalt	lim		1.99
03ZW441	458730	6773523	Quartz Vein	lim, Ag-Pb sulfide		0.37
03ZW442	458752	6773173	Altered Dike?	lim		0.72
03ZW443	458421	6772822	Quartz Vein			0.56
03ZW444	451339	6770833	Volcaniclastic Hornfels		chl(5%)	0.45
03ZW445	451827	6772067	Diorite Hornfels		chl(2%)	16.30
03ZW446	451724	6771993	Gray Dike			11.33

Sample	UTM E	UTM N	Lithology	Ore Minerals	Veins	Magnetic Susceptibility
03ZW447	451661	6771922	Volcaniclastic Hornfels		chl(2%)	0.56
03ZW448	451647	6771841	Breccia		chl	0.13
03ZW449	451632	6771672	Mudstone hornfels		chl	3.09
03ZW450	451647	6771598	Breccia	lim		0.21
03ZW451	451674	6771527	Gray Dike			0.47
03ZW452	451662	6771471	Gray Dike			0.56
03ZW453	451585	6771303	Diorite Hornfels		chl(2%)	0.86
03ZW454	451439	6771053	Mudstone Hornfels		chl	1.07
03ZW455	451234	6770802	Alt Metavolcanic Hornfels		qtz	0.38
03ZW456	460756	6772670	Sawpit Pluton			0.21
03ZW457	460776	6772694	Volcaniclastic Hornfels	py		1.12
03ZW458	458840	6771263	Dacite Sill Hornfels	lim		0.56
03ZW459	457713	6769890	Alt Metavolcanic Hornfels	lim		2.41
03ZW460	457602	6769770	Basalt Hornfels			5.52
03ZW461	457606	6770172	Volcaniclastic Hornfels			6.75
03ZW462	457569	6770247	Basalt Hornfels			32.37
03ZW463	456195	6770410	Quartz Monzonite			21.17
03ZW464	456216	6770329	Altered Igneous	lim		0.66
03ZW465	456218	6770306	Quartz Vein	Ag-Pb sulfide		
03ZW466	456226	6770292	Altered Igneous			0.01
03ZW467	456256	6770255	Altered Igneous			0.24
03ZW468	456256	6770168	Monzodiorite			19.60
03ZW469	456402	6770009	Quartz Diorite			7.30
03ZW470	456382	6769727	Pink Dike			4.65
03ZW471	456437	6769356	Monzodiorite			13.73
03ZW472	456398	6768692	Basalt Hornfels			37.37
03ZW473	449884	6769030	Gray Dike			0.60
03ZW474	450156	6769640	Gray Dike			12.93
03ZW475	452245	6768815	Quartz Monzodiorite			0.68
03ZW476	452519	6768734	Diorite Hornfels			5.66
03ZW477	452389	6768743	Quartz Monzodiorite	py		0.45
03ZW478	452170	6768836	Pink Dike			2.94
03ZW479	457594	6770920	Basalt Hornfels			0.71
03ZW480	454295	6771361	Granodiorite			0.72
03ZW481	454500	6771604	Altered Igneous			0.29
03ZW482	454489	6771594	Granodiorite			6.51
03ZW483	454476	6771557	Quartz-Feldspar veins			
03ZW484	454496	6771396	Altered Igneous			0.34
03ZW485	454638	6771162	Monzogranite	co,py,mo	qtz-ser	0.68
03ZW486	453348	6771738	Granodiorite Dike			0.27
03ZW487	453327	6771846	Siltstone Hornfels	py		0.28
03ZW488	453368	6771783	Quartz-Sulfide vein	sulfide		
03ZW489	453832	6772676	Conglomerate Hornfels		qtz-chl	8.10
03ZW490	453838	6772839	Altered Metaconglomerate	py,lim		0.26
03ZW491	452126	6771252	Diorite Hornfels			0.65
03ZW492	453127	6771195	Conglomerate Hornfels			2.83

Sample	UTM E	UTM N	Lithology	Ore Minerals	Veins	Magnetic Susceptibility
03ZW493	452874	6771194	Granodiorite Dike			5.14
03ZW494	452992	6771136	Dacite Hornfels			0.61
03ZW495	453523	6771807	Granodiorite Dike			8.70
03ZW496	453647	6772164	Gray Dike	py, co, bis	qtz-chl	0.34
03ZW496B	453647	6772164	Volcaniclastic Hornfels			
03ZW497	450971	6765276	Altered Quartz Diorite			0.19
03ZW498	454687	6770998	Quartz Monzodiorite	mo, mal		
03ZW499	454777	6770916	Quartz Monzodiorite	co	qtz	7.16

Appendix B: Compositional chemical data and analysis technique.

I. XRF major oxide data as wt%. Lab number signifies (1) ALS Chemex or (2) UAF analysis

Sample	SiO2	Al2O3	Fe2O3	CaO	MgO	Na2O	K2O	Cr2O3	TiO2	MnO	P2O5	SrO	BaO	LOI	Total	Lab
03JF018	50.2	18.5	12.8	4.81	6.99	5.75	0.47		1	0.25	0.07				101	2
03ZW006	56.6	16	11.1	7.11	6.26	3.74	1.11		0.97	0.24	0.18				103	2
03ZW012	54.4	18.2	9.42	6.72	4.77	3.02	0.57	0.01	0.88	0.19	0.12	0	0.1	1.4	99.8	1
03ZW068	58.6	16.6	6.53	4.6	3.49	4.17	1.61	<0.01	0.71	0.09	0.11	0	0.1	3.3	99.9	1
03ZW121	66.6	15.1	4.31	1.64	1.94	3.93	2.77	0.01	0.48	0.08	0.11	0	0.1	2.6	99.7	1
03ZW142	73.4	16.3	3.74	1.7	1.11	5.35	1.48		0.4	0.08	0.07				104	2
03ZW147	59	15.2	7.05	5.01	3.51	3.46	1.6	0.01	0.72	0.1	0.2	0.1	0.1	3.7	99.8	1
03ZW176	64.6	15.3	3.53	3.36	1.59	3.35	2.85	0.01	0.59	0.07	0.17	0.1	0.2	4	99.6	1
03ZW179	61.8	16.1	5.06	4.63	2.79	3.25	3.11	0.01	0.73	0.08	0.23	0.1	0.1	1.3	99.2	1
03ZW189	66.5	15	2.5	3.72	0.97	2.62	2.75	<0.01	0.34	0.05	0.1	0	0.1	5	99.6	1
03ZW195	56.5	16.5	5.33	5.19	2.01	4.01	1.99	<0.01	0.79	0.12	0.25	0.1	0.1	6.2	99.1	1
03ZW196	67.7	15.4	2.77	1.91	1.13	4.01	2.9	0.01	0.38	0.06	0.12	0.1	0.2	2.9	99.5	1
03ZW213	66.4	15.6	4.67	3.35	1.55	4.04	1.39	<0.01	0.52	0.07	0.1	0	0.1	2.1	99.9	1
03ZW265	65	15.4	3.65	2.76	1.76	3.86	2.99	0.01	0.56	0.07	0.17	0.1	0.2	3.3	99.7	1
03ZW267	63.8	15.1	3.44	3.59	1.59	3.05	2.92	0.01	0.58	0.06	0.17	0.1	0.2	5	99.5	1
03ZW273	57	18.2	6.48	6.21	3.4	3.41	2.73	0.01	0.94	0.1	0.33	0.1	0.2	0.4	99.4	1
03ZW276	57.7	15.9	7.45	3.82	3.65	3.8	2.66	0.01	1.25	0.12	0.28	0.1	0.1	2.8	99.7	1
03ZW277	68.9	15	4.14	1.42	2.26	4.21	1.62	0.01	0.45	0.09	0.09	0	0.1	1.4	99.6	1
03ZW279	59.9	16.8	5.81	4.79	2.62	3.4	3.81	0.01	0.99	0.09	0.33	0.1	0.2	0.4	99.1	1
03ZW282	53.1	17.4	7.69	7.46	5.46	3.1	1.4	0.01	1.09	0.13	0.36	0.1	0.1	2.2	99.7	1
03ZW283	60.1	16.9	5.83	5.37	3.39	3.16	2.98	0.01	0.8	0.09	0.25	0.1	0.1	0.8	99.8	1
03ZW284	51.6	16.2	8.28	5.21	7.01	3.41	1.87	0.02	1.36	0.15	0.44	0.1	0.1	4	99.7	1
03ZW285	52	18	11.4	5.45	5.46	2.63	0.7	<0.01	1.03	0.22	0.15	0	0	2.8	100	1
03ZW293	57.3	17.5	7.11	5.1	3.14	3.5	3.24	0.01	0.94	0.1	0.42	0.1	0.2	1.1	99.7	1
03ZW294	61.8	17	4.95	4.73	2.28	3.6	2.86	0.01	0.77	0.08	0.29	0.1	0.2	0.8	99.4	1
03ZW297	64.5	16.8	4.27	1.7	0.94	4.13	5.15	0.01	0.61	0.11	0.19	0	0.2	1	99.7	1
03ZW298	56	18.2	7.75	5.22	3.71	3.26	0.7	0.01	1.08	0.1	0.15	0	0	3.7	100	1
03ZW317	65	15.6	3.6	3.63	1.94	3.18	2.97	0.01	0.56	0.07	0.16	0.1	0.1	2.7	99.6	1
03ZW331	65.7	14.9	3.27	2.69	1.62	3.17	3.42	0.01	0.51	0.06	0.16	0.1	0.2	3.9	99.7	1
03ZW333	73.4	16.7	3.04	0.19	0.24	5.2	2.08		0.49	0.02	0.03				101	2
03ZW337	52	16.3	9.22	8.26	6.22	3.03	0.73	0.03	1.59	0.17	0.27	0.1	0.1	1.6	99.4	1
03ZW341	68.6	15.3	4.19	1.41	1.57	4.49	1.51	0.01	0.48	0.07	0.09	0	0.1	1.8	99.6	1
03ZW347B	58.7	16.8	5.98	5.64	3.73	3.12	3.26	0.02	0.89	0.09	0.27	0.1	0.1	0.9	99.6	1
03ZW351	72.4	21.5	3.37	0.03	0.52	0.96	4.03		0.22	0.02	0.03				103	2
03ZW355	62.3	16.2	4.86	4.89	2.88	3.23	2.94	0.01	0.73	0.08	0.21	0.1	0.1	0.7	99.2	1
03ZW356	63.4	15.9	4.64	4.48	2.74	3.49	3.13	0.01	0.68	0.07	0.2	0.1	0.1	0.8	99.7	1
03ZW357	66.7	15.5	3.65	3.81	1.88	3.29	2.98	0.01	0.58	0.05	0.17	0.1	0.1	0.6	99.5	1
03ZW357B	66.8	15.6	3.6	3.72	1.83	3.27	3.03	0.01	0.55	0.05	0.14	0.1	0.2	0.5	99.3	1
03ZW357C	77.7	12.1	0.79	0.54	0.12	3	5.03	0.01	0.1	0.01	0.02	0	0.1	0.3	99.8	1
03ZW358	66.7	15.7	3.68	3.92	1.88	3.51	2.83	0.01	0.54	0.07	0.16	0.1	0.1	0.5	99.6	1
03ZW359	68.6	15.5	3.11	3.08	1.46	3.29	3.31	0.01	0.47	0.05	0.13	0.1	0.2	0.7	99.9	1
03ZW359B	68.6	15.5	3.1	3.05	1.41	3.24	3.29	0.01	0.46	0.05	0.13	0.1	0.2	0.7	99.8	1

03ZW360	57.2	17.5	6.64	5.77	3.21	3.1	3.87	0.01	1.03	0.11	0.34	0.1	0.2	0.5	99.5	1
03ZW361	68	15.3	3.37	2.9	1.4	3.63	3.34	0.01	0.53	0.07	0.16	0.1	0.2	0.6	99.5	1
03ZW362	68.6	14.9	3.11	2.73	1.31	3.24	3.81	0.01	0.46	0.07	0.14	0.1	0.1	0.8	99.4	1
03ZW363	69.8	15	2.74	2.49	1.08	3.47	3.62	0.01	0.42	0.06	0.13	0.1	0.1	0.5	99.4	1
03ZW364	69.2	15.2	2.69	2.29	1.03	3.63	3.67	0.01	0.41	0.07	0.11	0.1	0.2	0.7	99.2	1
03ZW365	70.2	14.9	2.48	2.27	0.97	3.53	3.84	0.01	0.36	0.05	0.1	0.1	0.1	0.4	99.3	1
03ZW366	66	16	3.86	3.54	1.78	3.6	3.12	0.01	0.57	0.07	0.18	0.1	0.2	0.6	99.6	1
03ZW367	65.9	15.9	3.88	3.44	1.71	3.5	3.22	0.01	0.58	0.07	0.18	0.1	0.2	0.6	99.2	1
03ZW369	72.2	16.2	4.39	2.18	0.93	3.96	2.24		0.54	0.07	0.18				103	2
03ZW373	61	16.7	5.39	4.56	2.67	3.28	3.66	0.01	0.81	0.09	0.28	0.1	0.2	0.7	99.4	1
03ZW374	72.7	11.8	0.55	0.36	0.08	2.66	6		0.08	0.02	0				94.2	2
03ZW378	65.8	16.2	3.8	3.49	1.81	3.3	3.59	0.01	0.57	0.06	0.19	0.1	0.2	0.6	99.7	1
03ZW389	56.3	16.6	7.2	6.38	4.35	3.09	3.36	0.02	1.05	0.12	0.36	0.1	0.2	0.6	99.6	1
03ZW391	65.8	15.6	3.57	3.43	1.68	3.22	3.72	0.01	0.59	0.06	0.18	0.1	0.1	0.6	98.6	1
03ZW394	57.3	15.7	7.11	5.05	3.64	2.97	3.07	0.01	1.12	0.1	0.38	0.1	0.2	2.6	99.3	1
03ZW395	66.1	16	3.8	2.95	1.84	3.21	3.68	0.01	0.56	0.05	0.19	0.1	0.2	1.1	99.7	1
03ZW396	62.9	16.2	4.6	5.04	3.08	3.36	2.26	0.02	0.61	0.08	0.19	0.1	0.1	0.6	99.1	1
03ZW403	59.8	17.2	5.79	5.12	3.04	3.36	3.23	0.01	0.84	0.09	0.28	0.1	0.2	0.6	99.6	1
03ZW404	69.4	15	4.81	3.73	1.67	3.99	2.59		0.64	0.1	0.21				102	2
03ZW412	62.8	15.5	8.16	4.25	5.17	3.44	2.69		0.68	0.14	0.11				103	2
03ZW427	74.3	17.9	1.85	0.09	0.21	4.36	4.56		0.19	0.03	0.03				104	2
03ZW434	70.6	17.7	3.52	0.15	0.4	4.35	4.42		0.3	0.02	0.07				102	2
03ZW435	70.9	17.5	3.58	0.1	0.41	4.53	4.3		0.28	0.02	0.07				102	2
03ZW458	65.8	16.7	5.32	3.44	1.72	2.06	1.56		0.52	0.07	0.09				97.2	2
03ZW466	74.4	18.3	1.44	0.04	0.45	2.93	5.73		0.44	0.02	0.06				104	2
03ZW467	76.2	18.1	3.12	0.75	1.09	3.67	1.27		0.23	0.07	0.05				104	2
03ZW469	61.6	16.9	5.29	5.43	3.04	3.34	2.65	0.01	0.76	0.08	0.22	0.1	0.1	0.2	99.7	1
03ZW474	65.2	15.6	4.67	3.5	1.66	3.44	2.92	0.01	0.57	0.09	0.18	0.1	0.2	1	99.1	1
03ZW478	65.6	15.8	3.68	2.54	2	3.73	3.66	0.01	0.56	0.07	0.17	0.1	0.2	1.6	99.6	1
03ZW479	52.1	16.8	9.52	2.61	5.65	5.67	0.19	<0.01	0.9	0.12	0.14	0	0	5.8	99.5	1
03ZW481	68.2	18.4	3.21	4.17	0.63	2.67	3.41		0.38	0.07	0.1				101	2
03ZW482	66.1	15.7	3.58	3.23	1.64	3.21	3.84	0.01	0.53	0.05	0.17	0.1	0.2	1.2	99.5	1

II. Triple acid digestion followed by ICP-AES analysis. ALS Chemex analysis.

SAMPLE	Ag	Al	As	Au	Ba	Be	Bi	Ca	Cd	Ce	Co	Cr	Cs	Cu	Fe	Ga	Ge	Hf	Hg	In	K	La	Li	Mg	Mn	Mo	Na	Nb	Ni	P	Pb	Rb	S	Sb	Se	Sn	Sr	Ta	Te	Th	Ti	Tl	U	V	W	Zn
03ZW006	0.3	9.3	8.2	0.1	300	0.6	0.1	4.8	0.6	24	21	42	0.8	86.4	5.7	18	0.2	0.9	0	0.1	1	11	12	2.4	1600	0.9	3.2	1.4	15	780	15.1	15	<0.01	1.8	2	0.8	359	<0.05	<0.05	1.1	0.6	0.1	0.3	229	0.3	110
03ZW028	0	7.4	98	<0.01	640	0.6	0.1	0.1	0.1	32	5	9	1.1	8.4	2.6	15	0.1	0.4	0	0.1	2.1	15	16	0.2	503	4.2	0.1	3	2.7	130	5	39	<0.01	4.6	1	1.4	62	0.1	<0.05	4.4	0.1	0.3	2.3	19	0.4	33
03ZW142	0.1	7.5	14	0	200	0.6	3.4	1	0.1	23	4.6	26	2	39.1	1.9	13	0.1	1.4	<0.01	0	1	11	7.6	0.6	385	0.8	3.4	2.6	2.6	260	3.4	31	0.1	0.6	1	2.9	151	0.1	0.1	3.3	0.2	0.3	0.8	44	0.5	24
03ZW171	0.2	7.3	50	<0.01	480	0.6	0.2	4.5	0.8	21	12	62	0.8	34.8	4.9	15	0.1	0.9	0	0.2	1.3	10	4.8	1.4	1620	1.1	2.3	1.8	18	640	31.5	19	0.1	1.1	2	3.1	195	0.1	0.1	1.1	0.5	0.2	0.6	178	0.9	138
03ZW225	0.1	7.9	3.4	<0.01	120	0.7	0.2	5.2	0.1	30	19	21	0.6	6.4	18	20	0.3	1	0	0.2	0.5	12	6.8	2.1	5610	0.7	0.6	3.3	5.3	450	2.6	8.8	<0.01	0.3	1	4	112	0.2	0.1	1.3	0.4	0.1	0.4	140	0.3	167
03ZW227	0.1	0.8	0.6	<0.01	10	0.1	0	0.3	<0.02	2.7	0.8	103	<0.05	540	0.5	1.4	<0.05	0.2	<0.01	<0.005	0	1.2	1.4	0.1	63	1.4	0.2	0.4	3.3	20	0.8	0.3	0	0.2	<1	0.4	40	<0.05	<0.05	0.3	0	<0.02	0.1	5	0.5	4
03ZW257	0.3	6.4	72	0	10	0.6	3	10	0	17	48	38	2	580	12	17	0.2	1.5	0.1	0.6	0.1	8.1	15	1.3	1270	6	0.5	2.9	16	630	2.9	4.3	3	6.4	7	58	173	0.2	0.1	1.2	0.4	0.3	0.6	141	96	33
03ZW271	0.1	11	3.8	<0.01	580	1	0.1	0.9	0	37	24	43	4.9	34.2	5.5	26	0.2	0.3	0	0	3.6	15	36	1	767	6.2	1.2	4.2	20	990	4	85	0.2	0.8	2	1.5	61	0.2	0.1	2.7	0.8	0.5	0.7	245	0.7	43
03ZW274	0.1	11	14	<0.01	780	0.9	0.1	1.1	<0.02	31	5.7	36	5.8	19.8	5.7	24	0.2	0.2	0	0	1.8	14	20	1.6	497	2.8	3	1	5.9	680	5.2	41	0.4	0.3	3	0.4	326	<0.05	0.2	1.5	0.2	0.3	0.6	179	0.1	44
03ZW280	0.3	8.7	6.6	0	570	3.2	0.6	0	0.1	178	1.4	36	2.3	4.5	1.2	19	0.2	1.3	0.5	0	3.5	121	12	0.3	61	47	0	9.3	4.9	200	27.7	126	0	6.7	1	2.7	39	0.2	0.1	70	0.2	0.6	10	45	3.1	79
03ZW281	<0.02	9.9	5.2	0	1410	2	0.1	4.1	0.1	73	22	46	3.1	10.9	3.7	20	0.2	1.6	<0.01	0	2.7	42	16	2	675	1.3	2.9	8.1	41	1090	13.6	87	0	0.9	1	0.9	808	0.3	<0.05	23	0.4	0.4	4.4	125	1.4	54
03ZW288	0.2	9	18	0.1	340	1	0.1	5.8	0.2	23	37	42	3.3	218	8.2	22	0.2	1.2	0	0.4	1.1	11	22	5	3050	4.4	1.1	2	21	710	23.1	24	0	5.6	2	2.7	219	0.1	<0.05	1.3	0.2	0.5	1.1	389	0.5	145
03ZW292	0.2	2.8	12	1.4	10	0.4	0	5.8	0.1	5.6	7.3	27	0.7	28.6	2.7	5.2	0.1	0.2	1.2	0	0.2	3	20	2	644	11	0	0.2	6.9	200	7	11	0	8.9	<1	0.4	105	<0.05	<0.05	0.7	0.1	0.1	1.2	71	0.2	43
03ZW313	0.1	9.2	27	<0.01	320	0.5	0.3	3	0.2	14	40	51	0.7	105	8.5	18	0.2	1	0	0	0.6	6.7	18	2.7	1835	2.2	2.9	0.9	31	620	4.3	9.6	<0.01	0.4	1	1.3	296	<0.05	<0.05	1.2	0.6	0.1	0.4	229	0.4	158
03ZW333	<0.02	8.1	2.1	<0.01	50	0.4	0.7	0.1	<0.02	33	22	32	0.8	3.2	2	15	0.1	2.9	<0.01	0	1.5	15	3.3	0.1	15	7.2	3.6	1.2	2.9	130	2.3	29	1.6	0.3	2	0.9	69	0.1	0.2	2.3	0.1	0.2	1.5	55	0.4	4
03ZW339	1	8	20	0.1	950	2.3	30	0.8	0.1	70	8	37	7.5	148	2.1	17	0.2	0.7	0	0.1	2.9	39	15	0.8	204	1.9	2.2	4.5	12	720	10.1	178	<0.01	1.1	1	2.7	252	0.1	1.3	24	0.2	0.9	3.1	51	2.5	33
03ZW339B	0.7	6.2	11	0	710	2.2	0.3	0.2	0.1	37	2.4	42	6.5	66.8	0.8	13	0.1	0.9	<0.01	0	4.7	20	7.3	0.2	67	1	1.5	4.4	4.5	150	24.8	195	<0.01	0.6	1	0.8	124	0.1	<0.05	38	0.1	0.9	6.8	14	2.7	15
03ZW340	6.2	8.1	15	0.1	1080	2.8	40	1	0.6	80	7.2	59	7.8	1005	2	18	0.2	0.7	0	0.1	3.3	46	19	0.7	391	2.3	2.3	5.9	14	680	64	159	0	2	1	1.8	320	0.1	0.7	35	0.2	0.8	7	51	3.9	110
03ZW347	0.1	8.5	11	<0.01	1140	2.2	3.7	2.6	0.1	91	18	71	11	60.6	3.6	18	0.2	1.2	0	0	2.9	51	26	1.8	541	8.5	2.3	10	42	1180	19	182	0	1.3	1	2.3	580	0.5	0.1	26	0.4	0.9	6.7	123	38	57
03ZW348	0.9	9	8.7	0	1230	2.2	4.6	3.3	0.2	97	19	46	7.1	380	3.8	19	0.3	1.3	0	0.1	3	54	30	1.9	596	2.7	2.6	12	35	1320	21.1	149	0.1	1.3	1	2.4	766	0.5	0.1	29	0.5	0.8	6.1	127	2.5	66
03ZW349	2.4	7.7	237	0.1	560	0.8	0.9	1.5	16	32	8.9	41	2.2	112	2.5	14	0.2	0.9	0.1	0.1	1.9	16	10	0.7	626	1.3	1.9	2.9	3	330	168	56	0.1	6.7	1	1.6	96	0.2	0.1	3.3	0.2	0.3	0.9	58	1.6	1245
03ZW350	0.2	7.5	33	0.1	710	1.4	0.2	2.8	0.1	66	24	46	6.5	90.9	4.4	18	0.2	0.4	0	0	1.6	37	30	1.7	499	9	2	7	35	1140	9	102	0.1	0.5	1	1.8	488	0.3	0.1	10	0.4	0.5	2.5	122	1	52
03ZW354	0.3	5.1	28	0.2	10	0.7	0.1	6.1	0.2	8.1	17	26	0.6	101	3.1	8.2	0.1	0.1	1.2	0	0.1	3.8	39	2.3	543	0.5	0	0.2	12	370	8.1	2.8	0.2	18	1	0.3	172	<0.05	<0.05	0.7	0.3	0	1.7	122	0.2	60
03ZW369	0.2	8.5	2.9	6.9	790	1.8	156	1.3	0.1	74	7.8	19	1.5	2.4	2.4	17	0.2	2.3	<0.01	0	1.7	45	8.5	0.8	362	1.2	2.6	3.7	6.2	790	4.7	54	<0.01	1.4	1	0.8	375	0.1	131	26	0.2	0.2	5.2	63	0.1	27
03ZW377	1.4	9.2	31	0.2	1150	2.7	0.9	0.2	0.1	72	5.7	35	13	183	1.8	21	0.2	1	0	0.1	3.4	44	15	0.6	242	1.5	2.3	6.4	11	850	23.1	234	<0.01	1.5	1	2.3	206	0.3	0.4	26	0.2	1.2	3	64	10	39
03ZW379	0.9	8.7	12	0	1280	2.7	0.6	0.9	0.3	85	8.4	48	6.7	259	2.4	19	0.2	0.9	<0.01	0.1	3.3	48	25	1	363	2.9	2.5	7.9	16	820	14	191	<0.01	0.9	1	2	385	0.3	0.1	30	0.3	0.9	3.1	62	17	42
03ZW382	0.3	8.5	4.1	3.1	1320	2.5	19	1.9	0.1	74	8.7	44	7.4	158	2.4	19	0.2	0.9	<0.01	0	2.7	43	25	1	315	0.9	2.6	6.7	13	850	13.2	151	<0.01	0.6	1	2.3	497	0.1	1.5	23	0.3	0.8	3.8	60	3.3	30
03ZW383	0.6	1.4	20	1.3	160	0.4	3.6	0.2	0.1	12	2.7	105	1.6	25.9	0.6	3.2	0.1	0.2	<0.01	0	0.5	6.7	6.6	0.1	77	4.1	0.3	1.1	4.5	70	7.7	38	<0.01	2.5	<1	0.6	14	<0.05	1.9	3.6	0	0.2	0.4	14	3.6	5
03ZW386	1.2	8.4	24	2	1540	2.4	50	1.5	0.4	75	8.8	45	9.9	432	2.3	18	0.2	1.2	0	0.1	3.1	46	21	0.9	278	1.2	2.5	7	13	720	23	167	0.1	1.6	1	1.8	453	0.3	0.7	27	0.2	1	4.5	57	3	45
03ZW387	1.5	8.3	8.7	6.7	1090	2.6	23	1.9	0.3	78	8.2	39	7.7	288	2.2	19	0.2	1	0	0	2.9	46	23	0.8	294	2	2.4	5	12	770	17.3	169	<0.01	1.1	1	2.5	364	0.1	3.2	22	0.2	0.8	2.8	55	1.1	34
03ZW390	0.2	10	6.2	0	590	1.6	0.2	8.9	0.2	157	22	62	2.9	76.3	4.6	23	0.3	2.1	0	0.1	1.2	90	18	0.3	1040	2.2	0.1	6.2	51	1800	29.1	39	<0.01	1.8	2	2.3	262	0.1	<0.05	49	0.6	0.2	7.4	172	1.9	57
03ZW398	<0.02	11	5.9	0	70	2.1	0.3	0.1	0.3	132	14	48	2.2	30.1	3.2	20	0.2	1.3	0	0.1	0.6	63	47	0.3	432	0.6	0	9.5	44	1190	24.7	31	<0.01	2.2	1	2.2	88	0.4	<0.05	40	0.4	0.2	7.2	115	4.8	95

03ZW400	0.1	9.2	21	<0.01	1770	3	0.5	3	0.6	121	17	52	11	30.2	3.9	20	0.3	0.9	0	0.1	3.2	69	31	1.8	777	1.8	2.5	13	31	1380	28.9	154	0	1.4	1	2.7	674	0.6	<0.05	43	0.4	0.9	11	108	2.2	124
03ZW404	0	8.8	3.1	<0.01	1540	2	0.1	2.6	0.2	68	11	26	1.4	43.4	2.7	18	0.2	1.8	0	0	2.1	37	15	1.1	557	1.4	3	7.4	11	790	14.9	69	0	0.8	2	1.3	822	0.4	0.1	24	0.4	0.2	3.9	82	0.7	71
03ZW464	<0.02	8.8	5.7	<0.01	690	3.7	0.1	0.1	0.1	152	4.7	52	3.3	5.1	2.3	21	0.3	0.3	0	0	4.6	89	9.5	0.2	224	1	2.2	6.4	11	470	10.9	196	0	2.1	1	1.2	198	0.1	<0.05	122	0.2	0.4	19	48	0.7	34
03ZW465	22	1.6	21	0	210	0.7	1.1	0	0.8	16	3	179	0.8	20	1	3.8	0.1	0.3	2	0	0.7	9.4	28	0.1	403	6.5	0	0.2	8.8	120	6560	32	0.2	8.3	1	0.8	8.1	<0.05	0.2	6.1	0.1	0.1	1.3	27	0.1	99
03ZW466	<0.02	7.7	4.1	<0.01	1070	3	0.3	0	0.1	152	0.4	27	2.1	2.4	0.8	18	0.2	5.1	0.5	0	4	87	6.5	0.2	16	0.7	1.8	15	3.4	260	15.7	145	0.1	3.6	1	1.7	157	0.7	<0.05	112	0.2	0.3	9.6	40	4.1	15
03ZW467	0.3	7.3	2.3	0	320	0.6	0	0.4	0.1	17	4.4	40	0.9	172	1.6	13	0.1	0.2	0	0	0.8	7.8	16	0.8	304	2.9	1.8	1	4.7	170	10.1	30	0	0.4	1	0.3	187	<0.05	<0.05	1.7	0.1	0.2	0.3	29	1	18
03ZW481	<0.02	8.3	3.5	<0.01	940	1.6	0	2.4	0.1	34	4.3	14	5.4	3	1.6	17	0.1	2.3	0	0	2.4	21	12	0.3	357	1	2.1	3.6	3.2	450	14.3	100	<0.01	1.1	1	1.2	294	0.2	<0.05	7.7	0.2	0.5	3.5	38	0.7	47
03ZW483	0.1	3.6	24	0.1	540	1	0.1	0.1	0.1	29	1.9	41	2.6	6	0.6	7.6	0.1	0.8	<0.01	0	2.2	17	7.9	0.2	81	1.9	0.8	2	5.1	110	8.5	96	<0.01	1	<1	0.6	68	0.1	<0.05	17	0.1	0.5	2.1	12	1.7	12
03ZW484	<0.02	8.1	4.3	<0.01	850	2	0	1.8	0.1	34	4.7	22	4.9	5	1.8	17	0.1	2.4	0	0	2.4	20	23	0.3	350	1.2	0	3.4	4.5	530	10.9	104	<0.01	1.6	1	0.9	33	0.2	<0.05	7.8	0.2	0.5	2.8	43	1.5	48
03ZW485	0.8	8	11	0	1110	2.4	0.4	1.2	0.1	68	4.8	42	6.9	175	1.7	18	0.2	2.5	0	0	3.4	39	20	0.6	225	2.4	1.5	4.8	8.1	540	11.7	174	0	0.8	1	2	217	0.2	<0.05	25	0.1	0.7	5.4	40	1.3	34
03ZW488	0.1	8	133	<0.01	1040	0.7	0.2	0.2	0.3	27	9.2	47	2	26.9	7.3	22	0.2	1.7	0	0.1	1.9	12	26	2.9	1375	0.8	0.1	3.4	18	680	13	35	<0.01	0.2	1	3.3	20	0.1	<0.05	3.6	0.3	0.2	0.9	122	1.6	159
03ZW496	0.1	8.8	5.5	<0.01	1250	2.3	23	2.7	0.1	80	11	25	5.1	58.7	3	19	0.2	3.2	0	0	2.3	47	22	1.3	558	0.7	2.8	9	10	960	15	101	<0.01	1	1	1.8	646	0.6	0.2	22	0.4	0.5	7.4	89	9.4	63
03ZW496B	0	8.8	6.7	<0.01	1100	1.4	0.6	1.4	0.1	44	10	18	8.6	21.4	3.2	18	0.2	1.1	0	0	2.7	23	17	1.2	568	1	2.2	4	12	740	6.6	92	<0.01	0.5	2	1.8	275	0.1	0.1	4.1	0.4	0.6	1	91	0.9	57
03ZW499	1.2	9.2	5	0.2	1530	2.8	2.9	3	0.3	93	16	55	11	421	3.9	21	0.3	0.9	0	0.1	2.8	55	37	2	572	1.9	2.6	12	31	1200	18.3	161	0	0.6	2	3.3	645	0.5	0.1	26	0.5	0.8	6.6	117	2.3	75

III. Aqua regia digestion followed by ICP-AES analysis. ALS Chemex analysis.

SAMPLE	Ag	As	Au	Ba	Bi	Cd	Co	Cs	Cu	Hg	Li	Mn	Mo	Ni	P	Pb	Sb	Se	Te	U	V	Zn
03ZW015	0.78	3.9	0.029	570	0.25	0.31	11.1	0.79	499	0.02	7.2	760	4.26	13.9	270	5.2	1.04	0.7	1.22	0.06	82	67
03ZW018	0.05	15.8	0.003	70	0.4	0.15	18	0.11	25.2	1.09	3.4	625	1.97	17.7	480	3.5	0.53	0.3	0.41	0.38	74	116
03ZW030	0.03	4.3	<0.001	290	0.08	0.08	5.2	0.09	12.4	0.04	3.8	339	1.01	3.3	260	4.4	0.54	0.6	0.1	0.15	19	26
03ZW033	0.03	3.1	<0.001	110	0.07	0.02	22	0.3	6.8	0.01	8.5	406	0.91	11	670	0.8	0.1	2.2	0.2	0.08	117	21
03ZW035	0.09	30.2	0.001	520	0.05	0.2	17.6	0.48	53.5	<0.01	5.3	1405	2.37	13.6	420	9.5	1.76	0.8	0.08	0.13	66	36
03ZW046	0.04	6.9	0.003	330	0.74	0.04	10.6	0.15	83.2	0.01	5.8	340	0.48	6.9	620	2.2	0.13	3.3	0.54	0.11	142	33
03ZW048	0.02	3.1	<0.001	440	<0.01	0.02	23.9	0.37	11.6	<0.01	14.2	717	0.25	28.9	530	0.6	0.17	0.4	0.02	0.08	146	27
03ZW050	0.01	0.5	<0.001	520	<0.01	0.06	1.8	0.57	2.9	0.01	0.2	259	0.44	3	500	4.1	0.07	0.4	<0.01	0.2	9	17
03ZW053	0.06	3.2	0.001	70	0.1	0.11	14.7	<0.05	120.5	0.01	2	473	0.79	11.2	570	3.6	0.32	1.4	0.14	0.13	123	37
03ZW057	0.04	7.6	0.001	180	0.1	0.11	8	0.23	41.4	0.01	0.7	484	2.06	4.8	380	1.8	0.09	0.5	0.08	0.13	13	19
03ZW074	0.01	3.8	0.038	520	0.02	0.04	5.4	0.18	11.6	<0.01	5	142	0.91	4.5	380	1.5	0.16	0.6	0.08	0.22	36	15
03ZW077	0.17	14.6	0.011	250	0.12	0.15	3.5	0.25	16.6	0.01	2.6	287	11.1	4.8	180	12.6	0.85	0.3	0.01	0.18	20	22
03ZW086	0.08	7	<0.001	150	<0.01	0.24	8.8	0.31	6.6	0.01	0.7	2320	2.92	8.4	240	17.4	1.1	0.6	0.01	0.16	62	105
03ZW087	0.06	0.9	0.001	40	0.06	0.11	16	<0.05	123	<0.01	2.9	651	0.94	12	490	3.4	0.5	0.4	0.03	0.05	76	56
03ZW088	1.16	0.6	0.002	320	1.16	1.98	73.3	1.44	132000	<0.01	13.2	1385	0.61	6.8	500	11	0.13	0.8	0.51	0.07	170	393
03ZW093	0.6	1.8	0.008	200	0.19	2.22	3.3	0.17	676	0.01	2	550	1.66	6.6	60	50.1	0.14	0.3	0.1	<0.05	29	40
03ZW102	0.03	3.5	<0.001	230	0.21	0.01	5.1	0.06	32.3	0.01	1.1	47	0.47	4.6	460	2	0.1	2.8	0.34	0.07	95	5
03ZW111	0.09	2.1	0.091	250	0.02	0.38	5.6	0.55	24.4	<0.01	0.5	631	1.6	9.8	150	8.5	0.5	0.2	0.01	0.18	23	26
03ZW114	0.01	0.3	<0.001	190	<0.01	0.05	2.2	0.13	5.8	<0.01	0.6	210	0.6	5.4	90	2.5	0.08	<0.2	<0.01	<0.05	17	19
03ZW119	0.15	13	<0.001	1160	0.28	0.05	1	0.17	3.2	0.3	0.4	60	3.03	2.2	280	15.2	0.49	0.3	0.29	2.81	1	17
03ZW120	0.05	5.9	0.002	1640	0.43	0.05	0.6	0.39	3	0.16	0.7	50	2.36	2.9	300	24.4	0.53	0.3	0.11	3.23	1	11
03ZW122	0.32	92.9	0.001	50	0.14	0.08	0.7	0.31	8	0.11	3.5	62	2.01	3.1	80	57.3	2.29	0.3	0.03	2.12	<1	28
03ZW123	0.38	31.6	0.013	3370	<0.01	0.18	1.7	0.47	41.2	0.04	3.8	190	2.99	3.3	150	65.5	2.3	0.2	<0.01	0.06	40	89
03ZW127	0.08	3.5	0.029	70	<0.01	0.21	5.3	0.23	41.5	0.01	1.2	347	1.93	10.1	130	0.7	3	0.2	<0.01	0.05	29	11
03ZW130	0.07	26	0.003	480	0.1	0.04	13	0.95	44.5	<0.01	17	274	1.28	15.3	870	2.6	1.1	1.5	0.14	0.13	116	72
03ZW132	0.16	5.5	<0.001	140	0.12	0.07	37.4	0.31	252	<0.01	5.9	826	2.99	13.8	870	1.6	0.62	4.2	0.28	0.05	190	63
03ZW137	0.35	6.7	0.015	190	0.15	0.08	21.9	0.25	221	<0.01	6.9	183	4.3	18.7	400	2.2	0.29	1.9	0.35	0.06	97	21
03ZW139	0.02	1.7	<0.001	50	0.01	0.01	11.6	0.09	41.4	<0.01	1.2	76	0.73	14.6	1250	0.6	0.16	0.5	0.03	0.06	153	5
03ZW145	0.18	58.3	0.005	420	0.13	0.06	15	0.34	62.9	<0.01	10.2	673	3.03	19.2	510	6.7	1.56	1	0.2	0.09	58	81
03ZW165	0.09	5.7	0.002	520	0.12	0.28	4.8	1.04	15.3	<0.01	7.3	230	1.72	10	420	7.3	1.26	0.7	0.02	0.17	45	52
03ZW175	0.02	20	0.003	660	0.04	0.26	21.1	1.08	4.5	0.01	8.5	1365	0.13	58.9	450	2	0.59	0.4	0.01	0.06	83	49
03ZW178	0.11	16	0.002	60	0.05	0.1	7.3	0.51	15	<0.01	1.1	1075	4.15	10.4	240	16.1	4.12	0.5	0.03	0.82	36	60
03ZW180	0.02	1	<0.001	670	<0.01	0.02	2	0.29	6.1	<0.01	4.6	116	2.12	12.5	50	1.6	0.17	<0.2	<0.01	0.25	5	13
03ZW183	0.07	28.2	0.002	80	0.05	0.09	11	0.28	33	0.04	8.3	171	1.75	19.8	660	6.9	1.69	0.6	0.02	0.46	34	73
03ZW186	0.05	8	0.002	600	0.09	0.09	10	4.15	13.4	<0.01	12.4	439	1.28	6.5	1520	3.7	0.45	0.7	<0.01	0.22	81	84
03ZW204	0.03	2.6	<0.001	510	0.03	0.09	17.6	0.61	20.1	0.01	10.4	419	0.64	7.5	440	1.7	0.31	0.3	<0.01	0.11	39	79
03ZW205	0.04	9.5	0.018	160	0.04	0.05	26.1	0.29	47	<0.01	6.1	303	1.52	15.4	650	0.6	0.13	0.7	0.04	0.1	144	48
03ZW206	0.79	29.5	0.002	500	<0.01	59.4	11.2	0.66	99.6	0.02	1.9	1050	0.28	8.2	430	124	5.12	0.8	0.01	0.05	34	1650

SAMPLE	Ag	As	Au	Ba	Bi	Cd	Co	Cs	Cu	Hg	Li	Mn	Mo	Ni	P	Pb	Sb	Se	Te	U	V	Zn
03ZW209	0.11	6.9	<0.001	630	0.06	0.25	9	0.42	15.7	0.01	0.7	1105	1.77	5.4	420	7.8	2.13	0.8	<0.01	0.86	36	77
03ZW219	0.03	1	<0.001	90	<0.01	0.11	3.2	0.17	244	<0.01	1.4	168	0.51	6	150	1.2	0.08	0.2	<0.01	0.14	5	15
03ZW223	0.09	2.9	0.002	50	<0.01	0.15	9.8	<0.05	6.2	<0.01	0.5	292	0.54	8	190	6.6	0.56	1	0.1	0.12	102	7
03ZW224	0.06	4.1	<0.001	310	0.04	0.13	18	<0.05	44.8	<0.01	2.5	291	0.72	10.4	810	3.8	0.26	0.9	0.13	0.18	79	26
03ZW240	0.03	236	0.001	80	<0.01	0.06	5.8	0.28	14.8	<0.01	1.4	1825	4.81	3.6	220	4.8	2.64	0.6	0.03	<0.05	33	30
03ZW252	0.13	1.6	0.004	620	<0.01	0.36	12.8	2.02	51.3	0.01	9.3	399	0.33	6.8	140	4.5	0.61	0.3	<0.01	0.06	251	82
03ZW253	0.09	41.1	0.007	120	0.23	0.02	3.6	1.15	128	<0.01	5.4	96	0.59	2.4	410	1.4	0.79	1.4	0.12	0.56	50	12
03ZW256	0.27	7.6	0.02	350	0.02	0.3	5.1	10.2	193	0.01	4.3	229	0.52	8.1	740	5.4	0.76	0.6	0.01	0.31	82	39
03ZW258	0.11	235	0.014	170	0.84	0.21	8.3	1.64	29.5	<0.01	2.3	78	12.3	3	950	5.1	2.12	2.7	0.27	0.64	36	16
03ZW261	0.12	4.5	0.002	170	0.1	0.09	4.5	0.5	37.9	<0.01	3.9	349	0.97	4.4	330	6	0.53	0.8	0.05	0.2	27	33
03ZW262	0.18	7.5	0.001	120	0.17	0.21	12.8	0.11	11.8	<0.01	6.7	1280	0.18	3.2	950	3.9	0.55	0.8	0.04	0.11	21	75
03ZW269	0.03	6.7	0.002	30	<0.01	0.04	15.6	0.38	32.6	<0.01	2.4	320	1.54	7.3	50	0.4	0.13	<0.2	<0.01	<0.05	6	6
03ZW299	0.03	<2.0	0.003	310	<0.01	0.3	4.5	0.16	9.6	0.04	2.2	791	0.18	2.5	140	13.4	0.4	0.4	0.01	0.27	17	86
03ZW302	0.03	2.5	0.001	570	0.03	1.14	11	0.21	40.4	0.31	3.6	754	0.85	6.5	440	29.6	0.12	0.3	<0.01	0.58	41	134
03ZW306	2.19	21.6	0.004	520	0.67	10.5	19.4	1.3	36.6	0.04	15.2	647	2.36	5.9	480	913	3.44	2.5	1.08	0.09	190	1060
03ZW309	1.1	14.6	0.066	1240	<0.01	0.18	24.3	0.19	45.2	0.01	8.5	481	1.28	19.9	550	11.7	0.56	11.6	4.03	<0.05	70	42
03ZW319	0.06	25.4	0.001	180	0.01	0.06	16.7	0.22	4.1	0.11	14.6	526	0.38	4.2	800	5.9	0.34	0.7	0.06	0.08	61	114
03ZW326	0.08	4.3	0.003	210	0.21	0.1	14.6	0.51	10.6	<0.01	7.5	328	6.37	3.7	240	4.4	0.38	4.1	2.35	0.14	51	31
03ZW329	0.05	3.5	0.006	270	0.69	0.16	10.7	0.92	4	<0.01	6.9	154	3.05	2.8	350	3.7	0.45	1.4	0.72	0.19	48	23
03ZW332	0.08	1.6	0.003	100	0.04	0.1	6.1	0.89	4	<0.01	11.1	243	2.49	3.9	390	4.1	0.28	0.4	0.06	0.14	42	29
03ZW334	0.12	5.9	0.001	460	0.25	0.04	0.5	0.76	4	<0.01	2.9	30	1.78	1.4	140	1.9	0.47	1.7	0.16	0.18	38	5
03ZW344	0.88	9.4	0.091	50	0.83	0.18	11.6	1.48	658	0.01	4.4	1200	1.03	8	570	0.9	1.42	0.5	0.14	0.63	36	29
03ZW345	0.04	2.6	0.001	490	0.11	0.11	11.2	2.39	104.5	<0.01	17.1	198	3.16	12.8	880	0.5	0.33	0.4	0.03	0.41	85	21
03ZW346	0.08	3.3	0.003	290	0.11	0.16	27.2	3.91	70.9	<0.01	22.1	469	1.58	21.2	1190	3.7	0.54	1.1	0.09	0.25	210	48
03ZW351	0.23	51.5	1.735	1520	0.41	0.17	1.5	0.14	33.2	1.96	0.8	19	3.77	1.1	120	2.4	5.12	0.8	0.12	2.63	2	3
03ZW352	2.3	64.1	0.174	2510	0.33	1.35	26	1.6	98.3	0.01	14.3	960	1.56	12.8	490	27.2	1.94	1.4	0.13	0.14	200	354
03ZW353	0.9	2.7	10.9	560	0.04	0.1	21.1	5.44	1860	0.02	25.4	408	2.35	29	660	1.2	0.28	1	<0.01	0.5	186	55
03ZW384	0.09	0.8	0.012	1150	0.09	0.04	3	0.18	14.8	<0.01	0.4	10	2.5	2.3	40	1	0.14	0.7	0.15	0.3	4	2
03ZW405	0.2	40.4	0.011	460	0.09	0.04	7.6	2.92	15.1	0.05	9.6	472	2.85	2.3	390	9.6	2.32	<0.2	0.03	0.18	54	28
03ZW406	8.41	24.2	0.024	>10000	0.09	0.19	0.6	0.32	30.8	0.09	1.7	18	2.42	1.3	260	126	1.92	<0.2	0.01	0.5	2	26
03ZW408	0.14	20	0.003	6360	0.19	0.11	17.1	0.48	63.7	0.07	4.7	1375	0.87	15.6	700	7.3	1.44	0.5	0.02	0.16	82	65
03ZW409	0.29	37	0.001	360	0.18	0.33	14.4	0.52	30.8	0.02	3.2	2670	0.86	22.3	330	28	1.55	0.4	<0.01	0.09	54	74
03ZW410	0.1	14.8	0.001	230	0.06	0.2	11.8	0.48	24.5	0.02	5.5	1215	0.7	7.2	450	5.3	0.32	0.4	<0.01	0.16	58	75
03ZW412	0.09	6.2	0.002	890	0.05	0.08	16.2	2.14	40.2	<0.01	13.4	807	0.45	8.8	440	1.5	0.46	0.4	0.02	0.16	114	95
03ZW416	0.33	23.2	0.011	310	0.04	0.04	2.3	0.27	21.3	0.01	10.5	987	1.64	4.1	270	56.5	0.99	1.6	0.28	0.14	211	86
03ZW417	0.87	21.4	0.013	150	0.52	0.15	8.2	0.69	50.1	0.02	16.9	533	0.56	3.7	300	16.2	4.3	1.3	2.76	0.24	186	104
03ZW418	0.32	17.2	0.006	320	0.25	0.07	1.3	0.26	27.2	0.02	14.2	349	1.86	1.1	560	26	2.36	1	1.58	0.24	87	75
03ZW419	0.4	21.8	0.01	160	1.1	0.22	21.9	0.39	37.9	0.04	20	841	1.04	5.9	440	29.8	5.8	3.4	2.56	0.09	161	134
03ZW420	0.5	31.1	0.003	580	0.39	3.63	16.3	0.25	25.3	0.03	18.6	775	1.32	4.4	530	136	2.82	1.1	2.34	0.17	167	307
03ZW421	2.3	47.9	0.016	430	0.07	0.22	4.5	0.61	108	0.02	34.4	1075	0.62	11	260	323	5.53	1.2	1.5	0.4	216	244
03ZW423	0.05	100	0.002	740	0.02	0.27	4.6	0.2	15.8	0.11	1	318	1.9	1.8	1440	22.2	5.26	0.4	0.06	3.1	3	65

SAMPLE	Ag	As	Au	Ba	Bi	Cd	Co	Cs	Cu	Hg	Li	Mn	Mo	Ni	P	Pb	Sb	Se	Te	U	V	Zn
03ZW424	0.52	32.3	0.013	470	0.22	1.7	25	0.49	26.9	0.07	9.9	366	1.65	7	530	95.8	4.7	3.4	4.45	0.17	139	206
03ZW425	0.31	20.9	0.004	90	0.1	0.14	0.6	0.16	7.6	0.01	0.7	19	1.42	2.9	160	35.2	0.76	0.8	1.46	0.09	40	8
03ZW427	0.08	16.8	0.025	1940	0.16	0.03	3.3	0.12	61.1	0.06	0.3	47	1.24	2.9	150	7.5	0.99	0.4	0.05	4.81	1	5
03ZW428	0.09	481	0.06	210	0.06	0.09	10.4	0.07	20.4	0.74	1.4	1330	13.8	6.6	110	26.9	24	0.4	0.05	2.74	53	57
03ZW430	0.02	4.1	0.01	520	0.05	0.01	0.5	0.1	3.3	0.72	0.2	18	3.23	2.3	110	2.3	1.02	0.2	<0.01	1.89	1	3
03ZW432	0.05	5.2	0.017	720	0.11	<0.01	0.6	0.14	3.9	0.12	0.3	17	4.45	2.6	100	4.1	0.89	0.6	0.04	1.22	1	6
03ZW434	0.12	8.3	0.329	1600	0.55	0.02	0.5	0.1	12.2	0.09	0.2	24	3.23	2.2	280	5.7	2.59	0.4	0.15	2.34	1	6
03ZW435	0.04	7.6	0.033	1430	0.41	0.01	0.3	0.1	4.3	0.04	0.2	18	2.44	1.8	270	4.2	0.52	0.2	0.04	1.37	2	5
03ZW436	4.03	19.4	0.093	1520	0.19	0.09	8.9	0.19	48.9	0.07	2.7	217	5.66	6	190	28	0.98	5.7	3.1	0.06	49	32
03ZW437	0.05	8.1	0.014	1370	0.46	0.01	0.5	0.1	5.4	0.05	0.3	24	2.91	3.2	280	4.6	0.56	0.3	0.06	1.54	2	6
03ZW438	0.16	14.6	0.005	100	0.01	0.01	0.8	<0.05	68.9	0.04	0.2	11	1.42	2.9	740	1.6	0.76	27	5.41	<0.05	86	5
03ZW439	2.56	24.3	0.064	1110	1.12	0.09	14.6	0.43	79.6	0.12	6.1	301	5.09	14	390	139	1.44	9.8	2.87	<0.05	93	40
03ZW440	0.4	6	0.01	540	0.06	0.11	12.2	0.42	82.8	<0.01	38.1	299	1.5	18.5	310	7.1	0.21	3.6	0.18	0.09	164	114
03ZW441	9.88	53.8	0.723	150	0.14	0.05	0.7	0.11	31.5	0.28	0.2	23	3.23	4.6	40	31.9	10.1	1.7	0.84	<0.05	10	20
03ZW443	0.29	2.1	0.034	60	0.05	<0.01	0.8	<0.05	4	0.03	0.2	20	1.42	4.6	20	5	0.3	0.2	0.26	<0.05	2	2
03ZW450	0.21	32.7	0.014	110	0.42	0.13	14.8	0.13	121.5	0.03	1.2	268	1.54	9.5	480	8.3	0.68	0.5	0.14	0.09	31	63
03ZW455	0.1	203	0.005	360	0.33	0.35	9.6	0.19	23.4	0.01	2.8	421	1.73	6.1	280	5.5	0.41	0.2	0.02	0.11	14	55
03ZW458	0.02	19.2	0.001	90	0.01	0.1	6	0.26	56.9	0.04	1.6	320	0.59	5.5	230	1.8	1.56	0.3	<0.01	0.07	15	45
03ZW459	0.01	6.9	0.001	610	0.02	0.06	8.6	0.09	17.2	<0.01	6.8	425	0.49	2.2	510	2.2	0.07	0.3	<0.01	0.14	57	56
03ZW490	0.09	36.2	0.002	210	0.19	0.36	12	0.87	42.3	0.05	6.5	410	11.8	12.2	450	11.8	1.12	0.3	0.04	0.11	59	77

IV. Trace element chemical data. UAF analysis.

Sample	BA	CE	NB	RB	SR	Y	ZR
03JF018	137	21	2	11	258	17	46
03JF020	570	38	2	23	162	23	162
03ZW006	381	26	4	15	322	29	89
03ZW012	394	29	3	11	360	20	64
03ZW068	470	33	3	32	332	22	91
03ZW121	660	33	4	38	238	28	147
03ZW142	232	35	3	31	163	31	149
03ZW147	1159	56	7	32	743	16	128
03ZW176	1240	43	7	91	480	15	128
03ZW179	1196	84	12	119	617	20	188
03ZW189	549	28	4	93	170	14	101
03ZW195	1016	85	12	60	596	21	153
03ZW196	1444	33	4	91	406	12	109
03ZW213	572	35	3	20	319	25	132
03ZW265	1237	54	8	91	526	14	136
03ZW267	1226	51	7	88	395	15	124
03ZW273	1547	85	11	88	825	19	143
03ZW276	1109	59	9	64	578	18	120
03ZW277	597	35	3	24	183	21	131
03ZW279	1412	129	17	167	662	27	252
03ZW282	788	52	4	57	953	19	72
03ZW283	1123	88	12	129	608	20	182
03ZW284	866	66	14	55	557	20	142
03ZW285	299	25	3	14	263	25	69
03ZW293	1653	133	17	112	840	25	209
03ZW294	1344	69	10	99	711	16	150
03ZW297	1448	166	25	217	352	29	420
03ZW317	1186	63	8	85	509	14	136
03ZW331	1360	64	7	109	379	14	119
03ZW333	337	43	3	29	89	30	172
03ZW341	495	42	4	24	251	28	133
03ZW347	1281	96	12	133	683	22	187
03ZW351	1185	128	22	76	64	20	337
03ZW355	1156	72	10	106	557	17	149
03ZW356	945	64	11	119	480	19	148
03ZW357	1207	47	8	105	470	14	123
03ZW357B	1302	53	7	111	476	13	126
03ZW358	1121	60	7	92	484	14	119
03ZW359	1456	44	7	115	420	14	121
03ZW359B	1323	52	7	109	458	13	119
03ZW360	1467	91	13	136	691	24	167
03ZW361	1172	66	9	114	501	16	133
03ZW362	1092	70	8	126	458	14	120
03ZW363	1033	62	7	126	405	14	127
03ZW364	1313	62	8	129	399	15	147
03ZW365	1041	49	8	128	379	15	119
03ZW366	1268	81	9	106	577	16	133
03ZW367	1245	71	8	107	546	16	128
03ZW369	712	73	8	53	346	15	130
03ZW373	1341	110	14	141	636	21	194
03ZW378	1329	79	11	133	569	18	161
03ZW389	1375	110	16	139	747	25	164
03ZW391	1188	81	10	140	512	17	161
03ZW394	1641	106	15	137	584	26	239
03ZW395	1378	86	11	161	554	18	164
03ZW396	1068	60	7	78	591	15	128
03ZW403	1310	100	12	124	689	21	177
03ZW404	1421	51	8	65	728	15	132
03ZW412	847	25	3	46	275	26	118
03ZW427	1513	100	20	78	123	22	338

Sample	BA	CE	NB	RB	SR	Y	ZR
03ZW434	1327	130	20	69	162	15	346
03ZW435	1203	127	19	69	147	19	331
03ZW458	116	38	3	27	333	35	153
03ZW466	934	126	18	150	173	19	249
03ZW467	323	27	1	27	190	14	83
03ZW469	1230	73	9	97	615	18	156
03ZW474	1547	64	9	38	525	15	142
03ZW478	1517	48	7	117	492	15	136
03ZW479	104	24	3	4	178	24	70
03ZW481	873	31	4	96	285	12	99
03ZW482	1341	80	11	154	510	18	152

Appendix C: List of quartz-plagioclase-K-feldspar modal estimates

Estimated modal abundances from stained rock slabs.

Sample	Rock Unit	Qtz	Plag	Kspar	
03ZW055	Rex Creek Pluton	36	64	0	Tonalite
03ZW056	Sawpit Pluton	32	26	42	Monzogranite
03ZW104	Rex Creek Pluton	19	77	4	Quartz Diorite
03ZW108	Rex Creek Pluton	16	83	1	Quartz Monzodiorite
03ZW117	Sawpit Pluton	22	44	33	Monzogranite
03ZW148	Hornfels Diorite	4	94	1	Diorite
03ZW155	Hornfels Diorite	2	43	55	Monzonite
03ZW157	Hornfels Diorite	1	99	0	Diorite
03ZW200	Rex Creek Pluton	7	92	1	Quartz Diorite
03ZW214	Rex Creek Pluton	24	76	0	Granodiorite
03ZW220	Rex Creek Pluton	19	81	0	Quartz Diorite
03ZW260	Hornfels Diorite	7	91	1	Quartz Diorite
03ZW272	Bonanza Pluton	4	74	21	Monzodiorite
03ZW281	Bonanza Pluton	1	88	12	Monzodiorite
03ZW295	Bonanza Pluton	4	82	14	Monzodiorite
03ZW296	Bonanza Pluton	6	77	18	Quartz Monzodiorite
03ZW307	Bonanza Pluton	3	78	20	Monzodiorite
03ZW374	Bonanza Pluton	19	51	30	Quartz Monzonite
03ZW375	Bonanza Pluton	26	50	24	Granodiorite
03ZW376	Bonanza Pluton	25	67	8	Granodiorite
03ZW377	Bonanza Pluton	28	55	17	Granodiorite
03ZW380	Bonanza Pluton	23	63	15	Granodiorite
03ZW386	Bonanza Pluton	24	53	23	Granodiorite
03ZW392	Bonanza Pluton	27	67	6	Tonalite
03ZW393	Bonanza Pluton	27	55	18	Granodiorite
03ZW397	Bonanza Pluton	20	65	15	Quartz Monzodiorite
03ZW399	Bonanza Pluton	8	82	10	Quartz Monzodiorite
03ZW400	Bonanza Pluton	7	76	17	Quartz Monzodiorite
03ZW401	Bonanza Pluton	10	68	23	Quartz Monzodiorite
03ZW402	Bonanza Pluton	6	69	25	Quartz Monzodiorite
03ZW463	Bonanza Pluton	5	58	37	Quartz Monzonite
03ZW468	Bonanza Pluton	3	84	14	Monzodiorite
03ZW471	Bonanza Pluton	1	76	22	Monzodiorite

Sample	Rock Unit	Qtz	Plag	Kspar	
03ZW475	Rex Creek Pluton	12	58	30	Quartz Monzodiorite
03ZW477	Rex Creek Pluton	12	58	30	Quartz Monzodiorite
03ZW480	Bonanza Pluton	27	60	13	Granodiorite
03ZW485	Bonanza Pluton	30	32	38	Monzogranite

Appendix D: Microprobe analysis data.

UAF analysis. DL=detection limit

Sample	%Ag	%Au	%total	Fineness	Ag DL	Au DL	Grain	Location
03ZW353	8.4	91.0	99.4	916	0.16	0.17	1	
	8.4	90.1	98.6	914	0.16	0.17	1	
	8.9	89.8	98.7	910	0.18	0.16	1	
03ZW369	5.9	93.8	99.7	941	0.16	0.17	1	
	6.2	93.5	99.7	938	0.16	0.17	1	
	6.6	91.4	98.0	933	0.17	0.17	1	
03ZW382	12.3	86.1	98.4	875	0.15	0.17	1	
	13.2	88.9	102.1	871	0.16	0.17	1	
	12.1	87.5	99.7	879	0.16	0.17	1	
Spruce Placer	6.0	93.2	99.3	939	0.16	0.17	1	rim
	5.9	95.2	101.1	942	0.15	0.17	1	center
	6.3	94.9	101.3	938	0.16	0.17	1	rim
975727	10.2	88.8	98.9	897	0.16	0.17	1	
	10.3	88.8	99.1	896	0.15	0.17	1	
	9.8	87.9	97.7	899	0.15	0.17	1	
975721	8.4	88.9	97.3	914	0.16	0.17	1	center
	0.5	94.9	95.4	994	0.17	0.17	1	rim
	0.3	94.4	94.6	997	0.16	0.17	1	rim
975842	3.8	93.4	97.2	961	0.16	0.17	1	center
	3.9	93.6	97.5	960	0.16	0.17	1	edge
	3.6	93.0	96.6	962	0.17	0.17	1	edge
	%Bi	%Te	%S	%total	Bi DL	Te DL	S DL	Mineral
03ZW369	52.1	48.1	0.0	100.2	0.34	0.08	0.03	Tellurobismuthite
	51.2	48.2	0.0	99.4	0.34	0.08	0.03	Tellurobismuthite
	58.4	36.6	4.5	99.5	0.34	0.08	0.03	Tetradymite
	52.0	47.7	0.0	99.8	0.34	0.08	0.03	Tellurobismuthite
	52.2	48.2	0.0	100.4	0.34	0.08	0.03	Tellurobismuthite
	51.4	47.7	0.0	99.1	0.34	0.08	0.03	Tellurobismuthite
	51.4	47.4	0.0	98.9	0.34	0.08	0.03	Tellurobismuthite
	51.9	47.0	0.0	99.0	0.35	0.08	0.03	Tellurobismuthite
	51.6	48.4	0.0	100.0	0.34	0.08	0.03	Tellurobismuthite
	51.9	48.4	0.0	100.3	0.33	0.08	0.03	Tellurobismuthite
	51.6	47.8	0.0	99.5	0.35	0.08	0.03	Tellurobismuthite
Spruce Placer	52.2	33.9	4.1	90.2	0.33	0.07	0.03	Tetradymite
	58.9	35.9	4.8	99.6	0.34	0.08	0.03	Tetradymite
	59.9	36.7	4.9	101.4	0.34	0.08	0.03	Tetradymite
	59.9	36.1	4.7	100.7	0.34	0.08	0.03	Tetradymite
03ZW339	73.0	0.0	17.6	90.6	0.38	0.09	0.03	Bismuthinite
	71.3	0.0	18.1	89.4	0.37	0.09	0.03	Bismuthinite
	94.5	0.0	0.0	94.5	0.36	0.11	0.02	Bismuth

Appendix E: 40Ar/39Ar analytical data.

UAF Geophysical Institute Analysis.

UAF106-27 03ZW232 WR#1 Weighted average of J from standards = 0.002512 +/- 0.000006

Laser	Cum.	$^{40}Ar/^{39}Ar$	+/-	$^{37}Ar/^{39}Ar$	+/-	$^{36}Ar/^{39}Ar$	+/-	% Atm.	Ca/K	+/-	Cl/K	+/-	$^{40}Ar^*/^{39}Ar_K$	+/-	Age	+/-
(mW)	^{39}Ar	meas.		meas.		meas.		^{40}Ar							(Ma)	(Ma)
300	0.206	75.6526	2.0186	4.6844	0.1194	0.15396	0.00867	59.7	8.622	0.220	0.00527	0.00079	30.57	2.86	133.5	12.1
600	0.353	73.8210	0.9264	9.3107	0.1387	0.16716	0.00650	66.0	17.188	0.258	0.00950	0.00117	25.25	1.95	110.9	8.3
900	0.482	63.1966	0.7425	17.6998	0.2153	0.12858	0.00644	58.0	32.855	0.404	0.01097	0.00161	26.81	1.91	117.6	8.1
1200	0.584	41.6213	0.5387	17.5389	0.2267	0.06249	0.00877	41.2	32.553	0.426	0.01181	0.00183	24.73	2.63	108.7	11.2
1500	0.668	41.3980	0.4509	17.1959	0.1877	0.04697	0.01481	30.4	31.909	0.352	0.01174	0.00186	29.11	4.44	127.3	18.7
2000	0.772	46.3930	0.5466	23.0454	0.2729	0.06888	0.00890	40.2	42.929	0.516	0.00775	0.00286	28.16	2.68	123.3	11.4
2500	0.838	57.0671	0.9347	28.9640	0.4743	0.06672	0.02197	30.8	54.166	0.904	0.00462	0.00464	40.26	6.64	173.8	27.3
3000	0.889	59.5541	1.3658	51.0776	1.1792	0.09944	0.01879	42.9	96.944	2.315	0.00984	0.00507	35.15	5.76	152.6	24.0
9000	1.000	60.8574	0.6482	43.2494	0.4645	0.07732	0.00983	32.2	81.656	0.902	0.00888	0.00230	42.42	3.02	182.7	12.4
Integrated		60.6584	0.4368	19.6971	0.1074	0.10820	0.00347	50.3	36.611	0.202	0.00869	0.00069	30.53	1.08	133.3	4.6

03ZW232 WR#2 Weighted average of J from standards = 0.002512 +/- 0.000006

Laser	Cum.	$^{40}Ar/^{39}Ar$	+/-	$^{37}Ar/^{39}Ar$	+/-	$^{36}Ar/^{39}Ar$	+/-	% Atm.	Ca/K	+/-	Cl/K	+/-	$^{40}Ar^*/^{39}Ar_K$	+/-	Age	+/-
(mW)	^{39}Ar	meas.		meas.		meas.		^{40}Ar							(Ma)	(Ma)
300	0.103	100.0266	1.1113	3.2695	0.0387	0.24082	0.00474	70.9	6.012	0.071	0.00220	0.00160	29.14	1.23	127.5	5.2
600	0.251	65.6510	0.5526	4.8098	0.0424	0.10200	0.00274	45.4	8.853	0.078	0.00181	0.00119	35.96	0.85	156.0	3.5
900	0.378	65.7001	0.7643	13.1717	0.1534	0.13327	0.00350	58.5	24.377	0.286	0.00515	0.00139	27.51	1.06	120.6	4.5
1200	0.551	45.7733	0.4987	14.0257	0.1643	0.07269	0.00236	44.7	25.972	0.307	0.00590	0.00096	25.55	0.77	112.2	3.3
1500	0.637	41.6522	1.5924	15.3775	0.5966	0.04012	0.00842	25.7	28.501	1.117	0.00043	0.00583	31.24	2.76	136.3	11.6
1800	0.710	46.7229	0.3842	14.6312	0.1294	0.07369	0.00925	44.3	27.104	0.242	0.00596	0.00219	26.27	2.77	115.3	11.8
2100	0.760	51.7352	0.6202	19.4694	0.2321	0.06076	0.01444	31.9	36.182	0.437	0.00489	0.00307	35.67	4.34	154.8	18.1
2400	0.798	66.0131	0.8171	20.9835	0.2658	0.09273	0.01794	39.1	39.035	0.501	0.00703	0.00384	40.71	5.39	175.7	22.2
2700	0.829	71.0565	1.3003	23.3292	0.4229	0.10244	0.02278	40.2	43.466	0.800	0.00413	0.00507	43.16	6.86	185.7	28.1
3000	0.840	75.5687	8.6932	24.5350	2.8221	0.08095	0.07806	29.2	45.749	5.348	0.00419	0.04310	54.33	24.13	230.8	96.2
3300	0.858	73.9765	1.7694	26.0333	0.6223	0.12584	0.02520	47.6	48.591	1.182	0.00461	0.00413	39.38	7.58	170.2	31.3
3700	0.869	67.8215	2.6739	27.1328	1.0687	0.11803	0.03654	48.4	50.680	2.032	0.00201	0.00653	35.58	11.00	154.4	45.8
4200	0.885	65.4366	1.4628	28.1469	0.6264	0.11684	0.02219	49.6	52.610	1.193	0.00778	0.00441	33.61	6.68	146.2	27.9
9000	1.000	67.8465	0.3835	32.9854	0.1859	0.09205	0.00514	36.5	61.852	0.356	0.00880	0.00223	44.04	1.57	189.3	6.4
Integrated		62.3143	0.2969	15.3631	0.0750	0.10475	0.00221	47.8	28.474	0.140	0.00457	0.00088	32.81	0.67	142.9	2.8

03ZW295 BI Weighted average of J from standards = 0.002512 +/- 0.000006

Laser	Cum.	$^{40}Ar/^{39}Ar$	+/-	$^{37}Ar/^{39}Ar$	+/-	$^{36}Ar/^{39}Ar$	+/-	% Atm.	Ca/K	+/-	Cl/K	+/-	$^{40}Ar^*/^{39}Ar_K$	+/-	Age	+/-
(mW)	^{39}Ar	meas.		meas.		meas.		^{40}Ar							(Ma)	(Ma)
250	0.002	39.8589	1.1328	0.3346	0.0295	0.13242	0.02247	98.2	0.614	0.054	0.02418	0.00448	0.72	6.55	3.3	29.6
500	0.006	26.3389	0.4050	0.3428	0.0182	0.01922	0.01271	21.5	0.629	0.033	0.03079	0.00294	20.66	3.77	91.3	16.2
750	0.024	26.4071	0.1740	0.0915	0.0056	0.01183	0.00281	13.2	0.168	0.010	0.03041	0.00116	22.89	0.84	100.9	3.6
1000	0.089	25.5182	0.0466	0.0152	0.0009	0.00123	0.00088	1.4	0.028	0.002	0.03010	0.00024	25.13	0.26	110.4	1.1
1250	0.223	25.4256	0.2565	0.0078	0.0007	0.00013	0.00045	0.1	0.014	0.001	0.02951	0.00013	25.36	0.29	111.4	1.2
1500	0.327	25.4824	0.2974	0.0260	0.0088	-0.00010	0.00089	-0.1	0.048	0.016	0.02915	0.00023	25.49	0.40	112.0	1.7
1750	0.392	25.3971	0.0463	0.0294	0.0026	-0.00073	0.00143	-0.9	0.054	0.005	0.02938	0.00031	25.59	0.42	112.4	1.8
2000	0.449	25.4222	0.0492	0.0786	0.0022	0.00022	0.00108	0.2	0.144	0.004	0.03033	0.00030	25.34	0.32	111.3	1.4
2300	0.543	25.4553	0.0885	0.1134	0.0017	-0.00138	0.00122	-1.6	0.208	0.003	0.03248	0.00027	25.85	0.37	113.5	1.6
2600	0.701	25.1113	0.1191	0.0652	0.0007	-0.00023	0.00041	-0.3	0.120	0.001	0.03021	0.00019	25.16	0.17	110.5	0.7
3000	0.869	24.9295	0.2428	0.0512	0.0008	0.00027	0.00046	0.3	0.094	0.001	0.02912	0.00013	24.83	0.28	109.1	1.2
4000	0.990	25.2634	0.2451	0.1611	0.0104	0.00028	0.00142	0.3	0.296	0.019	0.03544	0.00302	25.17	0.49	110.6	2.1
9000	1.000	25.2905	0.2580	0.0515	0.0117	0.00121	0.00509	1.4	0.095	0.021	0.02841	0.00159	24.91	1.52	109.5	6.5
Integrated		25.3310	0.0717	0.0644	0.0016	0.00050	0.00030	0.6	0.118	0.003	0.03059	0.00037	25.16	0.11	110.6	0.6

03ZW295 HO Weighted average of J from standards = 0.002512 +/- 0.000006

Laser	Cum.	$^{40}Ar/^{39}Ar$	+/-	$^{37}Ar/^{39}Ar$	+/-	$^{36}Ar/^{39}Ar$	+/-	% Atm.	Ca/K	+/-	Cl/K	+/-	$^{40}Ar^*/^{39}Ar_K$	+/-	Age	+/-
(mW)	^{39}Ar	meas.		meas.		meas.		^{40}Ar							(Ma)	(Ma)
400	0.004	564.9709	15.1458	10.2205	0.2796	1.79286	0.05227	93.6	18.879	0.520	0.45839	0.01385	36.16	6.26	156.8	26.0
800	0.011	154.1140	1.6363	30.9058	0.3320	0.46187	0.01121	87.1	57.872	0.634	0.24487	0.00392	20.33	3.06	89.9	13.2
1200	0.022	94.8731	1.2870	51.0288	0.6923	0.26747	0.00793	79.3	96.848	1.359	0.11038	0.00222	20.31	2.18	89.8	9.4
1500	0.048	59.1746	0.2832	16.2589	0.0798	0.12822	0.00344	62.0	30.152	0.149	0.06935	0.00078	22.72	1.02	100.1	4.4
1800	0.084	44.9492	0.2460	14.9633	0.0899	0.07002	0.00238	43.6	27.726	0.168	0.13716	0.00110	25.60	0.72	112.4	3.1
2100	0.161	36.3755	0.1055	9.1649	0.0326	0.03940	0.00126	30.1	16.917	0.061	0.21032	0.00073	25.55	0.39	112.2	1.6
2500	0.260	34.8002	0.0995	6.5301	0.0280	0.03095	0.00086	24.9	12.033	0.052	0.17059	0.00083	26.23	0.27	115.1	1.1
3000	0.388	30.5455	0.0807	8.2769	0.0292	0.01691	0.00119	14.3	15.269	0.054	0.21117	0.00089	26.28	0.36	115.3	1.5
3500	0.488	31.0672	0.1823	8.3461	0.0555	0.01982	0.00086	16.8	15.398	0.103	0.18329	0.00127	25.95	0.30	113.9	1.3
4000	0.564	32.1592	0.2062	9.8554	0.0780	0.02554	0.00107	21.2	18.200	0.145	0.25451	0.00229	25.49	0.36	111.9	1.6
5000	0.950	28.4972	0.3797	7.9813	0.0619	0.01181	0.00030	10.2	14.721	0.115	0.20580	0.00155	25.71	0.39	112.9	1.6
9000	1.000	30.4751	0.2243	16.6869	0.1315	0.02105	0.00187	16.3	30.954	0.247	0.27169	0.00205	25.76	0.59	113.1	2.5
Integrated		35.7210	0.1573	9.6986	0.0290	0.03686	0.00034	28.5	17.909	0.054	0.20225	0.00066	25.69	0.18	112.8	0.8

03ZW365 BI#1 Weighted average of J from standards = 0.002512 +/- 0.000006

Laser	Cum.	$^{40}Ar/^{39}Ar$	+/-	$^{37}Ar/^{39}Ar$	+/-	$^{36}Ar/^{39}Ar$	+/-	% Atm.	Ca/K	+/-	Cl/K	+/-	$^{40}Ar^*/^{39}Ar_K$	+/-	Age	+/-
(mW)	^{39}Ar	meas.		meas.		meas.		^{40}Ar							(Ma)	(Ma)
250	0.001	30.7215	0.9824	0.8598	0.0590	0.09031	0.04293	86.7	1.578	0.108	0.02019	0.00881	4.07	12.66	18.4	56.8
500	0.006	10.7363	0.1199	0.6972	0.0139	0.02838	0.00717	77.8	1.280	0.025	0.03092	0.00293	2.37	2.12	10.7	9.6
750	0.017	6.8019	0.0357	0.3160	0.0065	0.01727	0.00299	75.0	0.580	0.012	0.02932	0.00109	1.69	0.88	7.7	4.0
1000	0.033	19.3270	0.0747	0.1304	0.0040	0.01441	0.00333	22.0	0.239	0.007	0.02288	0.00077	15.05	0.98	66.9	4.3
1250	0.083	25.1995	0.0677	0.0326	0.0013	0.00273	0.00063	3.2	0.060	0.002	0.02166	0.00030	24.37	0.20	107.2	0.8
1500	0.158	25.5526	0.0532	0.0228	0.0010	0.00099	0.00088	1.1	0.042	0.002	0.02167	0.00020	25.23	0.27	110.9	1.1
1750	0.235	25.8971	0.2802	0.0312	0.0011	0.00076	0.00050	0.9	0.057	0.002	0.02208	0.00018	25.65	0.32	112.6	1.4
2000	0.317	25.8859	0.4307	0.0403	0.0014	0.00064	0.00095	0.7	0.074	0.003	0.02238	0.00026	25.67	0.51	112.7	2.2
2300	0.410	26.4121	0.1658	0.0649	0.0010	0.00139	0.00040	1.5	0.119	0.002	0.02292	0.00014	25.98	0.20	114.0	0.9
2600	0.512	26.9304	0.1687	0.0961	0.0009	0.00136	0.00038	1.5	0.176	0.002	0.02340	0.00018	26.51	0.20	116.3	0.9
3000	0.642	26.5503	0.1912	0.1138	0.0008	0.00098	0.00025	1.1	0.209	0.001	0.02353	0.00013	26.24	0.21	115.2	0.9
4000	0.873	25.9742	0.1476	0.1268	0.0008	0.00057	0.00023	0.6	0.233	0.001	0.02290	0.00011	25.79	0.16	113.2	0.7
9000	1.000	25.7810	0.1608	0.0481	0.0009	0.00085	0.00061	1.0	0.088	0.002	0.02082	0.00016	25.50	0.24	112.0	1.0
Integrated		25.7044	0.0669	0.0850	0.0003	0.00163	0.00019	1.9	0.156	0.001	0.02261	0.00006	25.20	0.09	110.7	0.4

03ZW365 BI#2 Weighted average of J from standards = 0.002512 +/- 0.000006

Laser	Cum.	$^{40}Ar/^{39}Ar$	+/-	$^{37}Ar/^{39}Ar$	+/-	$^{36}Ar/^{39}Ar$	+/-	% Atm.	Ca/K	+/-	Cl/K	+/-	$^{40}Ar^*/^{39}Ar_K$	+/-	Age	+/-
(mW)	^{39}Ar	meas.		meas.		meas.		^{40}Ar							(Ma)	(Ma)
250	0.002	22.2670	0.3994	0.9424	0.0203	0.07114	0.00817	94.2	1.730	0.037	0.02189	0.00160	1.29	2.41	5.8	10.9
500	0.006	7.5124	0.1160	0.6806	0.0112	0.01933	0.00254	75.6	1.249	0.021	0.02944	0.00071	1.82	0.75	8.3	3.4
750	0.015	9.1814	0.1062	0.2640	0.0040	0.01137	0.00158	36.5	0.485	0.007	0.02625	0.00057	5.81	0.47	26.2	2.1
1000	0.030	20.1603	0.4075	0.1129	0.0038	0.00363	0.00285	5.3	0.207	0.007	0.02427	0.00065	19.07	0.93	84.4	4.0
1250	0.058	25.0085	0.1183	0.0417	0.0008	0.00331	0.00050	3.9	0.077	0.002	0.02415	0.00013	24.00	0.19	105.6	0.8
1500	0.102	25.7118	0.2547	0.0361	0.0005	0.00139	0.00144	1.6	0.066	0.001	0.02467	0.00035	25.28	0.49	111.1	2.1
1750	0.159	26.3218	0.2677	0.0470	0.0006	0.00133	0.00018	1.5	0.086	0.001	0.02507	0.00018	25.91	0.27	113.7	1.2
2000	0.223	26.2631	0.2335	0.0683	0.0004	0.00096	0.00020	1.1	0.125	0.001	0.02527	0.00014	25.96	0.24	114.0	1.0
2300	0.300	26.7125	0.2239	0.0975	0.0006	0.00071	0.00016	0.8	0.179	0.001	0.02572	0.00018	26.48	0.23	116.2	1.0
2600	0.397	26.5772	0.3305	0.1094	0.0007	0.00064	0.00016	0.7	0.201	0.001	0.02570	0.00019	26.37	0.33	115.7	1.4
3000	0.525	26.1242	0.1499	0.1079	0.0003	0.00034	0.00009	0.4	0.198	0.001	0.02598	0.00011	26.00	0.15	114.2	0.7
4000	0.779	25.8257	0.1261	0.1038	0.0004	0.00037	0.00007	0.4	0.191	0.001	0.02601	0.00010	25.70	0.13	112.8	0.5
9000	1.000	25.4317	0.0889	0.0835	0.0003	0.00022	0.00006	0.2	0.153	0.001	0.02637	0.00008	25.35	0.09	111.4	0.4
Integrated		25.6262	0.0612	0.0951	0.0002	0.00095	0.00009	1.1	0.174	0.000	0.02581	0.00005	25.33	0.07	111.3	0.4

03ZW365 BI#3 Weighted average of J from standards = 0.002512 +/- 0.000006

Laser	Cum.	$^{40}Ar/^{39}Ar$	+/-	$^{37}Ar/^{39}Ar$	+/-	$^{36}Ar/^{39}Ar$	+/-	% Atm.	Ca/K	+/-	Cl/K	+/-	$^{40}Ar^*/^{39}Ar_K$	+/-	Age	+/-
(mW)	^{39}Ar	meas.		meas.		meas.		^{40}Ar							(Ma)	(Ma)
250	0.002	25.5004	0.4456	0.9193	0.0254	0.07288	0.01033	84.3	1.688	0.047	0.01786	0.00253	4.01	3.05	18.1	13.7
500	0.008	6.1012	0.1143	0.3836	0.0091	0.00583	0.00319	27.9	0.704	0.017	0.02784	0.00080	4.38	0.95	19.7	4.2
750	0.019	12.6330	0.1573	0.2216	0.0045	0.00651	0.00158	15.1	0.407	0.008	0.02490	0.00046	10.70	0.49	47.8	2.2
1000	0.038	19.5382	0.1794	0.1504	0.0022	0.00194	0.00097	2.9	0.276	0.004	0.02466	0.00043	18.95	0.34	83.9	1.5
1250	0.064	20.7693	0.1199	0.1190	0.0016	0.00078	0.00066	1.1	0.218	0.003	0.02481	0.00022	20.52	0.23	90.7	1.0
1500	0.101	22.2125	0.1156	0.0738	0.0011	0.00053	0.00049	0.7	0.135	0.002	0.02410	0.00024	22.03	0.18	97.2	0.8
1750	0.148	24.8559	0.5701	0.0492	0.0013	0.00173	0.00053	2.0	0.090	0.002	0.02421	0.00028	24.32	0.59	107.0	2.5
2000	0.210	25.8653	0.3054	0.0484	0.0009	0.00160	0.00085	1.8	0.089	0.002	0.02400	0.00015	25.37	0.40	111.4	1.7
2300	0.288	26.5677	0.3671	0.0503	0.0008	0.00055	0.00031	0.6	0.092	0.001	0.02404	0.00018	26.38	0.38	115.8	1.6
2600	0.386	26.3385	0.2143	0.0665	0.0007	0.00024	0.00022	0.2	0.122	0.001	0.02425	0.00014	26.25	0.22	115.2	1.0
3000	0.503	26.6966	0.1948	0.0817	0.0005	0.00044	0.00016	0.5	0.150	0.001	0.02442	0.00009	26.55	0.20	116.5	0.9
4000	0.748	26.6372	0.1374	0.1144	0.0005	0.00034	0.00007	0.3	0.210	0.001	0.02416	0.00014	26.52	0.14	116.3	0.6
9000	1.000	26.6896	0.1192	0.1949	0.0005	0.00019	0.00011	0.2	0.358	0.001	0.02428	0.00008	26.62	0.12	116.8	0.5
Integrated		25.7515	0.0703	0.1176	0.0003	0.00073	0.00009	0.8	0.216	0.000	0.02426	0.00005	25.52	0.08	112.1	0.4

03ZW365 HO#1 Weighted average of J from standards = 0.002512 +/- 0.000006

Laser	Cum.	$^{40}Ar/^{39}Ar$	+/-	$^{37}Ar/^{39}Ar$	+/-	$^{36}Ar/^{39}Ar$	+/-	% Atm.	Ca/K	+/-	Cl/K	+/-	$^{40}Ar^*/^{39}Ar_K$	+/-	Age	+/-
(mW)	^{39}Ar	meas.		meas.		meas.		^{40}Ar							(Ma)	(Ma)
200	0.003	156.3811	3.8617	4.2263	0.1100	0.51676	0.01809	97.5	7.776	0.203	0.08812	0.00487	3.98	3.81	17.9	17.1
400	0.020	32.9931	0.2053	1.3442	0.0109	0.10169	0.00391	90.8	2.469	0.020	0.06195	0.00089	3.02	1.15	13.6	5.2
600	0.039	34.4551	0.3463	1.5310	0.0159	0.08364	0.00323	71.5	2.812	0.029	0.06593	0.00142	9.84	0.94	44.0	4.1
900	0.077	35.6017	0.1235	0.7381	0.0045	0.05190	0.00164	43.0	1.355	0.008	0.03924	0.00041	20.30	0.49	89.7	2.1
1200	0.117	31.8273	0.1391	0.6529	0.0042	0.01834	0.00212	16.9	1.198	0.008	0.03207	0.00047	26.44	0.64	116.0	2.7
1500	0.174	32.9104	0.1873	2.3174	0.0162	0.01840	0.00304	16.0	4.259	0.030	0.04868	0.00149	27.66	0.91	121.2	3.9
2000	0.309	28.4881	0.2902	6.4944	0.0714	0.00819	0.00077	6.8	11.967	0.132	0.11642	0.00133	26.64	0.36	116.9	1.5
2500	0.484	27.3859	0.2300	7.6810	0.0786	0.00740	0.00120	5.9	14.164	0.146	0.13246	0.00150	25.88	0.42	113.6	1.8
3000	0.716	27.5574	0.3178	8.5827	0.0620	0.00819	0.00112	6.5	15.837	0.115	0.13657	0.00095	25.90	0.46	113.7	2.0
9000	1.000	27.2618	0.2474	10.0417	0.0170	0.00944	0.00033	7.5	18.546	0.032	0.13981	0.00036	25.36	0.27	111.4	1.1
Integrated		29.0098	0.1184	7.3226	0.0223	0.01576	0.00043	14.2	13.500	0.041	0.11843	0.00040	24.99	0.17	109.9	0.8

03ZW365 HO#2 Weighted average of J from standards = 0.002512 +/- 0.000006

Laser	Cum.	$^{40}Ar/^{39}Ar$	+/-	$^{37}Ar/^{39}Ar$	+/-	$^{36}Ar/^{39}Ar$	+/-	% Atm.	Ca/K	+/-	Cl/K	+/-	$^{40}Ar^*/^{39}Ar_K$	+/-	Age	+/-
(mW)	^{39}Ar	meas.		meas.		meas.		^{40}Ar							(Ma)	(Ma)
400	0.003	147.8383	7.9163	4.9664	0.2767	0.50594	0.05170	100.9	9.142	0.511	0.08906	0.01238	-1.33	13.07	-6.0	59.4
800	0.009	95.5976	2.8543	3.7484	0.1159	0.33801	0.03281	104.2	6.895	0.214	0.11069	0.00650	-4.04	9.25	-18.4	42.4
1200	0.018	48.2646	0.9220	2.8975	0.0574	0.16226	0.01309	99.0	5.326	0.106	0.09196	0.00268	0.51	3.77	2.3	17.1
1500	0.041	19.2639	0.1829	1.1146	0.0150	0.07066	0.01196	108.1	2.047	0.028	0.07705	0.00173	-1.56	3.53	-7.1	16.1
1800	0.067	16.6906	3.7314	1.1181	0.4508	0.17551	0.13654	310.8	2.053	0.828	0.09350	0.04107	-35.14	39.47	-166.7	196.2
2100	0.083	36.8010	0.2951	2.3478	0.0223	0.04020	0.00698	31.8	4.314	0.041	0.05759	0.00155	25.11	2.07	110.3	8.8
2500	0.124	28.1589	0.1283	2.5899	0.0131	0.01542	0.00255	15.5	4.760	0.024	0.06004	0.00055	23.81	0.76	104.8	3.3
3000	0.185	30.2824	0.0781	5.9982	0.0219	0.00895	0.00228	7.3	11.049	0.040	0.09572	0.00063	28.17	0.68	123.3	2.9
3500	0.240	30.4470	0.2205	9.1058	0.0813	0.01201	0.00193	9.4	16.807	0.151	0.13012	0.00119	27.72	0.61	121.4	2.6
4000	0.300	29.4191	0.1071	10.5750	0.0619	0.01289	0.00192	10.3	19.538	0.115	0.15401	0.00085	26.56	0.58	116.5	2.5
5000	0.418	28.5440	0.2202	11.6792	0.0955	0.00863	0.00090	5.9	21.594	0.178	0.17840	0.00156	27.05	0.34	118.6	1.5
9000	1.000	28.4315	0.1738	13.0757	0.0545	0.00931	0.00024	6.2	24.198	0.102	0.19430	0.00099	26.86	0.19	117.8	0.8
Integrated		29.2579	0.2023	10.7597	0.0709	0.02082	0.00347	18.3	19.882	0.132	0.16571	0.00147	24.05	1.05	105.8	4.5

03ZW471 BI Weighted average of J from standards = 0.002512 +/- 0.000006

Laser	Cum.	$^{40}Ar/^{39}Ar$	+/-	$^{37}Ar/^{39}Ar$	+/-	$^{36}Ar/^{39}Ar$	+/-	% Atm.	Ca/K	+/-	Cl/K	+/-	$^{40}Ar^*/^{39}Ar_K$	+/-	Age	+/-
(mW)	^{39}Ar	meas.		meas.		meas.		^{40}Ar							(Ma)	(Ma)
250	0.001	46.2154	1.5113	0.3110	0.0477	0.12908	0.02860	82.5	0.571	0.088	0.02396	0.00773	8.07	8.38	36.2	37.2
500	0.005	23.9526	0.2399	0.1402	0.0084	0.03852	0.00411	47.5	0.257	0.015	0.03029	0.00184	12.55	1.22	56.0	5.4
750	0.019	28.1005	0.2075	0.0428	0.0033	0.01224	0.00145	12.9	0.078	0.006	0.02967	0.00074	24.46	0.47	107.6	2.0
1000	0.049	26.4388	0.0658	0.0161	0.0013	0.00467	0.00066	5.2	0.029	0.002	0.02996	0.00025	25.03	0.21	110.0	0.9
1250	0.090	25.7881	0.1506	0.0118	0.0008	0.00005	0.00058	0.1	0.022	0.001	0.03031	0.00026	25.74	0.23	113.1	1.0
1500	0.142	26.2426	0.3603	0.0127	0.0008	0.00109	0.00044	1.2	0.023	0.001	0.03030	0.00029	25.89	0.38	113.7	1.6
1750	0.198	25.8703	0.5652	0.0126	0.0011	0.00110	0.00030	1.3	0.023	0.002	0.03034	0.00040	25.52	0.57	112.1	2.4
2000	0.257	25.8953	0.2127	0.0137	0.0006	0.00198	0.00075	2.3	0.025	0.001	0.03034	0.00026	25.28	0.31	111.1	1.3
2300	0.323	25.4041	0.3412	0.0152	0.0006	0.00032	0.00040	0.4	0.028	0.001	0.03091	0.00048	25.28	0.36	111.1	1.5
2600	0.404	25.5211	0.2529	0.0285	0.0005	0.00117	0.00020	1.3	0.052	0.001	0.03057	0.00011	25.15	0.26	110.5	1.1
3000	0.521	25.5045	0.1758	0.0382	0.0004	0.00030	0.00016	0.3	0.070	0.001	0.03072	0.00019	25.39	0.18	111.5	0.8
4000	0.762	25.4150	0.1441	0.0176	0.0002	0.00030	0.00007	0.3	0.032	0.000	0.03002	0.00011	25.30	0.15	111.2	0.6
9000	1.000	25.2564	0.0994	0.0684	0.0003	0.00026	0.00006	0.3	0.126	0.001	0.02985	0.00012	25.16	0.10	110.5	0.4
Integrated		25.5915	0.0682	0.0330	0.0002	0.00114	0.00008	1.3	0.061	0.000	0.03022	0.00007	25.23	0.07	110.9	0.4

03ZW471 HO Weighted average of J from standards = 0.002512 +/- 0.000006

Laser	Cum.	$^{40}Ar/^{39}Ar$	+/-	$^{37}Ar/^{39}Ar$	+/-	$^{36}Ar/^{39}Ar$	+/-	% Atm.	Ca/K	+/-	Cl/K	+/-	$^{40}Ar^*/^{39}Ar_K$	+/-	Age	+/-
(mW)	^{39}Ar	meas.		meas.		meas.		^{40}Ar							(Ma)	(Ma)
300	0.004	151.1691	3.8241	2.0504	0.0612	0.50715	0.02217	99.1	3.767	0.113	0.05239	0.00723	1.43	5.36	6.5	24.2
600	0.027	19.3243	0.0882	0.5842	0.0121	0.03732	0.00369	56.9	1.072	0.022	0.04517	0.00129	8.31	1.09	37.3	4.8
900	0.058	34.1396	0.1134	0.5106	0.0047	0.03048	0.00238	26.3	0.937	0.009	0.02973	0.00050	25.15	0.71	110.5	3.0
1200	0.114	32.1831	0.0861	0.4034	0.0021	0.01620	0.00075	14.8	0.740	0.004	0.03054	0.00031	27.41	0.23	120.1	1.0
1500	0.195	28.9786	0.0795	0.6684	0.0025	0.00612	0.00051	6.1	1.227	0.005	0.03251	0.00022	27.20	0.17	119.3	0.7
1800	0.299	28.5823	0.0858	0.9404	0.0036	0.00277	0.00055	2.6	1.727	0.007	0.03925	0.00024	27.82	0.18	121.9	0.8
2100	0.438	27.3313	0.4998	0.8845	0.0043	0.00249	0.00043	2.5	1.624	0.008	0.03750	0.00024	26.65	0.52	116.9	2.2
2500	0.669	26.6322	0.2787	1.1869	0.0049	0.00226	0.00017	2.2	2.180	0.009	0.03469	0.00015	26.04	0.28	114.3	1.2
2900	0.857	26.5293	0.3246	3.4860	0.0157	0.00270	0.00026	2.0	6.411	0.029	0.03628	0.00020	26.02	0.33	114.2	1.4
3300	0.929	26.3992	0.1690	13.8551	0.0905	0.00321	0.00080	-0.4	25.654	0.169	0.03602	0.00037	26.70	0.29	117.1	1.3
3700	0.952	26.7535	0.1971	19.1216	0.1659	0.00920	0.00200	4.8	35.528	0.312	0.03804	0.00062	25.76	0.63	113.1	2.7
4100	0.959	26.3193	0.4124	20.4987	0.3167	0.00597	0.00523	0.9	38.121	0.597	0.04215	0.00238	26.42	1.62	115.9	6.9
5000	0.974	27.0794	0.1845	44.5961	0.3118	0.01490	0.00316	3.9	84.274	0.607	-0.03645	0.10490	26.77	0.98	117.4	4.2
9000	1.000	28.2916	0.2584	138.6763	0.5970	0.04749	0.00162	12.8	279.703	1.324	0.05556	0.00069	27.09	0.59	118.8	2.5
Integrated		27.9411	0.1144	7.4754	0.0116	0.00872	0.00021	7.2	13.783	0.022	0.03533	0.00154	26.02	0.13	114.2	0.6

03ZW474 BI#1 **474B_1** Weighted average of J from standards = 0.002512 +/- 0.000006

Laser	Cum.	$^{40}Ar/^{39}Ar$	+/-	$^{37}Ar/^{39}Ar$	+/-	$^{36}Ar/^{39}Ar$	+/-	% Atm.	Ca/K	+/-	Cl/K	+/-	$^{40}Ar^*/^{39}Ar_K$	+/-	Age	+/-
(mW)	^{39}Ar	meas.		meas.		meas.		^{40}Ar							(Ma)	(Ma)
250	0.005	51.1107	1.2448	2.8473	0.0755	0.17564	0.01958	101.2	5.234	0.139	0.01883	0.00621	-0.61	5.66	-2.8	25.7
500	0.020	12.1118	0.1515	1.5419	0.0210	0.02475	0.00571	59.6	2.832	0.039	0.04041	0.00138	4.89	1.69	22.0	7.6
750	0.054	8.3198	0.0392	0.6493	0.0048	0.01383	0.00247	48.7	1.192	0.009	0.03507	0.00065	4.25	0.73	19.2	3.3
1000	0.093	15.2832	0.0411	0.5336	0.0037	0.02158	0.00199	41.5	0.979	0.007	0.02699	0.00069	8.92	0.59	40.0	2.6
1250	0.153	21.0347	0.2471	0.3291	0.0061	0.01727	0.00130	24.2	0.604	0.011	0.02517	0.00053	15.93	0.43	70.8	1.9
1500	0.263	25.6434	0.2897	0.2093	0.0029	0.00436	0.00162	5.0	0.384	0.005	0.02307	0.00051	24.34	0.56	107.1	2.4
1750	0.377	27.1175	0.1163	0.4038	0.0023	0.00222	0.00088	2.3	0.741	0.004	0.02437	0.00037	26.47	0.28	116.1	1.2
2000	0.463	24.6891	0.1611	0.6133	0.0040	0.00463	0.00098	5.4	1.126	0.007	0.02567	0.00029	23.35	0.33	102.8	1.4
2300	0.555	25.6667	0.2706	0.7050	0.0075	0.00044	0.00112	0.3	1.294	0.014	0.02980	0.00280	25.57	0.43	112.3	1.8
2600	0.625	26.6327	0.3033	1.1161	0.0246	0.00551	0.00757	5.8	2.049	0.045	0.03262	0.00066	25.08	2.26	110.2	9.6
3000	0.712	24.4586	0.0931	0.8552	0.0071	0.00534	0.00508	6.2	1.570	0.013	0.02259	0.00065	22.93	1.50	101.0	6.4
4000	0.970	25.4847	0.2413	1.3776	0.0058	0.00167	0.00058	1.5	2.530	0.011	0.02274	0.00015	25.09	0.29	110.3	1.3
9000	1.000	20.0232	0.0833	0.2541	0.0055	0.00233	0.00235	3.4	0.466	0.010	0.00567	0.00077	19.33	0.70	85.5	3.0
Integrated		24.1193	0.0801	0.8009	0.0024	0.00606	0.00077	7.2	1.470	0.004	0.02501	0.00029	22.37	0.24	98.6	1.1

03ZW474 BI#2 **474B_2** Weighted average of J from standards = 0.002512 +/- 0.000006

Laser	Cum.	$^{40}Ar/^{39}Ar$	+/-	$^{37}Ar/^{39}Ar$	+/-	$^{36}Ar/^{39}Ar$	+/-	% Atm.	Ca/K	+/-	Cl/K	+/-	$^{40}Ar^*/^{39}Ar_K$	+/-	Age	+/-
(mW)	^{39}Ar	meas.		meas.		meas.		^{40}Ar							(Ma)	(Ma)
250	0.002	69.8515	2.3169	4.2912	0.1580	0.19586	0.03073	82.4	7.896	0.292	0.01523	0.01157	12.30	8.92	54.9	39.2
500	0.011	11.8359	0.1121	1.9794	0.0224	0.04111	0.00816	101.6	3.637	0.041	0.04125	0.00265	-0.19	2.41	-0.9	10.9
750	0.041	5.0075	0.0194	0.6341	0.0042	0.01360	0.00211	79.8	1.164	0.008	0.03279	0.00087	1.01	0.62	4.6	2.8
1000	0.075	8.0687	0.0247	0.5512	0.0032	0.01252	0.00194	45.5	1.012	0.006	0.02788	0.00071	4.38	0.57	19.8	2.6
1250	0.113	14.3929	0.0506	0.5126	0.0047	0.01434	0.00175	29.2	0.941	0.009	0.02620	0.00072	10.17	0.52	45.5	2.3
1500	0.155	18.1120	0.0640	0.5768	0.0034	0.01272	0.00184	20.5	1.059	0.006	0.03140	0.00061	14.37	0.55	64.0	2.4
1750	0.206	19.4121	0.0534	0.4078	0.0021	0.01032	0.00074	15.6	0.748	0.004	0.03057	0.00021	16.37	0.22	72.7	1.0
2000	0.269	22.9870	0.0520	0.3084	0.0020	0.01084	0.00062	13.8	0.566	0.004	0.02879	0.00017	19.78	0.19	87.5	0.8
2300	0.349	27.3967	0.0673	0.2914	0.0016	0.00974	0.00051	10.4	0.535	0.003	0.02792	0.00013	24.52	0.16	107.8	0.7
2600	0.431	30.4630	0.2310	0.4119	0.0040	0.01030	0.00091	9.9	0.756	0.007	0.03096	0.00053	27.43	0.34	120.2	1.5
3000	0.505	33.1919	0.1814	0.5815	0.0036	0.01030	0.00079	9.0	1.067	0.007	0.03300	0.00052	30.18	0.29	131.8	1.2
4000	0.749	35.3138	0.2110	1.0790	0.0030	0.00349	0.00032	2.7	1.981	0.006	0.03906	0.00011	34.36	0.23	149.4	1.0
9000	1.000	30.5946	0.2839	0.9636	0.0020	0.00141	0.00011	1.1	1.769	0.004	0.04186	0.00030	30.24	0.29	132.1	1.2
Integrated		27.8684	0.0904	0.7539	0.0011	0.00749	0.00022	7.8	1.384	0.002	0.03527	0.00012	25.69	0.11	112.8	0.5

03ZW474 HO#1 **474H_1** Weighted average of J from standards = 0.002512 +/- 0.000006

Laser	Cum.	$^{40}Ar/^{39}Ar$	+/-	$^{37}Ar/^{39}Ar$	+/-	$^{36}Ar/^{39}Ar$	+/-	% Atm.	Ca/K	+/-	Cl/K	+/-	$^{40}Ar^*/^{39}Ar_K$	+/-	Age	+/-
(mW)	^{39}Ar	meas.		meas.		meas.		^{40}Ar							(Ma)	(Ma)
400	0.003	126.1942	15.5943	3.6072	0.5172	0.43480	0.14485	101.6	6.634	0.953	0.19972	0.03627	-2.05	39.85	-9.3	181.5
800	0.009	71.5232	2.5524	2.3572	0.0882	0.20813	0.01980	85.8	4.332	0.162	0.19925	0.00955	10.18	5.45	45.6	24.1
1200	0.024	39.8303	0.6293	1.0881	0.0203	0.06204	0.00816	45.9	1.998	0.037	0.06518	0.00183	21.56	2.42	95.2	10.4
1500	0.044	32.4310	0.3836	0.9420	0.0126	0.03338	0.00546	30.2	1.730	0.023	0.05573	0.00118	22.62	1.63	99.7	7.0
1800	0.064	28.8942	0.3463	2.3113	0.0377	0.01078	0.00755	10.4	4.247	0.069	0.14441	0.00218	25.89	2.26	113.7	9.6
2100	0.089	29.0386	0.2374	4.4569	0.0382	0.01508	0.00285	14.2	8.202	0.070	0.19404	0.00238	24.96	0.87	109.7	3.7
2500	0.138	26.9725	0.0980	6.4620	0.0286	0.00408	0.00178	2.7	11.907	0.053	0.16712	0.00119	26.33	0.54	115.6	2.3
3000	0.226	26.1070	0.1253	6.8622	0.0384	0.00402	0.00092	2.6	12.648	0.071	0.14357	0.00079	25.52	0.30	112.1	1.3
3500	0.354	25.9291	0.2656	6.8610	0.0810	-0.00146	0.00245	-3.7	12.646	0.150	0.13479	0.00144	26.97	0.78	118.3	3.3
4000	0.440	25.9094	0.1027	7.1245	0.0300	-0.00042	0.00201	-2.5	13.133	0.056	0.13633	0.00085	26.66	0.61	117.0	2.6
5000	0.563	26.1880	0.1677	7.2157	0.0465	0.00282	0.00065	1.1	13.302	0.086	0.15227	0.00098	25.99	0.26	114.1	1.1
9000	1.000	25.7457	0.0914	8.3899	0.0123	0.00376	0.00018	1.9	15.479	0.023	0.17991	0.00026	25.37	0.11	111.5	0.5
Integrated		26.9822	0.0615	7.1840	0.0146	0.00701	0.00060	5.7	13.244	0.027	0.15875	0.00032	25.54	0.19	112.2	0.8

03ZW474 HO#2 **474H_2** Weighted average of J from standards = 0.002512 +/- 0.000006

Laser	Cum.	$^{40}Ar/^{39}Ar$	+/-	$^{37}Ar/^{39}Ar$	+/-	$^{36}Ar/^{39}Ar$	+/-	% Atm.	Ca/K	+/-	Cl/K	+/-	$^{40}Ar^*/^{39}Ar_K$	+/-	Age	+/-
(mW)	^{39}Ar	meas.		meas.		meas.		^{40}Ar							(Ma)	(Ma)
400	0.001	382.9427	45.7143	10.6323	1.2838	1.42350	0.19184	109.6	19.645	2.389	0.12268	0.02771	-37.19	26.91	-176.9	134.5
800	0.003	198.8530	7.3563	5.7575	0.2235	0.65949	0.03722	97.8	10.604	0.413	0.26464	0.01245	4.39	8.35	19.8	37.4
1200	0.008	50.5309	0.7827	4.0452	0.0687	0.14812	0.01653	86.1	7.442	0.127	0.11352	0.00426	7.05	4.85	31.7	21.6
1500	0.014	31.7665	0.5164	3.0699	0.0586	0.06957	0.00958	64.0	5.644	0.108	0.06115	0.00318	11.43	2.83	51.1	12.4
1800	0.021	30.7688	0.4466	5.6431	0.0880	0.06307	0.00888	59.3	10.392	0.163	0.04727	0.00293	12.57	2.63	56.1	11.5
2100	0.028	31.2588	0.7194	6.5804	0.1662	0.07012	0.01735	64.8	12.126	0.308	0.04263	0.00488	11.05	5.14	49.4	22.7
2500	0.038	34.8768	0.5746	4.6697	0.0833	0.07227	0.01315	60.3	8.594	0.154	0.06660	0.00322	13.89	3.89	61.9	17.0
3000	0.054	32.7345	0.2516	4.4529	0.0396	0.03341	0.00728	29.2	8.194	0.073	0.09699	0.00210	23.23	2.16	102.3	9.3
3500	0.099	30.5007	0.2397	5.7580	0.0492	0.01277	0.00262	11.0	10.605	0.091	0.13748	0.00127	27.23	0.81	119.4	3.4
4000	0.216	26.7690	0.1974	6.9191	0.0557	0.00473	0.00086	3.3	12.753	0.103	0.14354	0.00116	25.98	0.32	114.0	1.4
5000	0.423	26.2303	0.3430	6.7232	0.0935	0.00369	0.00062	2.2	12.390	0.173	0.13800	0.00191	25.73	0.39	113.0	1.7
9000	1.000	26.3273	0.2483	8.0833	0.0536	0.00519	0.00015	3.5	14.910	0.099	0.14934	0.00098	25.51	0.25	112.0	1.1
Integrated		27.6047	0.1647	7.3878	0.0367	0.01076	0.00034	9.5	13.621	0.068	0.14217	0.00070	25.07	0.19	110.2	0.8

975960 BI Weighted average of J from standards = 0.002512 +/- 0.000006

Laser	Cum.	$^{40}Ar/^{39}Ar$	+/-	$^{37}Ar/^{39}Ar$	+/-	$^{36}Ar/^{39}Ar$	+/-	% Atm.	Ca/K	+/-	Cl/K	+/-	$^{40}Ar^*/^{39}Ar_K$	+/-	Age	+/-
(mW)	^{39}Ar	meas.		meas.		meas.		^{40}Ar							(Ma)	(Ma)
100	0.004	17.3942	0.1629	0.1622	0.0062	0.05188	0.00207	88.2	0.298	0.011	0.09342	0.00184	2.05	0.61	31.9	9.5
150	0.007	6.9854	0.0823	0.0888	0.0071	0.01594	0.00201	67.6	0.163	0.013	0.09232	0.00169	2.25	0.59	35.1	9.2
200	0.015	8.3159	0.0616	0.0581	0.0033	0.00979	0.00047	34.9	0.107	0.006	0.08008	0.00106	5.40	0.14	83.0	2.2
300	0.042	7.8983	0.0396	0.0308	0.0010	0.00325	0.00036	12.2	0.057	0.002	0.08019	0.00058	6.91	0.11	105.6	1.6
450	0.115	7.4533	0.0300	0.0177	0.0003	0.00068	0.00007	2.7	0.032	0.001	0.07753	0.00073	7.23	0.04	110.2	0.5
600	0.219	7.3427	0.0482	0.0261	0.0003	0.00008	0.00007	0.3	0.048	0.001	0.07752	0.00055	7.29	0.05	111.2	0.8
750	0.387	7.2444	0.0253	0.0518	0.0002	0.00012	0.00004	0.4	0.095	0.000	0.07783	0.00027	7.19	0.03	109.6	0.4
900	0.538	7.1933	0.0306	0.0761	0.0005	0.00010	0.00005	0.3	0.140	0.001	0.07472	0.00027	7.14	0.03	109.0	0.5
1050	0.683	7.1718	0.0194	0.0688	0.0007	0.00021	0.00007	0.8	0.126	0.001	0.06208	0.00011	7.09	0.03	108.2	0.4
1200	0.747	7.1774	0.0450	0.0656	0.0010	0.00023	0.00013	0.9	0.120	0.002	0.06057	0.00045	7.09	0.06	108.2	0.9
1500	0.808	7.2432	0.0355	0.0393	0.0006	0.00038	0.00014	1.5	0.072	0.001	0.06616	0.00027	7.11	0.06	108.5	0.8
2000	0.836	7.2849	0.0305	0.0315	0.0010	0.00090	0.00030	3.6	0.058	0.002	0.06336	0.00054	6.99	0.09	106.8	1.4
2500	0.844	7.8406	0.0670	0.0130	0.0029	0.00151	0.00107	5.7	0.024	0.005	0.05873	0.00093	7.37	0.32	112.3	4.8
3000	0.856	7.7187	0.0537	0.0213	0.0013	0.00312	0.00053	12.0	0.039	0.002	0.05930	0.00045	6.77	0.17	103.5	2.5
8000	1.000	7.4412	0.0393	0.0324	0.0006	0.00061	0.00005	2.4	0.059	0.001	0.06823	0.00036	7.23	0.04	110.4	0.6
Integrated		7.3519	0.0112	0.0489	0.0002	0.00074	0.00003	3.0	0.090	0.000	0.07124	0.00012	7.11	0.01	108.5	0.5

976864 M Weighted average of J from standards = 0.002512 +/- 0.000006

Laser	Cum.	$^{40}Ar/^{39}Ar$	+/-	$^{37}Ar/^{39}Ar$	+/-	$^{36}Ar/^{39}Ar$	+/-	% Atm.	Ca/K	+/-	Cl/K	+/-	$^{40}Ar^*/^{39}Ar_K$	+/-	Age	+/-
(mW)	^{39}Ar	meas.		meas.		meas.		^{40}Ar							(Ma)	(Ma)
100	0.003	7.4673	0.0577	0.0378	0.0015	0.01328	0.00075	52.7	0.069	0.003	0.00176	0.00010	3.52	0.22	54.5	3.4
150	0.007	7.9195	0.0422	0.0326	0.0015	0.00850	0.00060	31.8	0.060	0.003	0.00172	0.00010	5.38	0.18	82.7	2.7
200	0.014	8.1926	0.0402	0.0258	0.0006	0.00489	0.00036	17.7	0.047	0.001	0.00103	0.00009	6.72	0.11	102.8	1.7
300	0.029	8.1921	0.0403	0.0174	0.0006	0.00253	0.00009	9.1	0.032	0.001	0.00077	0.00004	7.42	0.05	113.1	0.7
450	0.056	7.8696	0.0164	0.0122	0.0002	0.00140	0.00012	5.3	0.022	0.000	0.00066	0.00002	7.43	0.04	113.2	0.6
600	0.114	7.5424	0.0472	0.0074	0.0001	0.00063	0.00007	2.5	0.014	0.000	0.00049	0.00003	7.33	0.05	111.8	0.8
750	0.173	7.4774	0.0123	0.0073	0.0001	0.00055	0.00006	2.2	0.013	0.000	0.00049	0.00002	7.29	0.02	111.1	0.3
900	0.237	7.4007	0.0097	0.0159	0.0002	0.00048	0.00007	1.9	0.029	0.000	0.00049	0.00002	7.23	0.02	110.3	0.3
1050	0.311	7.3907	0.0241	0.0109	0.0001	0.00056	0.00003	2.2	0.020	0.000	0.00052	0.00003	7.20	0.03	109.8	0.4
1200	0.391	7.3487	0.0305	0.0107	0.0001	0.00052	0.00003	2.1	0.020	0.000	0.00050	0.00002	7.17	0.03	109.4	0.5
1500	0.473	23.4563	0.4503	0.0165	0.0003	0.05442	0.00064	68.6	0.030	0.001	0.00061	0.00006	7.35	0.42	112.0	6.3
2000	0.546	7.3536	0.0570	0.0362	0.0002	0.00053	0.00004	2.1	0.066	0.000	0.00076	0.00001	7.17	0.06	109.4	0.9
2500	0.624	7.4541	0.1587	0.0332	0.0004	0.00080	0.00006	3.1	0.061	0.001	0.00074	0.00003	7.19	0.16	109.8	2.4
3500	0.731	7.3396	0.1347	0.0640	0.0007	0.00084	0.00004	3.3	0.118	0.001	0.00101	0.00004	7.07	0.13	107.9	2.0
8000	1.000	7.3658	0.1068	0.0741	0.0007	0.00078	0.00004	3.1	0.136	0.001	0.00111	0.00004	7.11	0.11	108.6	1.6
Integrated		8.7442	0.0492	0.0379	0.0002	0.00524	0.00004	17.7	0.070	0.000	0.00079	0.00001	7.17	0.05	109.4	0.9

977056 BI Weighted average of J from standards = 0.002512 +/- 0.000006

Laser	Cum.	$^{40}Ar/^{39}Ar$	+/-	$^{37}Ar/^{39}Ar$	+/-	$^{36}Ar/^{39}Ar$	+/-	% Atm.	Ca/K	+/-	Cl/K	+/-	$^{40}Ar^*/^{39}Ar_K$	+/-	Age	+/-
(mW)	^{39}Ar	meas.		meas.		meas.		^{40}Ar							(Ma)	(Ma)
100	0.003	16.1099	0.1010	0.1236	0.0039	0.05068	0.00248	93.1	0.227	0.007	0.02361	0.00055	1.12	0.73	17.5	11.4
150	0.007	4.9061	0.0428	0.0791	0.0044	0.00989	0.00106	59.8	0.145	0.008	0.02347	0.00034	1.96	0.31	30.6	4.9
200	0.014	8.4727	0.0490	0.0506	0.0026	0.01121	0.00131	39.2	0.093	0.005	0.02115	0.00039	5.14	0.39	79.0	5.9
300	0.036	8.2456	0.0264	0.0207	0.0006	0.00537	0.00031	19.3	0.038	0.001	0.02013	0.00017	6.63	0.09	101.4	1.4
450	0.104	7.6743	0.0232	0.0066	0.0003	0.00090	0.00008	3.5	0.012	0.000	0.02040	0.00009	7.38	0.03	112.5	0.5
600	0.182	7.5224	0.0667	0.0080	0.0003	0.00013	0.00007	0.5	0.015	0.001	0.02058	0.00024	7.46	0.07	113.7	1.0
750	0.251	7.4474	0.0300	0.0240	0.0004	0.00038	0.00012	1.5	0.044	0.001	0.02038	0.00012	7.31	0.05	111.4	0.7
900	0.346	7.3880	0.0331	0.0550	0.0007	0.00013	0.00009	0.5	0.101	0.001	0.02030	0.00014	7.33	0.04	111.7	0.6
1050	0.490	7.3139	0.0188	0.0610	0.0003	-0.00007	0.00004	-0.4	0.112	0.001	0.01999	0.00010	7.31	0.02	111.5	0.3
1200	0.573	7.3232	0.0263	0.0285	0.0003	0.00005	0.00006	0.2	0.052	0.000	0.02020	0.00009	7.28	0.03	111.1	0.5
1500	0.658	7.3531	0.0184	0.0150	0.0002	0.00008	0.00010	0.3	0.027	0.000	0.02063	0.00008	7.30	0.04	111.4	0.5
2000	0.816	7.2584	0.0142	0.0395	0.0003	-0.00004	0.00006	-0.2	0.072	0.001	0.02121	0.00008	7.25	0.02	110.5	0.3
2500	0.854	7.3192	0.0168	0.0614	0.0007	0.00018	0.00027	0.7	0.113	0.001	0.02111	0.00018	7.24	0.08	110.5	1.2
3500	0.949	7.3032	0.0281	0.0203	0.0003	-0.00015	0.00010	-0.6	0.037	0.000	0.02031	0.00009	7.32	0.04	111.6	0.6
8000	1.000	7.2462	0.0165	0.0232	0.0002	-0.00001	0.00015	-0.1	0.042	0.000	0.01993	0.00013	7.22	0.05	110.2	0.7
Integrated		7.4038	0.0085	0.0336	0.0001	0.00048	0.00003	1.9	0.062	0.000	0.02049	0.00004	7.24	0.01	110.4	0.5

03ZW351 M Weighted average of J from standards = 0.002512 +/- 0.000006

Laser	Cum.	$^{40}Ar/^{39}Ar$	+/-	$^{37}Ar/^{39}Ar$	+/-	$^{36}Ar/^{39}Ar$	+/-	% Atm.	Ca/K	+/-	Cl/K	+/-	$^{40}Ar^*/^{39}Ar_K$	+/-	Age	+/-
(mW)	^{39}Ar	measured		measured		measured		^{40}Ar							(Ma)	(Ma)
200	0.0014	25.285	0.152	0.0127	0.0127	0.05663	0.00170	66.2	0.0232	0.0234	0.00301	0.00031	8.525	0.495	38.7	2.2
400	0.0068	30.109	0.199	0.0065	0.0034	0.03536	0.00060	34.7	0.0119	0.0063	0.00259	0.00008	19.633	0.235	87.9	1.0
600	0.0172	28.707	0.155	0.0019	0.0017	0.01336	0.00025	13.8	0.0036	0.0031	0.00148	0.00003	24.731	0.162	110.0	0.7
800	0.0365	27.578	0.174	0.0021	0.0014	0.00517	0.00015	5.5	0.0039	0.0025	0.00109	0.00004	26.021	0.174	115.5	0.8
1000	0.0636	26.778	0.133	0.0020	0.0008	0.00254	0.00008	2.8	0.0037	0.0014	0.00095	0.00002	25.999	0.133	115.4	0.6
1250	0.1030	26.102	0.132	-0.0003	0.0005	0.00112	0.00006	1.3	-0.0006	0.0010	0.00097	0.00002	25.743	0.132	114.3	0.6
1500	0.1472	25.759	0.121	-0.0010	0.0004	0.00066	0.00005	0.8	-0.0019	0.0008	0.00098	0.00002	25.535	0.121	113.4	0.5
1750	0.1994	25.662	0.121	-0.0008	0.0003	0.00067	0.00005	0.8	-0.0014	0.0006	0.00099	0.00002	25.434	0.122	113.0	0.5
2000	0.2581	25.507	0.112	-0.0005	0.0003	0.00060	0.00004	0.7	-0.0009	0.0005	0.00100	0.00002	25.300	0.112	112.4	0.5
2500	0.3465	25.431	0.131	-0.0007	0.0002	0.00046	0.00003	0.5	-0.0012	0.0004	0.00105	0.00002	25.266	0.131	112.3	0.6
3000	0.4685	25.392	0.116	-0.0002	0.0001	0.00046	0.00001	0.5	-0.0004	0.0002	0.00108	0.00002	25.229	0.116	112.1	0.5
4000	0.6723	25.316	0.115	-0.0003	0.0001	0.00044	0.00001	0.5	-0.0005	0.0002	0.00115	0.00001	25.158	0.115	111.8	0.5
5000	0.8962	25.322	0.118	-0.0003	0.0001	0.00047	0.00001	0.6	-0.0006	0.0001	0.00126	0.00002	25.154	0.118	111.8	0.5
8000	1.0000	25.313	0.116	-0.0004	0.0002	0.00062	0.00003	0.7	-0.0007	0.0003	0.00168	0.00002	25.101	0.116	111.6	0.5
Integrated		25.561	0.044	-0.0002	0.0001	0.00108	0.00001	1.2	-0.0004	0.0001	0.00119	0.00001	25.214	0.044	112.1	0.6